Plant virus-derived nanoparticles for the imaging and treatment of cancer

Coralie Gamper

UNIVERSITÉ DE STRASBOURG

ÉCOLE DOCTORALE Sciences de la vie et de la santé

CNRS-UPR2357 Institut de Biologie Moléculaire des Plantes

THÈSE présentée par :

Coralie GAMPER

soutenue le : **23 septembre 2019**

pour obtenir le grade de : **Docteur de l'université de Strasbourg**

Discipline/ Spécialité : Biotechnologie

Nanoparticules dérivées de virus de plante pour le traitement et l'imagerie du cancer

THÈSE dirigée par :

Monsieur HEINLEIN Manfred	Directeur de recherche, CNRS
Monsieur BAGNARD Dominique	MCU, université de Strasbourg

RAPPORTEURS :

Madame BARBERI-HEYOB Muriel	Professeur, université de Lorraine
Madame WEGE Christina	Professeur, université de Stuttgart

AUTRES MEMBRES DU JURY :

Monsieur REMY Jean-Serge	Directeur de recherche, CNRS
Monsieur BENNASROUNE Amar	MCU, université de Reims Champagne-Ardenne

I would like to thank my thesis jury for kindly accepting to evaluate my work. Thanks to Pr. Wege and Pr. Barberi-Heyob for agreeing to take time to read my thesis.

I would like to thank the director of the IBMP, the Dr. Laurence Drouard, and the director of the INSERM unit U1119, the Pr. Guy Mensah and their respective research unit for their welcoming.

I would like to thank the Dr. Gertraud Orend for her scientific advices during the course of my thesis.

I would like to thank my thesis director, the Dr. Manfred Heinlein for giving me the opportunity to realize my thesis in his lab and his help during the course of my thesis.

I would like to thank my thesis co-director, the Dr. Dominique Bagnard for his support since my master thesis. I appreciated your scientific advices and your help for the redaction of my thesis. I will miss a little bit your non volunteer "réécriture d'expressions françaises".

Thanks to Nicolas Baumberger and Laurence Hergott from the protein production platform of the IBMP for their technical support.

Thanks also to Mathieu Erhardt and Jérôme Mutterer from the microscopy platform of the IBMP for their technical advices.

Thanks to Sonia Boscà-San José who started this project and transmitted to me her technical knowledge. Even if we didn't work together for long, I appreciated your advices and your kindness.

Thanks to my former co-workers from Manfred's team. Thank you Nicolas for our discussions about the thesis difficulties and thank you Caiping for having collecting bacteria for me when I was blocked at Illkirch.

I thank my former co-workers from Dominique's team and especially Gérard, Michael, Caroline, Aurore, Lauriane and Marie.

I wish a good continuation with their thesis to Lucas and Dafni.

Thank you Caroline for your help with several experiments and your support during stressful period. I'm sure we will have other opportunities to go for a drink together !

Good luck with your retirement Gérard ! Our discussion (scientific or not) will certainly miss me.

Thank you Mika for the angiogenesis assays you done for me when I had no time to do them. It has been really nice working with you for more than 5 years now. I wish you the best for the rest of your career and good luck with future teenager Ambre !

Thank you Aurore for all our discussions about research, movies, books and so much more. You have endured my complaints so many times and gave me good advices to continue moving on, I will have not survive my thesis without you !

Lauriane you have been a wonderful support during these last two years. Your energy and your kindness have brought a welcome freshness to the lab. I wish you plenty of joy in your future works !

Marie I wish you all the best in your new career and a lot of happiness with your so nice little Danaá !

Fabien I wish you all the best for the rest of your career. Your jokes and movie suggestions have been appreciated !

Thanks to my parents, my sisters and my cousin for having supporting me through all these years and enduring me during some stressful moment ! Thank you Rébecca for having preparing my meal so often, I would have starved to death without you !

And finally, thank you Suzanne for your smile and your cuteness ! I am already proud to be your godmother and I can't wait for the moment we will travel together !

TABLE OF CONTENTS

List of figures and tables

Abbreviations

Ads: Adenoviruses
AE: Adverse events
Ahx: 6-aminohexanoic acid
AI: Aromatase inhibitors
APC: Antigen-presenting cells
BACTH: Bacterial adenylate cyclase two hybrid
CAFs: Carcinoma-associated fibroblasts
CARs: Chimeric antigen receptors
CCND1: Cyclin D1
CHO: Chinese hamster ovary
CNTs: Carbon nanotubes
CP: Coat protein
CPT: Camptothecin
Cx43: Connexin43
DCs: Dendritic cells
DMSO: Dimethyl sulfoxide
DOX: Doxorubicin
DTT: Dithiothreitol
EC: Endothelial cells
ECM: Extracellular matrix
EDA: Ethylenediamide
EGFR: Epidermal growth factor receptor
EndR: Endoplasmic reticulum
ER: Estrogen receptor
FBS: Fetal Bovine Serum
FDA: Federal drug administration
FRET: Föster resonance energy transfer
G: Generation
GBSS: Gey's balanced salt solution
GJIC: Gap junction intercellular communication
GpA: Glycophorin A
GQDs: Graphene quantum dots
Gy: Gray
HBSS: Hank's balanced salt solution
HER2: Human epidermal growth factor receptor 2
HER3: Human epidermal growth factor receptor 3
HT: Hormone therapy
HRP: Horse-Radish Peroxidase
HUVECs: Human umbilical vein epidermal cells
ICI: Immune checkpoint inhibitors
IFN-y: Interferon-y
IGFR1: Insulin growth factor receptor 1
iPDT: Interstitial photodynamic therapy
IRRs: Infusion-related reactions
LB: Lysogeny broth
LDS: Lithium dodecyl sulfate
LPHNPs: Lipid-polymer hybrid nanoparticles
mAb: Monoclonal antibodies
MAPK: Mitogen-activated protein kinase
MBP: Maltose binding protein
MBs: Microbubbles
MET: Mesenchymal-Epithelial Transition

MMPs: Matrix metalloproteinases

MP: Movement protein

MRI: Magnetic resonance imaging

miRNA: MicroRNA

MSN: Mesoporous silica nanoparticles

MTO: Mitoxantrone

mTOR: mammalian target of rapamycin

MTP: Membrane targeting peptide

MTT: 3-(4,5-dimethylthiazol-2-yl)-2,5-diphenyltetrazolium bromide

MWCNTs: Multi-walled carbon nanotubes

NHS: N-hydroxy succinamide

NPs: Nanoparticles

Nrp1: Neuropilin-1

Nrp2: Neuropilin-2

NCS: Neocarzinostatin

NSCLC: Non-small cell lung carcinoma

ORF: Open reading frame

OSCC: Oral squamous cell carcinoma

OVs: Oncolytic viruses

PAMAM: Polyamidoamine

PD-1: Programmed cell death 1

PDGF: Platelet-derived growth factor

PD-L1: Programmed death-ligand 1

pDNA: Plasmid DNA

PDT: Photodynamic therapy

PEG: Polyethylene glycol

PFA: Paraformaldehyde

PI3K:

PK: Pharmacokinetic

PKI: Protein kinase inhibitor

PA: Polylactic acid

PLA: Proximity ligation assay

PMAn: Poly(isobutylene-alt-maleic anhydride)

PR: Progesterone receptor

PS: Photosensitizer

PTEN: Phosphatase and tensin homologue

PTT: Photothermal therapy

PTX: Paclitaxel

PVP: Polyvinylpyrrolidone

QD: Quantum dots

RAF: Rapidly accelerated fibrosarcoma

RES: Reticuloendoplasmic system

RISC: RNA-interfering silencing complex

ROS: Reactive oxygen species

RT: Room temperature

RTK: Receptor tyrosine kinase

SDF-1: Stroma-derived factor 1

SDT: Sonodynamic therapy

SERMs: Selective estrogen receptor modulator

shRNA: Short hairpin RNA

siRNA: Small interfering RNA

SNPs: Spherical nanoparticles

SPIO: Superparamagnetic iron oxide nanoparticles

SPR: Surface plasmon resonance

SRS: Stereotactic radiation surgery

SWCNTs: Single-walled carbon nanotubes

TAA: Tumor associated antigens

TAMs: Tumor associated macrophages

TBP: Trastuzumab-binding peptide

TGFß: Tumor growth factor ß

TILs: Tumor-infiltrating lymphocytes

TMD: Transmembrane domain

TME: Tumor microenvironment

TMV: *Tobacco Mosaic Virus*

TNBC: Triple negative breast cancer

TNC: Tenascin-C

TPC: 5-(4-carboxyphenyl)-10,15,20-triphenyl-chlorin

US: Ultrasound

VEGF: Vascular endothelial growth factor

VEGFR2: Vascular endothelial growth factor receptor 2

I. Cancer biology and treatments

Cancer is one of the most predominant diseases in western countries. In 2014, 8.2 million deaths worldwide were due to cancer and this number is expected to reach 22 millions in 2035.

Cancer cells are characterized by several hallmark features, including sustaining proliferative signaling, evasion of growth suppressors, avoidance of immune destruction, replicative immortality, tumor-promoting inflammation, activation of invasion and metastasis, induction of angiogenesis, resistance to cell death, deregulation of cellular energetics, genome instability and mutation (**Figure 1**) (Hanahan and Weinberg, 2011).

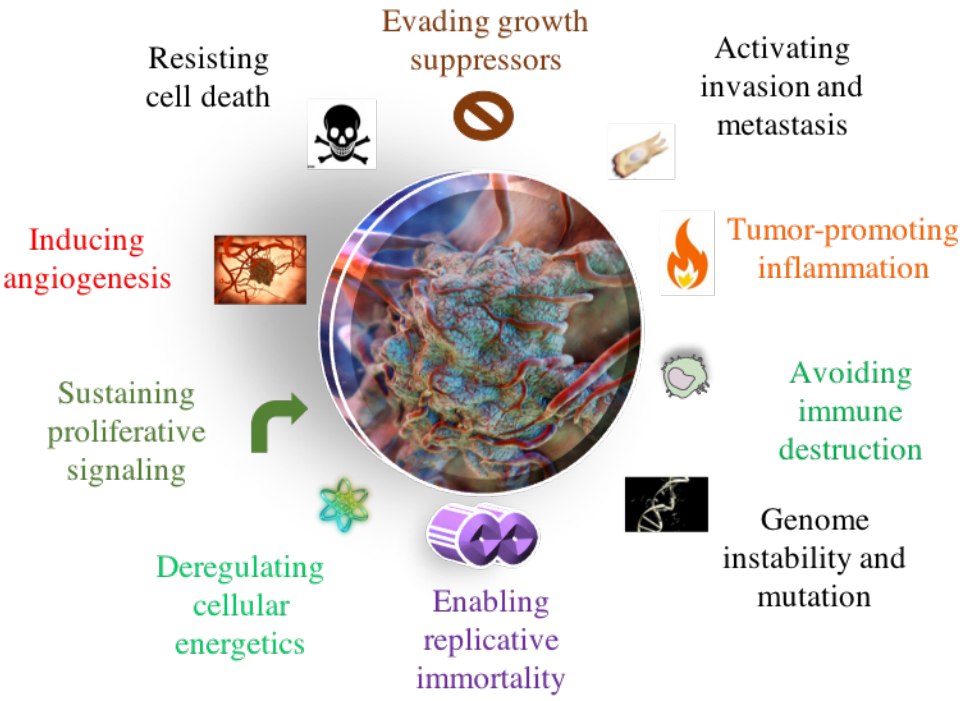

Figure 1 : Hallmarks of cancer.

Adapted from Hanahan and Weinberg (2011).

Moreover, tumor tissue is not exclusively composed of tumor cells but also of various other cell types such as endothelial cells, fibroblasts, and immune system cells

(macrophages, neutrophils, lymphocytes) that form the so-called stroma (**Figure 2**) (Dvorak, 1986).

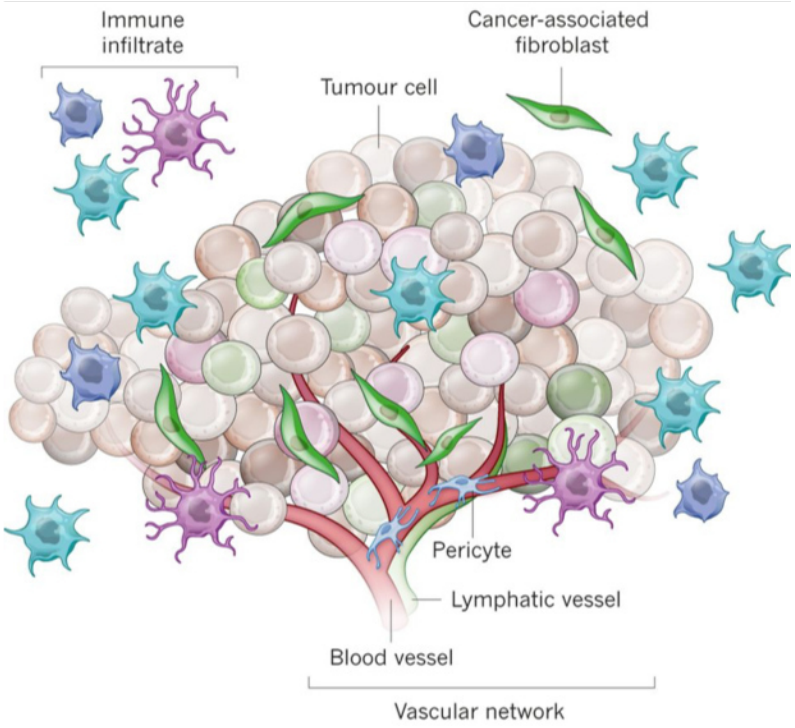

Figure 2: Tumor microenvironment.

The tumor is composed of various cells in addition of tumor cells. Immune cells and cancer-associated fibroblasts play a major role for creating a tumor-promoting environment. From Junttila and de Sauvage (2013).

The concomitance of all of these different features explains the complexity of cancer disease and, hence, the complexity encountered in developing an effective cancer treatment. Thus, many different therapeutic approaches have been investigated and among them I will focus on approaches aiming to benefit from the use of nanoparticles.

1. Cancer development

1.1. Genome alterations in cancer cells

The genome of cancer cells is highly unstable. Genome alterations are mainly affecting somatic cells but they can occur in germline cells thus leading to predisposition to cancer development. It has been highlighted that a single mutation is not sufficient to provoke the switch of healthy cells to cancer cells. Instead, from a primary mutation, additional mutations occurring in a sequential manner accumulate and then trigger the cancer phenotype (Croce, 2008; Vogelstein et al., 1988). This sequential process of alteration leads to the development of different clones of cancer cells derived from an initially mutated cell thereby creating intra-tumor heterogeneity. Although these mutations are critical for the appearance and development of many cancer types, there is, at this day, no efficient tool to avoid them and no approved drugs by which these mutations can be targeted.

1.1.1. Tumor suppressor genes

Tumor suppressor genes[1] are mainly involved in the regulation of proliferation and apoptosis. Their expression is downregulated or suppressed in cancer cells allowing them to proliferate indefinitely. p53 is a tumor suppressor gene altered in a wide variety of cancers (carcinoma, leukemia, lymphoma) and usually inactivated in more than 50% of the tumor type. Another tumor suppressor gene altered in cancer is PTEN (Phosphatase and Tensin Homologue). PTEN negatively regulates the PI3K/Akt/mTOR pathway, which is involved in cell proliferation (Dillon and Miller, 2014). Consequently, therapeutic strategies have been developed to restore p53 or PTEN activity in tumor cells. For example, delivery of PTEN protein to cancer cells has been achieved using several different nanocarriers such as silver nanoclusters (Arora et al., 2018) or lipid-like

[1] Tumor suppressor genes are defined as genes normally coding for proteins inhibiting tumor growth.

nanoparticles (Altınoğlu et al., 2016). In the same manner, p53 protein delivery to tumor cells has been investigated through several carriers and has exhibited a toxic effect on cancer cells *i.e* MDA-MB-231 breast cancer cells (Zhao et al., 2014). Tumor suppressor proteins such as p53 are very tightly regulated in healthy cells, thus it is important to deliver them specifically to cancer cells. Moreover, they have a low stability in the blood due to physic-chemical conditions (Chi et al., 2003), they are quickly eliminated by the macrophage phagocytic system and they are unlikely able to cross the cell membrane. In this regard, nanoparticles improved with targeting moiety would offer the possibility to load proteins and carry them directly to cancer cells.

1.1.1. Oncogenes

Oncogenes[2] encode proteins controlling apoptosis, cell proliferation or both. The most frequent alteration leading to the activation of oncogene is the chromosomic translocation. For example, the activation of c-MYC oncogene activation results from a translocation between chromosome 8 and 14 (Finger et al., 1986). This event leads to the creation of a novel gene resulting from the abnormal association of both chromosomes. MYC activation is associated with different cancers such as acute T-cell leukemia and Burkitt's lymphoma. Translocations can occur as a basis of a tumor initiation event or, later, during tumor progression.

A second type of genomic alteration provoking oncogene activation occurs by point mutations in proteins with critical roles in cell signaling. For example, mutations in RAS genes (KRAS, NRAS and HRAS) often implicated in cancer (colon cancer, Non-Small Cell lung cancer) (Slebos and Rodenhuis, 1992; Westra et al., 1993) are due to amino acid substitutions resulting in the constitutive activation of Ras proteins. Ras proteins are GTPase proteins which act on several proliferation pathways through MEK activation. Similar to translocations, point mutations can be the basis of the tumor-initiating event or occur during tumor progression.

[2] Oncogenes are defined as genes normally coding for proteins promoting tumor growth.

Another type of genomic alteration involved in cancer cell development is gene amplification. For example, Epidermal Growth Factor Receptor (EGFR), Rapidly Accelerated Fibrosarcoma (RAF) and MYC gene families are often amplified in cancer (Stefan and Bister, 2017). EGFR (also called ErbB-1 or HER1) amplification occurs in head and neck cancer and glioblastoma while EGFR2 (also called HER2/neu) amplification occurs in breast cancer and is associated with a bad prognosis (Press et al., 1997).

Because of their importance in the process of cancer development and progression, mutations have to be considered when developing anti-cancer drugs. Indeed, there are several examples of a direct link between the efficacy of drugs and amplified genes that they target (Yoshioka et al., 2018). For example, in the study of Yoshioka and colleagues, the sensitivity of different cell lines to the pan-HER inhibitor afatinib was correlated to their level of HER2 receptor expression. On the other hand, mutations are also the source of drug resistance (Shi et al., 2012) and can in extreme cases even be induced/selected by the drugs, creating a vicious circle favoring cancer. As a result, it is difficult to consider cancer mutations to develop therapeutic approaches because of the complex interplay between the target gene expression (gain or loss of expression) and functional mutations leading to hyper or hypo active proteins.

1.2. Cancer cell proliferation and survival

As already mentioned, cancer cells exhibit a high proliferation rate and suppress apoptosis. Several gene families are implicated in cancer cell survival and high proliferation. Cancer cells may use autocrine proliferative stimulation by producing growth factors and cognate receptors either themselves or by stimulating cells of the microenvironment which will produce growth factors in return (Bhowmick et al., 2004). As a result, therapeutic strategies have been investigated focusing on growth factor inhibition. EGFR family members and their signaling pathways are widely investigated as therapeutic target due to their role in sustained proliferation and survival of cancer cells. EGFR family receptors need to dimerize by either homo- or heterodimerization to

induce their activity. The most strongly implicated in cancer are HER1 and HER2, both carrying a tyrosine kinase activity within their intracellular domain (**Figure 3**). After dimerization, PI3/Akt/mTOR (**Figure 4**) or ERK 1/2 signaling pathways are activated, thus leading to a promotion of proliferation and survival of the cell (**Figure 5**) (Grant et al., 2002).

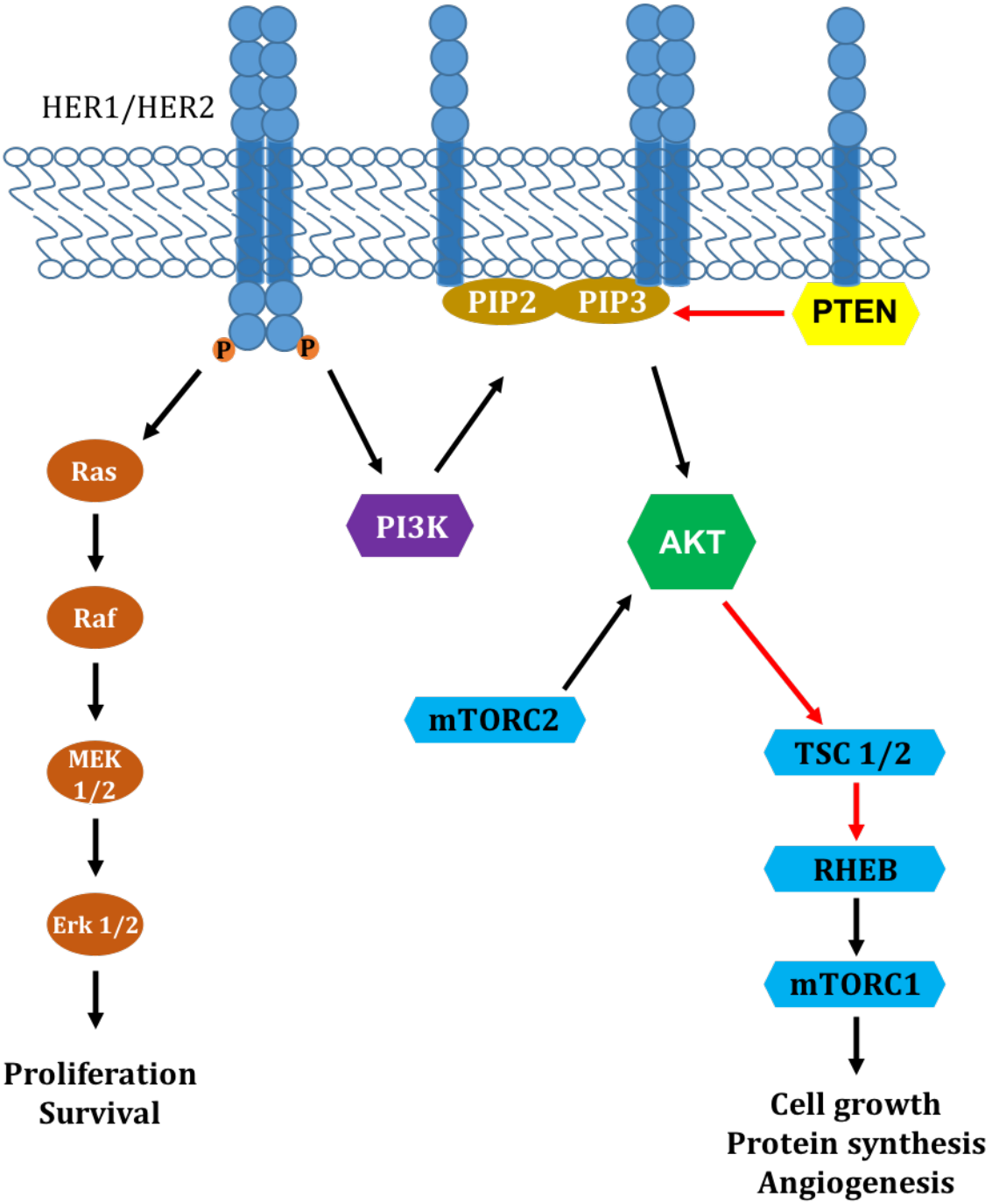

Figure 3: Tyrosine kinase receptor signaling pathway.

Ligand binding by tyrosine kinase receptor leads to receptor homo- or heterodimerization. This dimerization activates the RAS/RAF/ERK and the PI3/Akt/mTOR signaling pathways, which enhances cell proliferation and survival.

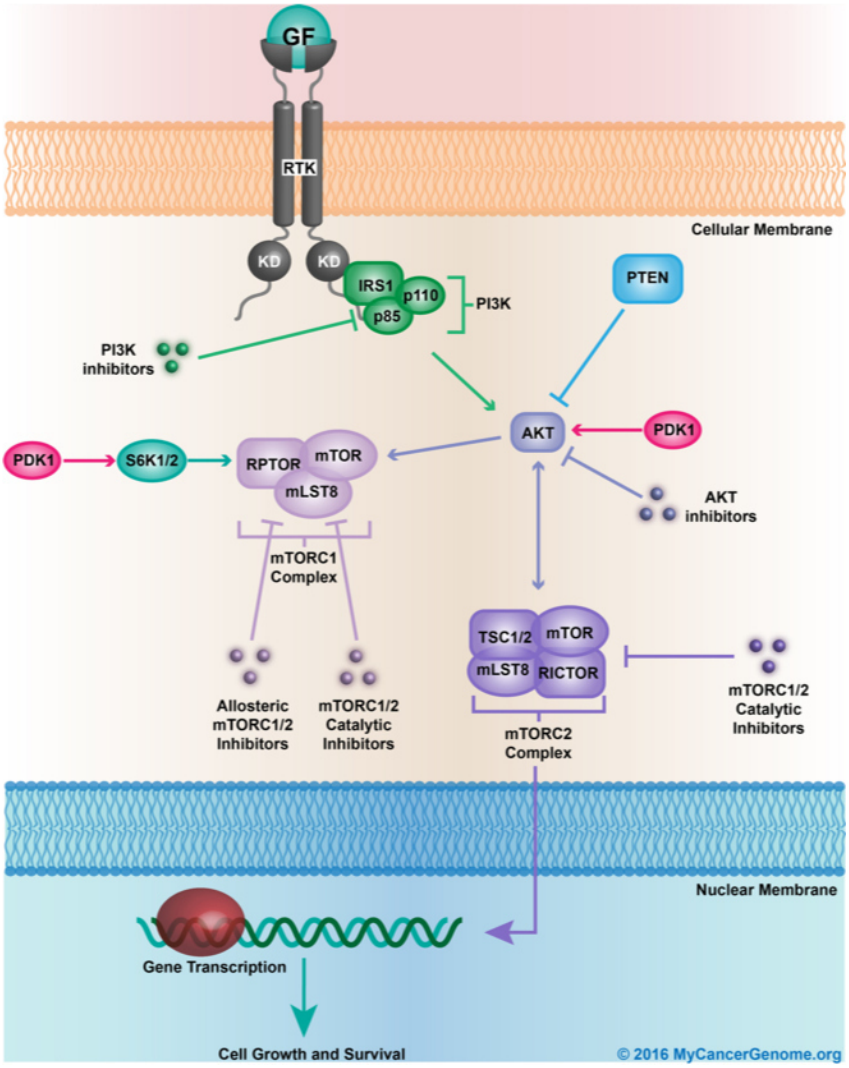

Figure 4: mTOR signaling pathway.

Ligand binding to tyrosine kinase receptor activates PI3K that phosphorylates Akt. Akt activates mTOR transcription factor favoring expression of tumor-promoting genes. Several inhibitors have been developed to target key proteins such as Akt and PI3K. From MyCancerGenome organization.

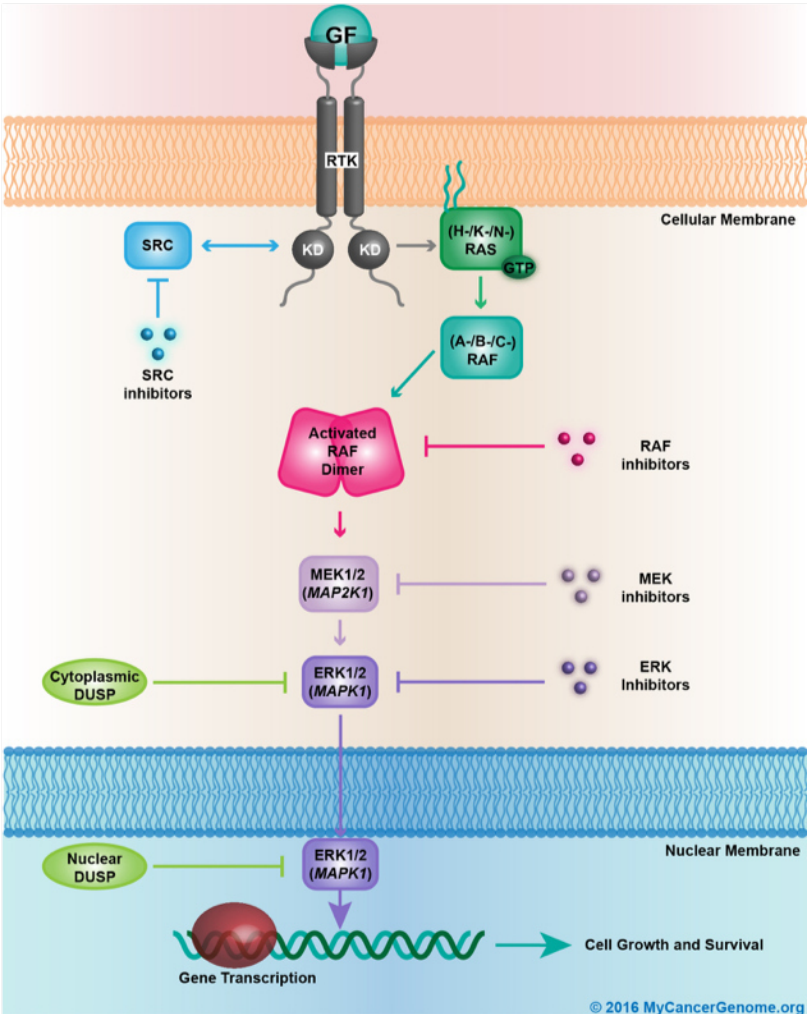

Figure 5: MAPK signaling pathway.

Growth factor binding to tyrosine kinase receptor leads to the activation of the RAS/RAF/MAPK pathway. This activation promotes cell survival and growth. Several inhibitors have been developed to target this pathway at multiple levels. DUSP, Dual specific phosphatase. From MyCancerGenome organization.

Consequently, important efforts have been made towards the development of drugs targeting these receptors and their signaling pathways e.g rapamycin (Sirolimus), a mTOR inhibitor, and rapamycin analogs (rapalogs). Although rapamycin has been shown to be efficient in pre-clinical animal models, it has demonstrated only modest beneficial effects on few malignant tumors in clinical trials. These failures can be explained by several potential mechanisms (Li et al., 2014). Indeed, since rapamycin and rapalogs have cytostatic but not cytotoxic effect, tumor growth started again at the end of the treatment (Bissler et al., 2008). Moreover, rapamycin does not cause the total

inhibition of mTOR-mediated processes such as autophagy and protein synthesis. To circumvent these issues, combinatorial strategies have been developed. For example, a polymeric nanoparticle was used to combine paclitaxel (PTX) and Everolimus (a mTOR inhibitor) and was shown to reduce tumor growth as well as paclitaxel side effects in several breast cancer tumor mouse models (Houdaihed et al., 2018). Moreover, the nanoparticle-based formulation allowed to deliver both PTX and Everolimus via the same route of administration, in this case intravenously, to maximize the chance to obtain similar pharmacokinetic (PK) profiles (e.g elimination rate, half-life circulation, biodistribution). This PK factor may be critical for achieving synergistic effects of drugs.

1.3. Loss of contact inhibition

Healthy tissues use regulatory mechanisms to control the number of cells to prevent abnormal tissue proliferation, which would otherwise lead to a modification of tissue architecture. It has been shown that diminution of certain types of connexins or gap junctions are common among human tumors. W.R Loewenstein hypothesized that the lack of gap junction proteins is linked to cancer (Loewenstein, 1979) and that connexins and gap junctions are required for cell-to-cell communication and for transmission of an antimitotic signal. This view was further confirmed by several studies that over time had accumulated evidences in this orientation (Budunova and Williams, 1994; Yotti et al., 1979). For example, connexin43 (Cx43) is less present in tumor tissue of certain cancer types such as breast cancer (Laird et al., 1999) and prostate cancer (Tsai et al., 1996). Gap junctions stay open during apoptosis allowing apoptotic factors to spread from one dying cell to another (Cusato et al., 2006). Thus, a reduction in the number of gap junctions and connexins would thereby reduce apoptosis in cancer cells.

Interestingly, several nanoparticle types have been shown to have an effect on connexins. For example, silver nanoparticles upregulate the expression of Cx43 thus leading to an increase in gap junction-mediated intercellular communication (GJIC) in human keratinocytes (Qin et al., 2018). In the opposite way, silica nanoparticles downregulate Cx43 expression in rat cardiomyocytes leading to a decrease in GIJC (Du et

al., 2017). These direct effects of nanoparticles on gap junctions and, therefore, on cellular communication may open an attractive perspective for the development of nanoparticles that target communication between cancer cells.

1.4. Inflammation in cancer

Early in 1863, the clinician Rudolf Virchow observed that leucocytes are present in neoplastic tissue and hypothesized that inflammation is linked to cancer (Balkwill and Mantovani, 2001).

Cancer cells present specific tumor antigens on their cell surface. These tumor antigens are recognized by immune cells, mainly dendritic cells (DCs), which trigger an anti-tumor response. Supported by secretion of chemokines such as cytokines and pro-inflammatory factor from cancer cells, DCs migrate into lymph nodes and present the tumor antigens to T cells (Blomberg et al., 2018). Consistently, several studies have shown a link between T cells, tumor infiltration, and cancer outcome (Galon et al., 2006). Indeed, Tumor-Infiltrating Lymphocytes (TILs) have been linked to a favorable disease outcome in multiple cancer types such as colorectal cancer (Ohtani, 2007) and breast cancer (Mahmoud et al., 2012). For example, it has been shown that the infiltration of tumors by cytotoxic T cells is a positive indicator in breast cancer tumor prognosis (Mahmoud et al., 2012) and especially in triple negative breast cancer (TNBC) (Liu et al., 2012b).

Myeloid immune cells are also implicated in the anti-tumor response (**Figure 6**). Macrophages, eosinophils or neutrophils can destroy tumor cells by phagocytosis or, more indirectly, by activating the T cells response by secretion of cytokines (Carretero et al., 2015; Katano and Torisu, 1982).

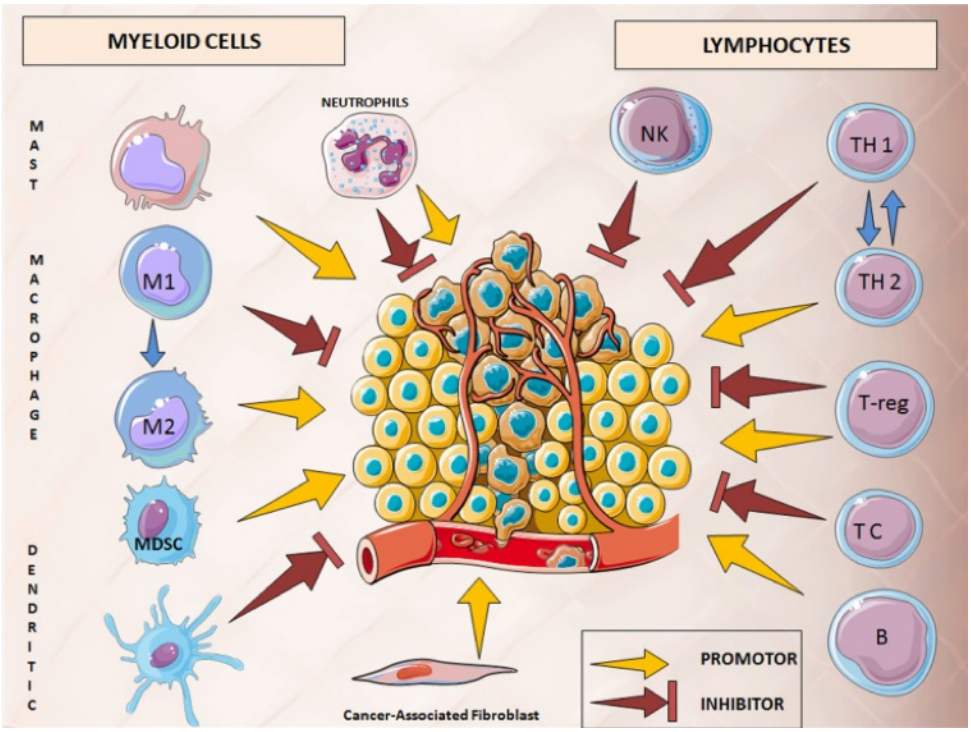

Figure 6: Implication of the immune system in tumor growth.

Cells from both innate and adaptive immune system can act as promotor or inhibitor of tumor growth. From Goubran et al. (2014).

However, during tumor progression the cancer cells manage to evade and subvert the immune system and even to exploit this system in favor of tumor growth. To do so, cancer cells produce cytokines such as Interleukin-10 (IL-10) or Tumor Growth Factor ß (TGFß), which induce the expression of a pro-tumor phenotype by various immune cell systems. A well-known class of these immune cells supporting tumor development is represented by Tumor Associated Macrophages (TAMs). TAMs secrete immunosuppressive cytokines that inhibit the activation of T cells. TAMs also secrete proteases that will remodel the ECM and thereby support tumor progression and invasion.

The dual role of the immune system in cancer progression complicates the understanding of the disease but it also opens therapeutic opportunities.

A new therapeutic strategy against cancer exploiting the immune system is called immunotherapy. This approach is described further below.

1.5. The activation of angiogenesis

Due to the high proliferation rate of cancer cells, the tumor volume increases rapidly. When the tumor reaches a certain critical volume, the supply of oxygen and nutrients through original blood vessels becomes insufficient and endangers the survival of cancer cells. To overcome this problem, cancer cells activate the development of new blood vessels through angiogenesis (**Figure 7**).

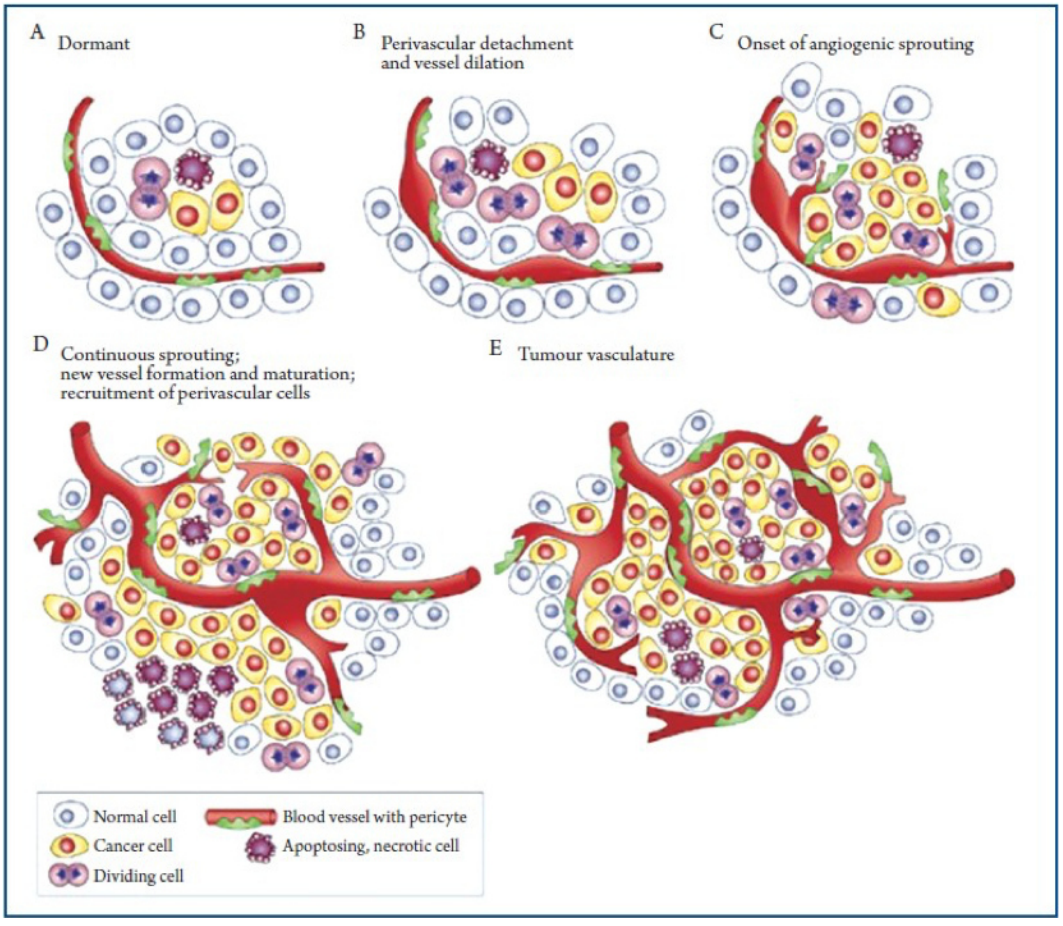

Figure 7: Tumor angiogenesis.

After reaching a critical tumor mass, the surrounding blood vessels aren't sufficient to support further tumor growth. Subsequently, tumor cells recruit perivascular cells and undergo EMT to create new blood vessels, thus developing their own tumor vasculature. From Cherry-Bohannan et al. (2011).

The activation of angiogenesis by cancer cells involves several steps. First of all, the hypoxia status in fast growing tumors inhibits the degradation of the Hypoxia-Induced Factor 1 (HIF1). The increased half-life of this factor leads to the expression of genes involved in angiogenesis, such as the genes encoding proteins of the vascular endothelial growth factor (VEGF) family (VEGFA, VEGFB, VEGFC, VEGFD, VEGFE,) (Fraisl et al., 2009) and Stroma-Derived Factor 1 (SDF-1). While VEGFA induces angiogenesis, SDF-1 attracts pro-angiogenic myeloid cells to the tumor site (Grunewald et al., 2006). At some point, the balance between anti-angiogenic and pro-angiogenic factors switches in favor of the angiogenesis. This critical step is called "angiogenic switch" (Hanahan and Folkman, 1996). Under pressure of pro-angiogenic factors, endothelial cells (ECs) derived from tumor-proximal blood vessels migrate to the tumor to form new vessels. To control EC migration, an EC subtype, called "Tip cell" pilots the other ECs (called "stalk cells") by following the pro-angiogenic factors gradient like JAGGED 1 (JAG1), Delta-Like 1 (DDL1) and Neuropilin-1 (Nrp1). Finally, tumor vessels are formed upon consolidation by pericytes recruited by the Platelet-Derived Growth Factor (PDGF) (Ribatti et al., 2011). Contrary to normal blood vessels, tumor blood vessels are generally leaky with more fenestration between ECs, less tight junctions between ECs and incomplete wrapping by pericytes (Ribatti et al., 2007).

In addition to EC recruitment, the formation of the new blood vessels to support tumor growth is also the consequence of cancer cells insertion in the newly formed vessels (Chang et al., 2000). This phenomenon has been particularly well described for brain tumors in which a subpopulation of cancer cells exhibiting stem cell like phenotypes are undergoing trans-differentiation to do so (Soda et al., 2011). Although still under debate, this feature of cancer stem cells is important in the context of anti-cancer drug design because these cells are largely the cause of tumor relapse. Previous work in the lab of D. Bagnard showed that inhibiting Plexin-A1 in glioblastoma inhibits its growth hence offering interesting therapeutic opportunities (Jacob et al., 2016). The leakage and permeability characteristics of these abnormal vessels facilitate the migration of cancer cells through the blood vasculature and allows the formation of metastases. Tumor-

associated vessel leakage is also the cause of passive drug targeting by penetrating the tumor bulk. It is important in the Enhanced Permeability and Retention (EPR) effect, a critical phenomenon for nanoparticles tumor accumulation *in vivo*.

Consequently, the targeting of the tumor vasculature by nanoparticles is of great interest. For example, it has been shown that gold nanoparticles inhibit angiogenesis and lung metastases development in a mouse model of melanoma (Li et al., 2017). In their study, Li et al., had demonstrated that gold nanoparticles have no effect on cell viability but could decrease endothelial cell migration by the reduction of the metalloproteinase-2 which is known to promote endothelial cells angiogenesis and migration (Ma et al., 2014). Moreover, Li et al., also showed that gold nanoparticles could inhibit the Epithelial-Mesenchymal Transition (EMT) of B16F10 melanoma cells.
In addition to this direct effect of certain types of nanoparticle on tumor vasculature, the nanoparticles offer the possibility to take advantage of the EPR effect to accumulate therapeutic compounds at the tumor site.

1.6. Invasion and metastasis

Cancer cells have the ability to invade surrounding tissues and to migrate to distant sites including new organs. Whereas healthy cells are bound to each other through extracellular matrix (ECM) thus maintaining tissue integrity, cancer cells develop strategies to remove their adhesion to the ECM and to remodel it. The main class of adhesion molecules is the integrin family; consistently, integrins expression is often deregulated in cancer.
Carcinoma-associated fibroblasts (CAF) are activated by cancer cells to produce matrix metalloproteinases (MMPs). These MMPs degrade integrins to decrease ECM stiffness and allowing cancer cells to increase their migratory behavior.
A major phenomenon implicated in the development of pro-invasive behavior of cancer cells is the EMT (**Figure 8**). The EMT is a multistep dynamic process that occurs naturally during embryogenesis. It is involved in gastrulation, tissue morphogenesis (Nieto et al., 1994) and wound healing (Savagner et al., 2005). It leads to the transition of cells

exhibiting an epithelial state (polarized function, localization of E-cadherin at the cell membrane) to a mesenchymal state. Moreover, EMT has been linked to the acquisition of certain stem cell properties (like self-renewal and the ability to differentiate into various cell types) by some cancer cells in some type of carcinoma [e.g mammary carcinoma (Mani et al., 2008)]. However, cancer cells don't undergo the entire transition to a complete mesenchymal state (Nieto et al., 2016). The number of intermediate phenotypes in cancer cells is still under debate and associated with various terms such as partial EMT, intermediate EMT, hybrid epithelial/mesenchymal, semi-mesenchymal or also incomplete EMT (Grigore et al., 2016). Cancer cells exhibiting intermediate EMT phenotypes are expected to show both epithelial (adhesion) and mesenchymal (migration) features.

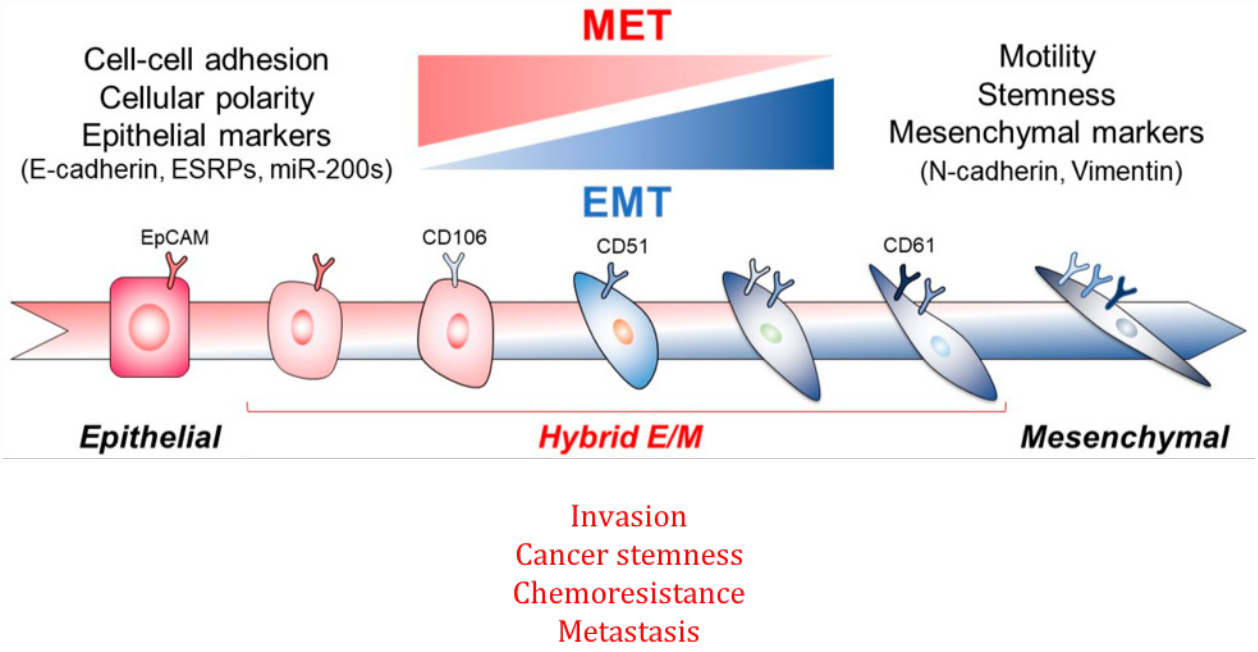

Figure 8: Epithelial-mesenchymal transition.

Under stimulation from the environment, tumor cells undergo EMT and acquire metastasis and invasion ability thus promoting tumor spreading. Adapted from Tsubakihara and Moustakas (2018).

The last decade of research has accumulated evidence linking the EMT to the invasion-metastasis cascade (Lambert et al., 2017), thus leading to the hypothesis that

the EMT program occurs in probably all carcinoma types and is critical in cancer cell dissemination (Guo et al., 2012).

During carcinogenesis, the EMT is activated in cancer cells by EMT-inducing transcription factors (EMT-TFs). The EMT and EMT-TFs are also involved in cancer cell resistance to several chemotherapeutic drugs and kinase inhibitors. For example, EMT-TFs such as SNAI1, SMUG and ZEB1 are involved in resistance to platinum-based chemotherapeutic drugs in various cancer types such as breast cancer (Lim et al., 2013). TGFß induces the EMT by binding to TGFßR1 and TGFßR2 leading to the formation of SMAD1-SMAD5-SMAD4 and SMAD2-SMAD3-SMAD4 complexes. These complexes function as transcription factors for genes implicated in cell invasion, angiogenesis and cell growth among other functions (Xu et al., 2009). TGFß thus induces the expression of important proteins implicated in cell invasion and metastasis, among them, Tenascin-C (TNC) (Saupe et al., 2013). TNC is an extracellular matrix (stroma) protein overexpressed in many cancer types and associated with poor prognosis (Ni et al., 2017; Sundquist et al., 2017). It has been shown that TNC expression is associated with lung metastasis in breast cancer patients (Insua-Rodríguez et al., 2018). Strikingly, TNC is implicated in resistance to chemotherapeutic drugs (Wang et al., 2016). Moreover, as TNC is only poorly expressed in the adult organism (Chiquet-Ehrismann et al., 2014), it constitutes a suitable target for cancer therapy.

Another protein involved in cancer invasion is the Nrp1. Nrp1 is a transmembrane protein expressed in glia cells as well as in some neurons and endothelial cells (Eichmann et al., 2005). It is overexpressed in various types of cancer cells (Bielenberg et al., 2006) and associated with a bad prognosis (Geretti and Klagsbrun, 2007). It has been shown that Nrp1 promotes EMT in oral squamous cell carcinoma (OSCC) (Chu et al., 2014) and several studies targeting Nrp1 demonstrated a decrease in cancer invasion and metastasis in gastric cancer (Peng et al., 2014), melanoma (Bai et al., 2015) and OSCC (Liu et al., 2015). The role of Nrp1 in cancer and its potential as a therapeutic target (Meyer et al., 2016) will be further discussed in the part II of this thesis.

Among the different hallmarks of cancer, the multiplicity of compensatory/redundant signaling pathways is a major hurdle for drug design. Strikingly, the nanoparticle technology offers the possibility to combine different treatments and thus target different pathways simultaneously, thereby reaching towards the Grail of anticancer drugs.

2. Cancer therapeutic strategies

Current cancer treatments include surgery, radiotherapy and chemotherapy. However, during the last century, a number of new approaches to treat cancer have been investigated.

2.1. Classical treatment

2.1.1. Surgery

Whenever possible, tumors are removed by surgical resection. However, the surgical approach has several disadvantages. Due to the infiltrating behavior of cancer cells, it is often necessary to remove tissues at the border of the tumor, possibly including healthy tissues. In the case of tumors attacking major organs such as the liver, lungs or brain, this can lead to important damages decreasing the patient's quality of life (Hatiboglu et al., 2018). Moreover, patient survival after surgery frequently depends on organs transplantation. To limit such problems as much as possible, surgeons need to be able to define the localization of the tumor as precisely as possible. Towards this aim, some new real-time tumor imaging techniques are under development. These new techniques allow the visualization of the tumor with cellular precision during surgery (Chi et al., 2014). However, such technique cannot be applied to tumors involving mobile tumor cells, such as leukemia.

Recently, live imaging using several types of nanoparticles (such as metallic nanoparticles) has led to an improvement in image-guided surgery *in vivo* (Zhu et al., 2017). Indeed, metallic nanoparticles exhibit optic and plasmonic properties which allow

them to be used as imaging agent. Moreover, metallic nanoparticles offer the possibility to be employed as a drug nanocarrier. The development of this type of nanoparticles and their application in cancer therapy will be discussed in the part III of this manuscript.

2.1.2. Radiotherapy

Radiotherapy (also called radiation therapy) is used in cancer treatment since more than a hundred years (Cosset, 2016). Although radiotherapy can be locally applied to cancer cells, healthy adjacent tissues are usually also exposed, thus leading to death of healthy cells (Taylor and Kirby, 2015). This causes numerous side effects usually including sore skin, tiredness, hair loss and vomiting. Additional side effects may occur depending on the treated zone (e.g. diarrhea when radiation is applied to abdominal or pelvic areas) (Lawrie et al., 2018).

Moreover, cancer cells are able to develop a resistance to radiation therapy through several mechanisms such as inhibition of reactive oxygen species (ROS) production, DNA damage repair, and inhibition of apoptotic pathways activated by radiation (Zhao et al., 2018).

Specific protocols to deliver radiation have been developed such as hypofractionated radiation therapy[3]. Two types of these protocols are used, the stereotactic body radiation therapy (SBRT, non-surgical radiation therapy used to treat functional abnormalities and small tumors of the brain) and the stereotactic radiation surgery (SRS, to treat body tumors).

While the induction of DNA damage is a major mechanism explaining the therapeutic effect induced by conventional radiation therapy, hypofractionated radiation therapy is thought to rely also on the modification of the tumor microenvironment (TME) (Arnold et al., 2018).

Indeed, cancer cell death induced by radiation leads to the release of cytokines [i.e Interferon-y (IFN-y)] able to activate the immune system, especially when the hypo-

[3] Radiation protocol applied during a shorter period of time and at higher doses compared to conventional radiation protocol

fractionated radiation protocol is applied. Indeed, several studies have shown that ablative doses of radiation [30 Gray (Gy)] induce a cytotoxic T-cell response through IFN-y release by cancer cells, which leads to a regression of the tumor (Filatenkov et al., 2015). However, the application of fractionated doses after the first large dose reduces the T-cell response. This could be explained by the death of the infiltrating lymphocytes due to the radiation. Thus, conventional radiation schedules may exert a negative effect on TME. To address this issue, the use of agents that block immunosuppressive signals has been investigated in combination with conventional radiation therapy. For example, treatment with a monoclonal antibody against the programmed cell death 1 protein (PD-1) in combination with fractionated radiation (5 x 2 Gy) in a dual-tumor mouse model led to a regression of both the irradiated tumor and distal tumors (termed abscopal effect) and this effect was correlated with the activation of a T-cell response (Dovedi et al., 2017).

In addition to these effects on the immune system, radiation therapy has also an effect on the tumor vasculature (Song et al., 1974). Large doses (higher than 10 Gy per fraction) induce major damage to the tumor vasculature leading indirectly to the death of cancer cells (Park et al., 2012). Single low doses, in contrast, induce a transient increase in tumor blood flow (Wong et al., 1973). Moreover, it has been demonstrated that endothelial cells survive at a 2 Gy dose of radiation (Kuwahara et al., 2014). Consistently, low doses of radiation (< 5 Gy) are linked to a promotion, rather than inhibition, of tumor angiogenesis and neovascularization. Moreover, *in vitro* studies have shown that low dose radiation causes a stimulation of VEGF production by stroma cells and phosphorylation of VEGFR2 (Vala et al., 2010). Thus, therapeutic strategies combining radiation and anti-angiogenic treatments have been investigated. For example, the blockade of VEGF signaling using antibodies in animal models has been shown to potentiate radiation effect (Truman et al., 2010). Moreover, as aforementioned, cancer cells can develop a resistance against radiation therapy. In order to overcome this issue, efforts have been made to develop radiosensitizers. Particularly, gold nanoparticles have

been greatly investigated because they own a good ability to sensitize cancer cells towards irradiation (Her et al., 2017).

2.1.3. Chemotherapy

Chemotherapy relies on the use of chemical drugs presenting a cytotoxic activity. Some chemotherapeutic drugs target microtubules. Paclitaxel, for example, is a drug from the taxane family, which binds to the end of polymerized β-tubulin. This causes the stabilization of the microtubules, which leads to the inhibition of cell division and to cell death.
The anthracyclin family is a class of antibiotics widely employed in cancer treatment as chemotherapeutic drugs. The main representative of this family is doxorubicin (DOX), which intercalates into DNA, thereby inhibits DNA synthesis, and cell division. Other chemotherapeutic drugs act as DNA damaging agents. One of these agents is Temozolomide, which is used in glioblastoma. The family of platinum anticancer agents, which includes cisplatin as the major representative, acts by crosslinking DNA, which inhibits DNA repair and synthesis.

Another class of chemotherapeutic drugs consist of topoisomerase I and II inhibitors. Topoisomerases are enzymes regulating DNA supercoiling by cleaving the DNA backbone. Thus, they play a critical role for DNA replication and repair. Their inhibition blocks the replication and repair of DNA in cells. Topoisomerase I inhibitors include irinotecan and camptothecin and topoisomerase II inhibitors include ectoposide and teniposide. It is known that also anthracyclin drugs exhibit topoisomerase II inhibition activity.

While clearly efficient on some tumor types, chemotherapies or combinations of chemotherapeutics show numerous side effects due to their lack of specific delivery and tumor targeting ability. For example, DOX is well known to produce cardiotoxicity.
Several alternative approaches have been developed with aim to circumvent these drawbacks. For examples, nanoparticles derived from a plant virus, Johnson grass

chlorotic stripe mosaic virus, have been used as a drug carrier to deliver DOX in a mouse model of TNBC (Alemzadeh et al., 2018). DOX was loaded inside the icosahedral nanoparticles, which were decorated with folic acid for targeting to cancer cells (FA-DOX-JgCSMV). The results show that the FA-DOX-JgCSMV particles were able to reduce tumor growth to the same extent as free DOX. Other carriers used for DOX delivery to tumors include cupper nanocubes (Li et al., 2019), co-polymer nanoparticles (Xu et al., 2018) and other virus-like nanoparticles (Finbloom et al., 2018). These different types of carriers are currently under further investigation and have the potential to increase the therapeutic effect of DOX.

2.2. Gene therapy

As mentioned above, cancer cells exhibit genomic alterations leading to an overexpression of genes promoting cell survival, proliferation, migration, avoidance of the immune system, and down regulation of genes controlling cell proliferation and invasion. One therapeutic strategy aims to re-establish a normal expression of these deregulated genes by strategies employing the expression of specific small interfering RNAs (siRNAs), short hairpin RNAs (shRNAs), microRNAs (miRNAs), or plasmid DNA (pDNA). miRNA are small non-coding RNA molecules (containing about 22 nucleotides) involved in post-transcriptional regulation of gene expression via base-pairing with complementary sequences within mRNA molecules. miRNA can act as a tumor suppressor genes or oncogenes. One important miRNA is miR-21, which regulates tumor suppressor genes, particularly PTEN. The expression of miR-21 is induced in several tumor types including glioblastoma, where it was discovered (Chan et al., 2005). miR.21 is overexpressed also in breast cancer and other tumor types (Volinia et al., 2006). miR-21 expression has been linked to the promotion of cancer cell proliferation, metastasis, and the inhibition of apoptosis (Pfeffer et al., 2015). Its overexpression was also linked to multi-drug resistance (Geretto et al., 2017) and radiation resistance in esophageal squamous cell carcinoma (Li et al., 2018a). Consequently, therapeutic strategies aim at the inhibition of miR-21. In a recent study, authors showed that renal carcinoma cells transfected with an anti-miR-21 oligonucleotides exhibited reduced invasive behavior

and an increase in their chemosensitivity to paclitaxel and oxaliplatin (Gaudelot et al., 2017).

shRNA are short oligonucleotide sequences that can loop back on themselves and form a stretch of dsRNA that is cleaved by Dicer. In biotechnology, shRNAs are delivered to the cells via an expression vector for transcription in the nucleus. The resulting pre-mature shRNA is processed in the cytoplasm by Dicer and the resulting siRNA (short oligonucleotide sequence which is synthetically produced or processed from a stretch shRNA by the Dicer enzyme present in the target cells) is integrated into an RNA-induced silencing complex (RISC) that uses the siRNA as a guide for the sequence-specific cleavage or translational repression of target mRNA.

Delivery of genetic material to cancer cells relies on vectors which can be non-viral or viral. Non-viral vectors are synthetically produced chemical molecules such as lipofectamine or FuGene. Plasmid DNA or siRNAs are encapsulated or bound to these vectors (Chira et al., 2015). Non-viral vectors are easy to produce and rarely the cause of an inflammatory reaction (Kaminski et al., 2002). Viral vectors are mainly derived from mammalian viruses, however there is an emerging interest in the development of bacteriophages and plant viruses as vectors (Lam and Steinmetz, 2018). These vectors and their employment as delivery system are explained in part III of this manuscript.

Several nanoparticle types have been used to deliver genetic material (Xiao et al., 2019). For example, graphene oxide has been employed to deliver a siRNA targeting survivin, a protein inhibiting the apoptosis in cancer cells (Wang et al., 2018). The authors showed that the siRNA was able to inhibit tumor growth *in vivo*. In another study, authors used lipoprotein nanoparticles to co-deliver DOX and miR-21 inhibitor to MCF-7 breast cancer cells resistant to DOX (Rui et al., 2017). They showed that this formulation was able to reverse drug resistance of cancer cells and had a synergistic antiproliferative effect *in vivo*.

2.3. Immunotherapy

A promising approach is to modulate the immune system, which is often deregulated in cancer disease. For example, as already mentioned, cancer cells secrete factors recruiting immune cells to promote changes in the microenvironment which are favorable to tumor development.

2.3.1. Vaccines for cancer treatment

The idea behind cancer vaccine development is to educate the immune system to target cancer cells. To this end, different strategies are employed, a) injection of whole tumor lysate into the bloodstream, b) dendritic cell vaccines, c) presentation of Tumor Associated Antigens (TAA), and d) the use of DNA-vaccines.

Dendritic cells (DCs) are Antigen Presenting Cells (APC). Vaccine-type dendritic cells are developed from blood isolated from the given patient followed by education of the immune system cells in this blood with antigens from tumor cells *in vitro*. This education induces the differentiation of the immune cells into DCs that are able to present the tumor antigens to other immune cells when injected back to the patient. In 2010, the Food and Drug Administration (FDA) approved the first therapeutic DC vaccine, which was named sipuleucel-T (Provenge®) and has been developed for the treatment of metastatic prostate cancer (Kantoff et al., 2010).

Although the normal immune system acts against cancer cells, its activity is reduced overtime if the stimulation by tumor antigens is insufficient. To circumvent this problem, DNA-vectors are employed as DNA vaccines that deliver bits of DNA coding for tumor-associated antigens (TAA) into cells. The transfected cells that produce the specific antigens are then capable of maintaining the cancer-controlling state of the immune system. Usually, adjuvants are required to support the recognition of the TAA by the immune system (Banday et al., 2015). Alternative approaches aim at methods to increase the specific TAA delivery to cancers. In this regard, several nanocarriers have

been studied as TAA carriers including gold nanoparticles (Mocan et al., 2015), liposomes (Thomann et al., 2011), and virus-like nanoparticles (Yin et al., 2012). Such nanocarriers offer the possibility to load large quantities of TAA and to ensure their sustained release, thus increasing the uptake of antigens by DCs leading to a sustained T cells activation (Prasad et al., 2011). Moreover, it is possible to load the nanocarriers with TAAs in combinations with adjuvants (Hamdy et al., 2011).

2.3.2. Immune checkpoint inhibitors (ICIs)

Normal cells carry specific immune checkpoints, molecules that are recognized by T cells and able to keep T cells in an inactivate state in order to prevent the immune system from attacking healthy cells. Some cancer cells exploit this checkpoint to avoid the recognition by T cells. For example, the programmed death-ligand 1 (PD-L1) is expressed on some cancer cell types and interacts with its receptor PD-1 expressed on T cells. To interfere with this checkpoint interaction, certain immune checkpoint inhibitors (ICIs) are being developed. One of these agents called pembrolizumab consists of antibodies that specifically target PD-1 and has been approved for treatment of several cancer types including metastatic or non-operable melanoma, head and neck cancer squamous cell carcinoma and cervical cancer (Larkins et al., 2017; Pai-Scherf et al., 2017). Due to their ability to block immune cell inactivation, the application of ICIs can lead to auto-immune responses with numerous side effects (Spain et al., 2016).

2.3.3. Chimeric antigen receptor (CAR)-expressing T cells (CAR-T cells)

A chimeric antigen receptor (CAR) is a genetically engineered chimeric receptor in which a part of a specific monoclonal antibody is combined with a signaling domain (Wilkins et al., 2017). To form CAR-T cells, T cells are extracted from the blood of the patient and then engineered to express CARs on their surface. The monoclonal antibody used to create each CAR determines its target. The second generation of CARs adds the

expression of co-stimulatory domain of receptor and the third generation includes an additional co-stimulatory domain to enhance T cell activation (**Figure 9**).

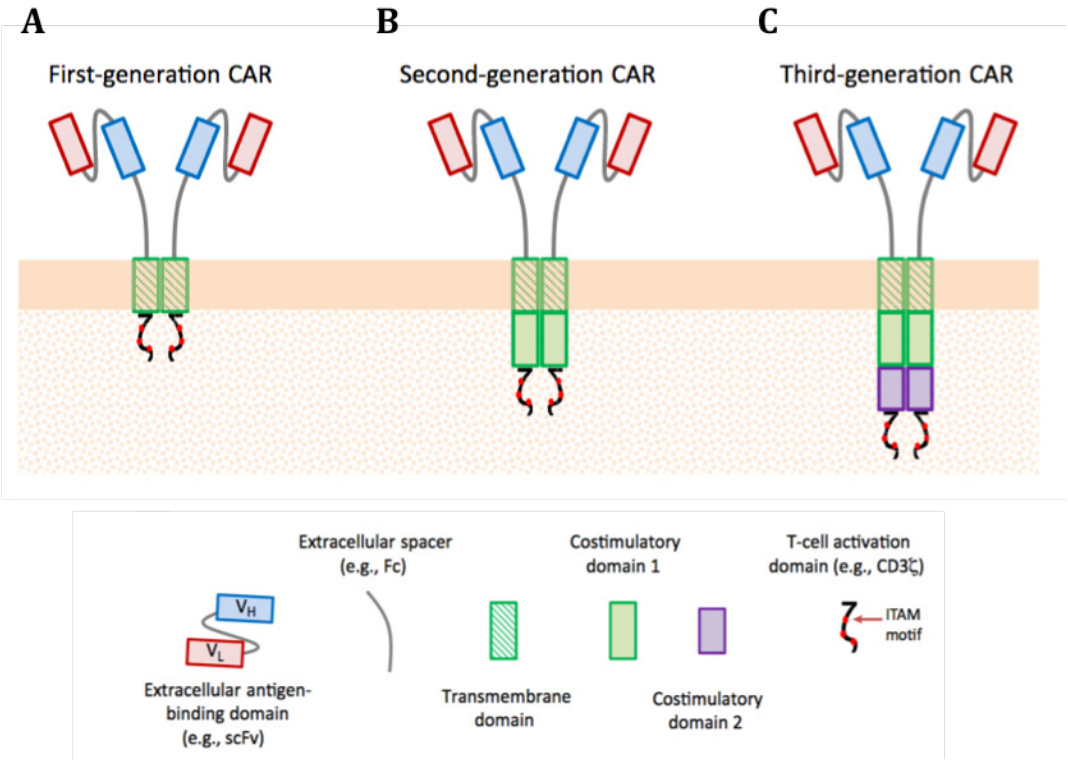

Figure 9: Successive generations of CARs.

(A) First generation of CARs associating antigen-binding domain with T-cell activation domain. (B) Second generation of CARs adds a costimulatory domain. (C) Third generation of CARs added a second costimulatory domain. From Chang and Chen (2017).

In 2017, the FDA approved the application of CAR-expressing T cells in advanced lymphoma for adults and acute lymphocytic leukemia for children (Liu et al., 2017). However, this approach requires further improvement before application to solid tumors. Indeed, the microenvironment of solid tumors exhibits several physical barriers that prevent infiltration by T cells. Moreover, immunosuppressive molecules are often expressed in high concentration within the tumor. To overcome these issues, one strategy aims to increase the cancer targeting ability of CAR-T cells. For example, CAR-T cells can be designed to target not only the cancer cells but also the tumor

microenvironment *e.g.* specific CARs T cells targeting VEGFR2 and thus, the tumor vasculature (Chinnasamy et al., 2010). This promising approach undergoes phase 1/2 clinical trials in liver cancer.

As described above, some cancer cells express PD-L1 to inhibit T cells activation. This mechanism of resistance is also effective against CAR-T cells (Tumeh et al., 2014). Therefore, CAR-expressing T cells have been engineered to secrete anti-PD-L1 antibodies thus restoring the function of these cells, at least *in vitro* (Suarez et al., 2016).

Interestingly, it is possible to couple the surface of CARs T cells to nanoparticles without impacting their function (Stephan et al., 2010). This opens the possibility to increase the specific delivery of therapeutic drugs loaded into nanoparticles using CARs T cells. The loaded therapeutic drug can be chosen to improve CARs T cells efficiency e.g. inhibiting immunosuppressive molecules (Siriwon et al., 2018).

Moreover, there is a new application area for nanoparticles targeting and remodeling the TME to increase immunotherapy (Gao et al., 2019). They have been used to target immunosuppressive enzymes (Zhu et al., 2012), the cytokines, the tumor extracellular matrix, and TAMs. This strategy aims to reverse the immunosuppressive environment instituted by the tumor in order to allow immunotherapeutic drugs to reach their targets.

2.4. Hormone therapy

Some cancers such as prostate cancer or Estrogen Receptor (ER) positive breast cancer, can be treated by hormone therapy (HT). HT is employed as neoadjuvant (treatment given before primary treatment which usually is surgery) or adjuvant therapy (treatment given after primary treatment). Prostate cancer cell growth is usually stimulated by androgens and, because androgens are mostly produced by testicles, one type of HT employed to treat prostate cancer consists of removing testicles by either surgery (orchiectomy) or by chemical castration using luteinizing hormone-releasing hormone agonists (Triptorelin, Leuprolide). ER positive breast cancer cells are stimulated by estrogen. Thus, HT in this case consists of approaches to reduce estrogen production or to inhibit estrogen binding to their receptor on cancer cells. Aromatase

inhibitors (AI) are used in postmenopausal women to block the production of estrogen from androgen by the aromatase enzymes. There are three AI used for treatment of breast cancer, letrozole (Femara), anastrozole (Arimidex) and exemestane (Aromasin). Interestingly, a recent study shows that premenopausal women could benefit from AI if their ovarian functions are suppressed (SOFT, Suppression of Ovarian Function Study published in 2015). For premenopausal women, rather a Selective Estrogen Receptor Modulator (SERM) is used. The SERM binds to ER thus inhibiting estrogen signaling and also cancer growth. The major SERM prescribed to treat breast cancer in premenopausal women is tamoxifen (Nolvadex in pill form and Soltamox in liquid form). The side effects of SERMs includes headache, weakness, blood clots and stroke.

However, another type of breast cancer characterized as 'triple negative breast cancer' (TNBC) is resistant to HT as it does not express ER, HER2 or progesterone receptor (PR), and this type of cancer represents 16% of all breast cancer types (Shah et al., 2012). This breast cancer is associated with a poor prognosis due to a high rate of relapse and a fast progression after relapse. The classical treatment protocol for TNBC involves neoadjuvant chemotherapy based on paclitaxel (Giordano et al., 2018). 15% of TNBC patients carry mutations in either the BRCA1 gene or the BRCA2 gene. These genes are tumor suppressor genes, both coding for proteins with DNA repair function. The BRCA1 mutation has been linked to a complete response (i.e tumor regression) when the patients were treated with cisplatin as a single-agent in a neoadjuvant protocol (Byrski et al., 2014).

Considering that TNBC patients lack a specific target for therapy, others strategies have been developed. For example, inhibitors targeting poly ADP ribose polymerase (PARP) like veliparib have shown positive results in clinical trials (Rugo et al., 2016).

However, TNBCs exhibit a high stromal and intratumoral level of TILs compared to other breast cancer types (García-Teijido et al., 2016) and high level of TILs is linked to a better clinical outcome for breast cancer patient (Denkert et al., 2010). TILs are also a prognostic factor and are correlated to an increased metastasis-free survival (Kreike et al., 2007), a decreased distant recurrence (Adams et al., 2014) and an improved overall survival (Adams et al., 2014). This important implication of the immune system in the

clinical outcome of TNBC has led to the employment of immunotherapeutic approaches. For example, pembrolizumab and atezolizumab (antibodies targeting PD-1 and PD-L1) are under investigation in both neoadjuvant and adjuvant settings.

2.5. Hyperthermia therapy

Hyperthermia therapy consists in the application of increased temperature (usually between 40°C and 45°C) to the whole or part of the body in order to kill cancer cells or to sensitize them to chemotherapy. Temperatures above 45°C are employed for thermal ablation. The main challenge encountered in this therapeutic approach is the destruction of cancer cells without damaging the healthy tissues. One strategy to achieve this goal consists in the use of metallic nanoparticles which can be excited by a magnetic field thus inducing an increased temperature of the particles. The coating of these nanoparticles with cancer cell targeting moieties allows the application for a more localized hyperthermia treatment. For example, ferric oxide nanoparticles carrying antibodies targeting the HER2 receptor accumulated at HER2 positive cells and caused cell death by hyperthermia upon application of a magnetic field *in vitro* (Zhang et al., 2011a).

Hyperthermia can support the efficiency of chemotherapeutic drugs by causing an elevation of tumor blood flow and vascular tumor permeability (Song et al., 2005). Interestingly, such synergistic effects between hyperthermia therapy and drug treatment can vary. For example, while hyperthermia therapy can have a synergistic with cisplatin there is no such affect if applied together with DOX (Lepock, 2005).

2.6. Photodynamic therapy (PDT)

The use of light as a therapeutic agent goes back to the ancient Greece, India and Egypt (Daniell and Hill, 1991) but was forgotten until the middle of 19th century. In 1903, Niels Finsen, a Danish physician, won the Nobel prize for the use of light to treat lupus vulgaris. However, this type of phototherapy wasn't dynamic and didn't introduce the use of a photosensitizer (PS). The first discovery of a photosensitizing agent was done by Prime, a French neurologist, who administrated eosin orally to his patient to treat

epilepsy and noticed that lesions appeared on skin areas exposed to light (Prime, 1900). In modern photodynamic therapy, a PS is activated in the presence of oxygen and under specific light (usually a laser) condition (**Figure 10**). The wavelength used depends on the PS, with a longer wavelength allowing a deeper tissue penetration. Generally, the wavelength used in clinics are around 630 nm. The change of the PS state from inactivated to activated induces a production of reactive oxygen species (ROS) and other radicals thus leading to cell death by apoptosis or necrosis. PSs differ with respect to chemical structure, excitation wavelength, and efficiency to produce ROS. The first PS authorized for treatment was the 'porfimer sodium' (Photofrin®), which is composed of porphyrin derivatives oligomers that can be excited at 630 nm. It is used in the treatment of esophagus cancer since 1995 and for the treatment of non-small cell lung (NSCL) carcinoma since 1998. The three main families of PS are based on porphyrin, chlorin and the dyes (e.g 5-aminolevulinic acid, silicon phthalocyanine 4) (Ormond and Freeman, 2013).

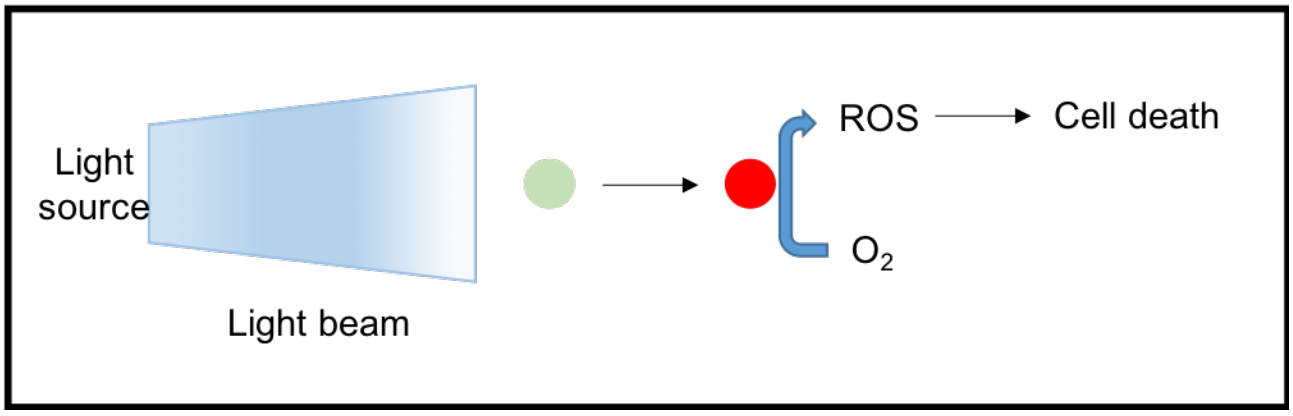

Figure 10: Mechanism of photodynamic therapy.

A light source generates a light beam that excites a photosensitizer. The excited photosensitizer transfers electrons to oxygen, thus creating ROS. These ROS damages tumor cell DNA leading to cell death.

As with many other treatments, also PS compounds can accumulate and cause damage in healthy organs (Mironov et al., 1992). Moreover, the requirement of light penetration reduces their therapeutic potential to tumor localized near the surface of tissues (Spikes, 1990). To overcome these limitations a new generation of PS compounds is under

investigation. Indeed, like other drugs, PS can also be conjugated to a targeting moiety to increase their accumulation at the tumor site. For example, a chlorin PS conjugated to a peptide targeting Nrp1 exhibited a fast accumulation at the tumor site within a mouse glioma model (Thomas et al., 2008).

Targeted delivery of PS compounds can also be achieved by combining them with cancer targeting agents on nanoparticles as a delivery platform (Lucky et al., 2015). Silica nanoplatform exhibiting Nrp1 targeting peptide on the surface and loaded with gadolinium for Magnetic resonance imaging (MRI) as well as chlorin for interstitial PDT (iPDT) was used for glioma treatment (Bechet et al., 2015). In this study, the authors used nanoparticles for MRI-guided implantation of an optic fiber for iPDT. In two different models of glioma tumor, nanoparticles loaded with gadolinium (with or without Nrp1 targeting peptide) were able to enhance the positive contrast in MRI enough to guide an optic fiber implantation for iPDT. Cerebral perfusion MRI was performed before and after iPDT to visualize modification in tumor perfusion after treatment. In both tumor type, a decrease in tumor perfusion was observed and even with nanoparticles not carrying Nrp1 targeting peptide. However, the perfusion was decreased up to 80% only in animals treated with nanoparticles carrying the peptide. Histological examination of brain tissue removed immediately after iPDT showed the presence of oedema and vascular disruption. Moreover, VEGF protein level was reduced after iPDT. These different results demonstrate the photodynamic activity *in vivo* induced by these functionalized nanoparticles.

In addition, two different types of polymer-lipid-PEG (polyethylene glycol) nanoparticles used as carriers of PS increased cellular uptake and caused stronger photocytotoxic activity as compared to the application of free PS (Pramual et al., 2017).

Unlike PDT, which is activated in the presence of oxygen and by specific light, photothermal therapy (PTT) depends on electromagnetic radiation, usually in the near infrared wavelength, to provoke an increase in temperature in the target tissue.

2.7. Ultrasound therapy

Over the last decade, ultrasound (US) had gained interest in the cancer drug delivery field. Originally used to image tumors using microbubbles (MBs) as contrasting agent, US can be used for targeted delivery of chemotherapeutic drugs by destructing microbubbles loaded with compounds. Micro- or nanobubbles are made of proteins (e.g albumin, lysozyme, avidine), surfactants (e.g TWEEN-40), polymer {e.g poly(D,L-lactic-co-glycolide)} or lipids (Sirsi and Borden, 2009). They can be coated or loaded with imaging agents, chemotherapeutic drugs (Fan et al., 2016), genetic materials (e.g siRNA, plasmid gene), or targeting peptides. Upon accumulation in the tumor through targeting moiety coating, the bubbles are destroyed with US, thus leading to a burst of drug release in the desired area.

More recently, nanobubbles (300-700 nm diameter) have been developed. Their reduced size allows them to more easily penetrate the leaky tumor vasculature and to enter into the tumor tissue.

High-intensity focused US is used for thermal tumor ablation (Alkins and Mainprize, 2018) while low-intensity focused US is employed for the release of drugs from phase-changeable nanoparticles (Cao et al., 2018).

2.7.1. Sonodynamic therapy (SDT)

SDT relies on the interaction between US and a chemical agent, called sonosensitizer. This therapy was inspired by PDT and begun to develop in 1980s. Indeed, some PS already used in PDT like porphyrin-based molecules have been proven to produce ROS when exposed to US (Kessel et al., 1994). US applied to a tumor area creates a phenomenon called “cavitation”, which forms water vapor bubbles in the milieu. The oscillating state of these bubbles induces high temperature and the formation of ·OH and ·H radicals as well as collapsing bubbles. Collapsing bubbles then interact with sonosensitizers leading to the creation of ROS, and the ROS, in turn, lead to cell death by apoptosis (**Figure 11**).

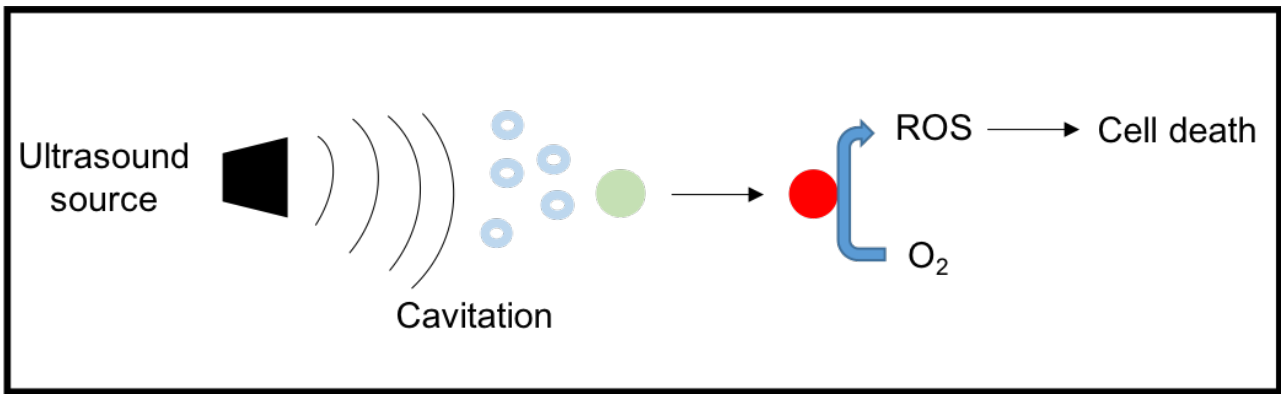

Figure 11: Mechanism of sonodynamic therapy.

An ultrasound source generates cavitation in the medium thus creating oscillating bubbles. These bubbles react with the sonosensitizer and cause its excitation. The excited sonosensitizer then creates ROS that damage cell DNA leading to cell death.

It has been hypothesized that another mechanism of action of SDT implies US creating light (a phenomenon known as sonoluminescence) thus leading to the activation of photosensitizer. Similar as in the in case of PDT, a major improvement in therapeutic potential can be expected from approaches that improve the specific delivery of sonosensitizer to the tumor site.

2.8. Targeted therapies

2.8.1. Use of small molecules inhibitors

As previously mentioned, both the RAS-RAF-MEK pathway and the PI3K/Akt/mTOR (mammalian target of rapamycin) pathway (Cantley, 2002) are upregulated in many cancer types. To inhibit these pathways, small molecule inhibitors have been developed (**Table 1**) (Tsimberidou, 2015). The activities of these molecules are often related to kinase inhibition, classifying most of these drugs within the protein kinase inhibitor (PKI) family (Roskoski, 2018). For example, the BRAF gene, which encodes BRAF kinase, is often upregulated in cancers such as melanoma cancer (Brose et al., 2002) and, therefore, its protein is the target of several inhibitors like dabrafenib (Tafinlar) (Long et al., 2012) and vemurafenib (Zelboraf) (Rochet et al., 2011).

Pathway/Target	FDA-Approved Drugs	Investigational Agents
RAS-RAF-MEK Pathway		
BRAF	Dabrafenib (Tafinlar)	Encorafenib (LGX818)
	Vemurafenib (Zelboraf)	GDC-0879
		PLX-4720
MEK	Trametinib (Mekinist)	Cobimetinib (GDC-0973)
		Selumetinib (AZD6244)
RAS		Tipifarnib
		Lonafarnib
PI3K/AKT/mTOR Pathway		
mTOR	Everolimus (Afinitor)	MLN0128
	Temsirolimus (Torisel)	JNK128
		AZD8055
		Ridaforolimus
PI3K		BKM120
		Copanlisib (BAY 80-6946)
		XL-147
		GDC-0032 (Taselisib)
		INK1117
		BYL719
		GDC-0941
PI3K and mTOR		BEZ235
		XL-765
		BGT-226
		GDC-0980
		PF4691502
AKT		MK2206
		GSK2141795
		BAY1125976
		GDC-0068

Table 1: Inhibitors of RAS-RAF-MEK pathway and PI3K/Akt/mTOR pathway.

Adapted from Tsimberidou (2015).

As previously described, EGFR family members are implicated in cancer growth. These proteins are targeted by kinase inhibitors. Erlotinib (Tarceva) targets the ATP binding site of EGFR and has been FDA-approved for metastatic non-small cell lung cancer and metastatic pancreatic cancer. Lapatinib (Tykerb) is a tyrosine kinase inhibitor of HER1 and HER2 that has been approved by the FDA for the treatment of advanced or metastatic breast cancer overexpressing HER2 in combination with capecitabine (Xeloda™) a chemotherapeutic agent inhibiting DNA synthesis (Medina and Goodin, 2008).

Although these inhibitors have shown efficiency in reducing tumor growth and in increasing patient survival, they also provoke many side effects, including severe cardiotoxicities (Chaar et al., 2018).

2.8.1. Targeting cancer cells with monoclonal antibodies

Another strategy to target receptors or ligands involved in cancer development consists in the employment of monoclonal antibodies (mAb) targeting specifically proteins overexpressed by cancer cells or by the TME (**Table 2**).

The main representative of monoclonal antibodies is bevacizumab (Avastin), which binds to the VEGF ligand and thereby interferes with its binding to VEGFR2 receptor, which inhibits angiogenesis usually induced by VEGFR2 activation.

As previously described, monoclonal antibodies can be used to target immune checkpoint inhibitors such as PD-1/PD-L1. Although pembrolizumab is the main representative of this category of monoclonal antibodies, other antibodies have been investigated to target ICI.

The employment of cetuximab, a monoclonal antibody targeting EGFR, in colorectal cancer in association with oxaliplatin-based chemotherapy increased patient overall survival but also caused complications due to the chemotherapy, which potentiates the side effects of cetuximab (Wen and Li, 2016). Other mAb are used to target the HER2 receptor, another member of the EGFR family, which is expressed in 20% of the breast cancer cases. Before the development of anti-HER2 therapies, HER2-positive breast cancer had a poor prognosis due to a high mortality rate at early stage of the disease and

elevated incidence of metastases (Slamon et al., 1987). Thus, an important number of therapeutic agents have been developed to target the HER2 receptor and its pathway (Ahmed et al., 2015). For example, a mAb called Trastuzumab (Herceptin®) is used in adjuvant therapy at early stages of breast cancer associated with HER2 overexpression. Trastuzumab targets the extracellular domain of HER2 receptor and, thus, inhibits its signaling. Moreover, Trastuzumab also inhibits HER2/HER3 dimerization in a ligand-independent manner, thus leading to an antiproliferative effect (Junttila et al., 2009). However, because Trastuzumab is unable to cross the blood-brain barrier, it is inefficient for the treatment of brain metastases.

Target	FDA-Approved Drugs
EGFR	Cetuximab (Erbitux)
	Panitumumab (Vectibix)
HER2	Pertuzumab (Perjeta)
	Trastuzumab (Herceptin)
VEGF ligand	Bevacizumab (Avastin)

Table 2: Monoclonal antibodies employed in cancer therapy.

Adapted from Tsimberidou (2015).

Some other receptors implicated in tumor growth are known to lack a signaling pathway and need to dimerize with other receptors to induce their biological effect. Thus, for this type of receptor it is important to block their dimerization.

All of these therapeutic approaches have demonstrated their potential in the treatment of cancer. However, due to the complexity of the cancer disease, it appears that an effective cancer treatment should combine different approaches while attempting to reduce side effects. In this aim, the use of nanoparticles exhibits suitable qualities.

II. Neuropilin-1

1. Neuropilin-1

The Nrp1 is a glycoprotein of 130 kDa that acts as a receptor for ligands belonging to different families such as VEGF-165 (Soker et al., 1998) or semaphorin 3A (He and Tessier-Lavigne, 1997). The receptor is composed of an extracellular domain formed by 840 amino acids (aa), a transmembrane domain of 25 aa, and an intracellular domain of 40 aa (**Figure 12**).

The extracellular domain of Nrp1 contains three sub-domains. The domain A, at the N-terminal extremity, is further structured in two sub-domains, a1 and a2. Similarly, also the sub-domain B is structured in two sub-domains domains, b1 and b2. Finally, the C sub-domain (also referred to as 'MAM' for meprin/A5/μ-phosphatase) is juxta-membraneous (Yelland and Djordjevic, 2016).
Members of the VEGF ligand family bind to the B domain of the Nrp1 (Nakamura et al., 1998), whereas Semaphorin ligands bind to the A domain through their N-terminal domain and also to the B domain through their C-terminal domain. Thus, Sema3A and VEGF-165 compete for binding to the Nrp1 B domain.
Contrary to the A and B domains, the C part contains no binding sites for ligands. However, several studies have shown that this part is important for receptor dimerization (Renzi et al., 1999).

As already mentioned, the transmembrane domain of Nrp1 consists of 25 aa. The laboratory of D. Bagnard demonstrated the critical role of this domain in the dimerization of the Nrp1 and, especially, the importance of the GxxxGxxxG motif within this domain (Roth et al., 2008).

The intracellular domain of Nrp1 does not carry any binding site or signaling motif and is not required for signal transduction (Chen et al., 1997).

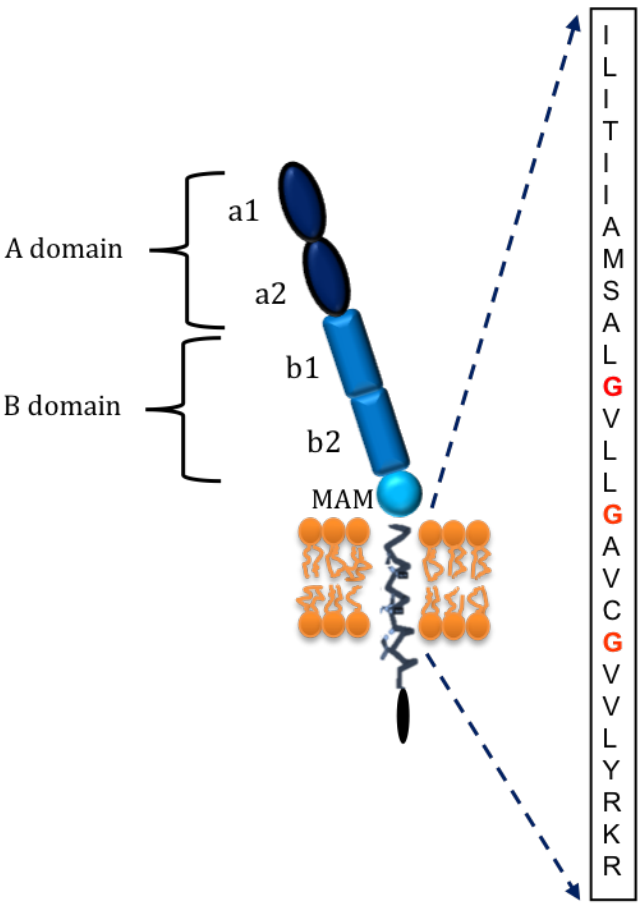

Figure 12: Structure of the Nrp1.

The extracellular part is composed of three domains, the A domain, B domain and MAM domain. The transmembrane domain contains the canonical GxxxGxxxG motif responsible for the dimerization and targeting by MTP-Nrp1.

Although the Nrp1 lacks a signaling domain on its intracellular part, it can still transduce its signal through dimerization with specific co-receptors (**Figure 13**).

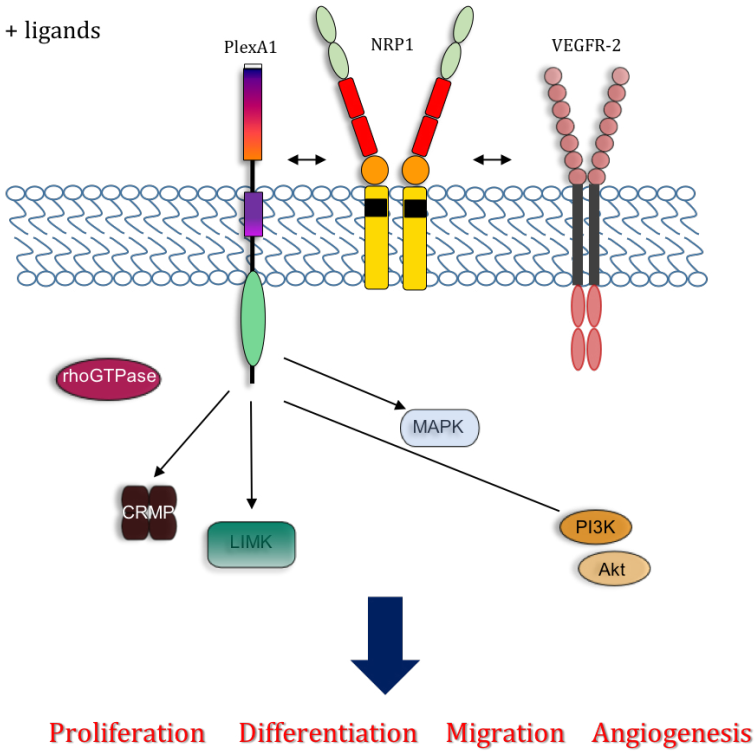

Figure 13: The Nrp1 signaling platform.

In presence of its ligand, Nrp1 dimerizes through its transmembrane domain with its partner receptors PlexinA1 and VEGFR2. These receptors induce specific biological effects through their respective signaling pathways.

The main co-receptors of Nrp1 are members of the plexin family. The plexins are transmembrane receptors of 240 kDa belonging to four classes, A to D (Tamagnone et al., 1999). The class A plexins include four members (PlexinA1 to PlexinA4), the class B plexins count three members (PlexinB1 to PlexinB3), and the class C and D plexins each have only one member (PlexinC1 and PlexinD1) each.

Another well-known partner of Nrp1 is VEGF receptor 2 (VEGFR2). It has been demonstrated that the binding of VEGF-165 to VEGFR2 is enhanced in the presence of Nrp1 (Fuh et al., 2000). Another study showed that VEGF-165 can bind both Nrp1 and VEGFR2 with distinct binding sites and thus supports the formation of the VEGFR2/Nrp1 complex (Soker et al., 2002). The Nrp1 also plays a role in epidermal growth factor receptor (EGFR)-mediated signaling (Rizzolio et al., 2012).

2. The role of the Neuropilin-1 in cancer

The Nrp1 is overexpressed in several tumor types including breast cancer and glioblastoma (Jubb et al., 2012; Meyer et al., 2016) and this overexpression has been linked to a bad prognosis for the patient (Geretti and Klagsbrun, 2007). It has been emphasized that Nrp1 is expressed in specific cell types supporting tumor growth, such as M2 macrophages (Caponegro et al., 2018). Genetic ablation of Nrp1 expression on microglia cells and macrophages in a glioma mouse model reduced tumor growth, thus supporting an important role of Nrp1 in tumor development (Miyauchi et al., 2016). Nrp1 was shown to be expressed also in dendritic cells and T cell subpopulations. Moreover, the formation of the Nrp1/VEGFR2 complex between tumor cells and endothelial cells is a predictive indicator for pancreatic cancer patient survival (Morin et al., 2018). Indeed, a high concentration of this complex is correlated with a poor chance of survival.

Nrp1 can also play a role in acquired drug resistance (**Figure 14**). Nrp1 expression is upregulated in melanoma cells treated with BRAF inhibitors as well as in breast cancer cells treated with HER2 targeted drugs (Rizzolio et al., 2018). This upregulation leads to the activation of JNK pathway which leads to the activation of EGFR or insulin growth factor 1 (IGFR1). The activation of these alternative proliferation pathways counteracts the inhibition of HER2 and promotes tumor cells proliferation.

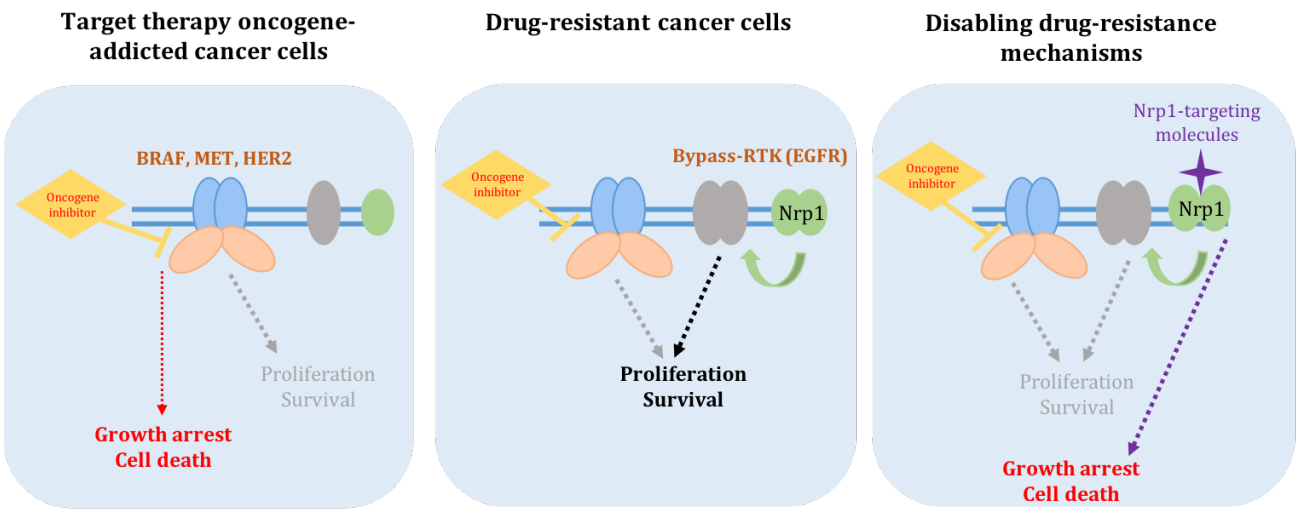

Figure 14: Nrp1-mediated drug resistance.

Oncogene inhibitors shunt activity of receptors favoring tumor cell proliferation and survival. However, in some drug-resistant cancer cells, compensatory mechanisms take place to restore cell proliferation and survival. One of these compensatory mechanisms is consisting of RTK such as EGFR activation caused by Nrp1 upregulation. Consequently, targeting of Nrp1 leads to growth arrest and cell death. Adapted from Rizzolio et al. (2018).

Considering the critical role of Nrp1 in cancer development, several approaches have been investigated to target this receptor for inhibition.

Using an indirect approach of library screening with antibodies binding to Kinase insert Domain Receptor (KDR, another name for VEGFR2), a research group discovered a heptapeptide (ATWLPPR) able to inhibit VEGF-induced endothelial cell proliferation *in vitro* and VEGF-induced angiogenesis in a rabbit corneal model *in vivo* (Binétruy-Tournaire et al., 2000). This peptide was further shown to inhibit VEGF165 binding to both Nrp1 and Nrp2 (neuropilin-2) receptors *in vitro* (Perret et al., 2004). In the same study, the heptapeptide was then radiolabeled with technetium-99m (^{99m}Tc) at the N-terminal part and injected in a mouse model of breast cancer tumor for a biodistribution assay. Interestingly, the radiolabeled heptapeptide was not able to bind to Nrp2 thus suggesting the importance of the N-terminal part of its sequence for the interaction with Nrp2. Indeed, the amide nitrogen groups of the three amino acids at the N-part (ATW)

were used to bind ^{99m}Tc through a mercaptoacetyl group. However, the labeled peptide was still binding to the Nrp1. The group of M. Barberi-Heyob later demonstrated that ATWLPPR peptide was binding to Nrp1 instead of KDR as initially proposed (Tirand et al., 2006). In this study, the authors coupled a chlorin-type photosensitizer (5-(4-carboxyphenyl)-10,15,20-triphenyl-chlorin, TPC) at the N-terminal end of the ATWLPPR peptide via a spacer (6-aminohexanoic acid, Ahx) to test its applicability for PDT. They demonstrated that the N-terminal part of the heptapeptide was not required for the binding to the Nrp1 receptor. Moreover, TPC-Ahx-ATWLPPR was eliminated from the blood compartment more efficiently than a commercial photosensitizer (Foscan®, Temoporfin) and accumulated rapidly in tumors. These results support the applicability of the ATWLPPR peptide for the targeting of Nrp1-expressing cells.

The ATWLPPR peptide has been further developed for its application in PDT by coupling it to different nanoparticle types, including superparamagnetic iron oxide nanoparticles (Niescioruk et al., 2017). Its coupling to liposomes loaded with paclitaxel increases the accumulation of the liposomes in MDA-MB-231 tumors *in vivo* (Cao et al., 2015).

The company Genentech used phage library screening to identify a human monoclonal antibody (MNRP1685A) against the Nrp1 (Liang et al., 2007). This antibody was shown to block VEGF binding to the b1b2 domain of Nrp1 in endothelial cells and to inhibit vascular remodeling. This antibody underwent two clinical trials so far. The first trial was aimed to evaluate a dose-escalating schedule of MNRP1685A administration to patients with advanced solid tumors (Weekes et al., 2014). However, the clinical benefit of MNRP1685A treatment was modest considering that a stable disease was the best observed response.

The second clinical trial evaluated the effect of MNRP1685A in combination with bevacizumab in patients with advanced solid tumors (Patnaik et al., 2014). However, this study revealed a high incidence rate of proteinuria, which led to a discontinuation of this approach.

While these approaches were aimed to target the extracellular domain of Nrp1, there is growing interest to target the oligomerization of Nrp1 with various co-receptors (**Figure 15**). Thus, although current therapeutic strategies focus on the targeting the extracellular domain or other protein targets in the downstream signaling pathway (Meyer et al., 2016), the lab of D. Bagnard developed an innovative strategy to interfere with the formation of Nrp1 complexes via its transmembrane dimerization domain.

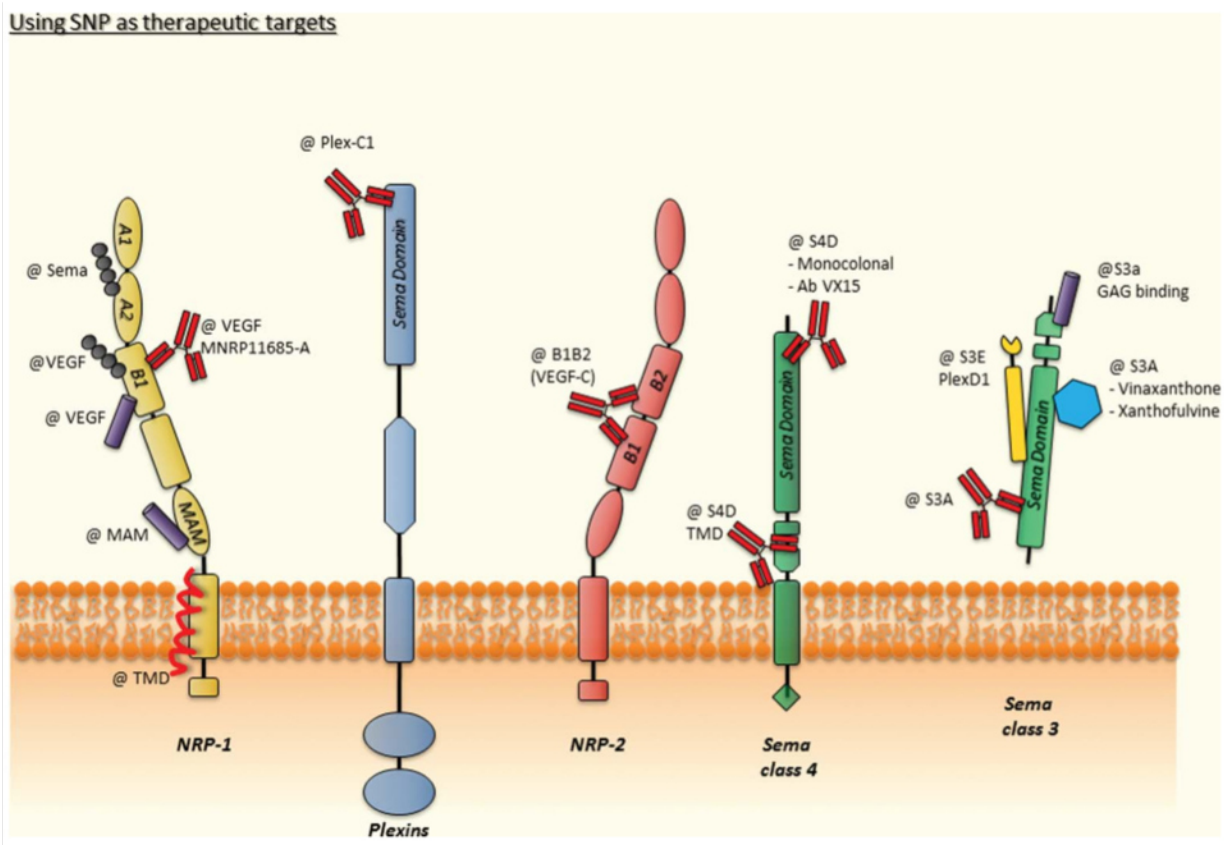

Figure 15: Therapeutic targets of the Semaphorin/Nrp/Plexin platform.

Current therapeutic compounds focus on targeting the extracellular domain of Semaphorin/Nrp/Plexin platform receptors. From Meyer et al. (2016).

3. Implication of the transmembrane domain in receptor activity

Many receptors interact and form complexes through interaction of their transmembrane domains (TMD) in order to transduce their signal. The importance of the TMD has been demonstrated for dimerization of tyrosine kinase receptors (Weiss and

Schlessinger, 1998) and for formation of T cell receptor complexes (Wucherpfennig et al., 2010). The TMDs are mainly structured by α-helices. The role of TMDs in receptor dimerization was initially discovered in 1976 when Furthmayr and Marchesi showed that Glycophorin A protein (GpA) forms dimers through its TMD (Furthmayr and Marchesi, 1976). GpA, which is a protein found on the surface of human erythrocytes, has a TMD of 23 residues (ITLIIFGVMAGVIGTILLISYGI) forming only a single α-helix. The hypothesis that the transmembrane helices are critical for homo- or hetero- dimerization (Bormann and Engelman, 1992) was corroborated for GpA by a mutagenesis screening technique (Lemmon et al., 1992a) and using a synthetic transmembrane peptide mimicking GpA transmembrane sequence (Lemmon et al., 1992b). Subsequent studies led to the description of a minimal motif composed of 7 amino acids (LIxxGVxxGVxxT; x stands for any amino acid) critical for GpA dimerization (Lemmon et al., 1994), which later was confirmed by a study employing Nuclear Magnetic Resonance spectroscopy (MacKenzie et al., 1997). Using the ToxR transcription activator system as a protein-protein interaction (PPI) reporter assay, Brosig and Langosch demonstrated that the central GxxxG motif was responsible for GpA dimerization (Brosig and Langosch, 1998). Application of another PPI reporter assay (TOXCAT) revealed that this motif is a frequent oligomerization motif (Russ and Engelman, 2000) and a statistical analysis demonstrated that the GxxxG motif is overrepresented in TMDs (Senes et al., 2000). The recurrent occurrence of glycines in this type of motif led to the proposition to call this motif the "glycine zipper motif". However, the motif of interaction rather is a "Small-xxx-Small" sequence, where Small is a small amino acid such as glycine, alanine or serine. Following the elucidation of the GxxxG motif as a key motif for dimerization, the GxxxG pattern was identified also in other transmembrane receptor proteins such as Integrin αIIb, HER2 and the neuropilins. The neuropilins represent a protein family that is highly conserved across species (Kawakami et al., 1996; Takagi et al., 1995). Nrp1 possesses a GxxxGxxxG motif critical for receptor dimerization and oligomerization, which is 100% conserved in birds, fishes, amphibians and mammals (Roth et al., 2008).

Although the GxxxG motif has been implicated in helix-helix interaction between some proteins, it is not automatically linked to such interaction for other proteins. Moreover, other similar motifs can be implicated in the interaction (Hubert et al., 2010). Nevertheless, given their implication in receptor interaction, it was suggested that the TMD plays an important role in receptor activity and thus in biological functions. A first demonstration of this implication was the discovery of a point mutation in the TMD of the Neu receptor (rodent form of HER2 receptor), changing a valine for a glutamic acid (Bargmann et al., 1986), which led to constitutive dimerization and activation causing cancer in rats (Weiner et al., 1989). The family of receptors that has been the most frequently used as a model for TMD interaction studies is the receptor tyrosine kinase (RTK) family and especially the EGFR subfamily.

Given the central role of the TMD in receptor dimerization, the laboratory of D. Bagnard developed synthetic membrane targeting peptides (MTPs) able to mimic the TMD and to interfere with receptor dimerization. First MTPs were shown to interfere with the dimerization and activation of the EGFR and HER2 receptors (Bennasroune et al., 2004). The specificity of inhibition was shown by application to Chinese hamster ovary (CHO) cells expressing a chimeric insulin receptor (IR) in which the TMD was replaced with the TMD of the EGFR or HER2 receptors (Bennasroune et al., 2005). In both cases, the specific MTPs interfered with autophosphorylation of the cognate chimeric IR.

After these encouraging results with MTPs targeting the interaction of members of the EGFR family, the laboratory of D. Bagnard extended this strategy to the targeting of interactions involving the Nrp1. This choice was motivated by previous works showing the importance of Nrp1 in forming signaling platforms in association with other receptors such as VEGFR1 (Bagnard et al., 2001) or plexins (Püschel, 2002). Moreover, a GxxxGxxxG motif was found in the TMD sequence of Nrp1 (**Figure 16**) and several experiments based on ToxLuc system (a modified TOXCAT system) and Föster Resonance Energy Transfer (FRET) had shown the ability of Nrp1 to homodimerize

through its TMD (Roth et al., 2008). Using the Bacterial Adenylate Cyclase Two Hybrid (BACTH) system (Karimova et al., 2001) to study the interaction between Nrp1 TMD and PlexA1 TMD, the group of D. Bagnard demonstrated that both receptors were able to self-assemble but also to form heterodimers following this order preference: Nrp1-Nrp1>Nrp1-PlexA1>PlexA1-PlexA1 (Aci-Sèche et al., 2014).

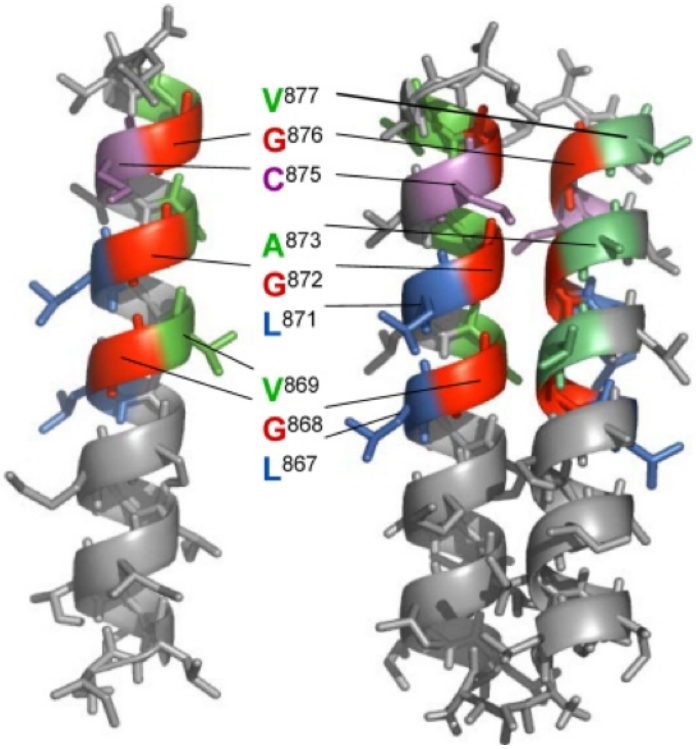

Figure 16: Nrp1-interfering peptide.

The critical glycines within the GxxxGxxxG interacting motif are highlighted in red.
From Roth et al. (2008).

A peptide mimicking the TMD of Nrp1 (MTP-Nrp1) produced by chemical synthesis was evaluated in preclinical models. Here, MTP-Nrp1 was able to inhibit VEGF-induced angiogenesis, migration and proliferation of Human Umbilical Vein Epidermal Cells (HUVEC) *in vitro* (Nasarre et al., 2010). Moreover, the specificity of MTP-Nrp1 was demonstrated using a mutant peptide (in which the three glycines were replaced by three valines), which was unable to inhibit angiogenesis, migration or proliferation of HUVEC. To investigate the possibility of using MTP-Nrp1 as an anti-cancer drug, a rat glioma

model (C6 cells) was used. Here, MTP-Nrp1 was shown to be active and able to inhibit Sema3A-induced oligomerization of Nrp1 as well as C6 proliferation and VEGF-induced cell migration. Experiments performed with a biotinylated version of MTP-Nrp1 demonstrated that the peptide stably integrated into the membrane within one hour and it was still detectable in the membrane after 24 hrs. Encouraged by these *in vitro* results, the applicability of MTP-Nrp1 for tumor inhibition was also evaluated in an *in vivo* model. Indeed, MTP-Nrp1 prevented glioma growth in an orthotopic brain tumor model induced by C6 cells. In this experiment, the C6 cells were first incubated either with MTP-Nrp1 at 10^{-8} M, or with the inactive mutant peptide, or with phosphate-buffered saline and then applied to mice by stereotaxic injection. Eight days after the injection, MRI analyses revealed that that the injection of MTP-Nrp1-incubated C6 cells produced up to 80% less tumors than the injection of C6 cells incubated with the controls. Subsequently, the activity of MTP-Nrp1 was also tested by application to already developed tumors, using a heterotopic tumor model. Here, cells of the U373MG glioma cell line, which expresses high level of Nrp1 (Hu et al., 2007), were injected into the flank of athymic nude mice. Mice carrying tumors were then randomized in two groups, one group receiving MTP-Nrp1 at 10^{-7} M in lithium dodecyl sulfate (LDS) and the other receiving only PBS (no effect of LDS on tumor growth has been previously shown). The mice were treated one time per day for 10 days via intraperitoneal administration. The results showed that mice treated with MTP-Nrp1 exhibit a significant reduction in tumor growth rate (final volume/initial volume) as compared to the control group (3.6-fold vs 7.9-fold).

Subsequently, the anti-cancer activity of MTP-Nrp1 was further evaluated by treatment of a murine model of breast cancer (Arpel et al., 2016). In this study, the authors firstly tested the activity on a syngenic model of breast cancer using MDA-MB-231cells. After validation of anti-proliferative effect of MTP-Nrp1 on 4T1 cells *in vitro,* the cells were injected subcutaneously in Balb/C mice to produce tumors. The mice were treated with MTP-Nrp1 at 1 $\mu g.kg^{-1}$ three times a week as soon as the tumors reached 200 mm^3. The results obtained had shown a reduction of the tumor growth up to 67% due to MTP-Nrp1 treatment. In the same study, the authors demonstrated the antiproliferative effect of MTP-Nrp1 on human breast cancer cell lines (MCF-7 cells, SK-BR-3 cells and 4T1 cells)

in vitro. MTP-Nrp1 was able to reduce cancer cell proliferation in both cell lines. Considering the highly metastatic behavior of MDA-MB-231 cells and the therapeutic challenge represented by the triple negative breast cancer, the authors decided to use MDA-MB-231 cells to evaluate MTP-Nrp1 anti-tumor effect *in vivo*. MDA-MB-231 cells expressing luciferase were injected in the mammary fat pad and tumor growth was monitored using a life imaging system. MTP-Nrp1 was injected three times a week by intraperitoneal injection. At the end of the treatment, the RECIST criteria analysis revealed that 100% of mice were responding to MTP-Nrp1 treatment with 25% of stable disease and 75% of partial response.

To test the effect of MTP-Nrp1 on metastasis formation, MDA-MB-231 were grafted by intra-cardiac injection in another in *vivo* protocol. The treatment with MTP-Nrp1 started two days after the cells grafting and metastasis formation. The tumor growth was monitored using bioluminescence in life imaging context using the NightOwl system. In this experiment, MTP-Nrp1 had reduced the number of metastasis (-62%) as well as their size (-83%) compared to control group. Moreover, the number of all the different type of metastasis observed was significantly reduced (brain, lung and bone). Interestingly, the overall survival of mice treated with MTP-Nrp1 was also better than the control group (only 16% of mice treated with MTP-Nrp1 died during the protocol lasting 92 days compared to 58% death in the control group). Two different types of pre-treatment protocols were then developed to evaluate the preventive anti-tumor effect of MTP-Nrp1. In one case the cells were incubated with MTP-Nrp1 during 1hr before the intracardiac grafting while in the other case the mice were under continuous pre-medication during 3 days before the grafting. This experiment demonstrated that MTP-Nrp1 is able to prevent metastasis formation.

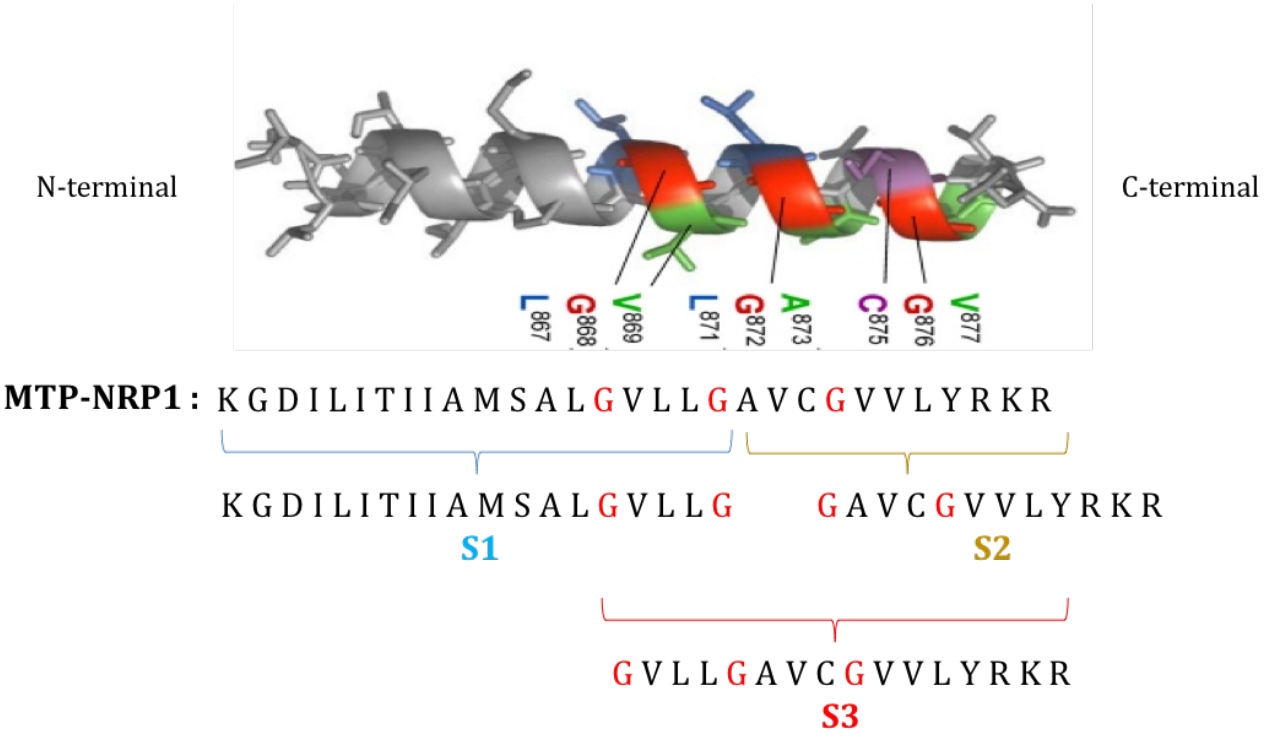

Figure 17: Short Nrp1-interfering peptides.

Short peptides partially overlapping with the MTP-Nrp1 peptide sequence. The S3 peptide contains the complete GxxxGxxxG motif. Adapted from Roth et al. (2008).

All of these results support the use of MTP-Nrp1 as a new anti-cancer drug. However, MTP-Nrp1 is a highly hydrophobic peptide which causes solubility issue. In order to increase its solubility, the current strategy uses LDS to form micellar structures incorporating the peptides. Alternative approaches used DMSO as a solubilizing agent. However, both vehicles are exhibiting potential toxicity and have limited potential for clinical use. Additional formulations of the MTP-Nrp1 would improve the translational value of this approach.

III. Nanoparticles (NPs)-based drugs delivery systems

The use of NPs as carriers for drug delivery in cancer treatment shows unique advantages as compared to naked drugs. NPs are at nanoscale size, exhibit a high surface-volume ratio and show a passive tumor targeting ability through the Enhanced Permeation and Retention (EPR) effect. The existence of the EPR effect was proposed by

Matsumura and Maeda in 1986 (Matsumura and Maeda, 1986), who investigated the accumulation of polymers fused to the tumor inhibiting antibiotic drug neocarzinostatin (NCS) (called smancs) in a tumor-bearing mouse model and found that the half-life of smancs in plasma was nine times longer than the half-life of non-conjugated NCS (18 minutes and 2 minutes respectively), and that smancs accumulated more rapidly in tumors than the non-conjugated NCS. It was assumed that these differences in retention and accumulation were due to: a) the high permeability of the tumor vasculature, b) poor uptake of molecule by lymphatic vessels, c) poor uptake of molecule by blood vessels and d) tumor hypervasculature. However, although the EPR effect is efficient for the accumulation of NPs in the rodent tumor model, the EPR effect was not efficient in the clinic (Danhier, 2016). Indeed, tumors developed in rodents exhibit important differences compared to human tumors (Nichols and Bae, 2014). Tumors in rodents grow quickly, usually in 2-4 weeks, while tumors in humans developed slowly, possibly during several years. This difference in growing speed leads to major differences between human and rodent tumors concerning both tumor microenvironment and tumor cells. Unlike human tumors, the tumors in rodent models are usually triggered by subcutaneous or orthotopic injection of a clonal population of cultured tumor cells and their fast expansion reduces the risk of genetic mutations. Rodent tumors are, therefore, composed of more homogenic cell populations and also show a higher tumor-to-body ratio as compared to the human tumor.

Based on this initial discovery supporting the potential of NPs in cancer-targeted drug delivery, research was focused on the development of NP carriers with increased therapeutic, imaging and tumor targeting abilities (**Figure 18**). This led to the emerging concept of "theranostic" NPs, which carry active agents to combine both therapeutic and imaging capabilities. In this regard, a wide range of NPs types has been tested, whereby each provides specific advantages and disadvantages (**Table 3**).

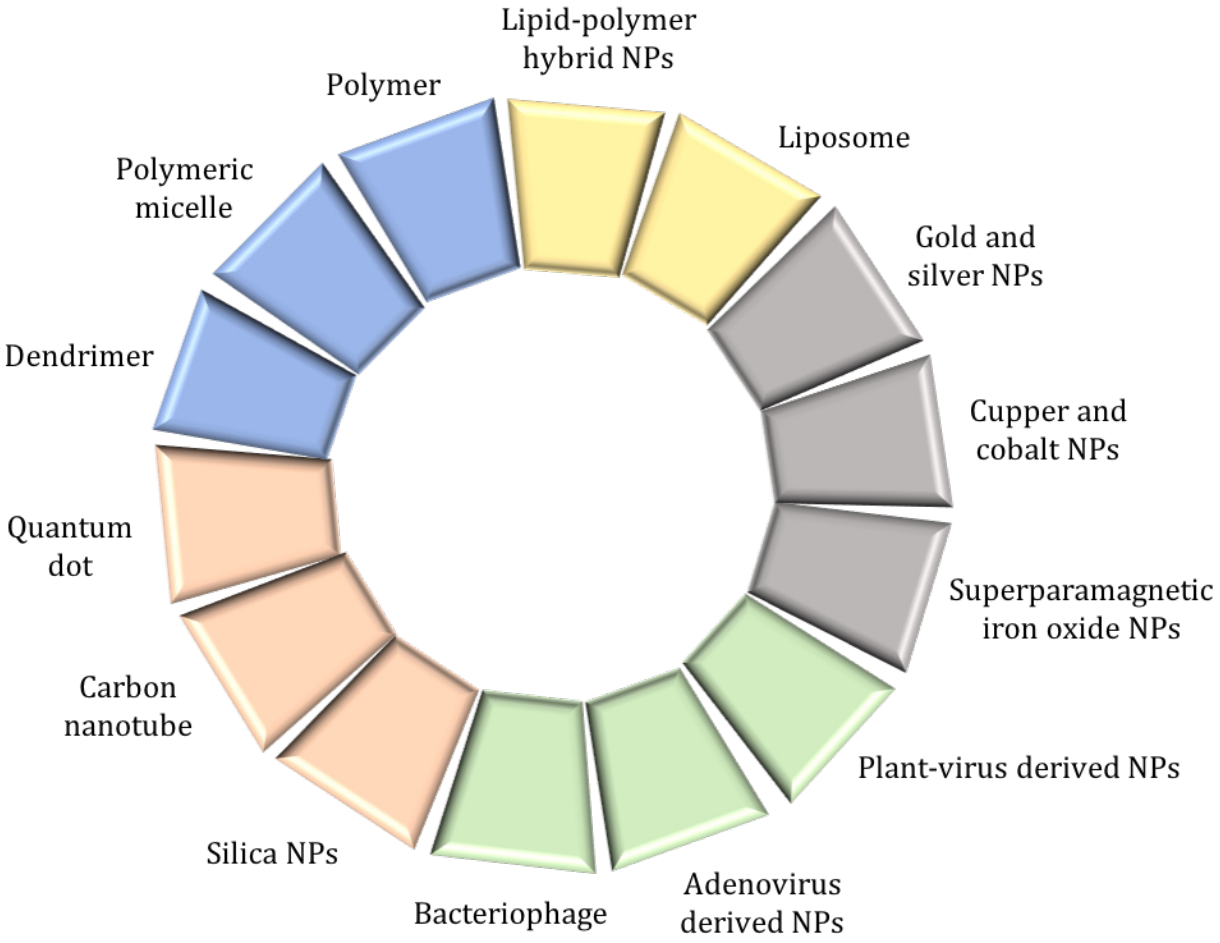

Figure 18: The main nanoparticles types.

1. Inorganic nanoparticles

1.1. Metallic nanoparticles

Metallic nanoparticles have inherent magnetic and electric properties that caused increasing interest in the biomedical field for their development as imaging agents. The main concerns about this type of NPs are their potential toxicity and retention in the body.

1.1.1. Gold and silver nanoparticles

Among metallic NPs, gold NPs (**Figure 19**) exhibit unique Surface Plasmon Resonance (SPR) and optical properties. They are used in a wide range of cancer therapy

(**Figure 20**). The preparation of gold NPs is based on the reduction of gold ions, usually from $HAuCl_4$ by chemical, physical or biological methods. The chemical method requires toxic chemicals and solvents as well as extreme pH and temperature conditions whereas biological methods are based on "green synthesis" using plant extracts as reducing agents (Singh et al., 2016a; Soshnikova et al., 2018). Also microorganisms are able to adsorb gold or silver atoms and to enzymatically reduce them to gold and silver NPs (Singh et al., 2016b). Gold NPs can be produced with different sizes, shapes (including nanorods, nanostars, nanocages and octagonal NPs) and physical properties.

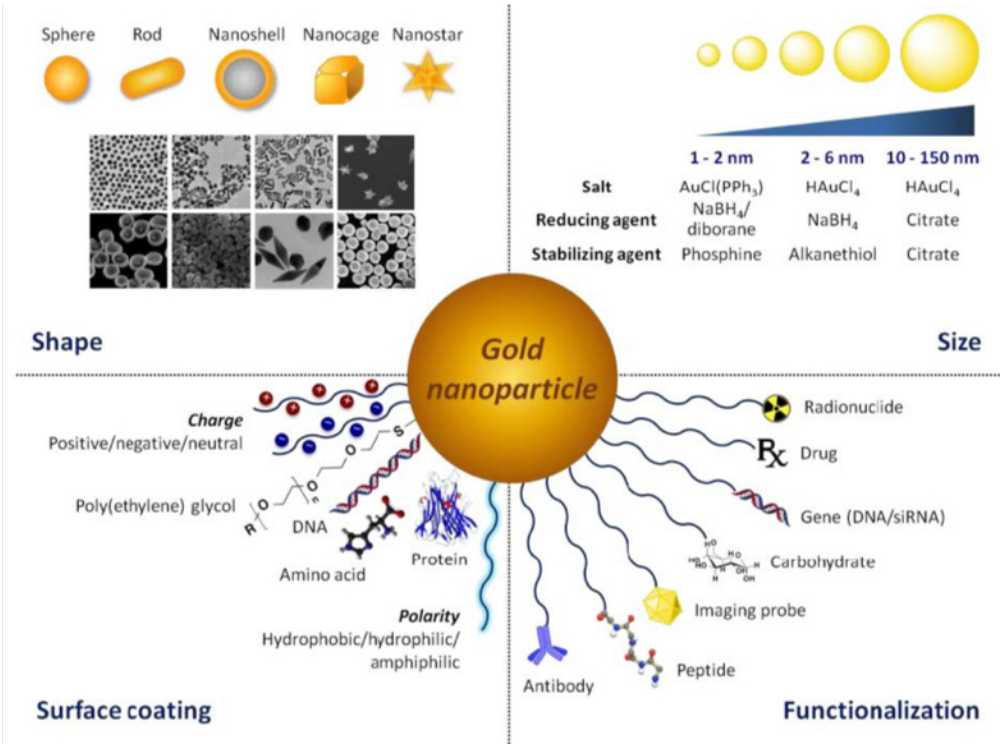

Figure 19: Gold nanoparticles.

Gold NPs come in various shapes and sizes (from 1 nm up to 150 nm). They can be functionalized to carry a wide range of therapeutic compounds as well as specific coating to increase their circulating time and their carrying ability. From Her et al. (2017).

The SPR property of gold NPs has been used to heat cancer cells thus leading to their destruction during photothermal therapy. Here, smaller gold NPs are preferred over

larger gold NPs because they adsorb light with a higher efficiency. The SPR of gold NPs is also used for photoimaging strategy but here rather large NPs are preferred due to their higher ability to scatter light.

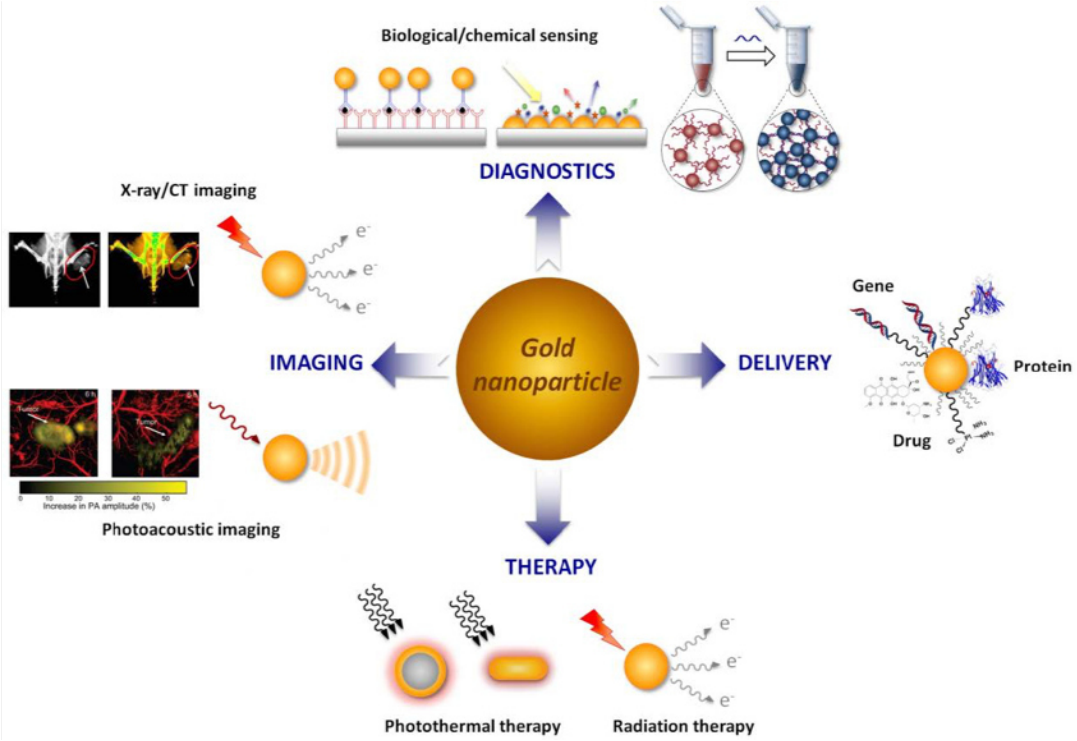

Figure 20: Main applications for gold nanoparticles.

Gold NPs are used for diagnostic, imaging, and delivery of therapeutics. Moreover, because of their specific physical properties they are also applied for photothermal and radiation therapy. From Her et al. (2017).

Similar to gold NPs, also silver NPs are used as carriers for drug treatment and imaging. When injected in the body, gold and silver NPs encounter plasma proteins leading to an adsorption of some of these proteins in the NPs. As a result of this phenomenon a "protein corona" is formed. Among these proteins collected in the corona are opsonins and fibrinogen (Dobrovolskaia et al., 2009), which lead to a recognition of the NPs by the immune system and to the removal from the blood flow by the reticulo-endoplasmic system (RES).

To avoid the recognition by the immune system, metallic and other NPs are coated with Polyethylene glycol (PEG). The chemical reaction leading to the coating of NPs by PEG is called PEGylation and the resulting particles are described as PEGylated NPs (Gupta et al., 2018). PEGylated carriers can avoid recognition by the immune system because PEG forms a hydrated layer preventing the non-specific adsorption of immunogenic substances, such as opsonin (Arakawa and Timasheff, 1985; Zhang et al., 1998).
However, studies have shown that anti-PEG antibodies are present in humans (Richter and Akerblom, 1984) and may affect the circulation time of PEGylated NPs (Grenier et al., 2018).

Although "naked" gold and silver NPs are both non-immunogenic and bio-inert, they are also not biodegradable, and their elimination from the organism is a major concern. Moreover, they provoke ROS-induced toxicity (Hsin et al., 2008) in various human, rat or murine cell lines (Foldbjerg et al., 2011; Hussain et al., 2005).
The size of silver NPs plays an important role in their cytotoxicity, whereby smaller silver NPs (2.8 nm) seem to exhibit a lower IC_{50} than bigger silver NPs (18 nm) (Zielinska et al., 2018). Whether small silver NPs are more efficient in killing cancer cells than larger silver NPs is a matter of debate (Liu et al., 2011).

Apart from gold and silver NPs, also other metal-based NPs based on copper oxide, cobalt oxide or zinc oxide are under investigation for applications in the cancer field (Vinardell and Mitjans, 2015).

1.1.2. Superparamagnetic iron oxide nanoparticles

The term superparamagnetic has been introduced in 1956 (Bean and Jacobs, 1956) to describe the capacity of ferromagnetic (Fe^{2+}) or ferrimagnetic (Fe^{3+}) materials to be transiently magnetized by a magnetic field. The surface of these materials is highly reactive and can be modified by conjugation (Ittrich et al., 2013). Superparamagnetic iron oxide nanoparticles (SPIO) are composed of a monomeric or polymeric iron oxide core stabilized by a coating that also prevents particles from aggregation. The coating can

consist of various components such as PEG, chitosan, polysaccharides, or lipids and can be conjugated with targeting moieties (antibodies, peptides). SPIO usually exhibit a uniform size distribution. They are used in biomedical imaging since 1980's, for example, as contrast agent in MRI (Hahn et al., 1990). When injected *in vivo* they are quickly removed from the blood flow by RES organs and cells. This leads to their accumulation mainly in liver, spleen and bone marrow (Laurent et al., 2010), which has been used for imaging of these organs. In cancer therapy they find applications for the delivery of therapeutic drugs or for inducing hyperthermia.

Coating of their surface with antibodies (Saesoo et al., 2018) or targeting peptides (Gao et al., 2018; Jia et al., 2018) has increased their ability to bind specifically to cancer cells and to reduce their uptake by RES. More recently, SPIO embedded in micelles or liposomes are being developed for application as theranostic NPs (Zheng et al., 2018).

1.2. Carbon NPs

Carbon NPs comprise fullerenes and carbon nanotubes as the main types.

The C60 Buckminster fullerenes are soccer-ball shaped molecules composed of 60 carbon atoms ($C_{60}H_{60}$) (**Figure 21A**). Although they are insoluble in water solvent, fullerenes can be solubilized by conjugation with molecule such as surfactants and polymers, making them suitable for use in the biological field. C60 fullerenes absorb light (Mroz et al., 2007), which leads to an excited state. This excited state can be quenched by phosphorescence or, in the presence of molecular oxygen, by the production of singlet oxygen, superoxide anions, and other ROS. This ROS-producing mechanism can be enhanced upon functionalization of the fullerenes with porphyrins or other photosensitizers, which allows to produce ROS under visible light. The phototoxicity of the functionalized fullerenes associated with enhanced ROS production under light has great potential for the treatment of cancers and other diseases by "photodynamic therapy (PDT)" (Constantin et al., 2010).

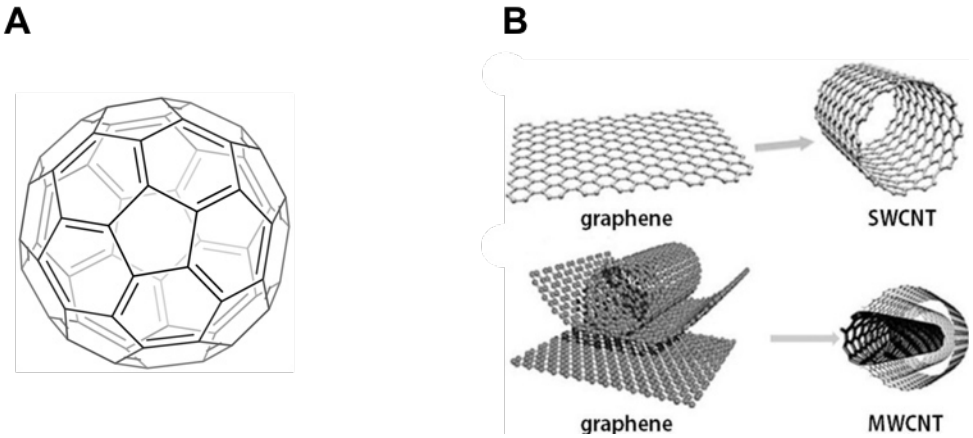

Figure 21: Structures of carbon nanoparticles.

(A) C60 fullerene exhibiting soccer-ball structure. (B) Single or multiple graphene sheets are used to create either SWCNT or MWCNT, respectively.

Carbon nanotubes (CNTs) were discovered by Sumio Iijima in 1991. Important features of CNTs include rich surface chemical functionalities, high aspect ratios, large surface areas and size stability even at the nanoscale (Iijima, 1991). CNTs are made by graphene sheets rolled into a cylinder shape. When made by a single graphene sheet they are called single-walled nanotubes (SWCNTs), while they are called multiwalled nanotubes (MWCNTs) when made with several graphene sheets (**Figure 21B**) (Elhissi et al., 2012). Native CNTs are insoluble in aqueous media but their solubility can be increased by functionalization, thus being suitable for biological applications. CNTs have been widely investigated as carriers for anticancer agents (chemotherapeutic drugs, genes, proteins) carriers and as mediators for PTT/PDT (Son et al., 2016). PEGylated SWCNTs loaded with DOX have shown increased antitumor activity (Liu et al., 2007) and similar results were obtained with MWCNTs loaded with DOX (Ali-Boucetta et al., 2008). To further increase their therapeutic potential, the CNTs loaded with drugs have been conjugated with targeting moieties such as folic acid and antibodies (Heister et al., 2009; Li et al., 2011).

Modified CNTs have shown potential use in immunotherapy of cancer through different applications. They have been successfully employed as artificial APC (Fadel et al., 2014)

or as carriers of peptide antigen to APC, thus increasing IgG responses (Villa et al., 2011), and in conjugation with tumor lysate to produce a tumor-cell vaccine (Meng et al., 2008).

In addition to their use as carriers, CNTs are also employed in photothermic and photodynamic therapies. CNTs are able to absorb near infrared light and this light absorption transfers heat to the tube. This property has been exploited in PTT (Gannon et al., 2007). Upon functionalization with antibodies, the PTT effect of CNTs can be specifically targeted to cancer cells (Xiao et al., 2009), thus increasing PTT efficiency by reducing destruction of healthy cells (Zhou et al., 2009). The possibility to load CNTs with drugs combines the application of PTT and antitumor agent, thus leading to a synergistic antitumor effect. A synergistic antitumor effect has been demonstrated to be occurring with the chemotherapeutic agent docetaxel (Wang et al., 2011) and with a siRNA (Wang et al., 2013).

1.3. Silica nanoparticles

Silica NPs are ceramic-based NPs that are used for biomedical purposes, but also in the car industry, in food, and cosmetical products. They are very stable and can be easily prepared at ambient temperature conditions with various size, shape and porosity. Their low size (50 nm) allows them to escape from the RES and they are biocompatible. They protect loaded drugs from denaturation in extreme pH and temperature conditions. Their surface can be modified by functional groups.

For example, silica NPs are employed in photodynamic therapy by carrying insoluble photosensitizers (Roy et al., 2003).

Among other porous silica NPs, also mesoporous silica NPs (MSN) are highly investigated as drug and imaging agent carriers (Wang et al., 2015).

1.4. Quantum dots

Quantum dots (QDs) are semiconductor (cadmium, selenide, zinc, etc…) nanocrystals with specific optical properties. They are composed of a core surrounded by a shell, both being semiconductors. The core and the shell exhibit different bandgap

(defined as the amount of energy required to elevate an electron from its ground state to the next energy level). The higher bandgap of the semiconductor material composing the shell confines the emission and excitation of the core and protects it from photobleaching (Walling et al., 2009). The composition of the core determines the wavelength of excitation and emission.

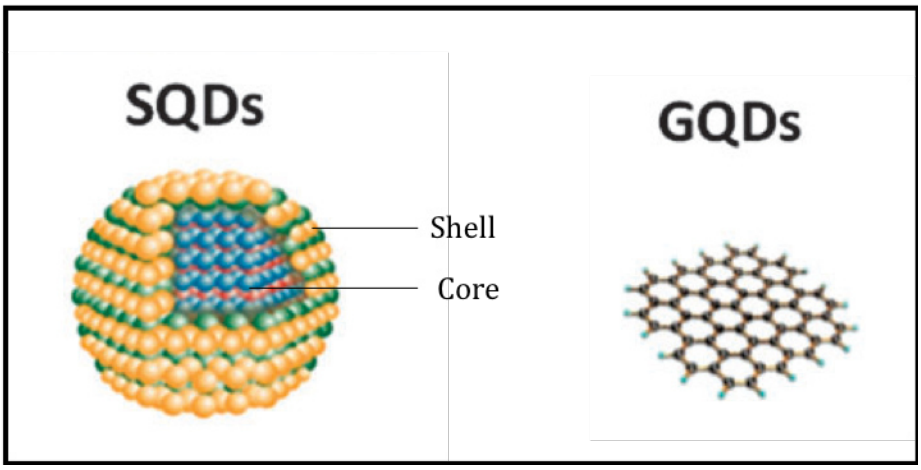

Figure 22: Semiconductor-based quantum dots and graphene quantum dots.
Adapted from Cayuela et al. (2016).

Compared to organic fluorescent dyes, QDs show exceptional brightness and stability (Chan and Nie, 1998). Despite these advantages, QDs are toxic to living systems (Sharma et al., 2017). Thus, modified QDs have been extensively developed.
QDs can be coated with antibodies or targeting peptide for specific delivery to cancer cells (Bilan et al., 2015).
A well-studied QD type applied in the cancer field is represented by the graphene QDs (GQDs). In contrast to other QDs, they are biocompatible (Kalluri et al., 2018) and have a higher loading capacity.

2. Organic nanoparticles

2.1. Polymer-based nanoparticles

2.1.1. Linear polymers

Linear polymers usually exhibit heterogeneous structure and different chain length in solution. Both cationic or anionic polymers can be used as nanocarriers depending on the charge of the compound to carry. For cationic therapeutic molecules (*e.g.* DOX) (Zhou et al., 2017), an anionic polymer such as dextran should be chosen, whereas in the case of siRNA therapy, a cationic polymer (*e.g.* chitosan) (Ripoll et al., 2018) can be used to neutralize the negative charges. PEGylation has been applied to shield polymer NPs against the immune system and to limit their uptake by immune cells.

Recently, researchers developed a linear polymer able to self-assemble into spherical nanoparticles by drug-triggering (Palvai et al., 2017). Poly (isobutylene-alt-maleic anhydride; PMAn) was conjugated with the hydrophobic drug paclitaxel (PTX) and the hydrophilic drug cisplatin. The PMAn-PTX conjugate formed 2D sheet, whereas the conjugation of cisplatin with PMAn-PTX led to self-assembly of a spherical particle.
At this point, the only commercialized polymeric particle is Abraxane® which is composed of the chemotherapeutic drug paclitaxel bound to an albumin. It was approved by the FDA in the USA for the treatment of breast cancer, NSCL carcinoma and pancreas cancer.

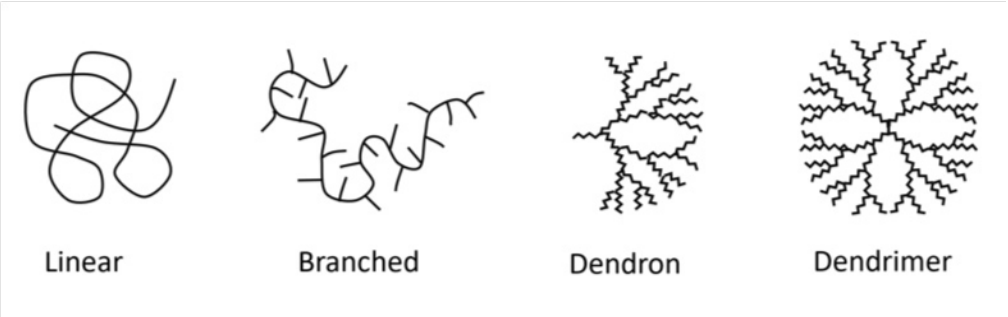

Figure 23: Different types of polymers.

2.1.2. Polymeric micelles

Amphiphilic polymers can self-assemble into micelles. They are composed of a hydrophobic core surrounded by a hydrophilic surface. This structure presents the advantage of being loadable with hydrophobic drugs in the core while coated with hydrophilic drugs or tumor-targeting ligands on the outer surface. In these polymeric micelles, drug release is mainly due to passive diffusion. However, a major limitation for the use of these polymeric micelles for drug delivery is their instability in the blood circulation leading to a fast and non-specific release of the drugs. Indeed, because polymeric micelles have a high critical micellar concentration (CMC), their dilution when injected systemically leads to their disassembly. In order to address this limitation, a new way to load drugs in polymeric micelles has been developed. In this case, the therapeutic agent is covalently linked to the polymer before assembly to micelles. These "conjugated micelles" are more stable and do not allow leakage of drugs by diffusion. For example, a polymer-drug conjugate (named Cellax) has been formed with PEG, acetylated carboxymethylcellulose (CMC) and docetaxel and shown to have a stronger antitumor effect with reduced toxicity compared to docetaxel alone (Ernsting et al., 2012). Moreover, employment of a cleavable linker between drug and polymer was designed to release the drug under controlled environment conditions such as pH, temperature or the presence of certain enzymes. A well-studied representative of these linker-carrying micelles is the PEG-Polylactic acid (PLA)-PEG micelle, which has been used as a carrier for chemotherapeutic drugs such as doxorubicin (Song et al., 2016) and docetaxel (Sim et al., 2018). A recent study in collaboration with D. Bagnard's lab led to the development of a cationic micelle loaded with a siRNA and the hydrophobic drug camptothecin (CPT) (Ripoll et al., 2018). Upon application to cells of the human breast cancer cell line MDA-MB-231 and to HeLa cells, both compounds preserved their cell killing properties as being part of the micelle. Moreover, as being combined together in micelles, the therapeutic compounds showed synergistic effects in a tumor mouse model following peritumoral injection.

2.1.3. Dendrimers

Dendrimers are nano-sized structures of globular shape with cavities, and which are biocompatible and well-defined in structure due to their chemical synthesis. They are formed by highly branched macromolecules composed of branching units (called dendrons) radiating from a central core. They are also called arborols or "cascade molecules". Each layer of dendrons is called a generation (G). More than a hundred of families of dendrimers exist depending on the type of atom chosen for the central core and the type of chemical groups added to them. The type of atom at the central core will influence the number of generations and also the number and size of the dendrimer's cavities. They are generated by two main approaches, a), the divergent way consisting of beginning from a central core then adding other atoms via chemical reactions to form the dendrons and b), the convergent way consisting of linkage of multiple dendrons until a central core is formed (**Figure 23**). The structure of dendrimers allows to present hydrophilic compounds at the surface while entrapping hydrophobic molecules in the cavities. The most commonly used dendrimers are the polyamidoamine (PAMAM) dendrimers commercialized under the name Starbust™. First described by Tomalia et al in the 1980's they are prepared by divergent synthesis with ammonia, cystamine or ethylenediamide (EDA). PAMAM dendrimers have been successfully loaded with various therapeutic agents, including DOX (Zhang et al., 2011b) and PTX (Teow et al., 2013). Polypropylenimine dendrimers commercialized under the name Astramol™ are another type of well-studied dendrimer.

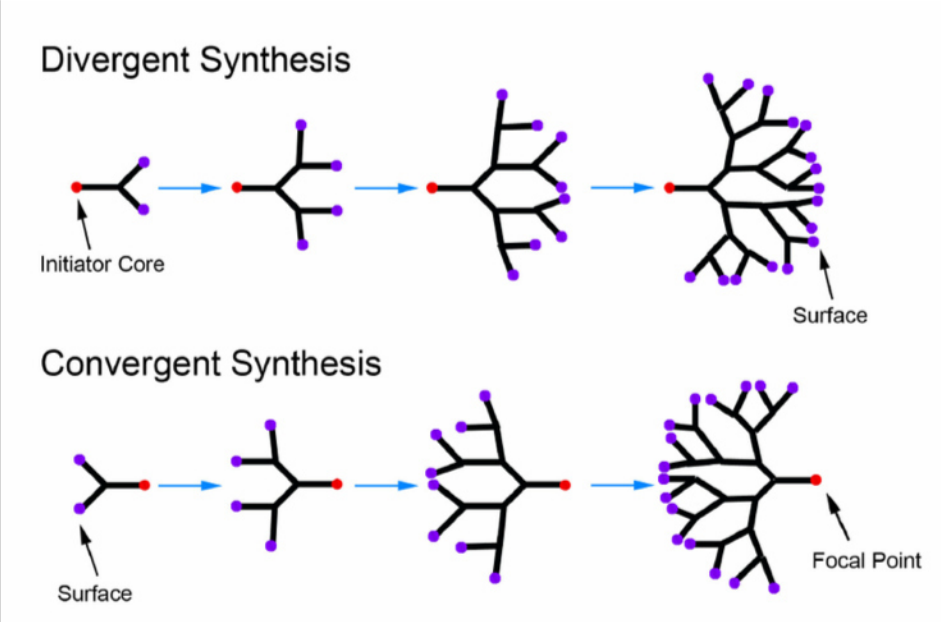

Figure 24: Dendrimer synthesis.

Dendrimers are produced by either divergent or convergent synthesis. From Pearson et al. (2012).

Recently, a research group achieved to bind doxorubicin to folic acid-coated dendrimers via a pH-sensitive linkage. These dendrimers were further entrapped with gold nanoparticle thus creating a theranostic nanoplatform for targeting cancer cell, delivering chemotherapeutic compound and allowing tumor imaging tumor under specific conditions (Zhu et al., 2018).

Dendrons formed during convergent dendrimer synthesis can be used to create a dendronizing system (Dockerry and Daniel, 2018) which allows other incorporated molecules to self-assemble (Rudick and Percec, 2008).

For example gold particles have been dendronized and used to deliver siRNA (Kim et al., 2012). The dendronization of a heparin-DOX conjugate increased the antitumor activity of DOX and reduced its toxicity (She et al., 2013).

2.2. Liposomes

Liposomes are used since several decades to increase the half-time of circulation and reduce the toxicity of chemotherapeutic drugs (Lee et al., 2017). They are composed of phospholipids (such as phosphatidylcholine or phosphatidylglycerol) that are mixed with specific amounts of cholesterol to form a lipid bilayer. Polar heads associate at the hydrophilic interface while hydrophobic chains remain packed together thus escaping the aqueous medium. Due to their structure they were first use as cell membrane mimics and only later became studied as potential carriers for hydrophobic drugs. Indeed, their specific structure allows loading of hydrophilic molecules into the liposome core while hydrophobic molecules are loaded within the lipid bilayer (**Figure 25**) (Soe et al., 2018).

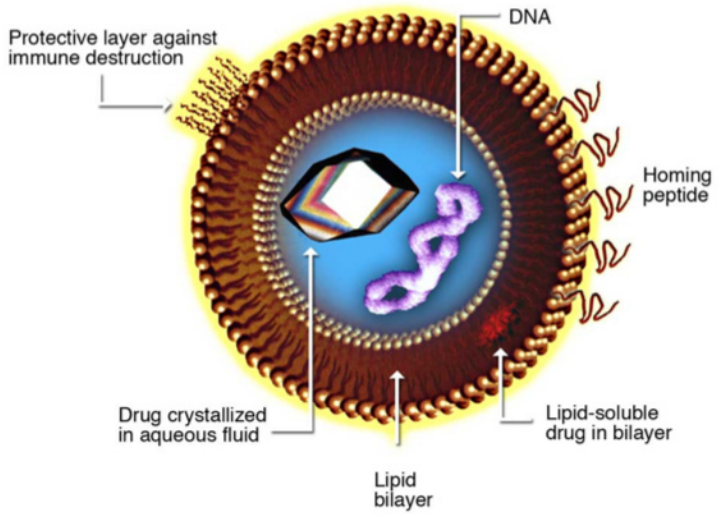

Figure 25: Liposome structure for drug delivery.

The liposome structure allows to load hydrophilic compounds into the core and hydrophobic compounds into the lipid bilayer. Coating of the liposome surface increases its targeting ability as well as its circulation time.

More recently, liposomes gained an increased interest as carrier for DNA or siRNA in cancer gene therapy (Mel'nikov et al., 2017; Saw et al., 2018). Here negatively charged, neutral or cationic lipids can be used. However, cationic lipids have the advantage to be easily bound to negatively charged DNA. Resulting complexes are called "lipoplexes".

Although liposomes exhibit advantages over naked drugs, they show poor biodistribution, recognition by the immune system resulting in quick elimination by RES and a lack in delivery specificity. To overcome detection by the immune system, liposomes were coated with PEG. The first PEG-coated liposome has been authorized by FDA in 1995 (Doxil® in the US; Caelyx® in Europe) for the treatment of AIDS and Kaposi's sarcoma.

However, although PEGylated liposomes show improved pharmacokinetic parameters, they have no improved therapeutic effect (Hong et al., 1999). They are still lacking specificity for cancer cells thus limiting delivery of therapeutic drugs to a tumor. As an improvement, researchers developed liposomes with targeted delivery or triggered release of therapeutic drugs, called "smart" liposomes (Riaz et al., 2018). Smart liposomes release their therapeutic cargo at the tumor site in response to physical factors of the tumor microenvironment such as acidic pH or hypoxia. For example, a research group recently incorporated nitroimidazole to a phospholipid bilayer of a liposome (Li et al., 2018b). Nitroimidazole is reduced by nitroreductase, an enzyme present in the hypoxic environment, thus resulting in the destabilization of the lipidic bilayer and a burst release of drugs contained in the liposome.

2.3. Lipid-polymer hybrid nanoparticles (LPHNPs)

LPHNPs are made by combining polymeric nanoparticles with lipids (Zhang et al., 2008). They consist of a polymeric core able to load hydrophobic drugs surrounded by a lipid monolayer, which reduces the loss of drugs by diffusion and enhances particle stability. Moreover, a layer of PEG (polysaccharide or polyvinylpyrrolidone, PVP) on the outer surface reduces the recognition of the particles by the immune system and enhances the circulation of LPHNP *in vivo*.

2.4. Virus-like nanoparticles

2.4.1. NPs derived from mammalian viruses

(a) Oncolytic virotherapy

Oncolytic virotherapy relies on the use of oncolytic viruses (OVs) to kill cancer cells but not healthy cells. The main feature of OVs is their ability to induce a lytic cycle in tumor cells. To do so, they may exploit a natural weakness of tumor cells (*e.g.* RAS pathway activation (Strong et al., 1998)) or be genetically modified for this objective.
Several different strains of viruses can be used in oncolytic virotherapy such as adenoviruses (Ads), Herpes simplex virus (HSV), reovirus, or vaccinia virus. In addition to their oncolytic property, some OVs promote an anti-tumor immunity. For example, reovirus induces an activation of dendritic cells (Prestwich et al., 2008) and HSV promotes a specific cytotoxic T cell activity against tumor cells (Toda et al., 1999). However, so far only one OV has been approved by the FDA, a genetically modified herpes virus called Talimogene Laherparepvec (T-VEC) used to treat metastatic melanoma (Pol et al., 2016).
Ads have shown efficient antitumor effects *in vitro* and are widely investigated in clinical trials. However, they are hepatotoxic and cause a strong immune reaction. As a result, Ads are mainly injected directly into the tumor, which, however, limits their potential efficacy against metastases. To circumvent this issue, scientists explore the possibility to hook them onto specific nanoparticles as carrier (Yokoda et al., 2017). For example, PAMAM dendrimers have been used to increase the safety profile of an Ads delivered systemically (Yoon et al., 2016). In this study, authors conjugated Ads and an anti-EGFR antibody to PEGylated PAMAM dendrimers. They showed that this formulation reduces Ads hepatotoxicity in a lung tumor model and also increases the selective killing of cancer cells by the active targeting of the anti-EGFR antibody.

These results demonstrate the potential application of NPs for the delivery of oncolytic viruses to target tissues, although additional studies are required.

(b) Mammalian viruses for therapeutics delivery in cancer

Although mammalian viruses have shown their utility in oncolytic virotherapy, they have also been extensively studied for drug delivery.

Adenoviruses are DNA viruses with icosahedral capsids and they infect several animal species including humans. By deleting genes involved in viral replication, it is possible to avoid the spreading of Ads in the organism while conserving their ability to enter cells and modify their genome. Ads are the most frequently used vector for cancer gene therapy under clinical trials (Kay, 2011).

2.4.2. NPs derived from bacteriophages

Bacteriophages are viruses that infect bacteria and not animal cells. They can have a filamentous shape (like the M13 phage) or a spherical shape (like the MS2 phage). Their capsid can be decorated with imaging or therapeutic agents by chemical conjugation or genetic engineering. They are used in a technique called “phage display” allowing the display of antibodies or peptide in the surface of the phage capsid (Nicastro et al., 2014). This technique is employed in cancer diagnosis by displaying peptides that are recognized by autoantibodies (Liu et al., 2012a). Phages are also employed to target cancer cells with antibodies able to target receptors that are overexpressed on cancer cells (Aanei et al., 2016) or molecules of the TME (Jin et al., 2014). Phages are also used to deliver therapeutic drugs for cancer therapy (Ju and Sun, 2017). For example, DOX has been successfully conjugated to the coat of filamentous M13 phages. It was shown that the drug was able to inhibit cancer cell growth after release (Bar et al., 2008).

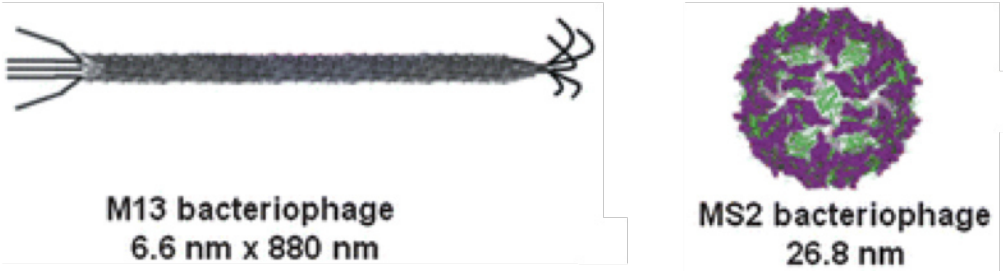

Figure 26: Bacteriophages.

Adapted from Li et al. (2010).

Phages have been genetically modified to have the ability to mediate gene expression in mammalian cells. Thus, they are also investigated as viral vectors for cancer gene therapy applications (Pranjol and Hajitou, 2015).

2.4.3. Plant virus-derived NPs

Contrary to mammalian viruses, plant viruses do not infect or replicate in animal cells and can be administrated at high doses (up to 100 mg/kg body weight) without showing toxicity (Singh et al., 2007). Moreover, their structures are well-known and are highly tunable by genetic or chemical modification (Bruckman and Steinmetz, 2014; Czapar and Steinmetz, 2017; Yildiz et al., 2011). Plant viruses like *Brome mosaic virus* (BMV), *Cowpea chlorotic mottle virus* (CCMV), *Cowpea mosaic virus* (CPMV), *Potato virus X* (PVX) and *Tobacco mosaic virus* (TMV) can be produced in gram quantities in plants and functionalized for the display of drugs, peptides, or fluorochromes using existing or engineered reactive amino acid side chains on the particle surface. Some viruses or their native or engineered coat proteins can also be produced in *Escherichia coli* or yeast. *In vitro* disassembly and reassembly can be used to purify the coat protein and load the assembled shell with drugs. Antigenic peptides fused to the particle by conjugation or translational fusion are broadly used for the development of vaccines. In the past, several plant virus-derived NPs have been engineered to target cancer, such as NPs derived from

CPMV, *Hibiscus chlorotic ringspot virus* (HCSRV), and *Red clover necrotic mosaic virus* (RCNMV).

Here, first, I will review one plant virus used in the cancer field and then focus on *Tobacco mosaic virus*, the virus employed in this research project.

(a) *Cowpea Mosaic Virus*

CPMV is an icosahedral virus with an approximate 27 nm diameter belonging to the *Comovirus* genus (**Figure 27**). Its capsid is composed of 60 coat proteins. CPMV shows no toxicity *in vivo* making it suitable for biomedical applications (Singh et al., 2007). Moreover, CPMV coat protein displays five reactive lysine residues, allowing it to be chemically conjugated to various compounds such as quantum dots (Medintz et al., 2005) or fluorescent dyes (Steinmetz et al., 2011).

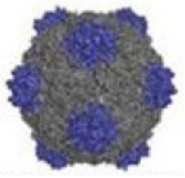

Figure 27: CPMV.

CPMV has an icosahedral structure that is 27 nm in diameter. Adapted from Bhaskar and Lim (2017).

Interestingly, CPMV exhibits a natural affinity for cancer cells due to its interaction with vimentin commonly expressed on cancer cells (Koudelka et al., 2009). CPMV is efficiently taken up by macrophages which could explain its effective tumor penetration which is even more enhanced if the particles are PEGylated (Agrawal and Manchester, 2012). The ability of CPMV to penetrate tumors and its internalization by endothelial cells (Koudelka et al., 2009) are features by which CPMV is suitable for intravital imaging as well as cancer treatment by PDT. For example, CPMV has been conjugated to the photosensitizer zinc ethynylphenyl porphyrin and shown in a mouse melanoma model

to target the photosensitizer into tumor cells and allow elimination by macrophages more efficiently than the photosensitizer alone (Wen et al., 2016).

CPMV has also been investigated as a drug carrier (Aljabali et al., 2013) and also raised interest as a NP for immunotherapy of cancer. Indeed, when locally applied to cancers, CPMV acts as an *in situ* vaccine by locally activating both the innate and adaptive immune systems. Thus, CPMV has been used as an *in situ* vaccine in mouse models for melanoma (Lizotte et al., 2016) and peritoneal ovarian cancer (Czapar et al., 2018).

(b) *Tobacco Mosaic Virus* (TMV)

i. General information about TMV

TMV was the first pathogen identified as a virus and has developed and maintained its status as a plant virus model system for more than 110 years (Scholthof et al., 2011). In 1892, the Russian botanist Dimitri Ivanovski observed an infectious agent in the sap of tobacco plants which, contrary to bacteria, was able to pass through the pores of a Chamberland filter. However, although Ivanovski discovered a new infectious agent that was smaller than bacteria, the term "virus" is credited to the Dutch microbiologist Martinus Beijerinck who repeated the experiment of Ivanovski in 1898.

TMV belongs to the *Tobamovirus* genus and has a single-stranded, positive-sense RNA genome of 6400 bases. The virus particle is rod-shaped, has a mass of 39,6 MDa (Butler and Klug, 1972) and its structural geometry has been resolved to 0,29 nm resolution by X-ray fiber diffraction and cryo-TEM techniques (Ge and Zhou, 2011; Namba and Stubbs, 1986; Namba et al., 1989). The particle consists of 2130 coat protein (CP) subunits assembled helically around the viral RNA (**Figure 28**). The right-handed helix shows an axial distance (pitch) between two CPs of 2,29 nm (Kendall et al., 2007). The rod is 300 nm long and 18 nm wide with a central channel of 4 nm containing the viral RNA. The virus particle is very stable and allows mechanically transmission (wind, water, handling) without insect vectors.

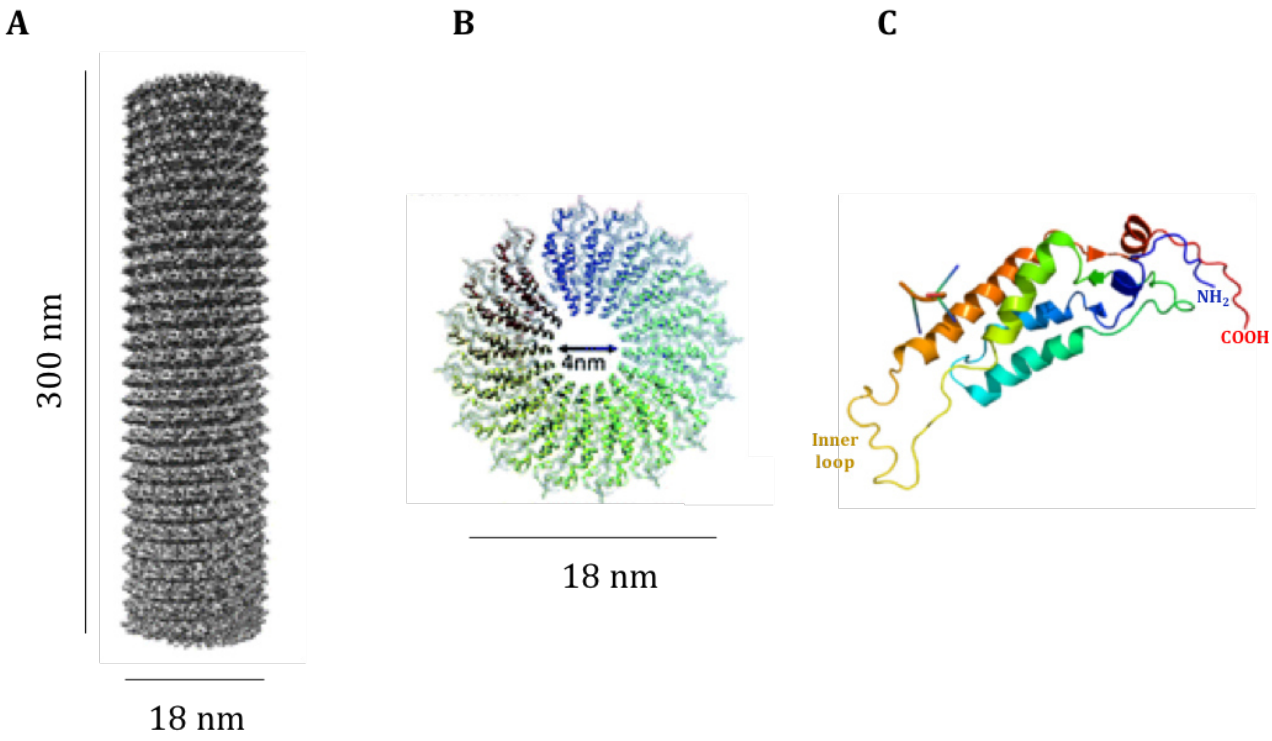

Figure 28: TMV structure.

(A) Rod shape of TMV, (B) frontal view of the rod showing the inner canal containing the viral RNA, (C) tertiary structure of the coat protein.

The virus exclusively infects plants, particularly plants belonging to the *Solanaceae*, such as tobacco, tomato, and pepper.

The viral RNA is capped at its 5' end and forms a tRNA-like structure at its 3' end. Four open reading frames (ORFs) encode small and large subunits (126 kDa and 183 kDa) of the RNA-dependent RNA polymerase (replicase), a 30 kDa movement protein (MP), and the 17,5 kDa coat protein (CP) (**Figure 29**). The large 183 kDa subunit of the replicase is translated by read-through of an amber stop codon that terminates the translation of the small 126 kDa subunit. Both subunits carry methyltransferase and helicase domains, but only the large subunit also contains the RNA-dependent RNA polymerase domain. However, although the 183 kDa protein is sufficient for replication, the 126 kDa suppresses antiviral RNA silencing and, therefore, strongly enhances the replication efficiency of the virus. Upon infection of a new cell, the virus disassembles in a process

called translational disassembly, whereby ribosomes cause the successive displacement of CP subunits as they move along the RNA for translation starting at the 5' end. The two replicase subunit are translated directly from viral RNA that enters the cell, whereas the MP and CP are translated from subgenomic RNAs produced during virus replication. The viral replication complexes (VRCs) that form at the cortical endoplasmic reticulum (EndR) are either transported by actin-myosin-driven movement along the membrane through plasmodesmata into adjacent cells to spread infection or remain anchored and give rise to viral factories that produce new virion progeny. The delicate mechanisms associated with replication and movement of TMV and other viruses, as well as viral interactions with host defense responses, have been described in numerous original articles and reviews (Pitzalis and Heinlein, 2017) and remain to be an important subject of ongoing studies (Das et al., 2018).

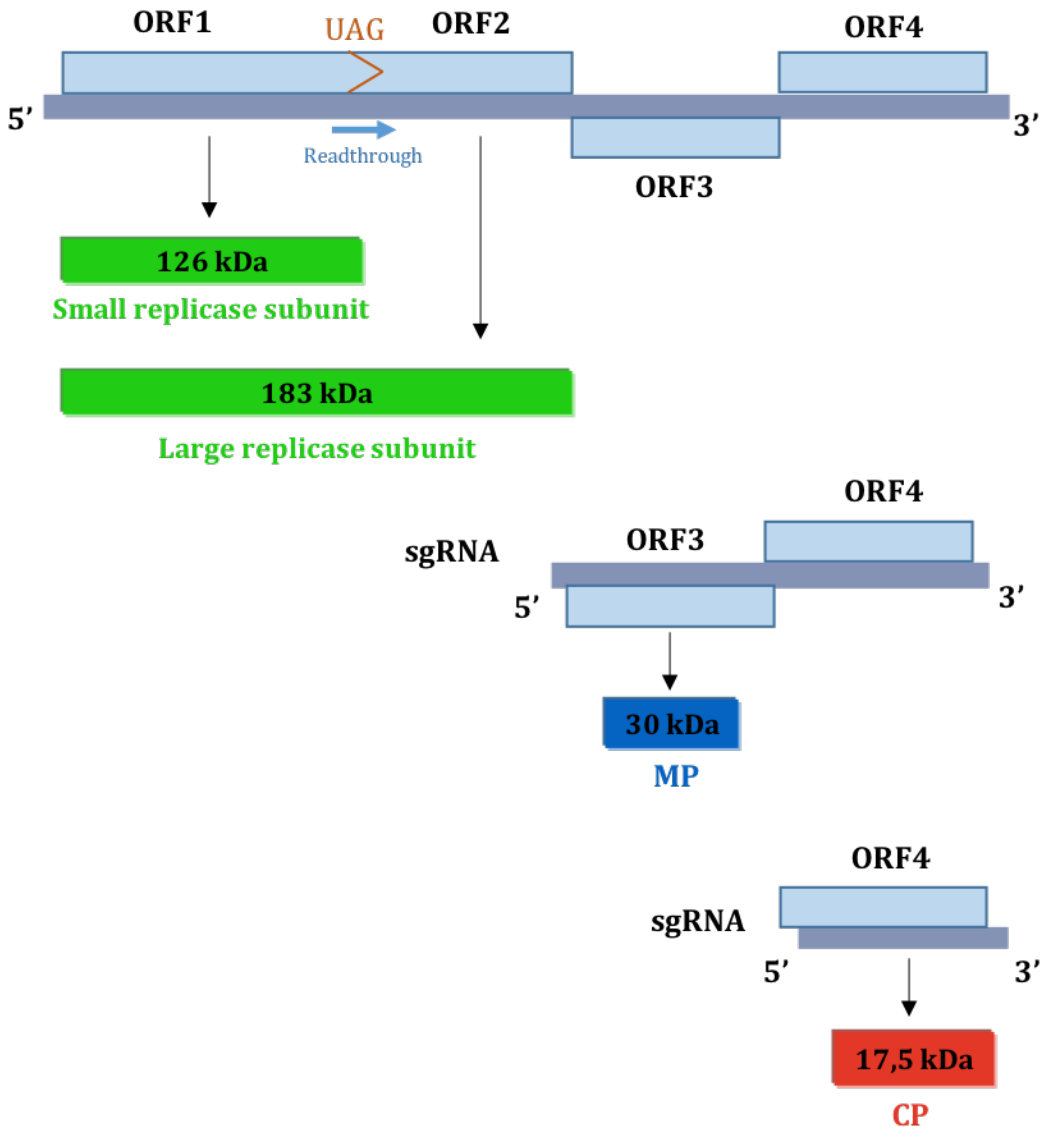

Figure 29: Genome organization of TMV.

Two ORFs encode a replicase due to ribosomal readthrough of a leaky stop codon. The third ORF encodes for the movement protein while the fourth ORF encodes for the capsid protein. sgRNA, subgenomic RNA.

TMV particles are stable over a large spectrum of temperature (up to 90°C) and pH (pH3,5-pH9) and resist various solvents including ethanol and also DMSO (Alonso et al., 2013), a solvent widely used in cancer therapy. Due to its stability the particle is used for applications as a nanocarrier in human medicine.

ii. TMV assembly

TMV assembly has been extensively studied over the last century (Creager et al., 1999; Scholthof, 2004) and is a textbook example for self-assembly. Each CP has a molecular mass of 17,5 kDa and consists of 158 amino acids with acetylated N-termini when produced *in planta*. The protein has a wedge-like shape with its wider side oriented toward the external surface of the rod. CP contains four alpha helices and both the N- and C- termini of the protein are located at the external surface of the rod. Three nucleotides of the viral RNA are associated with each CP subunit (Franklin, 1956). TMV is able to self-assemble *in vitro* (Fraenkel-Conrat and Williams, 1955; Schuster et al., 1980). Although this property was initially shown in the presence of viral RNA, further studies have shown that the protein assembles rod-like particles also in the absence of viral RNA at pH values below 6. Although the structure of the particles assembled in the absence of RNA is similar to the structure of the particles assembled in the absence of RNA, the length of the particles assembled in the absence of RNA is random, thus indicating that the RNA plays a critical role during particle formation and in determining particle length. Dependent mainly on pH, ionic strength, temperature, and CP concentration, assembly is initiated by the formation of CP oligomers collectively known as "protein A". The CP then further assembles into double-layered "disks" consisting of 34 CP subunits. Interaction of the disks with a specific stem-loop in the origin of assembly (OAS) near the 3' end of the viral RNA triggers the transformation of the disc into a helical state, by which the viral RNA is captured and threaded within the center of the growing particle as additional helical disks are added (Butler et al., 1977). Assembly beyond the disk state is dependent on CP acetylation. Thus, the assembly process will be interrupted at this stage, if the CP is derived from *E. coli* and not produced in plants. However, CPs derived from *E. coli* remain able to form stacked cylindrical aggregates (Hwang et al., 1994). Similar to assembly, the disassembly of the TMV particle is precisely controlled and initiated at the 5' end (Perham and Wilson, 1976).

iii. TMV in biotechnology

TMV is the basis of numerous biomedical, biomaterial and biosensor nanotechnologies (**Figure 30**) (Lomonossoff and Wege, 2018). In the following, I will briefly describe certain applications of TMV in the biomaterial field as well as applications in biomedical nanotechnology, such as vaccine development and drug delivery. TMV has been used as biotemplate for several metallic nanoparticles such as cobalt-platinum nanowires (Saunders and Lomonossoff, 2017) and gold nanowires (Wnęk et al., 2013). The fabrication relies on chemical functionalities of the amino acids within CP, which allow for electrostatic or complex binding of metal ions. The ions form oxides or are subsequently reduced to the metallic state. The wires are formed by either forming nanoscale tubes on the viral surface or inside the viral channel (usually occupied by the viral RNA), thus resulting in nanowires that are only 3-4 nm wide. Such nanowires have potential for the construction of nanoscale devices.

The TMV surface has been coupled with penicillinase to be used as a biosensor to detect penicillin (Koch et al., 2018), but also served as a scaffold for the coupling of other materials such as reporter dyes, contrast agents, light harvesting complexes, MRI imaging, or peptides for affinity binding, intravital targeting, or vaccination (Koch et al., 2016).

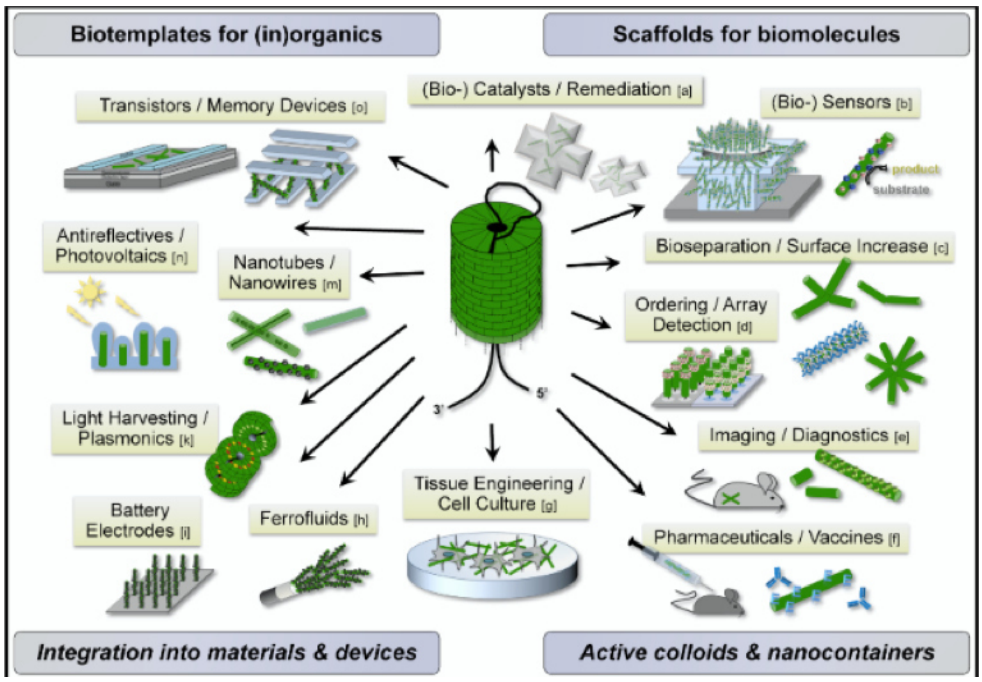

Figure 30: Applications of TMV in biotechnologies.

TMV is being used in a wide range of biotechnological fields including tissue engineering and biosensors. It is also used as template to build up inorganic materials. From Koch et al. (2016).

iv. TMV utilization in the vaccine field

Although TMV does not infect animals it is slightly immunogenic, as other biomaterials. Thus, treatment of animals with TMV triggers the activation of pattern-recognition receptors thus leading to the activation of T cells (Lebel et al., 2015). Moreover, the size and multivalent nature of TMV stimulates B cells and uptake by APC, leading to a functional cellular response in mice (Kemnade et al., 2014; McCormick et al., 2006). Because of its ability to stimulate the immune system TMV is suitable for generating vaccines against peptide antigens displayed on its surface.

Antigen peptides can be displayed on the particle surface by chemical coupling to one of the three surface-exposed regions of CP consisting of the N-terminal part, the C-terminal part and a loop between amino acids 55 to 60 (Namba and Stubbs, 1986). However, there is no reactive cysteine nor lysine residues in those regions. As a result,

TMV CP has been genetically engineered to create mutants with reactive lysine (Demir and Stowell, 2002) or cysteine into these regions for further chemical conjugation via N-hydroxy succinamide (NHS) chemistry (Smith et al., 2006).

Another strategy to display peptide antigens on the particle surface is provided by genetic engineering. Here, the coding sequence of the desired peptide is fused *in-frame* to the CP coding sequence close to the C-terminus or just before the STOP codon of CP. Such recombinant CP subunits were able to assemble particles and to display the encoded peptide on the particle surface.

In one of the earliest studies, this strategy was used to express malarial epitopes and to demonstrate that the virus was still able to replicate and to form particles in plants, therefore allowing to produce a vaccine subunit at low cost (Turpen et al., 1995). In another study, hybrid TMV particles carrying peptide epitopes of murine hepatitis virus (MHV) were isolated from infected plants and shown to trigger protective immunity in mice upon intranasal or subcutaneous administration (Koo et al., 1999).

Since 1995, numerous studies investigated the use of TMV and other plant viruses as nanoparticle vaccine and antigen carrier (Chen and Lai, 2013; McCormick and Palmer, 2008).

v. TMV as a delivery platform

Rods without the viral RNA can be loaded with therapeutic compounds (Czapar et al., 2016), while the external surface of CP can be conjugated with antibodies, imaging agents, peptides or chemotherapeutic drugs. Although (or because) humans produce antibodies against TMV (Liu et al., 2013), the virus causes no disease (Steinmetz and Evans, 2007).

The many advantages of TMV over other virus-like nanoparticles have led researchers to consider it as a suitable nanocarrier for drug delivery. In this respect, the behavior of TMV when in contact with mammal cells have been well studied during the recent years. TMV can enter but does not replicate in mammalian cells (Liu et al., 2016). TMV and TMV-derived materials can be delivered intravenously without inducing hemolysis or coagulation (Bruckman et al., 2014). More recently, it has been shown that

TMV can also form spherical nanoparticles (SNPs) under specific thermic conditions (Atabekov et al., 2011). These SNPs exhibit variable sizes of 50 nm to 800 nm. However, it appears that these nanospheres have a lower circulation time in the blood compared to nanorods and that they are cleared more rapidly from the tissue than the nanorods (Bruckman et al., 2014). Indeed, while nanorods are still detectable in the liver and the spleen at 24hrs after administration, the nanospheres are eliminated within one day.

Various studies have demonstrated that it is feasible to conjugate chemotherapeutic drugs to the CP leading to the formation of nanorods carrying those therapeutics. For example, Bruckman et al. successfully developed nanorods carrying doxorubicin (Bruckman et al., 2016). To show that these NPs are efficient for killing cancer cell *in vitro,* authors performed MTT proliferation assays on MDA-MD-231 and MCF7 breast cancer cell lines. Interestingly, in this study, the authors used heat to transform nanorods conjugated with DOX into loaded spherical NPs of TMV. These SNPs were also still able to kill cancer cells *in vitro*. In another study, Czapar et al. showed that TMV can be used to deliver the drug candidate phenanthriplatin, a platinum anticancer agent, to cancer cells (Czapar et al., 2016).
Recently, Lin and Steinmetz developed TMV nanorods loaded with mitoxantrone (MTO), an inhibitor of topoisomerase II that has been approved for application in advanced prostate cancer and metastatic breast cancer (Lin and Steinmetz, 2018). The authors showed that TMV-MTO exhibited a higher antitumor effect *in vivo* than MTO alone.

In addition to its employment in targeting cancer using chemotherapy, TMV has also been shown to be suitable for photodynamic therapy. Indeed, Lee and colleagues loaded a cationic porphyrin inside the inner channel of the TMV rod using electrostatic interaction with the negative charge from residues Glu97 and Glu106 (Lee et al., 2016). B16F10 melanoma cells were used to test cellular uptake and therapeutic efficacy. After 8h of incubation, the photosensitizer was efficiently released from the TMV rod, likely after being taken up by the endolysosomal compartment (Shukla et al., 2015). The

efficacy of cell killing was increased as compared to free PS. These results are encouraging for the development of the TMV as a new platform photosensitizer delivery.

TMV is also investigated as a carrier for imaging agents, such as MRI contrast agents (Bruckman et al., 2013) and fluorescent dyes (Wen et al., 2015). In a previous study, the lab of M. Heinlein conjugated TMV rods to a multi-photon absorbing fluorophore called 'BF3' (Niehl et al., 2015). This conjugate does not cross the blood-brain barrier and allowed to image the mouse brain vasculature over extended time after intravenous injection. However, some micro-vessels were obstructed by the large TMV-BF3 particle size indicating that further size modifications could be explored before potential clinical application.

As described above**,** TMV can be used as a carrier of peptides displayed on each CP subunit. Although most studies employ peptides as antigens for the production of vaccines against pathogens, the particles may also be employed for displaying peptides with therapeutic or targeting activity against cancers.

Trastuzumab is a monoclonal antibody which inhibits the growth of cancer cells by binding to the human epidermal growth factor receptor 2 (HER2) on the surface of these cells. Trastuzumab-binding peptides (TBP) were shown to be immunogenic and therefore capable of inducing the formation of HER2-inhibiting antibodies that block the propagation of HER2-carrying cancer cells. To enhance this immunogenicity, it has been attempted to create TMV particles displaying TPB on the surface. Using *Agrobacterium*-mediated co-delivery of binary vectors encoding TMV RNA and coat protein (CP) with a flexible linker $(GGGGS)_3$ and TBP as C-terminal extension into plant leaves such TMV particles could be produced. However, the formation of virions required the substitution of cysteine residues in the TBP, which illustrates that the tolerance for genetic fusions to the CP is dependent on the biophysical properties of the inserted amino acids. Moreover, although the recombinant TMV particles retained trastuzumab-binding capacity, mouse antibodies that formed against the particles failed to recognize HER2 on the surface of cancer cells (Frolova et al., 2010).

Nanoparticles	Advantages	Disadvantages
Metallic nanoparticles	Optical properties Surface Plasmon Resonance	Toxicity Retention in the body
Liposomes	Biocompatibility Carrying of hydrophilic and hydrophobic compounds	Poor biodistribution Quick elimination by RES
Polymeric micelles	Biocompatibility Carrying of hydrophilic and hydrophobic compounds	Instability in blood circulation
Dendrimers	Well-defined structure High solubility High functionalization possibilities	Toxicity
Adenovirus-derived nanoparticles	Biocompatibility Used for oncolytic virotherapy	Infectious in human
Bacteriophages	Biocompatibility Non infectious in humans Immunogenicity Used for phage display technique	Immunogenicity Clearance by the immune system
Plant-virus derived nanoparticles	Biocompatibility Non infectious in human Immunogenicity Well-defined structure High production yields in plants	Immunogenicity Clearance by the immune system
Quantum dots	High brightness Stability	Toxicity
Carbon nanotubes	Photoexcitability	Non water-soluble
Porous silica nanoparticles	Biocompatibility Stability High functionalization possibilities	Hemolysis Metabolic changes
Superparamagnetic iron oxide	Can be magnetized Highly reactive surface	Difficulty to control particle size

Table 3: Advantages and disadvantages of nanoparticles used in cancer treatment.

IV. Aims of the thesis

As previously discussed, the laboratory of D. Bagnard is exploring the possibility to use peptides that target the transmembrane domain (TMD) of Nrp1 as novel anti-cancer agents. However, due to the poor solubility of the hydrophobic TMD peptides and the lack of cancer targeting properties, this strategy faces several challenges. Given that TMV can be used as a carrier for various compounds including peptides, M. Heinlein and G. Orend (head of the team in which D. Bagnard was a member) conceived the idea to determine whether these challenges can be overcome by displaying the TMD mimicking peptide together with a cancer-targeting peptide (combining a killing peptide (Nrp1-TMD) with a cancer-targeting finding peptide: "FIND and KILL" strategy) on the TMV surface. In collaboration of D. Bagnard and G. Orend, the team of M. Heinlein engineered recombinant infectious clones of TMV encoding the virus with CP extended at its C-terminus by a linker peptide $(GGGGS)_3$ and fused with a peptide partially mimicking Nrp1-TMD sequence (CP-L-Nrp1) (**Figure 31**).

Figure 31: Nrp1 peptide fused to CP.

His_6 and MBP tags are fused to the N-terminal part of the protein. A flexible linker binds the peptide to the CP while increasing peptide movement possibilities.

However, although the recombinant virus was infectious in *Nicotiana benthamiana* plants, the CP fusion protein was trapped in membranes and unable to form virions. Instead, virion particles that could be recovered from infected plants contained the reverted wild type CP. Because the spread of TMV infection in plants is independent of CP (Holt and Beachy, 1991), the recombinant virus caused systemic infection despite of its dysfunctional CP. Given that recombinant TMV particles carrying the anticipated TMD peptide on its surface could not be produced in plants despite of infection, the strategy was changed by expressing the recombinant CP-L-Nrp1 protein in *E. coli*. To

increase solubility and to facilitate purification the CP-L-Nrp1 protein was expressed from plasmid pHMGWA linking the CP-L-Nrp1 protein to the maltose binding protein (MBP) and a histidine (His_6) tag at its N-terminus. When I started my PhD project, the Heinlein team already succeeded to purify soluble His_6-MBP-CP-L-Nrp1 fusion protein (now designated CPL-K) and, in collaboration with the team of D. Bagnard, to demonstrate its binding to cancer cells *in vitro*. This result and also first observations that the recombinant protein was capable to assemble disk-like particles encouraged the teams to further develop the FIND and KILL strategy using recombinant CPL-K and other peptide-carrying CP fusion proteins produced in *E. coli*. Therefore, the aim of my PhD thesis was to further develop the FIND and KILL strategy by

i) further evaluation of the biological activities of CPL-K on cancer cells;

ii) designing, producing, and evaluating the biological activities of a recombinant CP displaying a tumor-targeting FIND peptide (CPL-F) on cancer cells;

iii) combining CPL-K and CPL-F into nanoparticles by co-assembly and characterizing the effect of these particles on cancer cells.

As a finding peptide to produce CPL-F, I used the Nrp1-targeting heptapeptide ATWLPPR (CPL-F). This heptapeptide was shown to compete with VEGF165 binding to Nrp1 (Tirand et al., 2006) and was previously applied for the targeting of photosensitizer to tumor sites with the aim to develop targeted photodynamic therapy (Tirand et al., 2009; Bechet et al., 2010). Thus, following purification from *E. coli*, I evaluated the capacity of CPL-F to bind to cancer cells *in vitro* and *in vivo*.

Subsequently, I combined CPL-K and CPL-F in the same nanoparticles by co-assembly and tested their biological activity *in vitro*.

In parallel of the CPL-F development, I also produced two other CP fusion proteins, one carrying a transmembrane peptide targeting the HER2 receptor (CPL-K HER2) and another one carrying a peptide that targets TNC (CPL-F TNC).

In order to achieve these different goals, I used several human breast cancer cell lines and a human glioblastoma cell line. The different cell lines were chosen with regard to their target receptor expression and their clinical interest. Indeed, breast cancer is the most frequent cancer in women while glioblastoma represents the most frequent and aggressive tumor type in brain.

V. Materials and Methods

1. Animals

All *in vivo* experiments using animals described in this manuscript are approved by the CREMEAS (Comité Régional d'éthique en matière d'expérimentation animale de Strasbourg) under the authorization number 14058 2018031317278197.
Experiments were performed with athymic nude mice at 8 weeks (Charles River Laboratories) or on C57BL/6 mice at 8 weeks (Janvier Labs). Animals had access to food and water *ad libitum*. They were hosted in closed cages placed on a ventilated rack (Techniplast) within a conventional animal facility authorized by the French ministry of Agriculture (agreement number: E67-218-26).

2. Cell lines

In order to evaluate binding and biological activity of protein produced, different cell lines were used (**Table 4**). MDA-MB-231 cells, a human triple negative breast cancer cell line and U-118MG cell, a human glioblastoma cell line, were used for *in vitro* tests to determine the binding, disruption, proliferation and toxicity of CPL, CPL-K and CPL-F. The same lines were also used to perform *in vivo* biodistribution studies. To evaluate binding, proliferation and toxicity effect of CP-L-sHER2, I used MCF7 cells, a human breast adenocarcinoma cell line, as well as SK-BR-3, another breast cancer cell line. These two cell lines are known to express the Nrp1 and HER2 receptors.

As specificity control, Nrp1 knock-down cell lines for were established by lentivirus infection and shRNA silencing using a commercial kit (MISSION™ shRNA Sigma-Aldrich). In brief, 10 000 wild-type cells were plated in a 6-wells plate with culture medium (see below). Lentivirus particles carrying Nrp1 shRNA or control lentivirus particle without shRNA but instead a gene for green fluorescent protein (GFP) were added onto the cells (at a multiplicity of infection of three) and left for 24 hours at 37°C,

5% CO_2. The next day, the medium was refreshed to remove the particles. After two days in culture medium, the transfected cells were selected by addition of puromycin antibiotic to the medium.

All cell lines employed during this research work were cultured in Dulbecco's Modified Eagle's Medium (DMEM High Glucose, Dominique Dutscher) supplemented with 10% Fetal Bovine Serum (FBS, gibco®) and 1% of penicillin-streptomycin antibiotics (called UMED medium) and incubated at 37°C, 5% CO_2, 95% air.

Cell line	Tumor type	Origin	Nrp1 expression	HER2 expression
MDA-MB-231	Triple negative breast cancer	Human	+	-
MCF-7	Breast cancer	Human	+	+
SK-BR-3	Breast cancer	Human	+	++
U-118MG	Glioblastoma multiform	Human	++	+

Table 4: Cell lines used in this study and their receptor expression.

3. Protein production and purification

3.1. pHMGWA plasmid

The pHMGWA plasmid (Invitrogen) (**Figure 32**) carries *attR1* and *attR2* recombination sites for Gateway cloning as well as sequences encoding the His_6 and the Maltose Binding Protein (MBP). The MBP enhances the solubility of the protein of interest and is also used for protein purification using a maltose-column. The plasmid also provides an ampicilin resistance gene for selection of transformed bacteria.

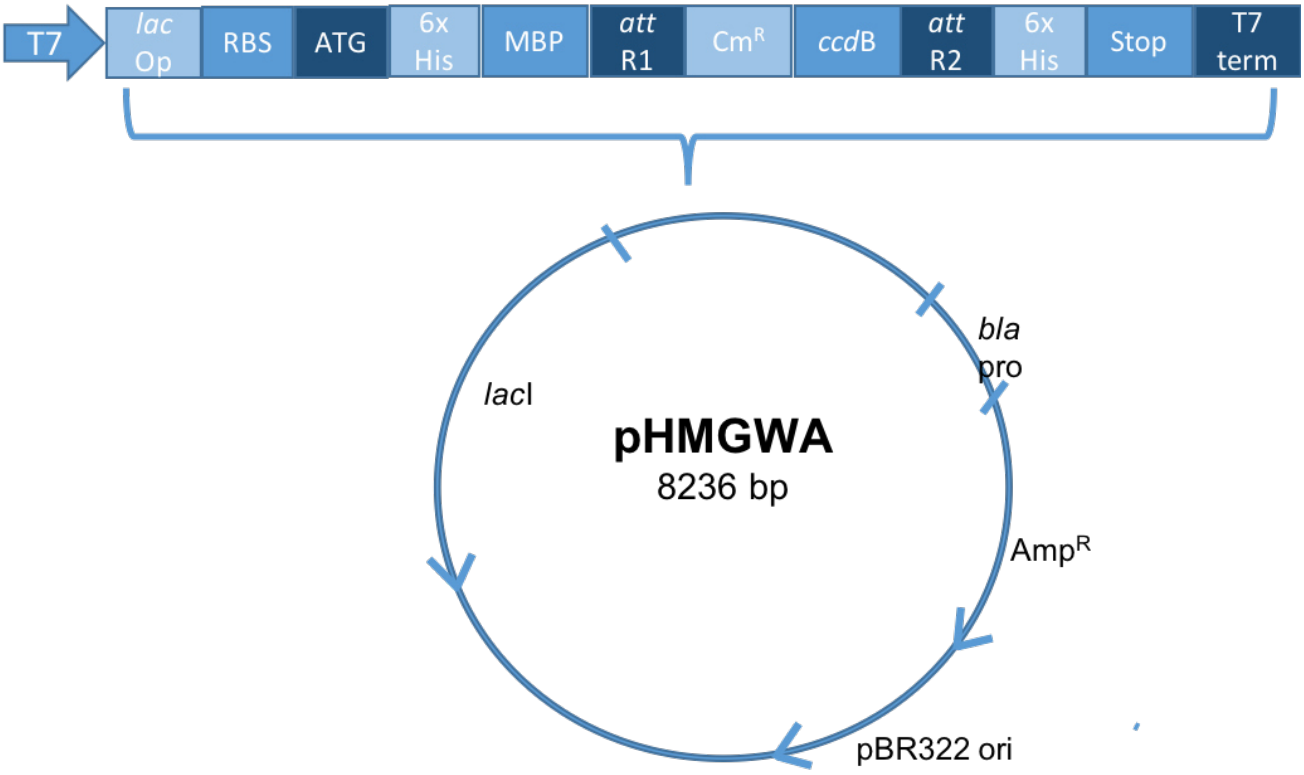

T7 promoter: 27 – 44
lac operator: 46 – 70
RBS: 100 – 106
Initiation ATG: 114 – 116
6His tag Nter: 126 - 143
MBP encoding sequence: 150 - 1247
attR1 recombination site: 1266 – 1390
Chloramphenicol resistance gene: 1499 – 2158
ccdB gene: 2500 – 2805
attR2 recombination site: 2846 – 2970
6His tag Cter: 2984 – 3001
Stop codon: 3002 – 3004
T7 termination region: 3069 – 3115
bla promoter: 3640 – 3738
Ampicillin resistance gene: 3739 – 4599
pBR322 origin: 4744 – 5417
lacI encoding sequence: 6788 – 7870 (reverse)

Figure 32: Map of the pHMGWA plasmid.

3.2. Plasmid production

The sequences of interest were inserted into pHMGWA plasmid using gateway technology (Invitrogen). The gateway system uses modified versions of recombinases from bacteriophages to clone sequences (**Table 5**). The sites recognized by these enzymes are called *att* sites. The first Gateway reaction (called BP reaction) was used to

recombine the DNA encoding the gene of interest into the pDonor vector via *attB* and *attP* sites. The attB1 and attB2 sites flanking my genes of interest were introduced by PCR suing the primer sequences shown in Table 5. Subsequently, a second Gateway reaction was used to transfer the DNA from the Donor vector to the pHMGWA destination vector via recombination between *attL* sites of the donor vector and *attR* sites of pHMGWA (**Figure 33**).

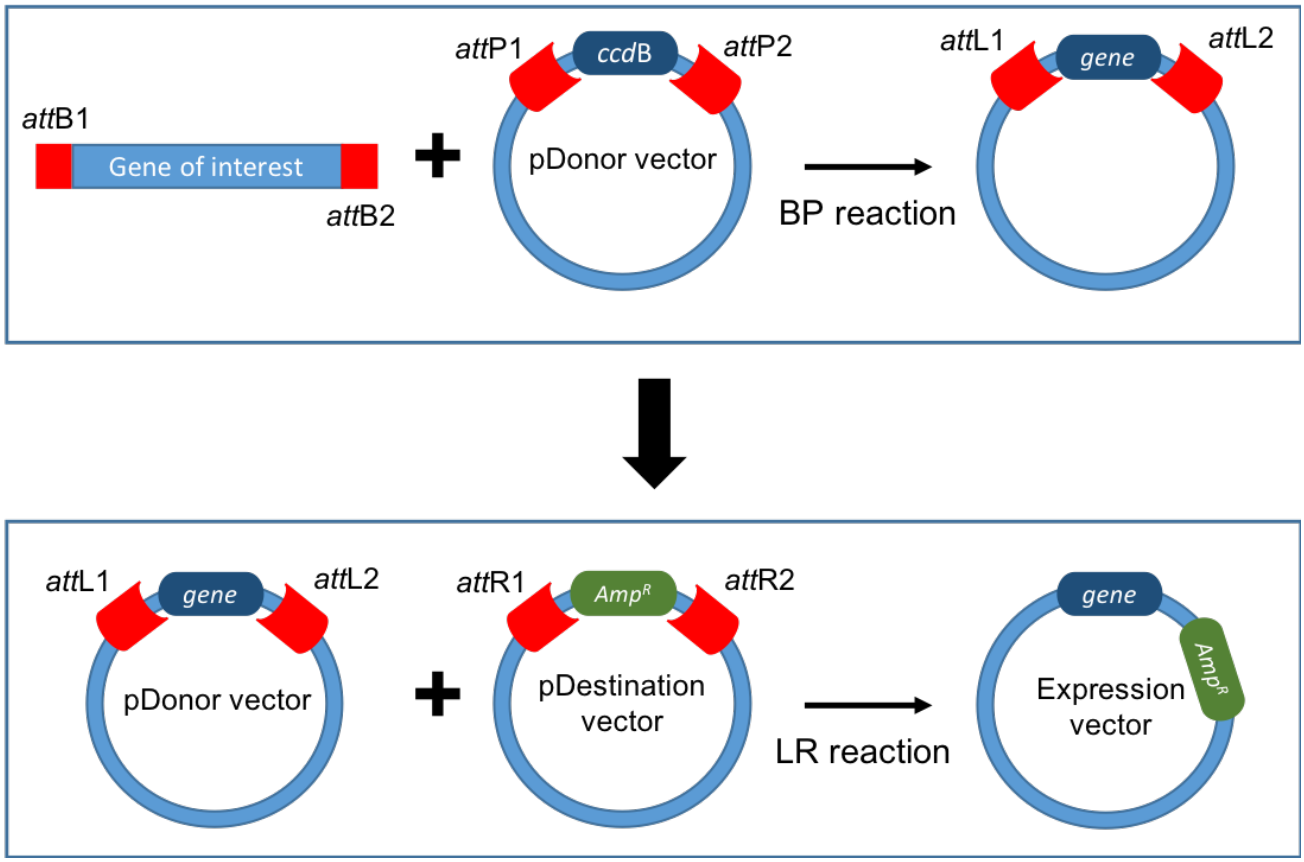

Figure 33: Gateway cloning technology.

Construction	Forward primer	Reverse primer
CPL-K	Phospho 5'-GGGGACAAGTTTGTACAAAAAAGCAGGCTTCGAAAACCTGTACTTCCAGGGTATGGCTTAC AGTATCACTACT-3'	Phospho 5'-GGGGACCACTTTGTACAAGAAAGCTGGGTTTTACCTCTTTCTATACAATACCACGCC-3'
CPL-F	Phospho 5'-GCAACTTGGCTTCCTCCTAGAGCAACTTGGCTTCCTCC-3'	Phospho 5'-TCTAGGAGGAAGCCAAGTTGCGGAACCCCCTCCGCCACTACC-3'
CPL-K HER2	Phospho 5' -GGCGTCGTCTTTGGCATACTGATTAAACGCCGTAAAACCCAGCTTTCTTGTACAAAGTTGGC -3'	Phospho 5' -CAGGACGACCACAAGGGAACCCCCTCCGCCACTACCG-3'

Table 5: Primers sequences used for LR reaction in gateway cloning.

3.3. Protein production

BL21 bacteria cells were transformed by heat shock with pHMGWA plasmid containing the sequence of interest. After one hour in Lysogeny Broth (LB) medium at 37°C with shacking, bacteria were plated on Petri dishes containing agar-solidified LB medium supplemented with ampicillin at 100 $ng.ml^{-1}$ for antibiotic selection. The plates were incubated at 37°C overnight. One of the bacterial colonies was transferred to 1 ml of liquid LB medium with ampicillin 100 $ng.ml^{-1}$ and the culture was grown for 8 hours at 37°C with shaking. Finally, 50 µl of the BL21 culture were transferred to 50 ml of NZY auto-inducing medium with ampicillin at 100 $ng.ml^{-1}$ and incubated for 36 hours at 20°C with shaking (**Figure 34**).

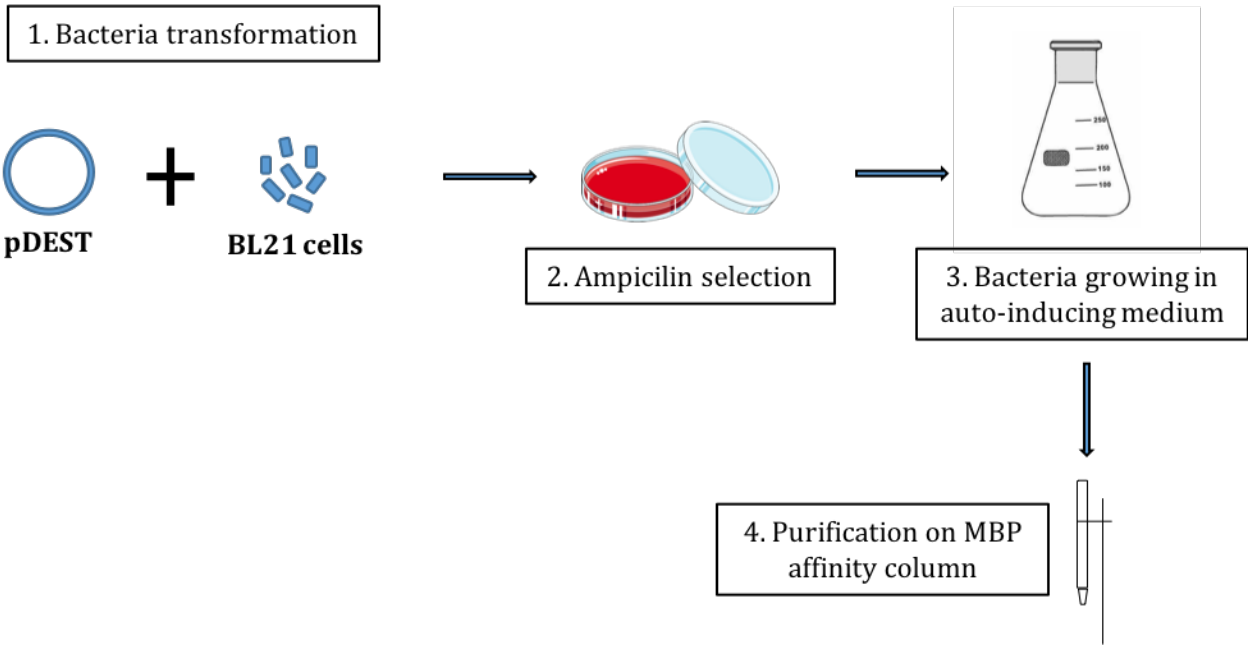

Figure 34: Protein production.

1. Bacteria are transformed by heat shock to integrate pDEST vector then 2. selected by antibody. 3. Transformed bacteria are allowed to grow in auto-inducing medium plus antibody to maintain the pressure of selection. 4. A the end of growing period, bacteria are lysed and soluble proteins undergo purification on MBP affinity column.

3.4. Protein purification using a MBPTrap column

After protein production by BL21 bacteria cells, an aliquot of each culture was used to measure the optical density (OD) at 600 nm (BioPhotometer, Eppendorf) and to calculate the volume of required lysis buffer consisting of 1% Triton X-100 diluted in Phosphate Buffer Saline (PBS) pH 7,2 (PBS pH 7,2 1x, gibco®) according to the following equation:

$V_{lysis\ buffer}$ (µl) = (OD/2) x $V_{culture}$ (ml) x 100.

The bacteria were collected by centrifugation of the culture at 4 000xg for 15 minutes at 4°C, resuspended in the required amount of lysis buffer and sonicated on ice at 60% for 10 minutes with intervals of 3s (Vibra Cell™ 75115 500W, Bioblock Scientific) until lysis. After centrifugation at 15 000 g for 20 minutes at 4°C the supernatant was filtered through 0,22 µm pore size filter units (Filtropur S 02, SARSTEDT) before application to the MBPTrap HP (GE Healthcare) column.

	Peptide sequence	Peptide molecular weight (Da)	Peptide GRAVY index	Fusion protein Molecular weight (Da)	Fusion protein Extinction coefficient	Fusion protein GRAVY index
CPL	NA	NA	NA	59 435	88 810	-0,267
CPL-K	GVLLGAVCGVVLYRKR	1703	1,069	61 120	90 425	-0,229
CPL-F	ATWLPPRATWLPPR ATWLPPR	2483	-0,529	61 901	105 310	-0,277
CPL-K HER2	LVVVLGVVFGILIKRR	1781	1,906	61 198	88 810	-0,205
HER2 K-LCP	LVVVLGVVFGILIKRR	1781	1,906	62 785	90 300	-0,252
CPL-F TNC	FHKHKSPALSPVGGG	1518	-0,507	63 560	90 300	-0,307

Table 6: Physical characteristics of the original peptides and their corresponding fusion proteins.

3.5. Dialysis

Nanoparticles assembled from CP and CP fusion proteins were produced by changing the pH of the protein solution. The protein solution was measured at 280 nm using a spectrophotometer (Multiskan GO, ThermoFisher) and set to at 1,8 $mg.ml^{-1}$ in PBS. The protein solution was sonicated for 10 minutes in a bath sonicator (FB 11201, Fisherbrand®) at 4°C set to an ultrasonic frequency of 80 kHz. Subsequently, two dialysis steps were performed. A first dialysis was performed to increase the pH of the protein solution to pH=8. Under these conditions, the CP exists to the majority in the disassembled "protein A" form. To perform this dialysis, I used dialysis devices (Slide-A-Lyser™ MINI Dialysis device 10K MWCO, 0,5 ml, ThermoFisher) consisting of a cup-like device with membrane connected to a conical tube of 15 ml. The tube was filled with 14 ml of dialysis buffer (KPO_4 pH 8 0,1M) and the cup-like device with 100 µl of the protein

solution. Dialysis device was then incubated at 4°C with slow agitation on a shaker overnight. Following this first dialysis step, a second dialysis was performed to decrease the pH to pH=6 to allow the CP to assemble. The buffer solution from the first dialysis was replaced with 0,1 M KPO_4 buffer at pH 6 and the dialysis device was again incubated at 4°C under low agitation overnight. At the end of the dialysis, the particles solution was filtered to remove all remaining proteins not assembled (Vivaspin 500, 100 kDa MWCO, GE Healthcare).

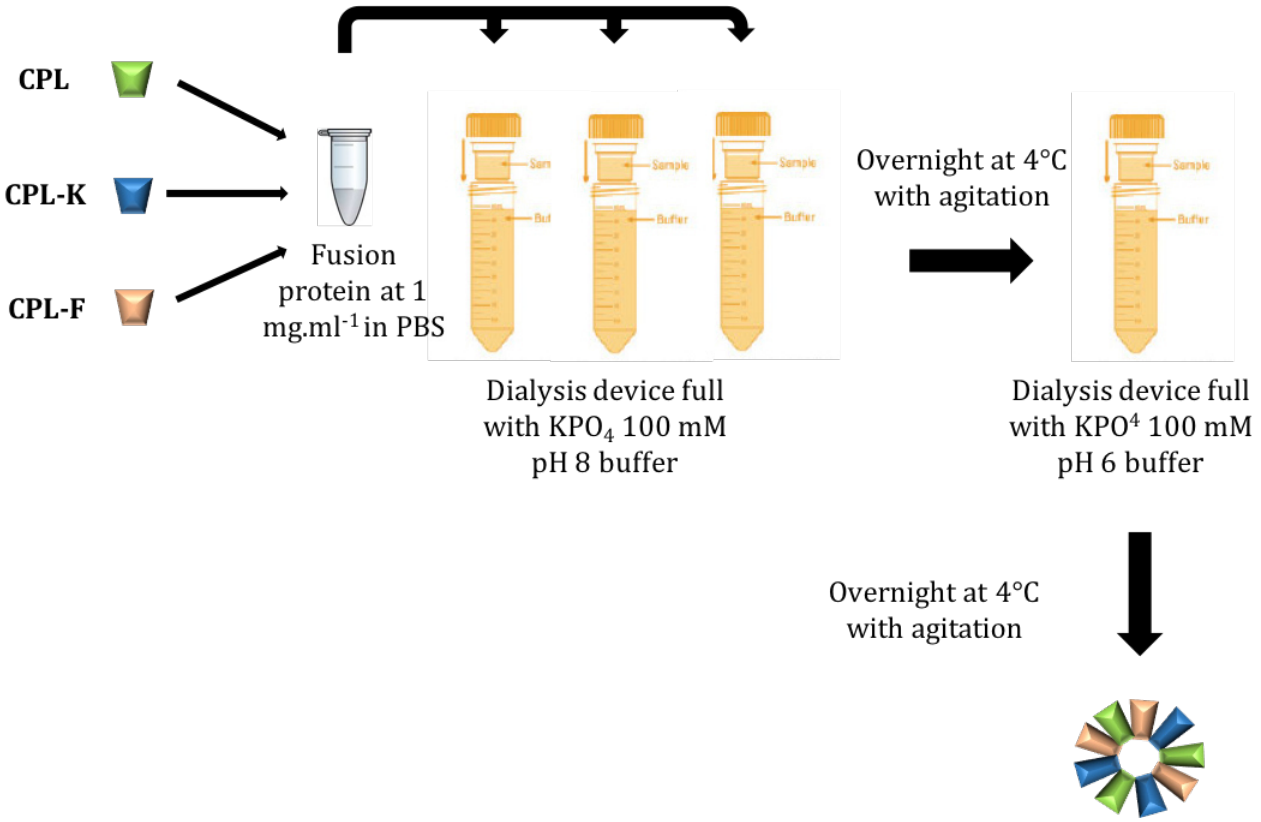

Figure 35: Dialysis procedure.

The different fusion proteins are set at 1 $mg.ml^{-1}$ then put separately in dialysis device with KPO_4 buffer at 4°C overnight to decrease the pH at 8. A second dialysis is then performed to decrease the pH at 6 to form nanoparticles.

4. Fusion protein characterization

4.1. Western blot

Purified proteins were verified by western blot analysis using pre-cast mini PROTEAN TGX Stain-free protein gels (Biorad). Proteins were denatured at 100°C with Laemmli buffer 1x (4x Laemmli Sample Buffer, Bio-Rad) and Dithiothreitol (DTT) for 5 minutes and loaded onto the gels for SDS Gel electrophoresis in Tris/Glycine/Sodium Dodecyl Sulfate buffer (10x TGS buffer, Bio-Rad) at 200V for 20 minutes. Proteins associated with the fluorophore compounds in the gel were imaged under 302 nm UV in a bio-imager (ChemiDoc™ Touch Imaging System, Biorad) and transferred onto nitrocellulose membrane using the Trans-Blot® Turbo™ Transfer System (Trans-blot Turbo, Biorad). The membrane was blocked with blocking buffer consisting of 5% milk (Blotting-Grade Blocker, Bio-Rad) and 0,1% Tween20 in PBS. Then primary antibody was applied to the membrane in blocking buffer and incubated overnight at 4°C with slow shacking. Subsequently, the membrane was washed three times for 5 minutes with PBS-0,1% Tween20 followed by incubation with Horse Radish Peroxidase (HRP)-conjugated secondary antibody diluted in PBS-0,1% Tween20 for 45 minutes under slow shaking at room temperature (RT). The membrane was again washed three times with PBS-0,1% Tween20 and the antibody-tagged protein bands were finally revealed by adding a mix of peroxide and luminol solution (Clarity™ Western ECL Substrate, Bio-Rad) and imaging the resulting luminescence in the bio-imager.

4.2. Dynamic light scattering (DLS)

The size distribution profile of assembled particles in the protein solution was measured by DLS using a Zetasizer Nano Range ZS equipment (Malvern Panalytical, Malvern, UK). 70 µl of protein solution at 1 $mg.ml^{-1}$ were loaded in a cuvette for measurement. The measure was done at 22°C and 50 mM NaCl solution was used as the "blank" control. The particle sizes were analyzed using Malvern software instructions.

4.3. Transmission electron microscopy (TEM)

After dialysis at pH 6, TEM was used for the imaging of created nanoparticles. 10 µl of the protein suspension were placed onto a cupper grid and allowed to dry for 10 minutes. Then, 10 µl of uranyl acetate were added onto the grid and left for 5 seconds before being removed. Subsequently, the sample was observed with a Hitachi H7500 transmission electron microscope at 80kV.

5. Functional assays

5.1. Proximity ligation assay

To test for and visualize an interaction between two proteins, the DuoLink® Proximity Ligation Assay (PLA) was used. In this assay the two proteins are detected by specific antibodies that are conjugated to oligonucleotides. If the two proteins are in close proximity these oligonucleotides are able to interact and can be ligated to a DNA circle together with additional oligonucleotides present in the reaction. The DNA cycle is then replicated by a polymerase and detected with fluorescently labeled oligonucleotide probes that bind to the locally amplified DNA (**Figure 36**).

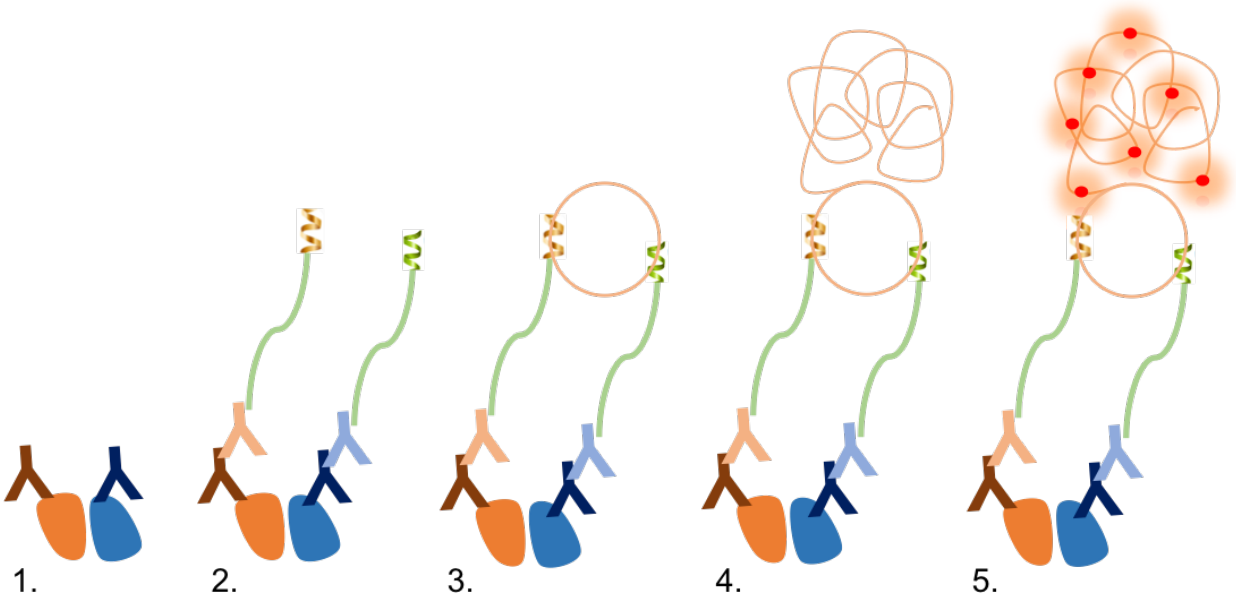

Figure 36: the proximity ligation assay (PLA).

1. Antibodies bind to their respective target receptor. 2. Secondary antibodies conjugated with ribonucleotide probes bind to primary antibodies. 3. Ligation of complementary probes by ligase enzyme thus forming cyclic DNA. 4. Amplification of cyclic DNA by polymerase enzyme. 5. Binding of fluorescent molecules to the amplified DNA.

The assay was performed with reagents provided in a kit (DuoLink® In Situ Detection Reagents Orange, Sigma-Aldrich) and according to the manufacturer's instructions. In brief, cells were plated in UMED medium in an 8-well plate (Permanox Labtek, Dominique Dutscher) and incubated at 37°C and 5% CO_2 (Forma Steri-cycle i160 CO2 Incubator, Thermo Scientific). One day later, cells were incubated for 10 minutes with CPL, CPL-K, CPL-F or CPL-K HER2 and then washed with PBS and fixed with 1% Paraformaldehyde (PFA) for 10 minutes (Paraformaldehyde 32%, Electron Microscopy Sciences). Following fixation, the cells were washed with PBS 2 times for 5 minutes and then incubated overnight at 4°C with a pair of antibodies diluted in PBS targeting the specific proteins (**Table 7**). After washing the samples with PBS 3 times for 5 minutes, they were incubated with secondary, oligonucleotide-conjugated antibodies diluted in PBS (DuoLink® In Situ PLA® Probe, Sigma-Aldrich). The complementary oligonucleotide and DNA ligase were added to form the DNA cycle during 30 minutes

followed by washing with PBS 3 times for 5 minutes and addition of the DNA polymerase. Finally, the fluorescent probes were applied under conditions protected against light. Cells were then mounted with a coverslip using DuoLink ® In Situ Mounting Medium with DAPI (Sigma-Aldrich) and observed with a fluorescence microscope. Sites of protein-protein interaction were detected as individual fluorescent dots. The observation of specific DAPI fluorescence allowed to localize the interactions in relation to the localization of the nucleus and to count them in individual cells. The interactions were quantified by counting the number of dots per image using ImageJ software. The number of dots was divided by number of nuclei in each image to obtain the average number of dots per cell.

Target	Species	Provider
NRP1	Mouse	Evitria
PlexinA1	Rabbit	Abcam ab23391
HER2	Rabbit	Cell signaling #2242S
HER3	Mouse	Millipore clone 2F12
MBP	Rabbit	New England Biolabs E8031S
CP	Rabbit	Homemade
Akt	Rabbit	Cell Signaling 9272S
P-Akt	Rabbit	Cell Signaling 9271S

Table 7: List of antibodies.

5.2. MTT proliferation assay

The MTT assay is a colorimetric assay based on the reduction of MTT, a water-soluble, yellow Tetrazolium salt [(3-(4,5-dimethylthiazol-2-yl)-2,5-diphenyltetrazolium bromide] into blue-violet, water-insoluble Formazan (Mosmann, 1983). To determine

cell proliferation with the MTT proliferation assay, 5 000 cells were plated on a 96-wells plate (Tissue Culture Plate, 96 well, Falcon) in 200 µl of UMED and incubated at 37°C, 5% CO_2. During the next day, the medium was removed and replaced with fresh medium containing the treatment (e.g. CP or CP-peptide at concentration from 10^{-5} M to 10^{-12} M). The cells were allowed to propagate for 48 hours before the culture medium was replaced by 100 µl MTT (Sigma-Aldrich) diluted at 1/50 in Gey's balanced salt solution (GBSS) (Sigma-Aldrich). After incubation for 4 hours at 37°C and 5% CO_2, 100 µl of isopropanol (Propanol-2 GPR RECTAPUR, VWR Chemicals) were added into each well to solubilize the formed formazan crystals. Optical density was measured at 570 nm (Multiskan GO, ThermoFisher).

5.3. MTT toxicity assay

The cells were plated on a 96-wells plate in 200 µl of UMED culture medium and incubated at 37°C, 5% CO_2. The day after, the medium was removed and replaced with fresh medium containing the CP alone or the CP-peptide and incubated for 4 hours at 37°C, 5% CO_2. At the end of the incubation the medium was replaced by 100 µl of MTT diluted in GBSS. The plate was incubated for 4 hours at 37°C, 5% CO_2 then 100 µl of propranolol (VWR Chemicals) were added in each well to solubilize formazan crystals. Optical density was measured at 570 nm (Multiskan GO, ThermoFisher).

5.4. Angiogenesis assay

Human Umbilical Vein Endothelial cells (HUVECs) were cultured at 37°C and 5% CO_2 in Endothelial Cell culture Medium (PromoCell) supplemented with endothelial cell growth supplement (0,004 $ml.ml^{-1}$), fetal calf serum (FCS, 0,02 $ml.ml^{-1}$), human epidermal growth factor (hEGF; 0.1 $ng.ml^{-1}$) and human basic fibroblast growth factor (hbFGF; 1 $ng.ml^{-1}$). For the assay, 15-well plates (ibidi) were coated with matrigel (Millipore) at 37°C for 1 hour. After the coating, five thousand HUVECs cells in 50 µl of culture medium containing test substances at the working concentration or not (control) were added to each well. The plates were incubated for 3 hours (37°C and 5% CO_2). At the end of the

incubation, the cells in each well were photographed under a microscope and the number of closed tubes were counted in 5 wells for each condition.

5.5. Migration assay

Cell migration was analyzed by imaging the number of cells moving away from a cell aggregate formed in hanging droplets of medium. To create these aggregates, U-118MG cells were cultured in UMED medium at 37°C and 5% CO_2 in T75 flask. When the flask had reached 70% confluency, cells were detached with trypsin (0,05% Trypsin-EDTA 1x, gibco®). After 5 minutes, the trypsin was inactivated with culture medium and cells were collected by centrifugation (5 minutes; 800 rpm) at RT and resuspended in 150 µl of medium. A Petri dish of 6 cm diameter was filled with 3 ml of culture medium and 20 µl drops of the cell suspension were deposed on the internal part of the lid of the Petri dish. The lid was then placed to close the dish and to incubate the cells above the medium at 37°C and 5% CO_2 overnight. The following day, aggregates formed by U-118MG cells were removed and cut into pieces of 30-50 µm in size (called aggregates) using tungsten needles under a binocular macroscope. Next, a 12x24 mm glass lamella was placed into a 6 cm Petri dish and coated with 20 µl chicken plasma. 15 to 20 aggregates were added onto the plasma. The plasma was then coagulated by addition of 20 µl thrombin and the whole mixture incubated for 45 minutes at RT. After complete coagulation, DMEM medium was carefully added into the Petri dish to cover the lamella without detaching the plasma clot. Treatments were performed by addition of test substances to the culture medium and incubation at 37°C and 5% CO_2 for 24 hours. Finally pictures of the aggregates were taken and the areas around the aggregates covered with migrated cells was determined with ImageJ software.

6. *In vivo* grafting of tumor cells

6.1. Subcutaneous tumor

To obtain tumor-bearing mice, MDA-MB-231 cells were grafted subcutaneously in 10 weeks-old female immunodeficient mice (Athymic nude mice, Charles River). Prior to

the grafting, cells were grown in a T75 flask and isolated using 3 ml of trypsin. After 5 minutes of incubation at RT, trypsin was deactivated with 3 ml of culture medium. Cells were centrifuged at 800 rpm for 5 minutes and the supernatant was removed. The cells were resuspended in 1 ml of 1x Hank's balanced salt solution (HBSS, gibco®) and aliquots of 1 $x10^6$ cells were created and were kept on ice in 100 µl HBSS until grafting. Mice were anesthetized with 3% isoflurane followed by injection of the cells into the flank using an insulin syringe. Mice were allowed to wake up in a separate box before being placed back to their cages with food and water *ad libitum*. Tumors were allowed to grow until they reached a size of 100 mm^3 before treatments were administered.

6.2. Biodistribution study

CPL, CPL-K Nrp1 and CPL-F Nrp1 were labeled with Alexa 647 via NHS Ester conjugation (Alexa Fluor™ 647 Protein Labeling kit, Invitrogen) following the manufacturer's instructions. In brief, 500 µl of protein at 2 $mg.ml^{-1}$ were stirred with the dye at RT for 1 hour using a magnetic stirrer. At the end of the incubation, the sample was loaded on a purification resin and eluted with PBS to collect the labeled proteins. Labeled proteins were injected in living 10 weeks-old female mice via intraperitoneal injection at a concentration of 10 $\mu g.kg^{-1}$. After specific intervals, mice were anesthetized (3% isoflurane) and placed into a NightOwl imager (Berthold) allowing to follow fluorescent signal in the living animal (**Figure 37**). Images of the fluorescent signal were acquired for 10 seconds (excitation filter 620 nm, emission filter 700 nm). At the end of imaging, the mice were sacrificed to remove organs for separate imaging.

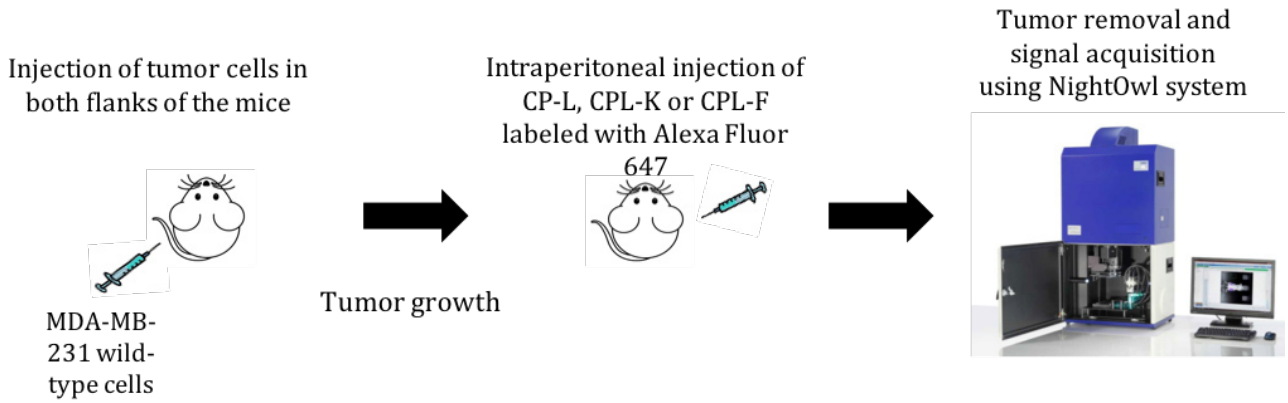

Figure 37: Scheme of the biodistribution experiments.

7. Statistical analysis

Data were analyzed with GraphPad (Prism 5) software. Statistical analyses included the Mann-Whitney test (for sample sizes of $n < 30$) and One-Way ANOVA for comparison between groups. Results are given as mean ± SD and are considered significant with a p-value < 0.05.

VI. Results

1. Development of fusion proteins exhibiting antiangiogenic and antimigratory abilities

Summary

The application of plant virus-derived nanoparticles as nanocarriers for therapeutic agents has gained strong interest in recent years. Especially, TMV has been widely investigated due to its numerous advantages. Indeed, genome and protein structure of TMV are well known thus allowing for genetic and chemical modification. The particles can be assembled *in vitro*, are very stable at a wide range of temperature and pH and do not infect humans.

Glioblastoma is the most frequent and deadly brain cancer. Breast cancer is the most common cancer among women. One subtype of breast cancer, called triple negative breast cancer, is still presenting a bad prognosis due to the lack of a specific treatment. Glioblastoma and triple-negative breast cancer cells are characterized by overexpression of the Nrp1. Thus, these two cancers were used as a model to evaluate our plant virus-derived nanoparticles carrying Nrp1-targeting peptides.

As shown in the attached manuscript, I could demonstrate that CPL-K (CP-linker-"Kill") binds to Nrp1 in cultured cancer cells leading to the disruption of Nrp1 complex formation with PlexA1 as well as to inhibition of downstream Akt survival signaling. Moreover, the application of the CPL-K is shown to inhibit angiogenesis and cell migration. CPL-F (CP-Linker-"Find"), which carries a peptide that does not integrate into the membrane but targets the extracellular domain of Nrp1 also binds to cultured cancer cells and inhibits Nrp1-dependent angiogenesis. Moreover, oligomers/nanoparticles assembled from CPL, CPL-K and CPL-F also show anti-angiogenic effects in a tubulogenesis assay. These observations provide evidence that the CP of TMV can be employed for generating a functionalized nanoparticle with biological activity. By fusing the highly insoluble transmembrane Nrp1 peptide to CP, we achieved the solubilization of this peptide while retaining its antiangiogenic activity.

Functionalized *Tobacco Mosaic Virus* Coat Protein Monomers and Oligomers as Nanocarriers for Anti-cancer Peptides

Coralie Gamper[1,2,3±], Caroline Spenlé[1,2,3±], Sonia Boscá[1±], Michael Van Der Heyden[2-3], Gertraud Orend[2], Dominique Bagnard[2,3*], Manfred Heinlein[1*]

[1]Université de Strasbourg, CNRS, IBMP UPR2357, F-67000 Strasbourg, France

[2]INSERM 1109, MN3T, The Microenvironmental Niche in Tumorigenesis and Targeted Therapy team and Tumor Microenvironment group, 67091 Strasbourg, France

[3]INSERM 1119, BMNST Lab, Fédération de Médecine Translationnelle, Labex Medalis, 67412 Illkirch, France

***** Co-corresponding authors

+ equal contribution

Correspondence should be addressed to:

Dr Manfred Heinlein

Institut de Biologie Moléculaire des Plantes du CNRS IBMP

CNRS - UPR235712, rue du Général Zimmer

67084 STRASBOURG France

manfred.heinlein@ibmp-cnrs.unistra.fr

or

Dr Dominique Bagnard

INSERM U1119- BMNST Lab, Labex Medalis

Pôle API, 300 Bvd S. Brant

67412 Illkirch

bagnard@unistra.fr

Running title: TMV-derived anti-cancer peptides nanocarriers

Keywords: Neuropilin, peptides, TMV, nanoparticles, cancer, angiogenesis

Abstract:

Components with self-assembly properties derived from plant viruses provide the opportunity to design biological scaffolds for the production of nanoscale objects for the ordered display of agents of diverse nature and with complementing functions. With the aim to design a functionalized nanoscaffold to targeting cancer, we tested the coat protein (CP) of *Tobacco mosaic virus* (TMV) as nanocarrier for an insoluble, highly hydrophobic peptide that targets the transmembrane domain of the Neuropilin-1 (Nrp1) receptor in cancer cells. We demonstrate that CPL-K (CP-linker-"Kill") binds to Nrp1 in cultured cancer cells leading to the disruption of Nrp1 complex formation with PlexA1 as well as to inhibition of downstream Akt survival signaling. Moreover, we show that the application of the CPL-K also inhibits angiogenesis and cell migration. CP was also fused to another peptide that does not integrate into the membrane but targets the extracellular domain of Nrp1. This fusion protein (CPL-F, CP-Linker-"Find") binds to cultured cancer cells as well and inhibits Nrp1-dependent angiogenesis. We demonstrate that oligomers/nanoparticles assembled from CPL, CPL-K and CPL-F also show anti-angiogenic effects in a tubulogenesis assay. Our observations provide evidence that the CP of TMV can be employed for generating a functionalized nanoparticle with biological activity. Remarkably, solubilization of the highly insoluble transmembrane Nrp1 peptide in a CP formula retained its anti-angiogenic activity.

Keywords: *Tobacco mosaic virus*, nanoparticle, nanocarrier, cancer, Neuropilin

Conflict of interest: The authors declare no conflict of interest

Introduction:

Nanoparticles play an ever-increasing role as carriers for transporting specific drugs to specific tissues and cells in order to combat diseases [1, 2], such as glioblastoma [3] and breast cancer [4] amongst others. Carrier-mediated drug delivery systems can offer many advantages over delivery of a physical mixture of multiple drugs. The advantages include prolonged half-life in the circulation provided by the carrier, reduced nonspecific uptake and, increased accumulation at the tumor site through passive enhanced permeation and retention (EPR) effects, and/or active targeting by incorporation of targeting ligands, endocytotic uptake thereby bypassing multidrug resistance, and "ratio-metric-dosing", that is, ability to tailor the relative ratios of each agent based on its pharmacological disposition. Moreover, a single delivery system carrying multiple drugs in the same platform can lead to controlled synchronised pharmacokinetics of each drug, resulting in improved treatment efficacy. Also, a single formulation improves solubility and bioavailability. Although many artificial nanoparticle platforms are under development [5], particular attention is given to nature-made nanoparticles based on plant viruses [6-11]. Virus-derived nanoparticles are particularly attractive because they are both biocompatible and biodegradable and show low antigenicity. Viral nanoparticles can be designed and engineered by genetic and chemical protocols. Plant viruses (unlike animal or human viruses) represent a safe platform since they do not cause diseases in humans [12]. Their size is in the nanometer range, thus enhancing permeability of tissues and retention in tumors [13-16]. They are suitable for both chemical and genetic manipulation, allowing the viral coat to be tailored for specific cell or tissue types, imaging purposes, and as a carrier for therapeutic cargo. Their multivalent nature enables the incorporation of multiple functionalities, thus allowing, for example, a cell targeting ligand and an imaging agent to be combined on the same platform [10].

The rod-shaped *Tobacco mosaic virus* (TMV) has been studied for more than a century [17, 18] and is the most economically and scientifically important plant virus [19]. The virus particle is 300 nm long and 18 nm in diameter and consists of a 6.7 kb long RNA encapsidated in a helical arrangement of 2130 identical copies of viral coat protein (CP), which is made of 158 amino acids and the structure of which is known [20-24]. The particle readily assembles *in vitro* [25-27] with a short stretch of 432 nts of its RNA (OAS, origin-of-assembly) that is sufficient for assembly [28]. Without RNA and at neutral pH, the CP assembles into a "20S aggregate

", a 18 nm double "disk" (or "nano-ring") comprising two layers of 17 CP units, which already can be used as nanoscale scaffold [Witus, 2011 #5667]. Dependent on the applied pH, ionic strength, and temperature, the protein can also be isolated as "Protein A" (a mixture of CP monomers, trimers, and pentamers) or helical rods of various length [29, 30]. These assemblies can be generated also with CP recombinantly expressed in *E. coli* [31-36]. The CP has several accessible sites for chemical modification at the outer and inner surface. The protein also offers the possibility to insert peptides at the N and C-terminus, as well as in a loop containing amino acid residues 59-66 for display on the surface of intact virions or CP assemblies [37]. This latter property is interesting because peptides and in particular cell penetrating peptides have clear beneficial effects in the context of cancer disease [38-40]. Among the different therapeutic approaches in which peptides are used, a recent strategy involves a peptide of 30 amino acids that mimics the transmembrane segment of Nrp1 (MTP-NRP1). Nrp1 is expressed in several human tumors where its high levels are associated with invasive tumor growth and worsened clinical outcome [41, 42]. Nrp1 is also highly expressed in tumor associated blood vessels [43]. Blocking Nrp1 signaling reduced tumor angiogenesis and tumor growth [44]. In particular, the MTP-NRP1 peptide was shown to inhibit Nrp1 and associated receptors, thereby blocking downstream signalling and reducing tumor angiogenesis [45-47].

The MTP-NRP1 peptide contains a double canonical GXXXG amino acid motif (G, glycine; x, any amino acid), known to promote and to stabilize interactions between transmembrane protein helices. Any mutation of the glycine residues in the GXXXG motif was shown to interfere with the tumor-suppressing activity of the peptide [45]. As compared to the classical approaches with drugs that target the extra- or intracellular domains of the NRP receptors [48, 49] or their ligand binding site, disruption of Nrp1-mediated signalling platforms by disrupting the interaction of Nrp1 with itself and other receptors within the membrane, represents a novel concept that has proven to inhibit tumor angiogenesis [46]. However, hydrophobic transmembrane peptides are highly insoluble in aqueous solutions and, therefore require the presence of detergents for solubilization. Moreover, due to low solubility, the production and purification of the peptides by chemical synthesis is expensive. In addition, MTP-NRP1 is only active upon integration in the plasma membrane. However, although MTP-NRP1 acts on tumors, it shows a large biodistribution profile in the whole body [46]. To improve delivery at the tumor site it is mandatory to couple this peptide to a targeting

moiety that promotes incorporation in the membrane of target cells only. Indeed, Nrp1 is an ideal candidate for anti-cancer targeting. It is highly expressed in tumor-associated blood vessels [43] and in malignant tumor cell lines, and its high expression correlates with aggressive clinical tumor behavior [41, 42]. A potential targeting moiety that could be combined with MTP-NRP1 is a heptapeptide (ATWLPPR) that was shown to compete VEGFA binding to Nrp1 [50]. This peptide has already been used for a targeted photodynamic therapy to deliver a photosensitizer to the tumor site, which improved tumor reduction [51, 52].

Here, we show a new method for mass production and purification of the highly hydrophobic MTP-NRP1 peptide by fusing it to the CP of TMV (CPL-K, for “kill”). This method was also used to produce a CP fusion protein displaying a three-tandem copy of the heptapeptide ATWLPPR (CPL-F, for “find”). We demonstrate that the fusion proteins are functional and retain the ability to assemble into disks, thus leading to the possibility to create multifunctional plant virus-derived nanoparticles in which the function of the different peptides can be used in a combined “find and kill” strategy, thereby enabling the delivery of biologically active peptides to target-expressing cells.

Results:

Characterization of CP fusion proteins produced in bacteria

Fusion proteins consisting of CP fused to a linker (L, $(GGGGS)_3$) and to the specific peptide at the C-terminus and to a poly-histidine-(His6)-maltose-binding-protein (MBP)-tag at the N-terminus were expressed in *E. coli* and purified on MBP Trap HP columns. As shown in **Figure 1a, b**, the isolated CP fusion proteins showed the expected molecular weight of 59 kDa for CPL, 61 kDa for CPL-K and 62 kDa for CPL-F, respectively in SDS-PAGE gels using the stain free method to visualize particles. Additional bands were also detected around 180 KDa for all constructs presumably due to multimerization of the proteins. Dynamic light scattering (DLS) analysis of recombinant proteins in PBS (pH 7.2) revealed that CPL, CPL-K and CPL-F form monodispersed solutions displaying small particles with hydrodynamic radii of 15.5 nm for CPL, 20 nm for CPL-K and 23 nm for CPL-F (**Figure 1, c-d**).

CPL-K interacts with Nrp1 and competes Nrp1 binding to Plexin A1

We investigated whether CPL-K binds to Nrp1 in living cells with a fluorescent Proximity Ligation Assay (PLA) applied to cultured MDA-MB-231 cells that naturally express Nrp1. We used antibodies recognizing MBP and Nrp1 to reveal the interaction between the recombinant protein and the target receptor. According to the atomic model of CP [21], the N- and C-termini of the CP are very close together. Thus, the N-terminally fused MBP is an excellent reporter for the interaction of the C-terminally fused MTP-NRP1 with NRP1-containing receptor complexes in the membrane of target cells. As shown in **Figure 2a**, only few fluorescent spots corresponding to non-specific binding were detected when1 µM CPL was added to the cells. However, numerous spots were counted when MDA-MB-231 cells were treated with 1 µM recombinant CPL-K protein reflecting the high capacity of CPL-K to bind Nrp1. The specificity of the interaction was assessed in two independent shRNA-expressing MDA-MB-231 cell lines in which *NRP1* was silenced. Indeed, both cell lines showed a significantly lower number of spots, suggesting that the amplification signal (red dot) is generated when CPL-K interacts with Nrp1 (**Figure 2, b-c).** To further demonstrate the interaction of CPL-K with Nrp1, we investigated whether CPL-K can interfere with dimerization of Nrp1 with PlexinA1. Therefore, we

determined the number of Nrp1/Plexin-A1 dimers at the surface of the wild type (WT) cells and in cells knocked down for NRP1. This assay was performed with cells of the glioblastoma U-118MG cell line previously shown to express Nrp1 and Plexin-A1 [53] as well as with cells of the metastatic breast cancer cell line MDA-MB-231, and the knockdown of NRP1 expression in both cell lines was confirmed by RT-qPCR (**Figure 3a, b**). Using the PLA with Nrp1 and PlexinA1 antibodies, numerous fluorescent spots were obtained when MDA-MB-231 and U-118MG cells were incubated with CPL, thus demonstrating that the high level of Nrp1/PlexinA1 dimers is not altered by CPL. Incubation of the cells with CPL-K, however, significantly reduced the number of spots thereby demonstrating the disruption of Nrp1/Plexin-A1 dimers in both cell types. As expected, cells of the respective *NRP1* knockdown lines showed only a low number of spots also in the presence of CPL, confirming the specific detection of Nrp1/Plexin-A1 dimers and their disruption by CPL-K. Quantification of spots revealed that CPL-K disrupted the Nrp1/Plexin-A1 dimers in the WT cells to the level observed in the Nrp1-silenced cells. Taken together, these observations indicate the capacity of CPL-K to bind Nrp1 and to interfere with the dimerization function of Nrp1.

CPL-K inhibits VEGFA-induced tumor cell migration and HUVEC tubulogenesis

We previously showed that disruption of the Nrp1/Plexin-A1 dimer suppresses VEGFA-induced migration of glioblastoma U-118MG cells [53]. To determine whether the CPL-K-induced disruption of NRP1/Plexin-A1 dimers produces similar effects, we performed a 3D migration assay. Therefore, U-118MG cell aggregates were grown in plasma clots in the presence or absence of VEGF and in the presence of either CPL or CPL-K. As seen in **Figure 4a** and **b**, VEGFA increased cell migration, as measured by the total surface of cells around the border of the aggregates in comparison to medium alone. Notably, VEGFA-induced migration was reduced with CPL-K to levels as seen without VEGFA, which was not the case with CPL that did not impact migration. The disruption of the Nrp1/Plexin-A1 complex was previously also shown to inhibit HUVEC tube formation on Matrigel [53]. Interestingly, HUVEC Matrigel tubulogenesis assays showed that CPL-K, but not CPL, has the same effect (**Figure 4 c, d**). Altogether, these results demonstrate that CPL-K inhibits VEGFA-induced migration and HUVEC tubulogenesis. Importantly, the anti-angiogenic activity of CPL-K is similar potent to that published for MTP-NRP1 also reaching a 30 % reduction [46].

CPL-F binds to Nrp1 and inhibits HUVEC tubulogenesis

The heptapeptide ATWLPPR was shown to bind Nrp1 and to facilitate cellular uptake of a coupled photosensitizing agent [51, 52]. To test the ability of this peptide to guide a tagged CP towards Nrp1, we produced a recombinant CPL-F (Find) peptide with three consecutive modules of the ATWLPPR peptide fused to the C-terminus of CP-L. By PLA using antibodies for MBP and Nrp1, we addressed whether CPL-F finds Nrp1 and indeed revealed a significant number of interactions between CPL-F and Nrp1 (**Figure 5a, b**). Next, we wanted to know whether CPL-F had an effect on HUVEC tubulogenesis, which was addressed in a Matrigel tubulogenesis assay. Again, CPL-F strongly inhibited HUVEC tube formation (Figure 5C-D).

CPL-K and CPL-F inhibit Nrp1-dependent Sema3A-induced downstream signaling

As Sema3A binds and activates Nrp1, we investigated whether CPL-F and CPL-K affected the phosphorylation of Act (P-Akt), which is an indicator of downstream signaling [54]. In determining P-Akt in Sema3A-stimulated MDA-MB-231 cells, we found that Sema3A stimulated the phosphorylation of Akt in the presence of CPL but not in the presence of CPL-K and the CPL-F (**Figure 6**). Thus, unlike CPL, CPL-K and CPL-F inhibit the ability of Sema3A to stimulate the signal transduction pathway leading to Akt phosphorylation.

A nanoparticle formulation of CPL/CPL-K/CPL-F inhibits HUVEC tubulogenesis

So far, we have shown that CPL-F and CPL-K are both active in inhibiting endothelial tubulogenesis. However, the two proteins likely act differently since CPL-F binds to the extracellular domain of Nrp1, whereas CPL-K rather interacts with the transmembrane sequences of Nrp1. Although both proteins are active on their own, the question arises whether their effects could be potentiated if combined in the same nanoparticle. As described in previous reports [31-36], bacterially expressed and purified CP can be assembled into different aggregates, which is dependent on pH, ionic strength, and temperature. To design a complex nanoparticle in disk formulation we reasoned that the active molecules (finding and killing moieties) should be spatially arranged in a way that they could reach their biological target and do not interfere with each other. Therefore, we added CPL to buffer the active moieties in an equimolar ratio comprising one third of the mix. In adaptation to reported conditions for the assembly of bacterially produced and modified CP [31], we

generated disk-like nanoparticles (NPs) by dialyzing CPL or an equimolar mixture of CPL, CPL-K, and CPL-F against 100 mM potassium phosphate pH 8.5 and then in a second step against the same buffer at pH 6.0 and 4°C. The presence of disk-like NPs formed from CPL (CPL-NPs) alone or from mixtures of CPL, CPL-K, and CPL-F (KF-NPs) was verified by electron microscopy (**Figure 7a**). To address whether the KF-NPs retained biological activity, we tested their effect in HUVEC Matrigel tube formation assays. As depicted in **Figure 7b-d**, the KF-NPs exhibited a significant anti-angiogenic effect whereas CPL-NPs had no effect.

Discussion:

We evaluated in this study the possibility to generate nanoparticles with anti-cancer properties. The general strategy was to merge three different tools providing a targeting mechanism (to find tumor cells), a tumor growth inhibitory mechanism (to kill tumor cells) and a protein scaffold to assemble the two find and kill moieties. To achieve such a Find and Kill approach we selected two types of peptides that previously have been demonstrated to have targeting (ATW-NRP1][52]) and inhibitory functions (MTP-NRP1 [46, 47]) towards Nrp1, a key molecule in promoting cancer growth. Nrp1 is a multivalent transmembrane receptor interacting with several other transmembrane molecules (mostly receptors) such as Plexin A1 and VEGFR and soluble binding partners such as Sema3A amongst others. Nrp1 exhibits multiple functions as e.g. promoting cell migration and angiogenesis, two properties that well justify targeting Nrp1 in tumors [43, 55]. As Nrp1 is overexpressed in several cancer types [41, 42, 56], it appears as an attractive therapeutic target both for reaching the tumor bed and to block tumor cell expansion in a variety of cancers. Whereas the ATW peptide binds to the ectodomain of Nrp1 and has been previously used as a cancer-targeting tool to enhance the photodynamic destruction of brain tumors [51, 52, 57], the hydrophobic MTP peptide targets the transmembrane domain of the receptor [45] and was shown to efficiently reduce tumor growth in breast or brain tumor models [46, 47]. However, because of its hydrophobic nature the production and solubilization of the peptide is difficult thereby slowing down its development and also presenting a problem in administration. Hence, to succeed in the production of nanoparticles bearing both the ATW and MTP peptides, we had to select a scaffold compatible with the very opposed biochemical/biophysical properties

of the two peptides. We selected the TMV-derived CP protein that had been linked to a short linker sequence (CP-L) and fused this to MBP to enhance solubility for nanoparticle production. This choice was based on previous reports having demonstrated the potency of TMV and TMV-derived proteins to vectorize various peptides and proteins [37, 58, 59]. This approach turned out to be suitable because the CP fusion proteins displaying either the Find (ATW) or the Kill (MTP) peptide sequences could easily be produced. The production reached a high yield with a concentration in the range of mg protein/ml. In solution, the proteins formed mono-dispersed, individual particles. Importantly, while expected for CP fusion protein carrying the hydrophilic ATW-NRP1 peptide (CPL-F), the MTP-NRP1 displaying protein (CPL-K) also was completely soluble without any requirement of detergent or solvent that usually is being mandatory for the solubilization of the native MTP-NPR1 peptide. The removal of the MBP severely impaired the production of CPL-K (data not shown). This is in line with our first trials using engineered TMV for production of the peptides in plants. Here, the high hydrophobicity of the MTP-NRP1 transmembrane peptide led to sequestration of CP to membranes. This blocked the synthesis of the virions, precluding our attempts to produce the peptide on intact virions in infected plants (data not shown). Hence, the bacterial approach we established is solving an important issue for the production and solubilization of MTP-NRP1 and other peptides targeting membrane domain sequences.

We next determined whether the particles conserved the biological properties of the MTP and ATW peptide sequences after fusion with CPL and MBP. The use of a proximity ligation assay confirmed that both the CPL-F and CPL-K particles conserved the capacity of the MTP and ATW peptides to bind Nrp1. The presence of the MBP tag allowed us to detect the MTP-NRP1 peptide at the membrane with specific antibodies thereby providing the most direct evidence for the interaction of the transmembrane domain-interacting peptide with its target inside the membrane, which so far was only indirectly possible by assaying the disruption of Nrp1 complexes by PLA [53]. The specificity of the CPL-F and CPL-K binding to the receptor was confirmed by using cells in which *Nrp1* expression was knocked-down. Remarkably, we observed a background signal with the CPL alone suggesting that this protein may stick to the membrane in a non-specific manner. When addressing the interaction of Nrp1 with Plexin-A1 at the cell surface we demonstrated in cultured U-118MG and MDA-MB-231 cells that the CPL-K peptide was able to disrupt this interaction. Complex disruption

presumably has an impact on the respective downstream signaling. Indeed, by using Sema3A as another Nrp1 interactor [60, 61] we demonstrated that both peptides blocked Sema3A-induced downstream Akt phosphorylation.

As potential anti-cancer tool the peptides should be able to inhibit cancer relevant events. Indeed, we showed that the CPL-F 'Find' and CPL-K 'Kill' particles reduced tumor cell migration and angiogenesis, in particular endothelial tube formation. Altogether, these results prove that the CP formulation of the Find and Kill peptides conserved their biological properties. We next examined whether we could use the self-assembly property of the CP protein to generate multifunctional particles. In adaptation to the protocol used by Bruckman [31], we produced nano-ring-like structures that we could image by electron microscopy. In terms of solubility, and accessibility of the active sites of the Find and Kill peptides in a mixed nanoparticle the relative ratio of CPL to the two other peptides is crucial. Here formation of cis-interactions and the risk of a too high solubility, potentially preventing the hydrophobic moiety to reach the cell membrane, should be considered. Nevertheless, nanoparticles created by assembling an equimolar mix of CPL-L, CPL-F, and CPL-K apparently retained a significant anti-angiogenic effect in the HUVEC-based tubulogenesis assays. The chosen approach of mixing the proteins does not guarantee a homogenous and organized distribution of the Find and Kill sequences within the assembled particles. It can also be expected that the large MBP moieties present on each of the assembled nanoparticle subunits hinders the proper display and optimal accessibility of the active sequences on the particle surface, which may explain the slightly lower anti-angiogenic activity as compared to each of the Find and Kill proteins alone. However, we demonstrate an easy way to produce complex nanoparticles decorated with different peptides by simply mixing the different monomers under conditions favorable for assembly. This proof of concept can now be further developed towards optimization and also for including other peptides with find and kill properties.

Conclusion:

Our data demonstrate that the CP protein of the TMV associated with the MBP protein can be used as a scaffold to assemble particles carrying various peptides with hydrophilic or hydrophobic properties. This polyvalent platform offers unprecedented possibilities to generate smart nanoparticles in high yields and

concentration. Presented here in the form of anti-cancer particles with a Find and Kill potential, the variation of the types of peptides that can be incorporated is almost unlimited.

Material and Methods:

Cell lines

U-118MG and MDA-MB-231 cells were grown in UMED medium consisting of Dulbecco modified Eagle medium (DMEM, Gibco, Thermo Fisher Scientific) supplemented with 10% fetal calf serum (Gibco), 100 µg/ml streptomycin, and 100 IU/ml penicillin (Sigma-Aldrich). MDA-MB-231 RNAi cell lines with reduced *NRP1* expression were generated by using NRP1-targeting shRNAs encoded by MISSION Lentiviral transduction particles (SHCLNV-NM_003873, Sigma-Aldrich). As control for the infected cells, a lentivirus carrying a GFP reporter was used (MISSION® TurboGFP™ Control Transduction particles SHC003V, Sigma-Aldrich). Infected cells were selected with puromycin (1 µg/ml). Two of the five different lentiviruses that were used for Nrp1 silencing showed significant reduced expression of Nrp1 (sh1NRP1 and sh2NRP1). Nrp1 silencing was determined by RT-qPCR. Here, total RNA was extracted using TRIzol Reagent® (Invitrogen), and converted to cDNA with the High-Capacity cDNA Reverse Transcription Kit (Applied Biosystems). Quantitative PCR was performed using the 7500 Real-Time PCR System (Applied Biosystems) and applying PowerUp™ SYBR™ Green Master Mix together with NRP1 primers GAT CATC CTG ATC ACC ATC ATC GCT ATG TCT GCT CTG GTT GTT CTG CTG GTT GCT GTT TGC GTT GTT GTT CTG TAC CGT AAA CGT and AATT ACG TTTA CGG TACA GAA CAA CAA CGC AAA CAG CAAC CAG CAG AAC AAC CAG AGC AGA CATA GCG ATGA TGG TGAT CAG GAT and the TaqMan™ Fast Advanced Master Mix together with hGAPDH Taqman probe (Hs02786624_g1) for normalization.

Plasmids

Bacterial expression plasmids pHis-MBP-CPL, pHis-MBP-CP-L-sNRP1, and pHis-MBP-CPL-3xF encoding CPL, CPL-K, and CP-LF were created by Gateway™ cloning using sequences of parental constructs pTMV-L, pTMV-L-Nrp1, and pTMV-F. pTMV-L-Nrp1 was created by replacing a PacI/KpnI fragment of the TMV cDNA (in

plasmid pUC3/12; [62]) encompassing nucleotides of CP and the TMV 3'UTR with a synthesized PacI/KpnI fragment (pUC-CP-L-NRP1 based on pUC cloning vector pIDTSMART:AMP; Integrated DNA Technologies, Leuven, Belgium) and containing the same part of TMV but in which a sequence encoding a flexible linker peptide (GGGGSGGGGSGGGGS) fused to the Nrp1 peptide (ILITIIAMSALGVLLGAVCGVVLYRKR) was inserted before the CP stop codon. TMV-L-sNrp1 encoding a shorter version of MTP-NRP1 (GVLLGAVCGVVLYRKR), TMV-L not encoding a targeting peptide, and TMV-F encoding one copy of the ATW peptide (ATWLPPR), were created by PCR using pUC-CP-L-Nrp1 as template. For TMV-L-sNrp1, pUC-CP-L-Nrp1 was used together with overlapping primers 5'-AGG CGG TAG TGG CGG AGG GGG TTC CGG AGT TCT CCT TGG TGC CGT CTG TGG-3' (forward) and 5'-CCA CAG ACG GCA CCA AGG AGA ACT CCG GAA CCC CCT CCG CCA CTA CCG CCT-3' (reverse) to shorten the MTP-NRP1-encoding sequence (sequence encoding part of the NRP1 peptide is underlined). After PCR, the methylated (parental) DNA was removed by digestion with DpnI. To remove the NRP1 peptide-encoding sequence from pUC-CP-L-NRP1 and create pUC-CP-L and pUC-CP-F, the forward primer 5'-GGT AGT CAA GAT GCA TAA TAA ATA ACG GATT-3' was used together with 5'-GGA ACC CCC TCC GCC ACT ACC GCC TCC-3' (reverse) or 5´-TCT AGG AGG AAG CCA AGT TGC AGT TGC AGG ACC AGA GGT CCA AAC C-3´ (reverse, sequence encoding the ATW peptide ATWLPPR is underlined), respectively. These primers border the NRP1 sequences to be deleted (for pUC-CP-L) or to be replaced (for pUC-CP-F) on both sides, thus allowing to amplify the rest of the plasmid. Both primers were phosphorylated at the 5' end to re-circularize the plasmid by ligation (T4 ligase). The plasmids pUC-CP-L-sNRP1, pUC-CP-L, and pUC-CP-F were digested with PacI and KpnI and the fragments ligated to the digested TMV, creating the constructs TMV-L-sNRP1, TMV-L, and TMV-F.

To create pHis-MBP-CPL, pHis-MBP-CPL-sNRP1, and pHis-MBP-CPL-3xF, the CPL and CPL-K fragments were amplified from TMV-L-sNRP1 with the primers (attB1 and attB2 recombination sites in bold; TEV protease recognition site in italics) 5'-GGG GAC AAG TTT GTA CAA AAA AGC AGG CTTC *GAA AAC CTG TAC TTC CAG GGT* ATG GCT TAC AGT ATC ACT ACT-3' (forward) and either 5'-GGG GAC CAC TTT GTA CAA GAA AGC TGG GTT TTAGGAACCCCCTCCGCCACTACC-3' (for CPL) or 5'- GGG GAC CAC TTT GTA CAA GAA AGC TGG GTT TTA CCT CTT TCT ATA CAA TAC CAC GCC-3' (for CPL-K) as reverse primer, and cloned into the donor vector pDONR/Zeo (Thermo Fisher Scientific, Waltham, MA, USA) to create pDONR-CP-L and pDONR-CP-L-K. CPL-1F was

amplified from TMV-F with primers 5'-GGG GAC AAG TTT GTA CAA AAA AGC AGG CTT CGA AAA CCT GTA CTT CCA GGG TAT GGC TTA CAG TAT CAC TACT-3' (forward) and 5'- GGG GAC CACT TTG TAC AAG AAA GCT GGG TTT TAT CTA GGA GGA AGC CAA GTT GC-3' (reverse, sequence encoding the ATW peptide ATWLPPR is underlined) and introduced into pDONR/Zeo to create pDONR-CP-F. To triplicate the ATW peptide, pDONR-CP-F was re-amplified with primers (ATW-encoding sequence underlined) 5´-GCA ACT TGG CTT CCT CCT AGA GCA ACT TGG CTT CCT CC-3' (forward) and 5'-TCT AGG AGG AAG CCA AGT TGC AGT TGC AGG ACC AGA GGT CC-3' (reverse), thus adding one additional copy of the ATW sequence to each side of the existing ATW sequence. Following ligation, the resulting plasmid pDONR-CP-3xF was re-amplified with primers 5'-AGG CGG TAG TGG CGG AGG GGG TTC CGC AAC TTG GCT TCC TCC TAG A-3' (forward, linker sequence is underlined) and 5'-CCA CCA GAC CCT CCA CCT CCA GTT GCA GGA CCA GAG GTC C-3' (reverse, linker sequence is underlined) to insert the linker (GGGGSGGGGSGGGGS) in front of the triplicated ATW peptide and creating pDONR-CP-L-3F. The donor plasmids pDONR-CP-L, pDONR-CP-L-K, and pDONR-CP-L-3xF were finally used for recombination with the destination vector pDEST-His-MBP (Addgene, Inc., Cambridge, MA, USA; [63]) to create pHis-MBP-CPL, pHis-MBP-CP-L-sNRP1, and pHis-MBP-CPL-3xF.

Protein Expression and Purification

The recombinant N-terminally His_6-MBP-tagged CP proteins were expressed in BL21 (DE3) pLysS (Novagen) *E. coli* cells upon selection with 100 µg ml^{-1} ampicillin. Cultures (50 ml or 300 ml) were grown for 40 hours at 25°C in ZYM5052 auto-inducing media. Upon lysis with xx proteins were purified on a MBP Trap HP column (GE Healthcare Life Science, Freiburg, Germany) in an ÄKTA Pure chromatography system (GE Healthcare Life Science, Freiburg, Germany) and eluted with 10 mM maltose in PBS. Peak fractions were pooled and dialyzed against PBS pH 7.4 using a HiTrap DST column (GE Healthcare Life Science, Freiburg, Germany). Protein concentrations were determined with NanoDrop 2000 UV-Vis equipment (Thermo Scientific, Wilmington, DE, USA). Protein expression and purification steps were monitored by analysis of total, soluble and eluted fractions by SDS-PAGE.

Electrophoresis gel and western blot

Before protein extraction, cells were treated with CPL-K or CPL at 10^{-6} M during 1hr then stimulated with Sema3A at 100 ng.ml^{-1} during 30 minutes as previously described elsewhere[44]. After lysis in Laemmli buffer (Sigma) supplemented with protease inhibitors (Roche) and phosphatase inhibitor (sodium orthovanadate), protein samples were separated in 4-20% pre-casted polyacrylamide gels (PROTEAN TGX Stain-free protein gels, Biorad) by SDS gel electrophoresis in Tris/Glycine/Sodium Dodecyl Sulfate buffer (Bio-Rad) at 300V for 18 minutes. Proteins were transferred onto nitrocellulose membrane using the Trans-Blot® Turbo™ Transfer System (Trans-blot Turbo, Biorad) and antibodies Akt and phospho-Akt (Cell signaling), and their respective secondary antibodies coupled with HRP (Biorad) were used. The blots were developed with ECL (Biorad), imaged with a bio-imager (Chemidoc™ Touch Imaging System, Biorad), and normalized using the stain free technology.

Dynamic light scattering (DLS) analysis

The size distribution profile of particles in the protein solutions was measured by DLS using a Zetasizer Nano Range ZS equipment (Malvern Panalytical, Malvern, UK). 70 µl of protein solution at 1 mg.ml^{-1} were loaded in a cuvette for measurement. The measurements were done at 22°C and with 50 mM NaCl as empty control. The analysis of particle sizes was performed according to the Malvern software instructions.

Proximity ligation assay (PLA)

Cells were seeded on PERMANOX slides (Lab-Tec) overnight, and then treated with 10 µM CPL, CPL-K or CPL-F monomers for 1 h. After fixation with 1 % para-formaldehyde (PFA) for 10 minutes, cells were permeabilized with PBS containing 0.1 % Triton-x-100. The samples were treated overnight with appropriate combinations of primary antibodies (mouse anti-NRP1 (Evitria)/rabbit anti-MBP (New England Biolabs, E8031S) for detection of CP fusion protein binding to Nrp1; anti-NRP1 (Evitria)/ rabbit anti-PlexA1 (Abcam, ab23391) for detection of receptor protein dimer disruption at 4°C in PBS. Subsequent steps of the assay were performed according to manufacturer's recommendations described in the Duolink In Situ Fluorescence Protocol with

components of the Duolink PLA and Duolink In Situ Detection Orange kits (Sigma-Aldrich). Finally, cells were mounted with a coverslip using Duolink ® In Situ Mounting Medium with DAPI (Sigma-Aldrich). Pictures of the labeled cells were taken using AxioZoom (Zeiss, Axio Imager Z1) using DAPI and wavelength is more appropriate. Fluorescent signals (dots) were quantified with ImageJ software.

Cell migration assay

Cell migration was analyzed by imaging the number of cells moving away from a cell aggregate formed by the hanging drop method (Nasarre et al., 2009). According to this method, U-118MG cells were cultured in UMED medium at 37°C and under 5% CO_2 using a T75 flask. Upon reaching 70% confluency, the cells were detached with trypsin (0.05% Trypsin-EDTA 1x, gibco®), collected by centrifugation (5 minutes; 800 rpm) at room temperature (RT), and resuspended in 150 µl of UMED medium. A Petri dish of 6 cm diameter was filled with 3 ml of culture medium and 20 µl drops of the cell suspension were deposed on the internal part of the lid of the Petri dish. The lid was then placed to close the dish and to incubate the cells above the medium at 37°C and 5% CO_2 overnight. The following day, aggregates formed by the U-118MG cells were removed and cut into pieces of 30-50 µm ('explants'). Next, a 12x24 mm glass cover-slip was placed into a 6 cm Petri dish and coated with 20 µl chicken plasma. Subsequently, 15 to 20 'explants' were added onto the plasma. The plasma was then coagulated by addition of 20 µl thrombin followed by incubation at room temperature. Upon completion of coagulation, DMEM medium was added into the Petri dish to cover the cells. To these cell aggregates CPL proteins were added at 10^{-6}M in culture medium at 37°C and 5% CO_2 for 24 hours. Microphotographs of the cell aggregates were taken (Nikon, Eclipse TS100) and the areas around the aggregates covered with migrated cells were determined with ImageJ software.

Angiogenesis assay

Human Umbilical Vein Endothelial cells (HUVECs) were cultured at 37°C under 5% CO_2 in Endothelial Cell culture Medium (PromoCell) supplemented with endothelial cell growth supplement (ECGS; 4 µl.ml^{-1}), fetal calf serum (FCS, 20 µl.ml^{-1}), human epidermal growth factor (hEGF; 0.1 ng.ml^{-1}) and human basic fibroblast growth factor (hbFGF; 1 ng.ml^{-1}). For the assay, plates (15 u-slide Angiogenesis, Ibidi plates, Biovalley) were

coated with Matrigel (Millipore) at 37°C for 1h. Then five thousand HUVECs cells in culture medium (50 µl) with the CPL proteins at 10^{-6} M were added to each well for 3 hours (37°C, 5% CO_2). The cells in each well were imaged by DIC microscopy (Leitz DM RB, Leica) and the number of closed tubes was counted for 5 wells per condition.

Disk Assembly

To assemble disk oligomers from hybrid CP monomers, the monomer concentration was set to 2 $mg.ml^{-1}$ prior to dialysis, as recommended [31]. The samples were initially dialyzed against 100 mM potassium phosphate pH 8.5 at 4ºC for 24 h in a Slide-A-Lyzer MINI dialysis unit (10 kDa MWCO) to generate the protein A form. For assembly, the sample was dialyzed against 100 mM potassium phosphate pH 6 at 4 ºC for 24 h. To assemble disks from different monomers, equal volumes of the different CPL proteins in 100 mM potassium phosphate pH 8.5 were mixed and dialysis of the mix sample was performed in potassium phosphate at pH 6 for 24 h.

TEM imaging

An 8 µl protein sample was deposited onto a Formvar coated nickel grid for 1 minute. The excess of solution was removed with filter paper. The grid was stained with uranyl acetate (15 µl at 2%) and the excess of stain was removed and dried. Subsequently, the sample was observed with a Hitachi H7500 transmission electron microscope at 80kV.

Statistical analysis

Data were analyzed with GraphPad (Prism 5). Statistical analyses were performed using Mann-Whitney test (for sample $n < 30$) and One-Way ANOVA for comparison between groups. Results are given as mean $\pm$ SD and considered significant for $p < 0.05$.

Acknowledgements

The work has been supported by grants from the University of Strasbourg Institute of Advanced Study (USIAS) and the Ligue Contre Le Cancer (Conférence de Coordination Inter-régionale, 2016 and 2017) to MH, and a PhD fellowship from the Ligue Nationale Contre le Cancer to CG.

Figure Legends

Figure 1: Analysis of CPL, CPL-K and CPL-F. a, b) SDS-Page gel with stain free method to visualize CPL, CPL-K (a), and CPL-F (b) particles. The respective molecules are in the range of the estimated sizes of 59 kDa (CPL), 61 kDa (CPL-K) and 62 kDa (CPL-F). c) DLS measurement of CPL, CPL-K and CPL-F. Measurements were performed three times independently. d) Hydrodynamic radius obtained by DLS for the different proteins.

Figure 2: **CPL-K interacts with Nrp1 in MDA-MD-231 cells.** a, b) Proximity ligation assays (PLA) with MDA-MB-231 cells treated either with 1 µM CPL or 1 µM CPL-K and using antibodies against the cellular Nrp1 protein together with antibodies against the MBP part of CPL and CPL-K. Nrp1 forms complexes with CPL-K (red fluorescent dots) but not with the CPL control protein. Nrp1/CPL-K complexes are formed in normal cells (a) but not in cells of two different cells lines in which Nrp1 expression is knocked down (sh1NRP1, sh2NRP1) (b). Scale bar, 10 µm. c) Quantification of Nrp1/CPL-K interactions (fluorescent dots per cell) in cell lines expressing shRNA constructs or not (C = control). N = 3 experiments, 5 to 10 imaging fields were quantified per condition and replicate experiment. *, $p < 0.05$; ***, $p < 0.0005$, ns>0.05 (non-parametric ANOVA test followed by Dunn's multiple comparison test).

Figure 3: CPL-K disrupts Nrp1/PlexinA1 complex formation. a, b) Downregulation of Nrp1 with shRNA constructs (sh1, sh2) in MDA-MB-231 cells (a) and U-118MG cells (b) as determined by RT-qPCR. c-f) PLA imaging (c, d) and quantification (e, f) of Nrp1/PlexinA1 complex formation as determined by PLA with antibodies for Nrp1 and PlexA1 in the presence of 1 µM CPL or CPL-K with MDA-MB-231 (c e) and U-118MG

cells (d, f) and, upon knockdown of Nrp1. Scale bar, 20 µm. **, $p < 0.005$ (one way ANOVA and Dunn's multiple comparison test).

Figure 4: CPL-K inhibits cell migration and angiogenesis. a, b) Observation (a) and quantification (b) of U-118MG cell migration in a 3D coagulated chicken plasma matrix. Results are normalized to the cell migration observed in medium without VEGFA. The relative surface of migration (%) was determined with Image J. N = 3 independent experiments, 5-30 explants measured per condition for each experiment. *** $p < 0.0001$ ** $p < 0.001$ Mann-Whitney test. c, d) Observation (c) and quantification (d) of HUVEC tubulogenesis on Matrigel 4 hours after seeding in complete medium. Scale bar, 100 µm. Results are normalized to tubulogenesis in the presence of CPL. Note a 37% decrease of tube formation with CPL-K. N = 9 independent experiments. ***p = <0.0001 Mann-Whitney test.

Figure 5: **CPL-F interacts with Nrp1** a, b) Observation (a) and quantification (b) of interaction of CPL and CPL-F with MDA-MB-231 cells as determined by the PLA with antibodies against Nrp1 and MBP. Scale bar, 10 µm. Quantification of Nrp1/CPL and Nrp1/CPL-K complexes per cell. N = 3 independent experiments with 5 - 10 imaging fields analyzed per condition. ***, $p < 0.0001$ Mann-Whitney test. c, d) Observation (c) and quantification (d) of tube formation of HUVECs four hours after treatment with CPL or CPL-F. Scale bar, 100 µm. Note a 52% decrease in the formation of tubes with CPL-F. N = 4 experiments. ***, $p < 0.0001$, Mann-Whitney test.

Figure 6: **CPL-K and CPL-F inhibit Sema3A-induced Akt phosphorylation.** a, b) Representative western blot (a) and quantification of western blot signals (b) of Akt and P-Akt in MDA-MB-231 cells upon stimulation with Sema3A. Note that Sema3A-induced P-Akt levels are suppressed by CPL-K and CPL-F but not by CPL. N = 3 experiments. *, $p < 0.05$, one-way ANOVA and Dunn multiple comparison test.

Figure 7: Characterization of monotype and mixed CPL nanoparticles by EM imaging and effect on angiogenesis. a) TEM images of nanoparticle assemblies (disks) derived from CPL and from a mixture of CPL, CPL-K, and CPL-F (KF). Scale bar, 100 nm. c-d) Observation (b) and quantification (c, d) of the tubule formation by HUVECs in matrigel. The number of tubes per field was measured four hours after cell plating and upon addition of the different CPL assembly formulations. N = 3 experiments, five wells quantified per condition for each experiment. Scale bar, 100 µm. Note that CPL and CPL-NP do not inhibit tube formation. In contrast, particles made of the mixture of CPL, CPL-K and CPL-F (KF-NP) significantly reduce tube formation. N = 3 experiments. ns > 0.01; **, $p < 0.001$ Mann-Whitney test.

References and Notes

1. Emerich, D. F.; Thanos, C. G., *J Drug Target* **2007,** *15* (3), 163-83.
2. Miller, G., *Science* **2012,** *336* (6079), 286.
3. Li, M.; Deng, H.; Peng, H.; Wang, Q., *J Nanosci Nanotechnol* **2014,** *14* (1), 415-32.
4. Saadeh, Y.; Leung, T.; Vyas, A.; Chaturvedi, L. S.; Perumal, O.; Vyas, D., *J Nanosci Nanotechnol* **2014,** *14* (1), 913-23.
5. Lee, J. H.; Nan, A., *J Drug Deliv* **2012,** *2012*, 915375.
6. Czapar, A. E.; Steinmetz, N. F., *Curr Opin Chem Biol* **2017,** *38*, 108-16.
7. Wen, A. M.; Steinmetz, N. F., *Chem Soc Rev* **2016,** *45* (15), 4074-126.
8. Steinmetz, N. F., *Nanomedicine* **2010,** *6* (5), 634-41.
9. Steinmetz, N. F.; Calder, G.; Lomonossoff, G. P.; Evans, D. J., *Langmuir* **2006,** *22* (24), 10032-7.
10. Young, M.; Willits, D.; Uchida, M.; Douglas, T., *Annu Rev Phytopathol* **2008,** *46*, 361-84.
11. Lewis, J. D.; Destito, G.; Zijlstra, A.; Gonzalez, M. J.; Quigley, J. P.; Manchester, M.; Stuhlmann, H., *Nat Med* **2006,** *12* (3), 354-60.
12. Steinmetz, N. F.; Evans, D. J., *Org Biomol Chem* **2007,** *5* (18), 2891-902.
13. Hashizume, H.; Baluk, P.; Morikawa, S.; McLean, J. W.; Thurston, G.; Roberge, S.; Jain, R. K.; McDonald, D. M., *Am. J. Pathol.* **2000,** *156*, 1363-80.
14. Maeda, H.; Wu, J.; Sawa, T.; Matsumura, Y.; Hori, K., *J Control Release* **2000,** *65* (1-2), 271-84.
15. Allen, T. M.; Cullis, P. R., *Science* **2004,** *303* (5665), 1818-22.
16. Cho, C. F.; Ablack, A.; Leong, H. S.; Zijlstra, A.; Lewis, J., *J Vis Exp* **2011,** (52), 2808.
17. Craeger, A. N.; Scholthof, K. B.; Citovsky, V.; Scholthof, H. B., *Plant Cell* **1999,** *11*, 301-8.
18. Scholthof, K. B., *Annu Rev Phytopathol* **2004,** *42*, 13-34.
19. Scholthof, K. B.; Adkins, S.; Czosnek, H.; Palukaitis, P.; Jacquot, E.; Hohn, T.; Hohn, B.; Saunders, K.; Candresse, T.; Ahlquist, P.; Hemenway, C.; Foster, G. D., *Mol Plant Pathol* **2011,** *12* (9), 938-54.
20. Namba, K.; Stubbs, G., *Science* **1986,** *231* (4744), 1401-6.
21. Namba, K.; Pattanayek, R.; Stubbs, G., *J Mol Biol* **1989,** *208* (2), 307-25.

22. Sachse, C.; Chen, J. Z.; Coureux, P. D.; Stroupe, M. E.; Fandrich, M.; Grigorieff, N., *J Mol Biol* **2007,** *371* (3), 812-35.

23. Ge, P.; Zhou, Z. H., *Proc Natl Acad Sci U S A* **2011,** *108* (23), 9637-42.

24. Fromm, S. A.; Bharat, T. A.; Jakobi, A. J.; Hagen, W. J.; Sachse, C., *J Struct Biol* **2015,** *189* (2), 87-97.

25. Fraenkel-Conrat, H.; Williams, R. C., *Proc Natl Acad Sci U S A* **1955,** *41* (10), 690-698.

26. Okada, Y., *Adv Biophys* **1986,** *22*, 95-149.

27. Butler, P. J., *Philos Trans R Soc Lond B Biol Sci* **1999,** *354* (1383), 537-50.

28. Sleat, D. E.; Turner, P. C.; Finch, J. T.; Butler, P. J.; Wilson, T. M., *Virology* **1986,** *155* (2), 299-308.

29. Klug, A., *Philos Trans R Soc Lond B Biol Sci* **1999,** *354* (1383), 531-5.

30. Durham, A. C.; Finch, J. T.; Klug, A., *Nat New Biol* **1971,** *229* (2), 37-42.

31. Bruckman, M. A.; Soto, C. M.; McDowell, H.; Liu, J. L.; Ratna, B. R.; Korpany, K. V.; Zahr, O. K.; Blum, A. S., *ACS Nano* **2011,** *5* (3), 1606-1616.

32. Brown, A. D.; Naves, L.; Wang, X.; Ghodssi, R.; Culver, J. N., *Biomacromolecules* **2013,** *14* (9), 3123-3129.

33. Shire, S. J.; McKay, P.; Leung, D. W.; Cachianes, G. J.; Jackson, E.; Wood, W. I.; Raghavendra, K.; Khairallah, L.; Schuster, T. M., *Biochemistry* **1990,** *29* (21), 5119-26.

34. Zhou, K.; Eiben, S.; Wang, Q., *ACS Appl Mater Interfaces* **2016,** *8* (21), 13192-6.

35. Hwang, D. J.; Roberts, I. M.; Wilson, T. M., *Arch Virol Suppl* **1994,** *9*, 543-58.

36. Dedeo, M. T.; Duderstadt, K. E.; Berger, J. M.; Francis, M. B., *Nano Lett* **2010,** *10* (1), 181-6.

37. Smith, M. L.; Fitzmaurice, W. P.; Turpen, T. H.; Palmer, K. E., *Curr Top Microbiol Immunol* **2009,** *332*, 13-31.

38. Liu, X.; Yang, T.; Han, Y.; Zou, L.; Yang, H.; Jiang, J.; Liu, S.; Zhao, Q.; Huang, W., *ACS Appl Mater Interfaces* **2018,** *10* (37), 31008-18.

39. Klimpel, A.; Lutzenburg, T.; Neundorf, I., *Curr Opin Pharmacol* **2019,** *47*, 8-13.

40. Baig, M. H.; Ahmad, K.; Saeed, M.; Alharbi, A. M.; Barreto, G. E.; Ashraf, G. M.; Choi, I., *Biomed Pharmacother* **2018,** *103*, 574-81.

41. Bielenberg, D. R.; Pettaway, C. A.; Takashima, S.; Klagsbrun, M., *Exp Cell Res* **2006,** *312* (5), 584-93.

42. Grandclement, C.; Borg, C., *Cancers (Basel)* **2011,** *3* (2), 1899-928.

43. Zachary, I., *Chem Immunol Allergy* **2014,** *99*, 37-70.

44. Miao, H. Q.; Klagsbrun, M., *Cancer metastasis reviews* **2000,** *19* (1-2), 29-37.

45. Roth, L.; Nasarre, C.; Dirrig-Grosch, S.; Aunis, D.; Cremel, G.; Hubert, P.; Bagnard, D., *Mol Biol Cell* **2008,** *19* (2), 646-54.

46. Nasarre, C.; Roth, M.; Jacob, L.; Roth, L.; Koncina, E.; Thien, A.; Labourdette, G.; Poulet, P.; Hubert, P.; Cremel, G.; Roussel, G.; Aunis, D.; Bagnard, D., *Oncogene* **2010,** *29* (16), 2381-92.

47. Arpel, A.; Gamper, C.; Spenle, C.; Fernandez, A.; Jacob, L.; Baumlin, N.; Laquerriere, P.; Orend, G.; Cremel, G.; Bagnard, D., *Oncotarget* **2016,** *7* (34), 54723-32.

48. Prud'homme, G. J.; Glinka, Y., *Oncotarget* **2012,** *3* (9), 921-39.

49. Meyer, L. A.; Fritz, J.; Pierdant-Mancera, M.; Bagnard, D., *Cell Adh Migr* **2016,** *10* (6), 700-8.

50. Tirand, L.; Frochot, C.; Vanderesse, R.; Thomas, N.; Trinquet, E.; Pinel, S.; Viriot, M. L.; Guillemin, F.; Barberi-Heyob, M., *J Control Release* **2006,** *111* (1-2), 153-64.

51. Thomas, N.; Bechet, D.; Becuwe, P.; Tirand, L.; Vanderesse, R.; Frochot, C.; Guillemin, F.; Barberi-Heyob, M., *Journal of photochemistry and photobiology. B, Biology* **2009,** *96* (2), 101-8.

52. Bechet, D.; Tirand, L.; Faivre, B.; Plenat, F.; Bonnet, C.; Bastogne, T.; Frochot, C.; Guillemin, F.; Barberi-Heyob, M., *Pharmaceutical research* **2010,** *27* (3), 468-79.

53. Jacob, L.; Sawma, P.; Garnier, N.; Meyer, L. A.; Fritz, J.; Hussenet, T.; Spenle, C.; Goetz, J.; Vermot, J.; Fernandez, A.; Baumlin, N.; Aci-Seche, S.; Orend, G.; Roussel, G.; Cremel, G.; Genest, M.; Hubert, P.; Bagnard, D., *Oncotarget* **2016,** *7* (36), 57851-65.

54. Arpel, A.; Sawma, P.; Spenle, C.; Fritz, J.; Meyer, L.; Garnier, N.; Velazquez-Quesada, I.; Hussenet, T.; Aci-Seche, S.; Baumlin, N.; Genest, M.; Brasse, D.; Hubert, P.; Cremel, G.; Orend, G.; Laquerriere, P.; Bagnard, D., *Cell Rep* **2014,** *8* (6), 1714-21.

55. Geretti, E.; Klagsbrun, M., *Cell Adh Migr* **2007,** *1* (2), 56-61.

56. Jubb, A. M.; Strickland, L. A.; Liu, S. D.; Mak, J.; Schmidt, M.; Koeppen, H., *J Pathol* **2012,** *226* (1), 50-60.

57. Thomas, N.; Tirand, L.; Chatelut, E.; Plenat, F.; Frochot, C.; Dodeller, M.; Guillemin, F.; Barberi-Heyob, M., *Photochem Photobiol Sci* **2008,** *7* (4), 433-41.

58. Folwarczna, J.; Moravec, T.; Plchova, H.; Hoffmeisterova, H.; Cerovska, N., *Prot Expr Purif* **2012,** *85* (1), 152-7.

59. Lomonossoff, G. P.; Wege, C., *Adv Virus Res* **2018,** *102*, 149-176.

60. He, Z.; Tessier-Lavigne, M., *Cell* **1997,** *90* (4), 739-51.

61. Gu, C.; Limberg, B. J.; Whitaker, G. B.; Perman, B.; Leahy, D. J.; Rosenbaum, J. S.; Ginty, D. D.; Kolodkin, A. L., *J Biol Chem* **2002,** *277* (20), 18069-76.

62. Holt, C. A.; Beachy, R. N., *Virology* **1991,** *181*, 109-17.

63. Nallamsetty, S.; Austin, B. P.; Penrose, K. J.; Waugh, D. S., *Protein Sci* **2005,** *14* (12), 2964-71.

Figure 1

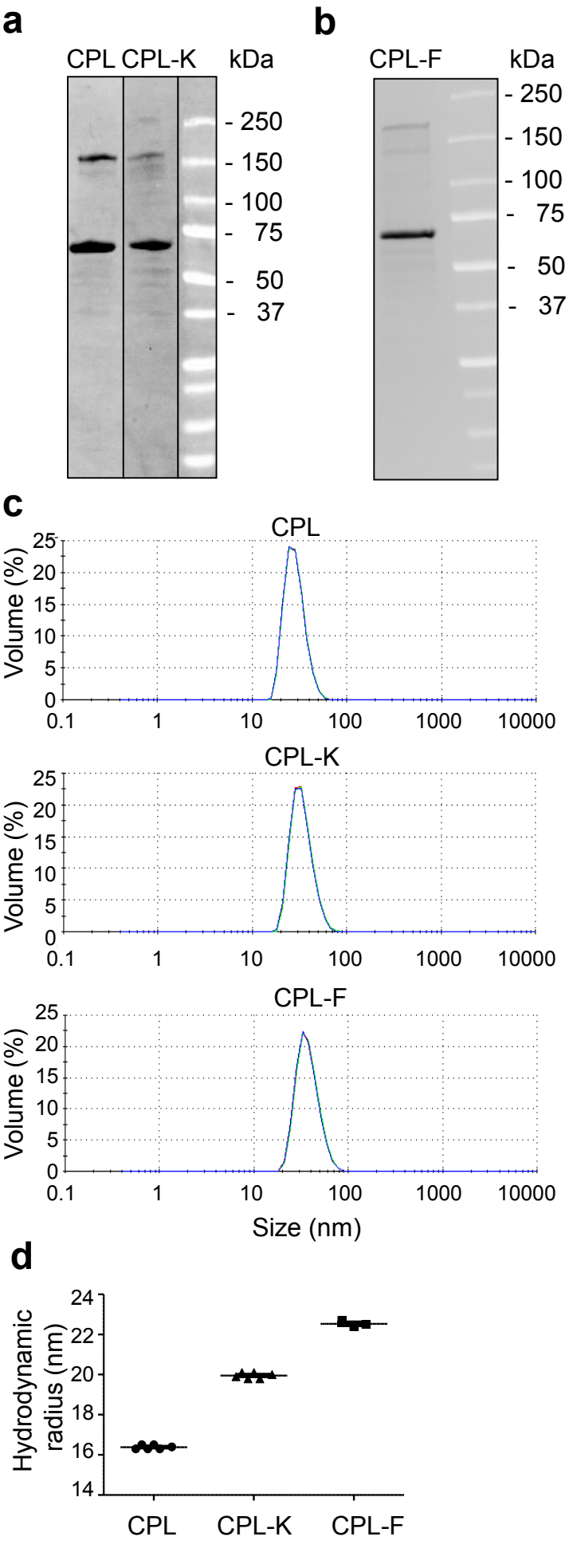
a
CPL CPL-K kDa
- 250
- 150
- 100
- 75
- 50
- 37
b
CPL-F kDa
- 250
- 150
- 100
- 75
- 50
- 37
c
CPL
CPL-K
CPL-F
Volume (%)
0
5
10
15
20
25
0.1
1
10
100
1000
10000
Size (nm)
d
Hydrodynamic radius (nm)
14
16
18
20
22
24
CPL
CPL-K
CPL-F

Figure 2

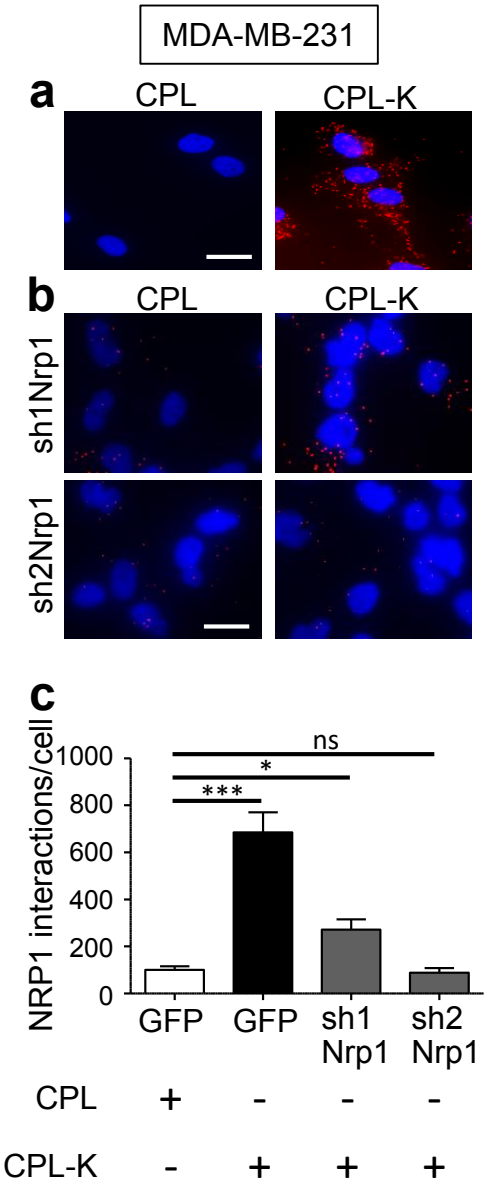
MDA-MB-231
a
CPL
CPL-K
b
CPL
CPL-K
sh1Nrp1
sh2Nrp1
c
NRP1 interactions/cell
1000
800
600
400
200
0
ns
*
***
GFP
GFP
sh1 Nrp1
sh2 Nrp1
CPL + - - -
CPL-K - + + +

Figure 3

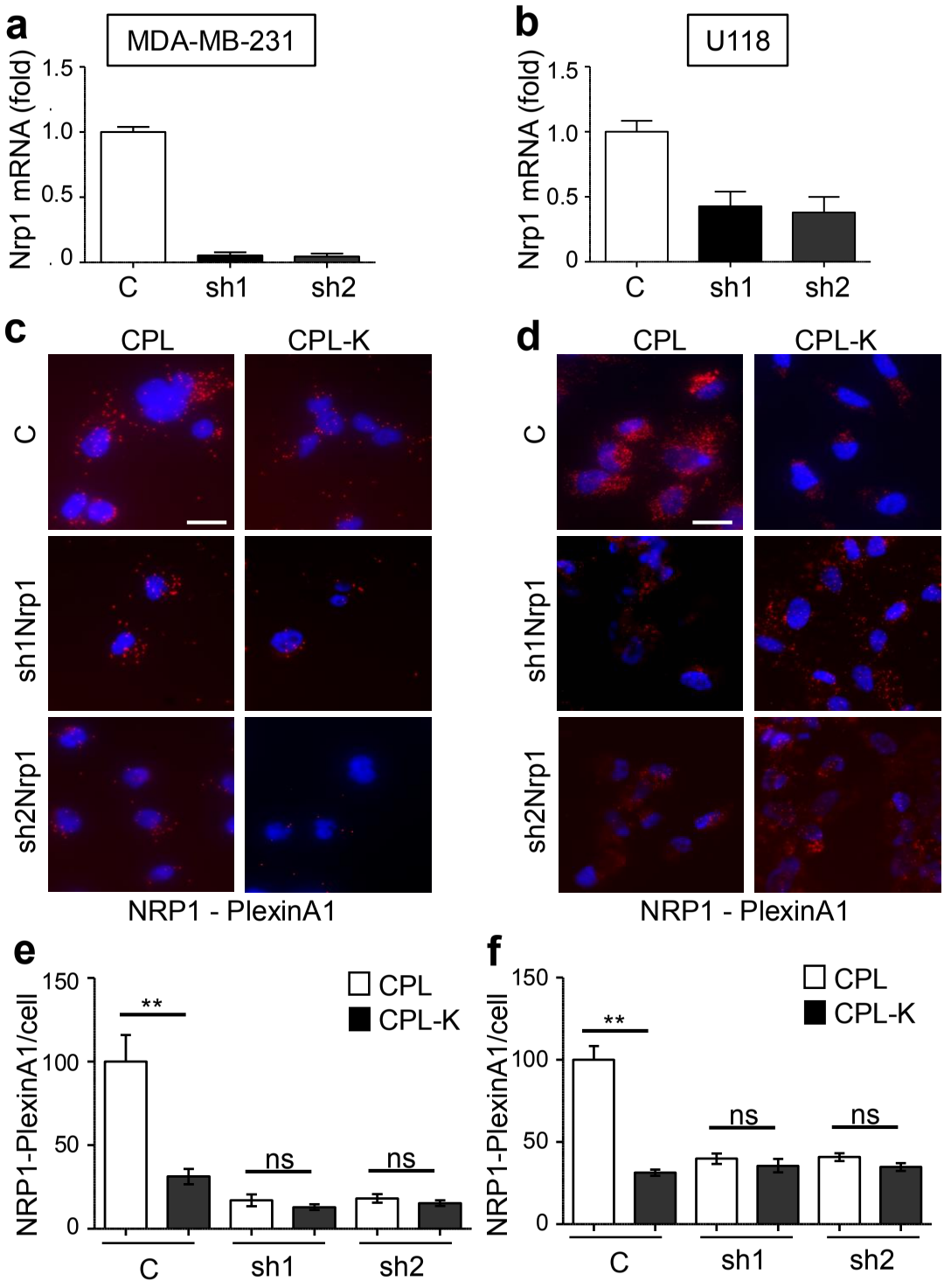
a
MDA-MB-231
Nrp1 mRNA (fold)
1.5
1.0
0.5
0
C
sh1
sh2
b
U118
Nrp1 mRNA (fold)
1.5
1.0
0.5
0
C
sh1
sh2
c
CPL
CPL-K
C
sh1Nrp1
sh2Nrp1
NRP1 - PlexinA1
d
CPL
CPL-K
C
sh1Nrp1
sh2Nrp1
NRP1 - PlexinA1
e
NRP1-PlexinA1/cell
150
100
50
0
**
ns
ns
CPL
CPL-K
C
sh1
sh2
f
NRP1-PlexinA1/cell
150
100
50
0
**
ns
ns
CPL
CPL-K
C
sh1
sh2

Figure 4

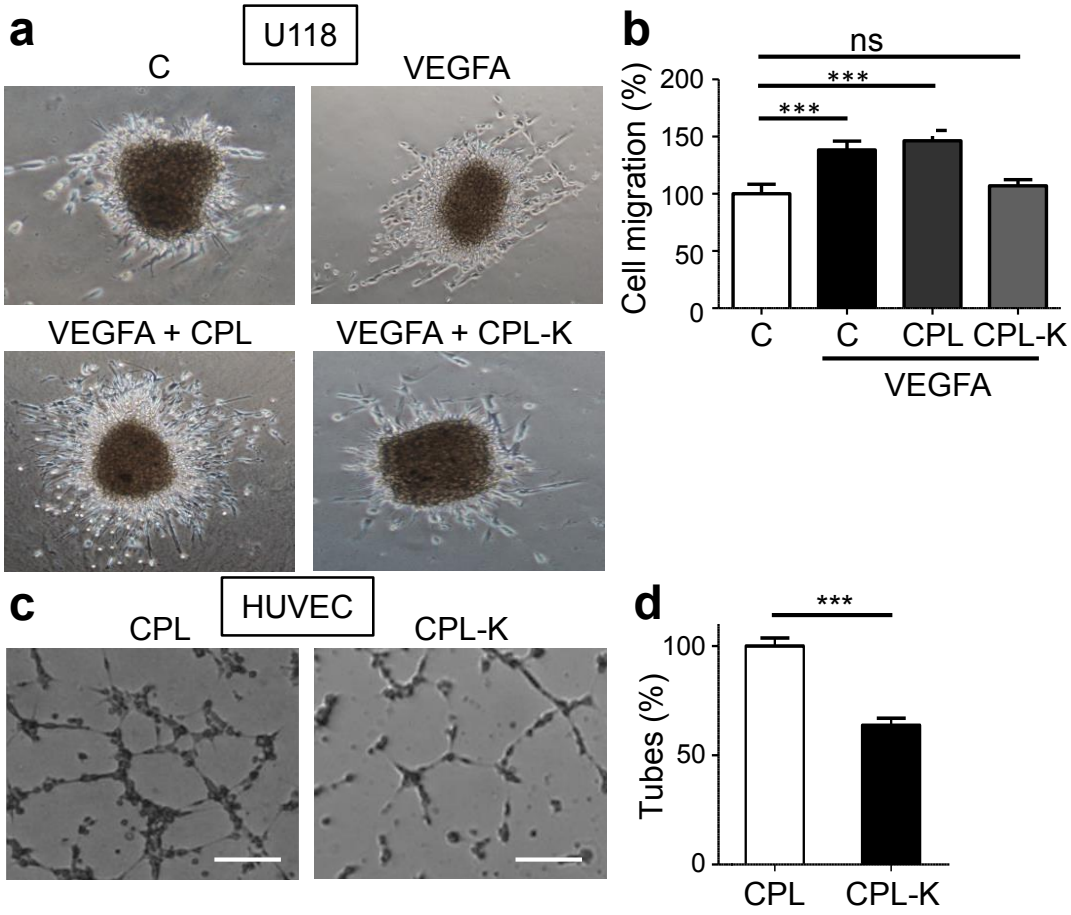
a
U118
C
VEGFA
VEGFA + CPL
VEGFA + CPL-K
b
ns
***
***
Cell migration (%)
200
150
100
50
0
C
C
CPL
CPL-K
VEGFA
c
HUVEC
CPL
CPL-K
d
***
Tubes (%)
100
50
0
CPL
CPL-K

Figure 5

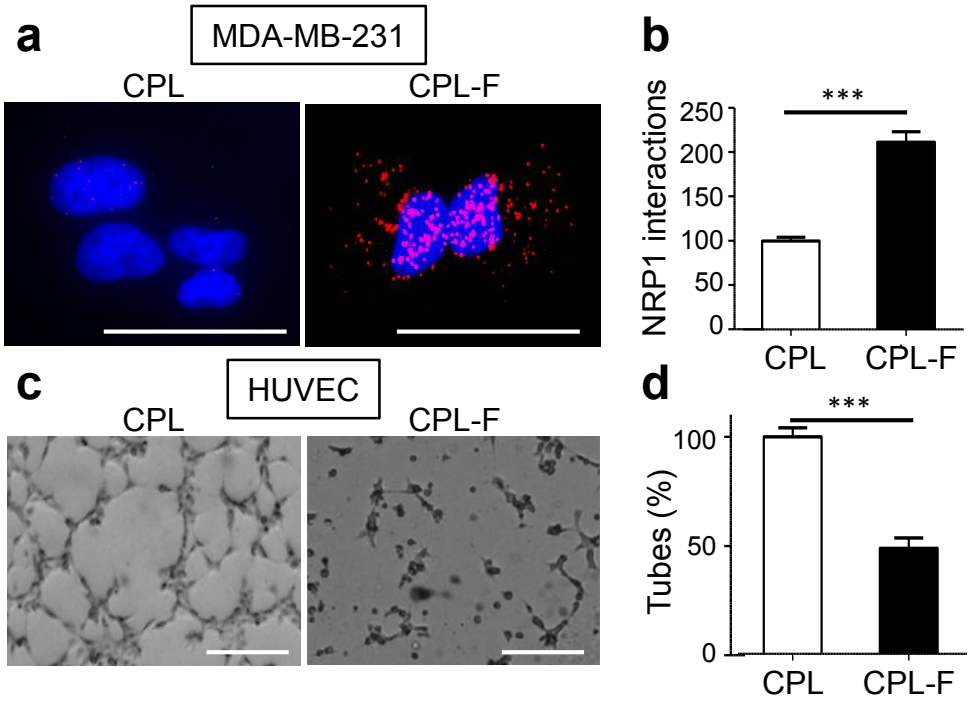
a
MDA-MB-231
CPL
CPL-F
b
NRP1 interactions
250
200
150
100
50
0
***
CPL
CPL-F
c
HUVEC
CPL
CPL-F
d
Tubes (%)
100
50
0
***
CPL
CPL-F

Figure 6

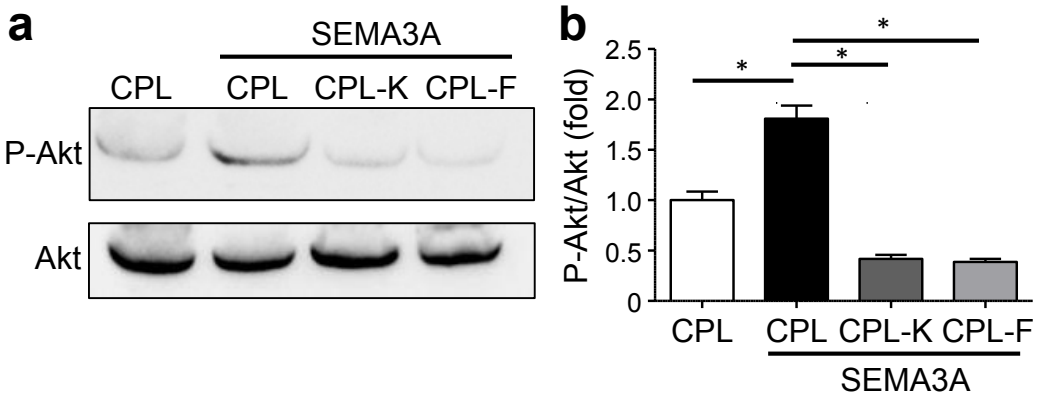
a
SEMA3A
CPL
CPL
CPL-K
CPL-F
P-Akt
Akt
b
P-Akt/Akt (fold)
2.5
2.0
1.5
1.0
0.5
0
*
*
*
CPL
CPL
CPL-K
CPL-F
SEMA3A

Figure 7

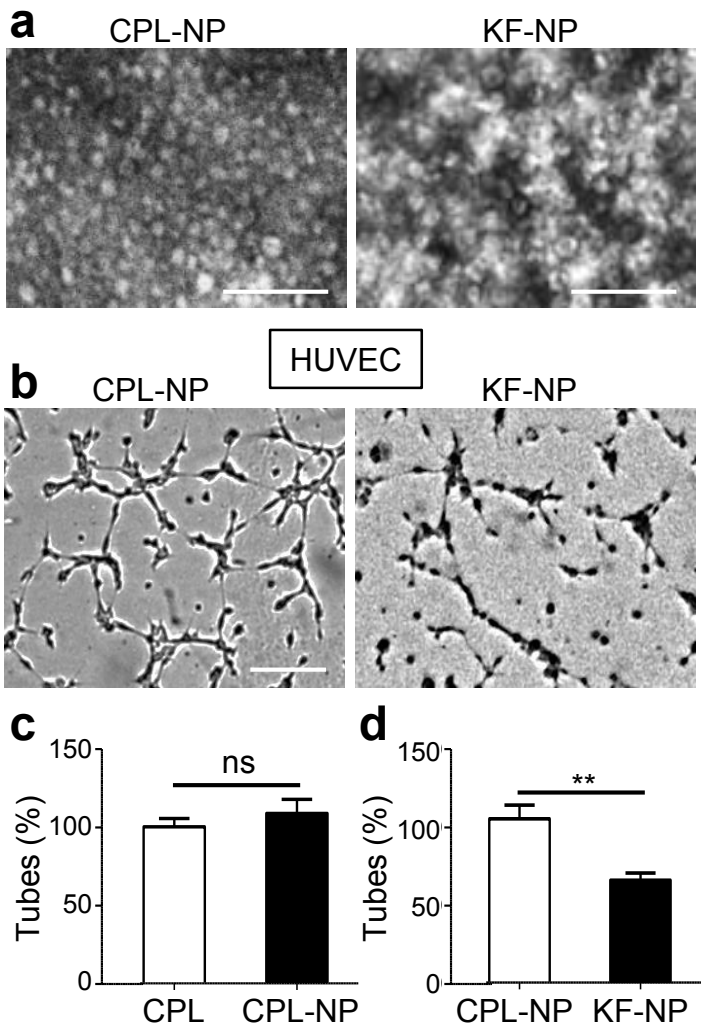
a
CPL-NP
KF-NP
HUVEC
b
CPL-NP
KF-NP
c
Tubes (%)
150
100
50
0
ns
CPL
CPL-NP
d
Tubes (%)
150
100
50
0
**
CPL-NP
KF-NP

2. Biodistribution studies

After the validation of the biological activity of CPL-K and the targeting ability of CPL-F *in vitro,* I investigated the *in vivo* behavior of the fusion proteins through several biodistribution assays. In order to evaluate the behavior of the fusion proteins in the murine organism, CPL, CPL-F and CPL-K were labeled with Alexa 647 fluorophore using a commercial kit as described in paragraph V.6.6.2.

2.1. Biodistribution of CPL-F and CPL-K on tumor-bearing mice

To address the potential selective tissue enrichment of the peptides in disease conditions, I examined their biodistribution in immunodeficient nude tumor-bearing mice. In the first experiment I compared the biodistribution of $CPL^{Alexa647}$ and $CPL\text{-}F^{Alexa647}$ while in another experiment the biodistribution of $CPL^{Alexa647}$ was compared with that of $CPL\text{-}K^{Alexa647}$. 10 weeks old mice were grafted by subcutaneous injection of MDA-MB-231 cells into the left flank. When the tumor reached the size of 100 mm^3, the mice were randomized between the $CPL^{Alexa647}$ group and the $CPL\text{-}F^{Alexa647}$ group for the first experiment and between the $CPL^{Alexa647}$ group and the $CPL\text{-}K^{Alexa647}$ group for the second experiment. Each group was composed of six mice. Following intraperitoneal injection, the biodistribution patterns of $CPL^{Alexa647}$, $CPL\text{-}F^{Alexa647}$ and $CPL\text{-}K^{Alexa647}$ indicate a classical profile for peptides with a rapid elimination process from the body. Interestingly, the images of whole mice showed some retention of $CPL^{Alexa647}$ in tumors even after 24 hours, whereas $CPL\text{-}F^{Alexa647}$ did not. Dissection of organs of mice 1 hour (**Figure 38**) or 24 hours (**Figure 39**) after injection with dye-labeled $CPL^{Alexa647}$, $CPL\text{-}F^{Alexa647}$ and $CPL\text{-}K^{Alexa647}$ showed the majority of the proteins being present in kidneys and liver and all of them were also present in tumors, thus revealing no difference in the specific targeting / retention between $CPL^{Alexa647}$, $CPL\text{-}F^{Alexa647}$ and $CPL\text{-}K^{Alexa647}$. However, the distribution of the proteins may be dictated by various strong but unspecific parameters that overshadow the specific effect of Nrp1-targeting peptides.

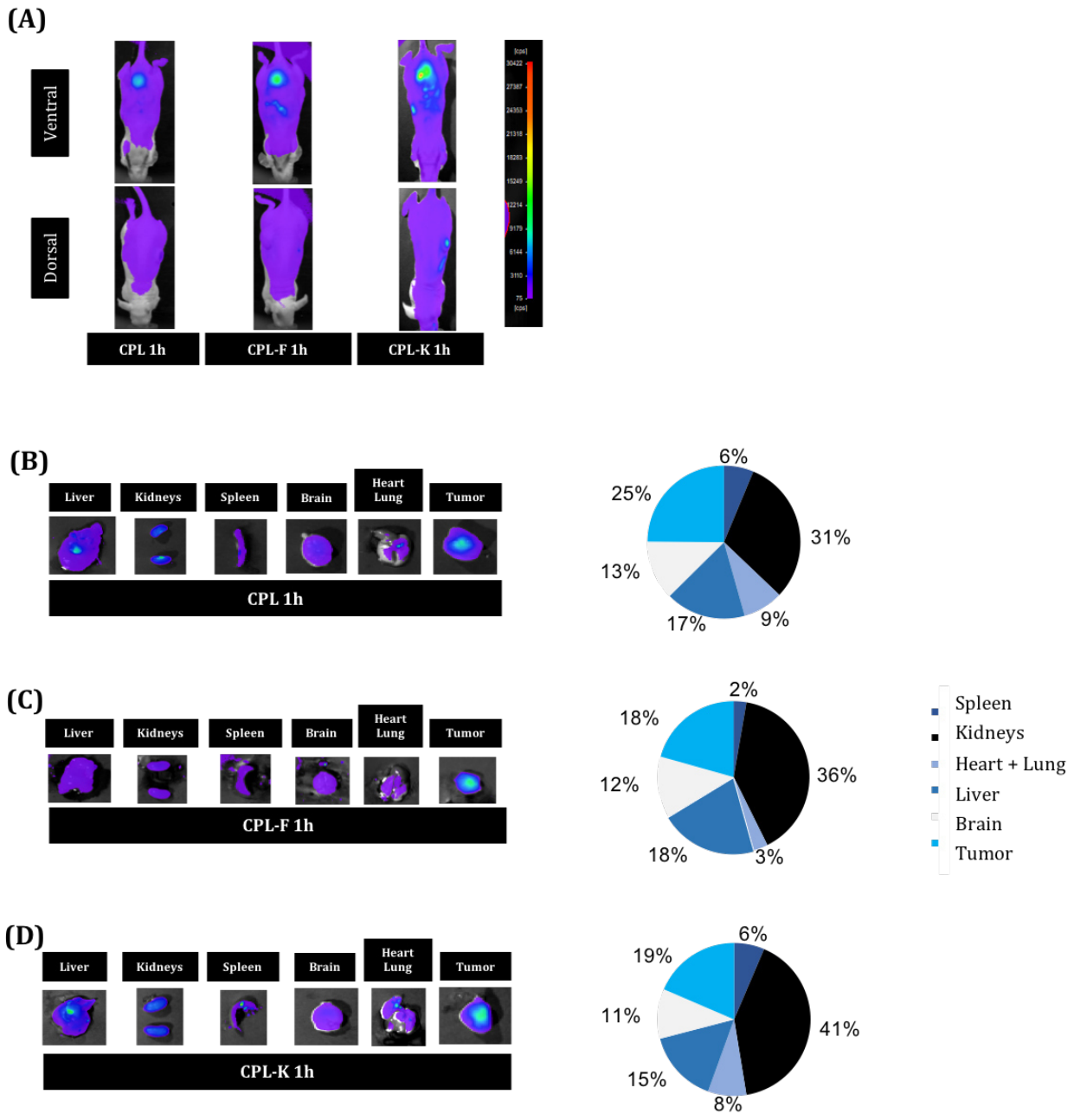

Figure 38: Biodistribution of CPL, CPL-F and CPL-K on tumor-bearing mice at 1hr after intraperitoneal injection.

(A) Signal acquired for one representative mouse for each condition 1h after intraperitoneal injection. Upper row ventral view, lower row dorsal view. (B) Representative collection of organs removed 1h after intraperitoneal injection of CPL, (C) CPL-F or (D) CPL-K. Their respective graphs show the repartition of the mean total signal acquired between the different organs. N = 3 mice per experimental group.

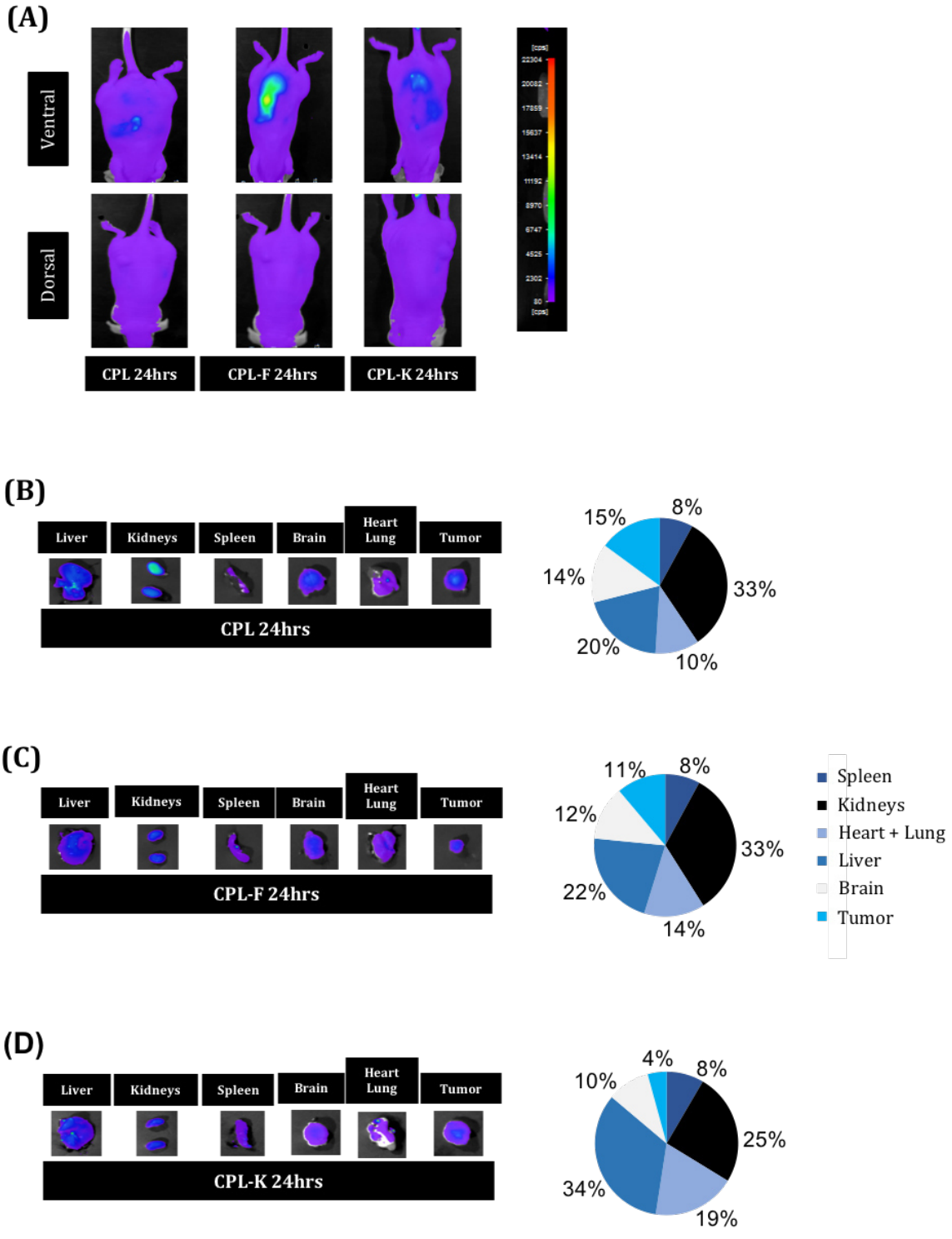

Figure 39: Biodistribution of CPL, CPL-F and CPL-K on tumor-bearing mice at 24hrs after intraperitoneal injection.

Images of organs from animals injected with: (A) CPL$^{Alexa\ 647}$ and corresponding graphs of mean signal repartition, (B) CPL-F$^{Alexa\ 647}$ and corresponding graphs of mean signal repartition or (C) CPL-K$^{Alexa\ 647}$ and corresponding graphs of mean signal repartition. N = 3 mice per experimental group.

These results highlight that the CPL without any peptide tends to show retention in many organs and in the tumor (up to 25% of the total signal). In order to verify whether the CPL is driving the biodistribution of the peptides thereby masking the finding property of CPL-F particles, we decided to repeat the experiments with mice grafted with wild-type MDA-MB-231 cells in comparison to mice grafted with MDA-MB-231 cells in which the expression of Nrp1 is diminished by silencing.

2.2. Biodistribution of CPL-F and CPL-K in mice bearing wild-type tumors versus mice bearing tumors knocked-down for Nrp1

In order to evaluate the specific targeting of CPL-F *in vivo*, a double tumor model was used. Here, immunodeficient nude mice were grafted with $1x10^6$ MDA-MB-231 wild-type cells in one flank and $1x10^6$ MDA-MB-231 cells knocked-down for Nrp1 into the other flank. When the tumors in both flanks had reached 100 mm^3 in size, the mice were randomized into two groups. One mouse had to be removed from the study because it didn't develop a wild-type tumor. One group of two mice was injected with $CPL^{Alexa647}$ and the other group of three mice was injected with $CPL\text{-}F^{Alexa647}$ (both compounds at 10 $\mu g.kg^{-1}$). At 1 hour post-injection, the mice were sacrificed and the tumors removed to acquire images of the fluorescent signal distribution (**Figure 40A**). For normalization of signal between tumors, the signal in each tumor was divided by the tumor area. The observations derived from this experiment indicated no difference between the wild-type tumor and the knock-down Nrp1 tumor in the $CPL^{Alexa647}$ group. However, the $CPL\text{-}F^{Alexa647}$ signal was reduced in the Nrp1 knock-down tumors as compared to the wild-type tumors (-35%).

While not reaching statistical significance this experiment showed the selectivity of the F peptide for Nrp1. However, the strong non-specific signal observed with CPL prevented a clear demonstration of the finding capability of CPL-F (**Figure 40B**).

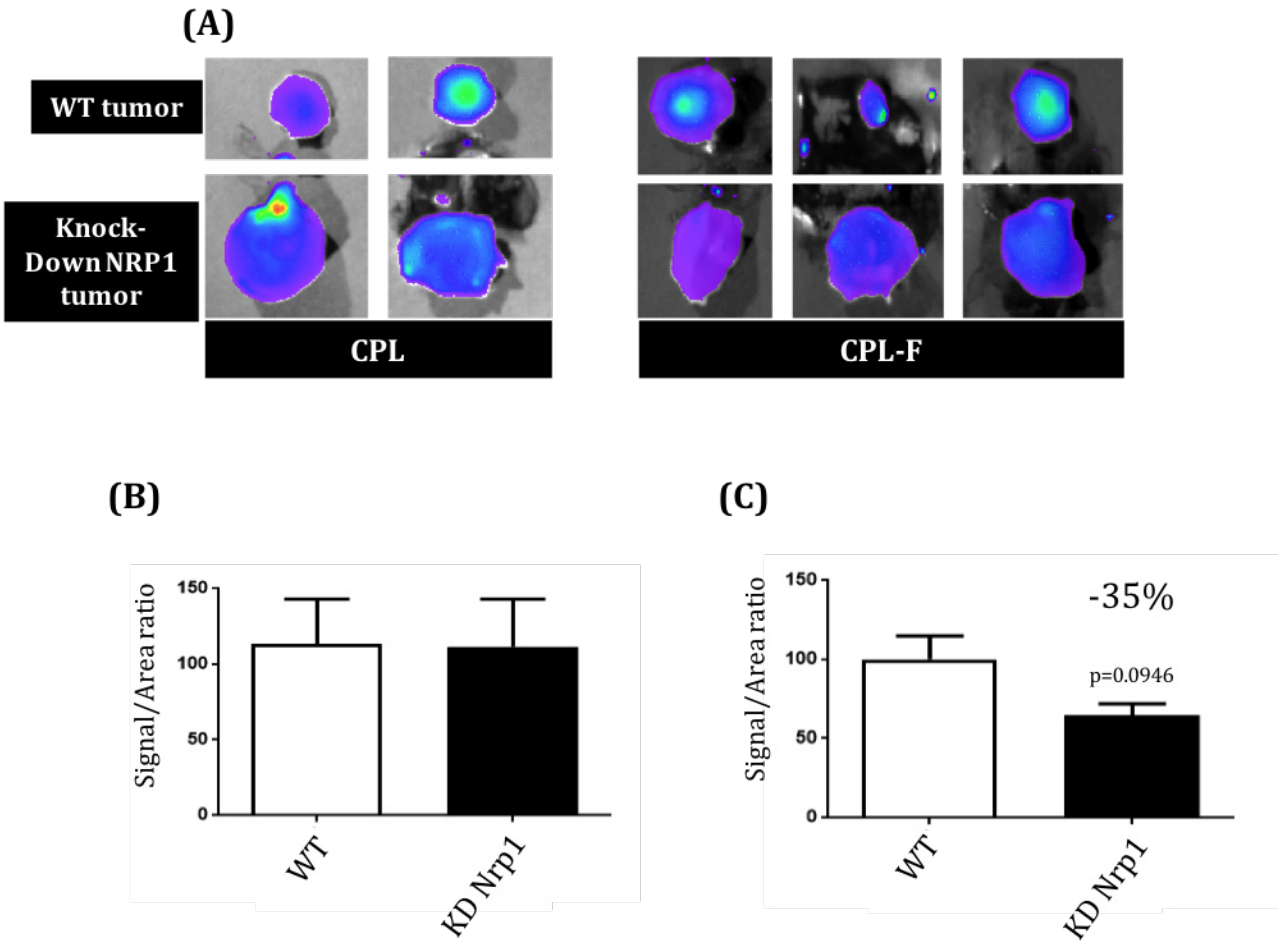

Figure 40: Tumor targeting of CPL-F.

(A) Images of extracted tumor 1h after intraperitoneal injection. Upper row WT tumors, lower row tumors knock-down for Nrp1. (B) Signal/Area ratio acquired for mice injected with CPL Alexa 647 for both tumor type. There is no significant difference between signal acquired in WT tumor compared to knock-down tumor. N= 2 mice. (C) Signal/Area ratio acquired for mice injected with CPL-F Alexa 647 for both tumor type. N= 3 mice. There is a tendency showing less signal in the knock-down Nrp1 tumor but it is not statistically significant. P=0.0946 Mann-Whitney test.

2.3. Biodistribution of CPL-F on immunocompetent mice

The biodistribution of injected CPL-F was also tested in immunocompetent mice. Here, six C57BL/6 mice were randomized between two groups. One group was treated with 10 $\mu g.kg^{-1}$ $CPL^{Alexa647}$ and the other group was treated with 10 $\mu g.kg^{-1}$ $CPL\text{-}F^{Alexa647}$. Fluorescent imaging of the injected mice revealed that the $CPL^{Alexa647}$ and $CPL\text{-}F^{Alexa647}$ proteins are distributed throughout the mouse body within 5 minutes and accumulate in

the bladder after 4 hours, thus indicating a rapid elimination profile (**Figure 41**). Imaging of dissected organs revealed no significant difference in the biodistribution at three different time points after injection (5 minutes, 1 hour, 24 hours). As in the previous experiment, the intensity of fluorescent signal was divided by the area of the measured organ for normalization. Figure 34 shows the signal distribution for each time point.

At 5 minutes post-injection, 49% and 48% of the total signal was localized in the kidneys in the $CPL^{Alexa647}$- and in the CPL-$F^{Alexa647}$- group, respectively. The second major organ that displayed a strong signal was the liver with 33% of the total signal in the $CPL^{Alexa647}$ group and 40% in the CPL-$F^{Alexa647}$ group. In both groups, the remaining signal s was localized in the brain (14% and 8%) and in the heart-lung (4% for each group).

At 1 hour post-injection, the kidneys still exhibited the majority of the signal in the $CPL^{Alexa647}$ and CPL-$F^{Alexa647}$ groups (30% and 44% respectively). Similarly as was already seen after 5 minutes, the liver showed 27% of the total signal in $CPL^{Alexa647}$ group and 26% in the CPL-$F^{Alexa647}$ group. The percentage of signal acquired in the heart-lung was 23% in the $CPL^{Alexa647}$ group and 19% in the CPL-$F^{Alexa647}$ group. Moreover, at that time point a fluorescent signal was also detectable in the spleen of both groups, representing 17% of the total signal in the $CPL^{Alexa647}$ group and 11% in the CPL-$F^{Alexa647}$ group. While a weak signal was detected in the brain of $CPL^{Alexa647}$ group mice (only 2% of the total signal), no signal was detected in the brain of the CPL-$F^{Alexa647}$-treated mice.

At 24 hours post-injection, the majority of the fluorescent signal was detected in the kidneys (37% in both groups). 28% and 37% of the fluorescent signal accumulated in the liver in the $CPL^{Alexa647}$ and CPL-$F^{Alexa647}$ groups, respectively. Fluorescent signal in the brain of mice in the $CPL^{Alexa647}$ group represented 17% of the total whereas that in the CPL-$F^{Alexa647}$group represented 16%. 13% of the total fluorescent signal accumulated in the heart-lung of the $CPL^{Alexa647}$ group, whereas the CPL-$F^{Alexa647}$ group accumulated only 2% of the total signal in this tissue. The spleen accumulated 4% and 8% of the total fluorescent tissue signal in the $CPL^{Alexa647}$ and CPL-$F^{Alexa647}$ groups, respectively.

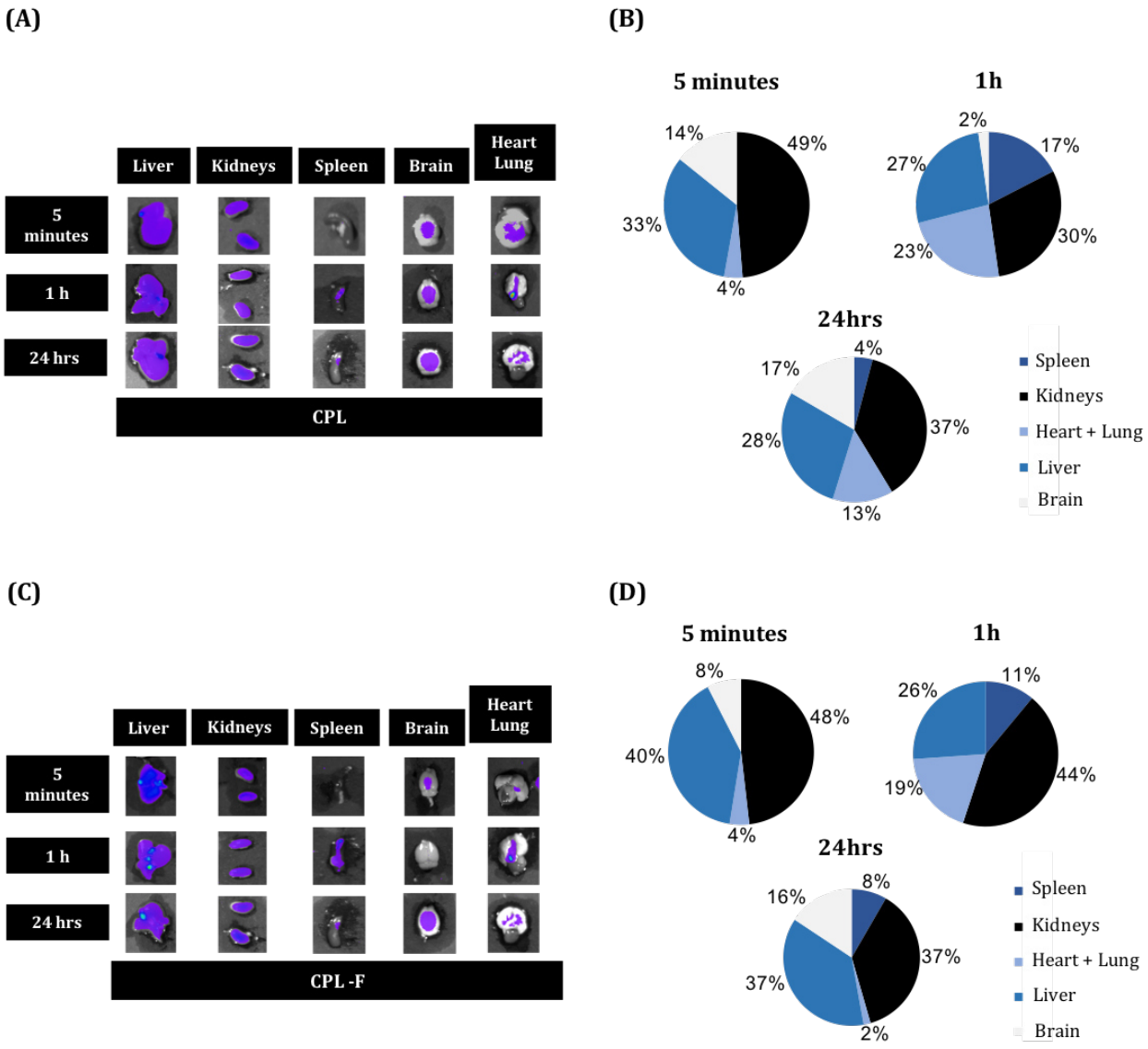

Figure 41 : Biodistribution of CPL-F in immunocompetent mice.

C57BL/6 mice were injected intraperitoneally with CPL or CPL-F labeled with Alexa 647 and organs were removed at different time point post-injection: 5 minutes, 1 hour and 24 hours. (A) Collection of organs from a representative mouse injected with CPL for each time point. (B) Graphs of signal repartition in the different organs at each time point for mice injected with CPL. N=3 mice. (C) Collection of organs from a representative mouse injected with CPL-F for each time point. (D) Graphs of signal repartition in the different organs at each time point for CPL-F. N=3 mice.

This experiment has shown that the CPL and CPL-F fusion proteins are taken up by the classical elimination organs, i.e. the kidneys and the liver. There was also detectable signal in Nrp1-expressing tissues (brain, heart-lung). However, overall, the

two proteins showed similar distribution profiles with only minor variations. Importantly, fluorescent signal was still detectable after 24 hour time point which suggests that the proteins undergo retention and delayed elimination.

3. Extension of the strategy with other peptides

In parallel with the analysis of the CPL-F and CPL-K *in vivo* biodistribution, I fused CPL with other peptides for targeting of other cancer-related mechanisms. The first peptide as a new alternative "killing" peptide known to interfere with the HER2 receptor transmembrane domain (MTP-HER2) (Arpel et al., 2014). The second alternative peptide binds to the extracellular matrix protein TNC, which is enriched around cancer tissues, and was tested as an alternative "finding" peptide.

The construct coding for His-MBP-CPL-HER2 (CPL-K HER2) was engineered in the lab whereas the other plasmid construct coding for His-MBP-CPL-TNC (CPL-F TNC) was synthesized by a company (Genescript). The CPL-K HER2 and CPL-F TNC fusion proteins were produced in *E. coli* and showed the expected molecular size upon SDS gel electrophoresis (**Figure 42**). The proteins also occur in higher molecular weight forms which may due to the presence of oligomers as described for the Nrp1 derived peptides.

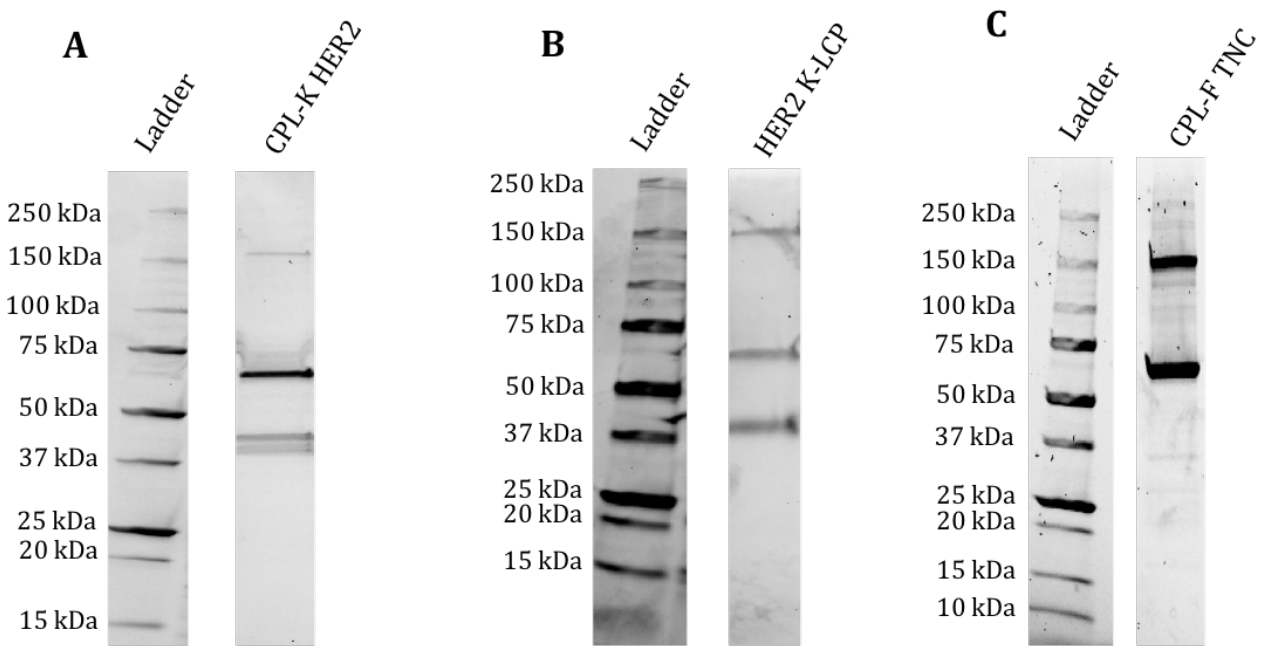

Figure 42: Gel migration of CP fusion protein.

Protein gel showing the migration of (A) CPL-K HER2, (B) HER2 K-LCP and (C) CPL-F TNC.

3.1. CPL-K HER2 induces a reduction of Akt phosphorylation level, binds to HER2 receptor and is able to disrupt its interaction with HER3 receptor

Using the proximity ligation assay with MCF-7 cells it was shown that CPL-K HER2 binds to HER2 receptor (**Figure 43A-B**). Moreover, the same assay demonstrated that the treatment of MCF-7 cells with CPL-K HER2 inhibits the interaction of between HER2 and HER3 receptors by 25 % (**Figure 43C**). The treatment of the cells with CPL-K HER2 also led to a reduction in Akt phosphorylation (**Figure 43D-E**), thus indicating that CPL-K HER2 has the capacity to interfere with downstream signaling pathways.

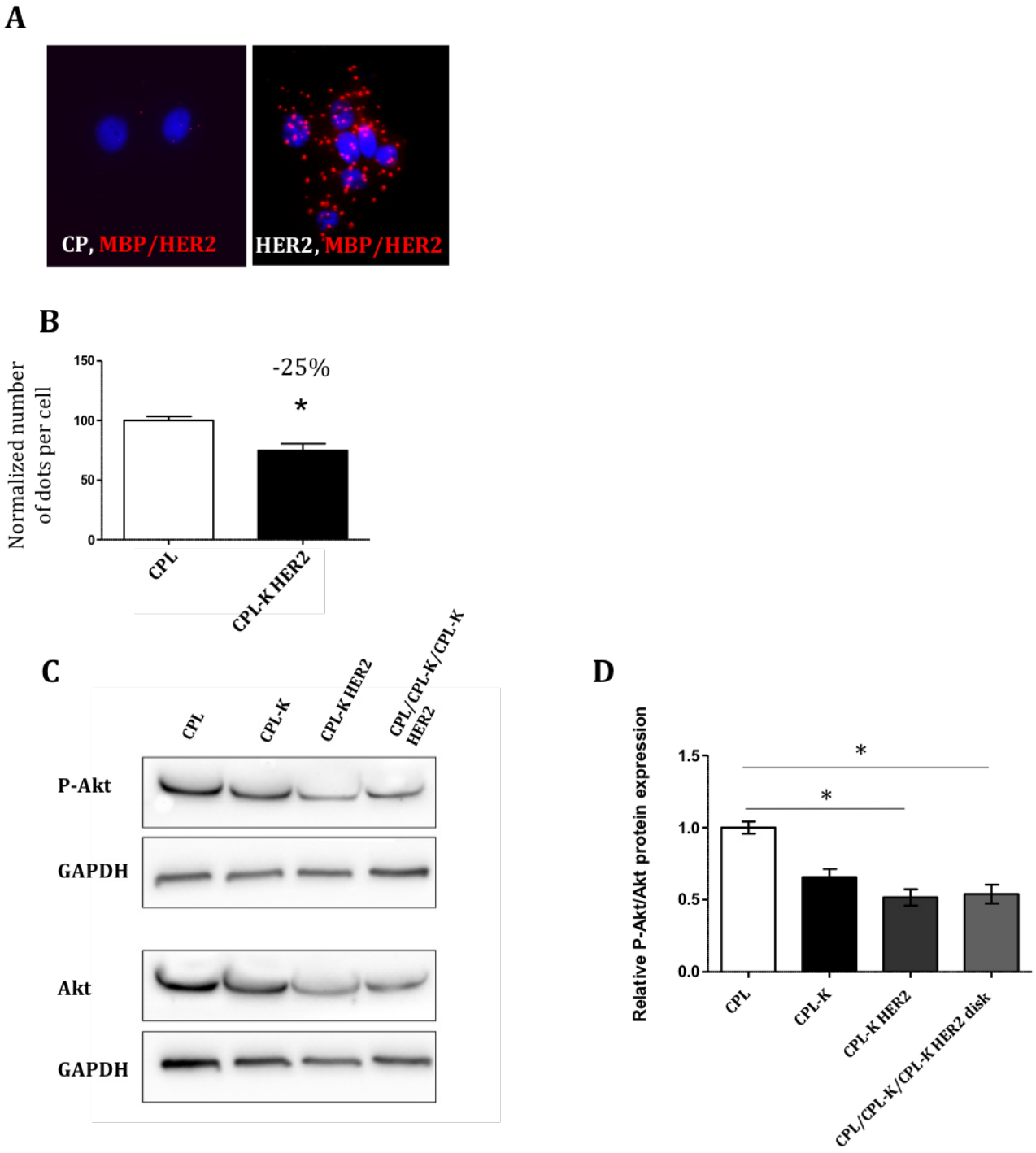

Figure 43: CPL-K HER2 binding and disruption activity.

(A) CPL-K HER2 binds to HER2 receptor on MCF-7 cells and (B) disrupts HER2/HER3 dimerization on MCF-7 cells. (C) Western blot showing level of Akt phosphorylated and dephosphorylated in different treatment conditions in MCF-7 cells. (D) Quantification of Akt phosphorylation in treated cells. N=3. $P<0.05$ (One-way ANOVA).

3.2. CPL-K HER2 shows no effect on cell proliferation

Based on these encouraging results showing that CPL-K HER2 binds to HER2 and interferes with HER2-HER3 interaction and downstream signaling, I performed proliferation assays to determine if CPL-K HER2 could interfere with the propagation of cancer cells. However, MTT proliferation assays failed to demonstrate an effect of CPL-K HER2 on the propagation of MCF-7 cells (**Figure 44**).

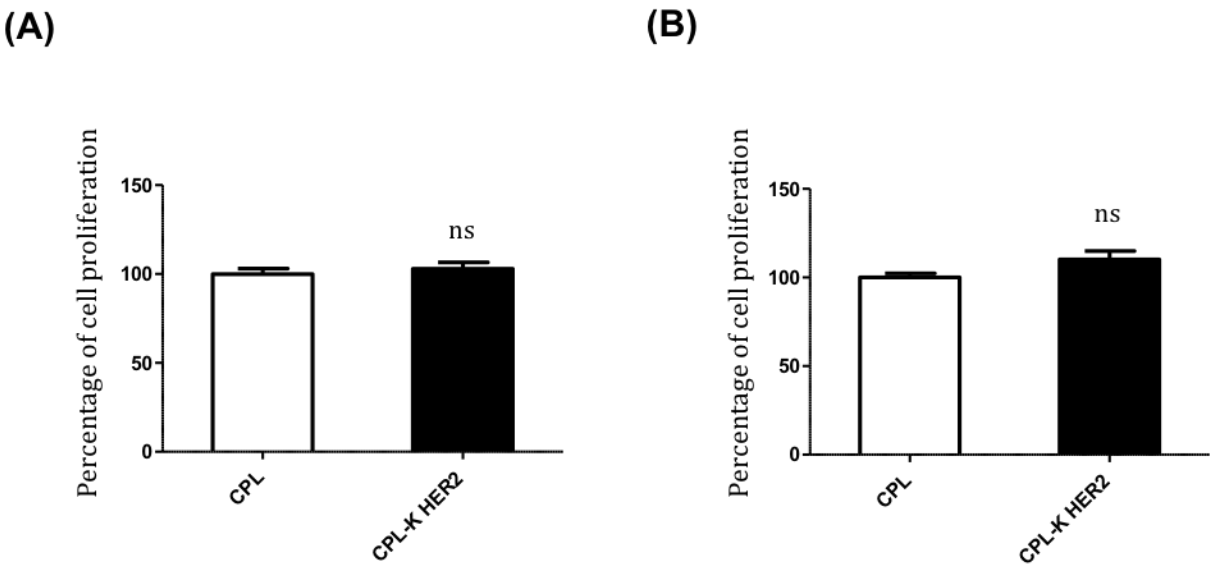

Figure 44: MTT proliferation assay on MCF-7 cells.

(A) Treatment of MCF-7 cells with CPL-K HER2 does not produce statistically significant difference in cell proliferation as compared to the treatment with CPL. Both proteins were applied with a concentration of 10^{-5} M. (B) Treatment of MCF-7 cells with 10^{-6} M CPL and 10^{-6} M CPL-K HER2. ns, not significant (Mann-Whitney test). N=2.

4. Nanoparticles assembly and evaluation

The nanoparticles carrying killing and finding peptide were further tested in tubulogenesis assay on HUVECs. Preliminary experiments with nanoparticles assembly with only CPL-K protein show that these nanoparticles lack antiangiogenic effect (**Figure 45A**). However, when a CPL moiety is added in the same quantity as CPL-K, the antiangiogenic effect is retrieved (**Figure 45B**).

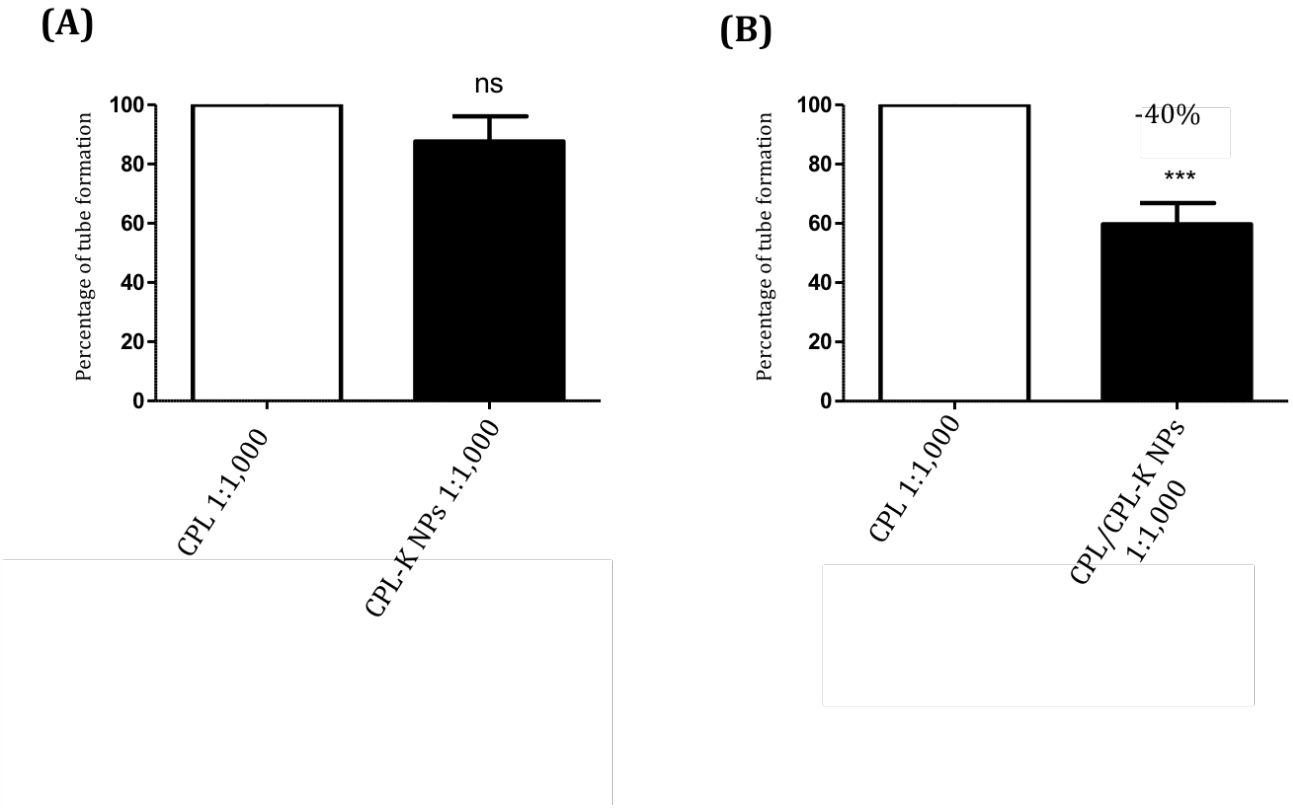

Figure 45: CPL-K NPs lack antiangiogenic effect which is retrieved with CPL/CPL-K NPs.

(A) Nanoparticles assembled from CPL-K fusion protein has no impact on HUVEC tubulogenesis. N=3 (Mann-Whitney test). (B) When a CPL moiety is added for nanoparticles assembly with CPL-K, the resulting NPs lead to 40% inhibition of HUVEC tubulogenesis. $p<0.0001$, n=3 Mann-Whitney test.

Nanoparticles carrying both peptide were then assembled. Due to the complexity to evaluate precisely both peptide concentration after the dialysis, we considered the same concentration for both peptide and performed cascade dilution. When diluted at 1:100, 1:1,000 and 1:10,000 CPL nanoparticles show no effect on angiogenesis thus supporting their absence of toxicity (**Figure 46**). Surprisingly, CPL/CPL-K/CPL-F nanoparticles lacks antiangiogenic effect when diluted at 1:100 (**Figure 47A**). This may be explained by a high concentration of big aggregates that prevent peptide integration into the membrane due to steric hindrance. However, at higher dilution (1:1,000 and 1:10,000) CPL/CPL-K/CPL-F nanoparticles exhibited an antiangiogenic effect (-20% and -18% respectively) (**Figure 47B**).

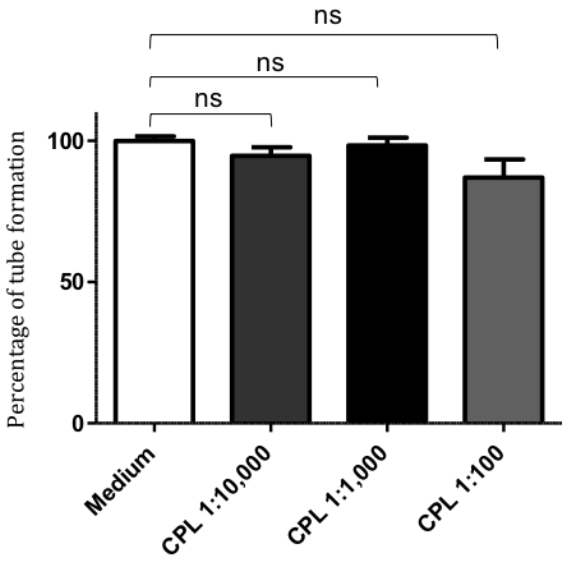

Figure 46: CPL nanoparticles show no effect on angiogenesis.

CPL NPs have no effect on HUVEC tubulogenesis. Eight wells minimum quantified in each condition. N=3. One-way ANOVA test.

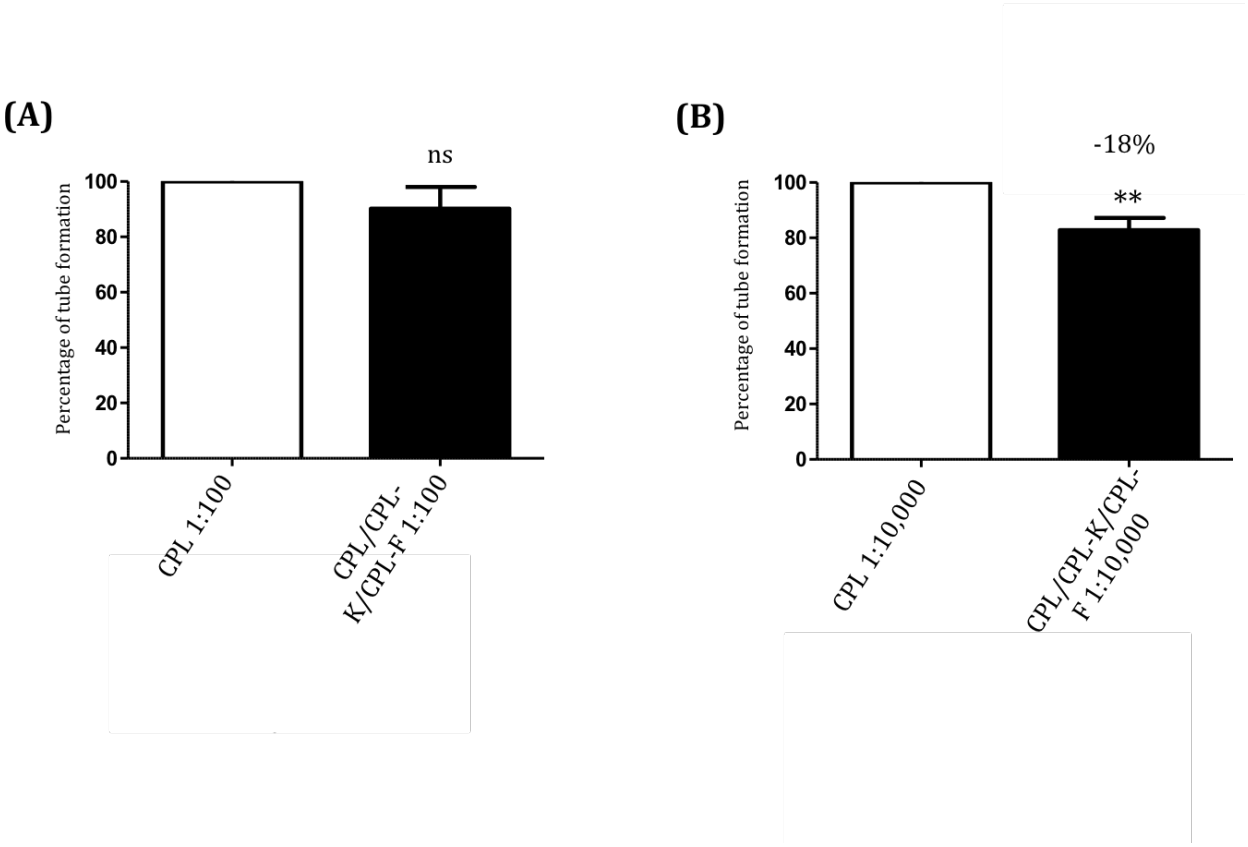

Figure 47: CPL/CPL-K/CPL-F NPs lack anti-angiogenic effect at 1:100 but retrieve it at 1:10,000.

(A) CPL/CPL-K/CPL-F NPs diluted to 1:100 don't inhibit HUVEC formation of tubes. n=2 (Mann-Whitney test). (B) When the NPs dilution is stronger, the antiangiogenic effect is retrieved. p-value < 0.005. N=5 (Mann-Whitney test).

VII. Discussion and perspectives

1. Protein production and characteristics

The aim of this thesis was to create TMV-derived nanoparticles as nanocarriers for peptide agents that target cancer cells and interfere with cancer cell signaling and growth. The starting idea was to infect plants with recombinant TMV virus expressing the CP fused at its C-terminus with specific anti-cancer peptides, to isolate recombinant virions, and to use the CP purified from virions and carrying different peptides for the *in vitro* assembly of multi-functionalized virus-derived nanoparticles. We envisioned to use this approach to combine peptides that interfere with cancer cell signaling platforms (cancer cell "killing"-"K"-peptides) formed by Nrp1 or HER2 with peptides able to guide nanoparticles to cancer cells through specific binding to cancer proteins ("finding"- "F"-peptides). The approach of using CP monomers isolated from virions for nanoparticle assembly was promising as TMV was previously shown as potential tool for displaying foreign peptides on its virion surface and that such modified virions can be produced in infected plants (Röder et al., 2017). However, this was mainly demonstrated for soluble peptides and extensively used for antigen presentation and vaccine production (Fujiyama et al., 2006; Pérez Filgueira et al., 2004; Saejung et al., 2007). The attempt to use a similar C-terminal fusion to the CP to produce virions that display a short linker sequence (L) with MTP-Nrp1 on their surface upon infection failed because the hydrophobic peptide interfered with virion assembly. Even by using a shorter peptide (MTP-sNrp1, GVLLGAVCGVVLYRKR) which carries the critical glycine residues but has reduced hydrophobicity (GRAVY index of 1.106 instead of 1.73), this methods showed itself not applicable in the context of producing virions with peptide derived from TMD. As an alternative approach to produce the TMD mimicking peptide-fused CP-derivatives, the modified CP was fused to MBP and His_6 tag at its N-terminus and produced in *E. coli*. Here, the shorter peptide (MTP-sNrp1, GVLLGAVCGVVLYRKR) with a reduced intrinsic hydrophobicity (GRAVY index of 1.106 instead of 1.73) was used. Expression in *E. coli* turned out to be an efficient strategy because we obtained large amount of the His_6-MBP-

CPL-sNrp1 recombinant protein, referred to as CPL-K. Similar high amounts of protein were also obtained upon expression of the CPL control protein (same protein without specific peptide), CPL-F (CPL fused to a soluble peptide targeting the extracellular domain of Nrp1, ATWLPPR), CPL-K HER2 (CPL fused to a peptide targeting the TMD of HER2), and CPL-F TNC (CPL fused to a soluble, TNC-binding peptide, FHKHKSPALSPVGGG). Even the highly hydrophobic long Nrp1-TMD peptide could be produced in large amount (up to 5 $mg.ml^{-1}$) using this strategy.

This opened the possibility to use this bacterial expression strategy to generate nanoparticles based on CP for assembly. Interestingly, proteins produced without the His_6 tag were insoluble. This observation is consistent with previous work by Pierre Hubert having shown that a fusion to MBP is not sufficient to solubilize MTP-Nrp1 (unpublished data).

Analysis of the isolated proteins by western blot revealed the expected molecular sizes. Moreover, slower migrating additional bands indicated the presence of oligomeric form of the proteins. These detergent- and high temperature (up to 95°C)- resistant aggregates may be explained by intrinsic affinity of both the CP and the fused peptides to interact and to assemble to higher order structures. Dynamic Light Scattering analysis showed that the protein solutions (in PBS) were monodisperse. This remarkable solubility was demonstrated for period of times up to 30 days.

Therefore, this strategy can be used to produce large amount of hydrophobic peptide and for a cheaper cost than chemical synthesis.

2. Fusion proteins interact with their targets

After the successful purification of CPL, CPL-K and CPL-F we have wondered if the peptides were still able to bind to their respective targets and to disrupt their dimerization with partner receptors. To test this, a proximity ligation assay, a technique allowing to visualize close interactions (distance <40 nm) of two targeted proteins, was used. The results obtained with MDA-MB-231 and U-118MG cell lines exposed to CPL-K

and CPL-F show that unlike the CPL control protein, both peptide fusion proteins bind to the surface of these cells thus indicating that the small Nrp1 TMD and Nrp1 ectodomain targeting peptides conserve the ability to bind to Nrp1 even though they are fused to a much larger His_6-MBP-CP moiety. This important observation encouraged the further use of His_6-MBP-CP moiety as a peptide carrier. It should be noted that CPL exhibited some background signal thus suggesting limited unspecific binding to the cell membrane. It would be important to test whether the signal to noise ratio can be reduced by using lower concentrations of the proteins. This background signal seen *in vitro* may also explain the background observed *in vivo*. In our *in vivo* model, CPL is retained in the tissues and tumors in the same manner as CPL-K and CPL-F. Thus, the high protein concentration used for injection (10 $\mu g.kg^{-1}$) may cause an increased elimination time from the body and the high concentration retained in the body may overshadow the specific binding of the peptide fused proteins at the specific target sites. It would be important to repeat the experiments with lower protein concentrations although this may cause a risk of reaching the limit of detection of the fluorescent peptides with the NightOwl system used to monitor the biodistributions. It is also possible that the specific targeting of the peptides *in vivo* is inhibited by chemical modification of the proteins with the fluorescent Alexa 647 tag. Radiolabeling could be an alternative way for achieving a realistic analysis of the biodistribution of the fusion proteins.

3. Conservation and loss of biological activities

3.1. Anti-angiogenesis activity

The results obtained in angiogenesis assays demonstrate that unlike the CPL control protein, CPL-K and CPL-F exhibit an inhibitory effect on angiogenesis. Thus, CPL alone, while exhibiting nonspecific binding to the membrane, does not own any anti-angiogenesis ability thereby strengthening the specificity of the effect induced by CPL-K and CPL-F.

The sMTP-Nrp1 peptide used to create CPL-K contains the C-terminal domain of Nrp1 and the two GxxxG motifs (called S3 peptide). This short peptide has been previously

shown to inhibit angiogenesis and cell migratory (Thesis of Laurent Jacob, University of Strasbourg). Indeed, angiogenesis assays on HUVECs have demonstrated that sMTP-Nrp1 treatment leads to an angiogenesis inhibition of 21.6% ($p<0.05$). However, the complete MTP-Nrp1 leads to an inhibition of 38.1% of the angiogenesis ($p<0.001$). Interestingly, our CPL-K, which contains the sMTP-Nrp1 peptide inhibits angiogenesis by 37% ($p<0.0001$) thus having a stronger anti-angiogenic activity than the pure sMTP-Nrp1 peptide.

It has been demonstrated that also the native ATWLPPR heptapeptide exhibits an anti-angiogenic effect on HMVECs and HUVECs (Starzec et al., 2006). Indeed, in their early work Starzec and collaborators have shown that the heptapeptide inhibits the VEGF-induced tube-like formation of HMVECs and the VEGF-induced formation of micro-vessels by HUVECs co-cultured with fibroblasts. Our assays show a conservation of the antiangiogenic property of ATWLPPR after fusion to His_6-MBP-CPL. Altogether, our results demonstrate that the two Nrp1 targeting peptides can be fused to CPL to produce nanoparticles without negatively affecting their biological properties.

3.2. Anti-migratory activity

To further validate the biological function of the CPL-fused peptides I also performed *in vitro* cell migration assays. Previous works of the D. Bagnard's laboratory have shown that MTP-Nrp1 has an anti-migratory effect if applied to aggregates of U373MG (human glioblastoma cell line). In these previous assays the migration of cells was induced by VEGF treatment, MTP-Nrp1 was then applied to determine if the peptide causes a reduction of the number of aggregates exhibiting migratory cell chains (called positive aggregates). Thus, while the control VEGF group exhibits 45% positive aggregates, the number of positive aggregates was reduced to 10% ($p<0.05$) in the MTP-Nrp1-treated group. Also the sMTP-Nrp1-treated group exhibited only 18% ($p<0.05$) of positive aggregates thus attesting the anti-migratory activity of the short peptide. In my work I used U-118MG cells and demonstrate that CPL-K (containing the sMTP-Nrp1 peptide) induces a reduction of the VEGF-induced cell migration by 22% as compared to

cells treated with CPL control protein. Thus, this second functional assay confirmed the biological activity of the peptides fused to CPL and strengthened the whole strategy.

3.3. Anti-proliferative activity

It has been previously demonstrated that MTP-Nrp1 exhibits antiproliferative activity on murine and human breast cancer cells (Arpel et al., 2016), and the same was also shown for the sMTP-Nrp1 peptide on human breast cancer cell lines (data unpublished). However, the CPL-K fusion protein had no antiproliferative effect on U-118MG cells as determined by MTT proliferation assays (data not shown). CPL-fusion proteins containing the full-length MTP-Nrp1 peptides should be tested. The lack of antiproliferative effect of CPL-K could be explained by a partial antagonism of the TMD. Indeed, the laboratory of D. Bagnard has previously developed two other short peptides targeting different part of the Nrp1-TMD (**Figure 17**). The first peptide (S1) mimics the N-terminal part and the first GxxxG motif, while the second peptide (S2) mimics the second GxxxG motif and the C-terminal part. The sNrp1 peptide present in CPL-K mimics the two GxxxG motifs and the C-terminal part of the Nrp1 TMD. When the S1 and S2 peptides were tested in angiogenesis assays, antimigratory assays and in an *in vivo* treatment assay (thesis of L. Jacob), S1 inhibited angiogenesis as efficiently as MTP-Nrp1 while S2 had completely lost the effect. However, S2 inhibited cell migration to the same extend as the full length MTP-Nrp1 whereas the S1 peptide showed only reduced effects on cell migration as compared to MTP-Nrp1. This showed that different parts of the Nrp1 TMD are involved in the formation of different receptor complexes and downstream signaling pathways leading to the different responses on cell proliferation, cell migration and angiogenesis triggered by Nrp1. The sMTP-Nrp1 used in the present project is the S3 peptide and therefore is expected to antagonize the S3- rather than the S1-mediated responses of the TMD, as is confirmed by the effect of CPL-K on cell migration. The lack of the anti-proliferative effect of CPL-K could be explained by the missing N-terminal part of the peptide. This part may have an important function in positioning the peptide to properly align with the key sequences involved in the signaling of the different functions.

Moreover, the large CPL moiety likely prevents full penetration of the peptide into the membrane and thereby the optimal inhibition of the two GxxxG motifs involved in Nrp1 activity.

Similarly, CPL-F was also unable to inhibit proliferation of MDA-MB-231 cells or U-118MG cells. However, this result is not surprising. Although the pure ATWLPPR peptide inhibited endothelial cells proliferation *in vitro* (Binétruy-Tournaire et al., 2000) its effects on the proliferation of tumor cells remains unclear. Starzec and coworkers demonstrated that the heptapeptide is unable to inhibit the proliferation rate of MDA-MB-231 *in vitro* (Starzec et al., 2006). Moreover, although the growth of tumors induced by a xenograft with MDA-MB-231 cells was inhibited at 45% after administration of the ATWLPPR peptide, the tumor cell proliferation index was not changed. However, the intratumoral endothelial area and the intratumor vessel density was reduced (-22% and -25% reduction, respectively). Therefore, it appears that the ATWLPPR peptide induces a tumor growth inhibition through its effect on angiogenesis but not through an effect on proliferation. This is consistent with our results showing that CPL-F lacks an antiproliferative activity on tumor cells. However, even if the CPL-K and CPL-F fusions proteins show no antiproliferative effects, their antiangiogenic effects are strong enough to envision a therapeutic effect *in vivo*.

As previously mentioned, I used also a peptide targeting the HER2 TMD in fusion to CPL. This peptide is even more hydrophobic than sMTP-Nrp1 (GRAVY index of 1.906 vs 1.106 respectively). The biochemical analysis of the purified CPL-K HER2 on by SDS-PAGE confirmed the expected size of the produced fusion protein and also indicated that a fraction of the protein adopt an oligomeric form (25%). The CPL-K HER2 protein was shown to bind to the HER2 receptor and was also able to disrupt the interaction of HER2 with HER3. However, we could not demonstrate any antiproliferative effect of CPL-K HER2. This effect was addressed with a MTT test based on metabolic level for up to 48 hours of treatment and with high concentrations reaching from 10^{-6} M to 10^{-5} M. As for the CPL-K (sNrp1), this lack of a biological effect on cell proliferation could be explained by the position of the His_6-MBP-CP tag at the N-terminal part of the MTP-

HER2 peptide. The N-terminal part of the HER2-TMD is important for the heterodimerization of HER2 receptor with EGFR (Escher et al., 2009) and its fusion to the His_6-MBP-CP moiety may interfere with the optimal interaction of the peptide with the targeted TMD of HER2. The importance of a free N-terminal part of MTP-HER2 was demonstrated by a PhD student working in parallel during the course of my thesis. Indeed, a chemically synthesized MTP-HER2 peptide with a conjugate function and a water solubilizing group at the N-terminal part showed a loss of antiproliferative activity while the same sequence modified at its C-terminal part with the same conjugate conserved its biological effect.

To investigate a possible role of the N-terminal modification in the loss of the antiproliferative activity of MTP-HER2, I designed a fusion protein sequence in which I fused the MTP-HER2 peptide to LCP-MBP-His_6 at its C-terminal end. The designed plasmid sequence was sent to Genescript company for synthesis. I produced the protein in *E. coli* following the same procedure as for the purification of the other fusion proteins. However, although we were able to purify the MTP-HER2- LCP-MBP-His_6 fusion protein (K HER2-LCP), the yield was lower than the yield obtained with the other fusion proteins. Indeed, while the yields were usually in the average of 1-2 $mg.ml^{-1}$, I was able to purify only 0.5-0.8 $mg.ml^{-1}$ of K HER2-LCP. Moreover, K HER2-LCP also did not show any antiproliferative activity.

All these data clearly demonstrate that by fusion to His_6-MBP-CPL large amounts of TMD peptides with high solubility can be produced. However, this study also shows that the length of the TMD sequence and the positioning of the tag is critical to conserve the biological activity of the TMD peptides. Future studies should investigate whether the addition of linkers of different nature or modifying the size of fusion proteins at the N- and C-termini could lead to optimization. For now, this work provides a starting point for the production of TMV-derived nanoparticles containing cancer targeting and inhibiting properties to fight with cancer cells.

4. Nanoparticles formation

It is well known that wild-type CP has the capacity to self-assemble under specific pH and temperature conditions. In the absence of viral RNA and at pH 8.5, 100 mM phosphate buffer, CP proteins remain in the protein A form when stored at 4°C (Butler, 1984). Bruckman and coworkers designed a fusion protein produced in *E. coli* with a His_6 tag placed at the C-terminal part of CP to investigate the impact of the tag on CP assembly (Bruckman et al., 2011). Structure analysis with TEM have shown that the addition of the His_6 tag causes dramatic changes in the behavior of CP in assembly. Indeed, Bruckman and his collaborators used unfused, wildtype CP purified from TMV-infected plants as a control and compared its assembly conditions to those of His_6-TMV-CP. They found that His_6 tag carrying CP isolated from bacteria forms disks over a wider pH range. Thus, while WT-TMV-CP remains in the protein A form at pH 8, disks are already observed for His_6-TMV-CP under the same condition. Moreover, the disks were the most predominant species formed by His_6-TMV-CP in solution even at low ionic strength (100 mM phosphate buffer) when stored at 4°C while WT-TMV-CP returns in protein A form under these conditions.

In our case, we have chosen to fuse His_6-MBP to the N-terminal part of the CP to let the C-terminus free for fusion to the TMD peptide. Indeed, the C-terminal part of CP is on the outer surface, which is mandatory to allow the peptide to reach its target. To our knowledge, it is the first construct fusing the His_6 tag and the MBP at the N-terminal part of TMV CP. Therefore, we performed dialysis to analyze the assembly and to visualized the disk structure with TEM. Although TEM pictures revealed the presence of disk-like structures, it appears that they do not represent the major form in solution. Indeed, most of the pictures showed the presence of aggregates lacking any particular structure. Interestingly, the disk-like structures were observed only after dialysis at pH 6. The presence of MBP in the protein probably impacts the structure of CP. Indeed, the MBP has been used in more than a hundred cases to help for crystallizing other proteins (Waugh, 2016). The aggregation may also reflect the strong interaction capability of the fused TMD peptides.

In order to obtain more precise informations concerning the structure of the protein at various pH, we could perform X-ray crystallography experiments or also Small Angle X-ray Scattering to analyze these objects in solution.

Subsequent to the confirmation that His_6-MBP-CPL is able to form disk-like structure, we investigated the assembly of nanoparticles from His_6-MBP-CPL (CPL) units containing the killing and finding peptides (CPL-K and CPL-F). First trials with CPL-K assemblies failed to demonstrate antiangiogenic activity *in vitro*, which can be due to the strong interaction between hydrophobic peptides, which are too closely clustered together if assembled next to each other. Therefore, to allow spacing between the hydrophobic peptides we mixed CPL-K with an equal amount of CP before assembly. The resulting assemblies nanoparticles exhibited an antiangiogenic effect on HUVECs comparable to that of non-assembled CPL-K protein (40% and 37% inhibition respectively). The possibility to add a moiety of finding peptide to the nanoparticles was the also quickly tested (CPL/CPL-K/CPL-F nanoparticles). By imaging of the nanoparticles with TEM the presence of disk-like structure in the solution could be demonstrated.

For nanoparticle assembly, we used equal amounts of the different proteins and assumed a homogeneous repartition throughout nanoparticles upon assembly. However, while each individual particle may contain an equal ratio of killing and finding moiety, it is also possible that some nanoparticles contain only one type of fusion protein. Further experiments using fluorescently tagged subunits or labeling individual nanoparticles with specific antibody targeting the finding and killing peptides could allow to further optimize the assembly conditions and to correlate the biological effects of the nanoparticles with their specific composition.

The nanoparticles carrying killing and finding peptide were tested in tubulogenesis assays using HUVECs. As described in the paragraph VI.4, the CPL/CPL-K/CPL-F nanoparticles did not show an antiangiogenic effect at high concentration (1:100 dilution). This may be explained by a high concentration of large aggregates that

prevent peptide integration into the membrane due to steric hindrance. However, when applied at higher dilutions (1:1,000 and 1:10,000), nanoparticles were able to inhibit the formation of vessels-like structures by the HUVECs. The CPL/CPL-K/CPL-F nanoparticles showed a weaker inhibitory effect on angiogenesis than CPL-K nanoparticles (-20% vs -40%), which may be explainable by the overall lower amount of killing peptide in the solution. Nonetheless, the inhibition remains significant thus encouraging further evaluation of the nanoparticles *in vivo*. Indeed, in the presence of the finding moiety, CPL/CPL-K/CPL-F nanoparticles should target the tumor bed more efficiently than the CPL-K nanoparticles, thus improving the anti-tumor effect of the killing peptide.

VIII. Bibliography

Aanei, I.L., ElSohly, A.M., Farkas, M.E., Netirojjanakul, C., Regan, M., Taylor Murphy, S., O'Neil, J.P., Seo, Y., and Francis, M.B. (2016). Biodistribution of antibody-MS2 viral capsid conjugates in breast cancer models. Mol. Pharm. *13*, 3764–3772.

Aci-Sèche, S., Sawma, P., Hubert, P., Sturgis, J.N., Bagnard, D., Jacob, L., Genest, M., and Garnier, N. (2014). Transmembrane recognition of the semaphorin co-receptors neuropilin 1 and plexin A1: coarse-grained simulations. PLoS One *9*, e97779.

Adams, S., Gray, R.J., Demaria, S., Goldstein, L., Perez, E.A., Shulman, L.N., Martino, S., Wang, M., Jones, V.E., Saphner, T.J., et al. (2014). Prognostic value of tumor-infiltrating lymphocytes in triple-negative breast cancers from two phase III randomized adjuvant breast cancer trials: ECOG 2197 and ECOG 1199. J. Clin. Oncol. Off. J. Am. Soc. Clin. Oncol. *32*, 2959–2966.

Agrawal, A., and Manchester, M. (2012). Differential uptake of chemically modified *Cowpea mosaic virus* nanoparticles in macrophage subpopulations present in inflammatory and tumor microenvironments. Biomacromolecules *13*, 3320–3326.

Ahmed, S., Sami, A., and Xiang, J. (2015). HER2-directed therapy: current treatment options for HER2-positive breast cancer. Breast Cancer Tokyo Jpn. *22*, 101–116.

Alemzadeh, E., Dehshahri, A., Dehghanian, A.R., Afsharifar, A., Behjatnia, A.A., Izadpanah, K., and Ahmadi, F. (2018). Enhanced anti-tumor efficacy and reduced cardiotoxicity of doxorubicin delivered in a novel plant virus nanoparticle. Colloids Surf. B Biointerfaces *174*, 80–86.

Ali-Boucetta, H., Al-Jamal, K.T., McCarthy, D., Prato, M., Bianco, A., and Kostarelos, K. (2008). Multiwalled carbon nanotube-doxorubicin supramolecular complexes for cancer therapeutics. Chem. Commun. Camb. Engl. 459–461.

Aljabali, A.A.A., Shukla, S., Lomonossoff, G.P., Steinmetz, N.F., and Evans, D.J. (2013). CPMV-DOX delivers. Mol. Pharm. *10*, 3–10.

Alkins, R.D., and Mainprize, T.G. (2018). High-Intensity Focused Ultrasound ablation therapy of gliomas. Prog. Neurol. Surg. *32*, 39–47.

Alonso, J.M., Górzny, M.Ł., and Bittner, A.M. (2013). The physics of *Tobacco mosaic virus* and virus-based devices in biotechnology. Trends Biotechnol. *31*, 530–538.

Altınoğlu, S.A., Wang, M., Li, K.Q., Li, Y., and Xu, Q. (2016). Intracellular delivery of the PTEN protein using cationic lipidoids for cancer therapy. Biomater. Sci. *4*, 1773–1780.

Arakawa, T., and Timasheff, S.N. (1985). Mechanism of polyethylene glycol interaction with proteins. Biochemistry *24*, 6756–6762.

Arnold, K.M., Flynn, N.J., Raben, A., Romak, L., Yu, Y., Dicker, A.P., Mourtada, F., and Sims-Mourtada, J. (2018). The impact of radiation on the tumor microenvironment: effect of Ddose and fractionation schedules. Cancer Growth Metastasis *11*, 1179064418761639.

Arora, N., Gavya S, L., and Ghosh, S.S. (2018). Multi-facet implications of PEGylated lysozyme stabilized-silver nanoclusters loaded recombinant PTEN cargo in cancer theranostics. Biotechnol. Bioeng. *115*, 1116–1127.

Arpel, A., Sawma, P., Spenlé, C., Fritz, J., Meyer, L., Garnier, N., Velázquez-Quesada, I., Hussenet, T., Aci-Sèche, S., Baumlin, N., et al. (2014). Transmembrane domain targeting peptide antagonizing ErbB2/Neu inhibits breast tumor growth and metastasis. Cell Rep. *8*, 1714–1721.

Arpel, A., Gamper, C., Spenlé, C., Fernandez, A., Jacob, L., Baumlin, N., Laquerriere, P., Orend, G., Crémel, G., and Bagnard, D. (2016). Inhibition of primary breast tumor growth and metastasis using a neuropilin-1 transmembrane domain interfering peptide. Oncotarget *7*, 54723–54732.

Atabekov, J., Nikitin, N., Arkhipenko, M., Chirkov, S., and Karpova, O. (2011). Thermal transition of native *Tobacco mosaic virus* and RNA-free viral proteins into spherical nanoparticles. J. Gen. Virol. *92*, 453–456.

Bagnard, D., Vaillant, C., Khuth, S.T., Dufay, N., Lohrum, M., Puschel, A.W., Belin, M.F., Bolz, J., and Thomasset, N. (2001). Semaphorin 3A-vascular endothelial growth factor-165 balance mediates migration and apoptosis of neural progenitor cells by the recruitment of shared receptor. J. Neurosci. Off. J. Soc. Neurosci. *21*, 3332–3341.

Bai, J., Zhang, Z., Li, X., and Liu, H. (2015). MicroRNA-365 inhibits growth, invasion and metastasis of malignant melanoma by targeting NRP1 expression. Cancer Biomark. Sect. Dis. Markers *15*, 599–608.

Balkwill, F., and Mantovani, A. (2001). Inflammation and cancer: back to Virchow? The Lancet *357*, 539–545.

Banday, A.H., Jeelani, S., and Hruby, V.J. (2015). Cancer vaccine adjuvants--recent clinical progress and future perspectives. Immunopharmacol. Immunotoxicol. *37*, 1–11.

Bar, H., Yacoby, I., and Benhar, I. (2008). Killing cancer cells by targeted drug-carrying phage nanomedicines. BMC Biotechnol. *8*, 37.

Bargmann, C.I., Hung, M.C., and Weinberg, R.A. (1986). Multiple independent activations of the neu oncogene by a point mutation altering the transmembrane domain of p185. Cell *45*, 649–657.

Bean, C.P., and Jacobs, I.S. (1956). Magnetic granulometry and super-paramagnetism. J. Appl. Phys. *27*, 1448–1452.

Bechet, D., Auger, F., Couleaud, P., Marty, E., Ravasi, L., Durieux, N., Bonnet, C., Plénat, F., Frochot, C., Mordon, S., et al. (2015). Multifunctional ultrasmall nanoplatforms for vascular-targeted interstitial photodynamic therapy of brain tumors guided by real-time MRI. Nanomedicine Nanotechnol. Biol. Med. *11*, 657–670.

Bennasroune, A., Fickova, M., Gardin, A., Dirrig-Grosch, S., Aunis, D., Crémel, G., and Hubert, P. (2004). Transmembrane peptides as inhibitors of ErbB receptor signaling. Mol. Biol. Cell *15*, 3464–3474.

Bennasroune, A., Gardin, A., Auzan, C., Clauser, E., Dirrig-Grosch, S., Meira, M., Appert-Collin, A., Aunis, D., Crémel, G., and Hubert, P. (2005). Inhibition by transmembrane peptides of chimeric insulin receptors. Cell. Mol. Life Sci. CMLS *62*, 2124–2131.

Bhaskar, S., and Lim, S. (2017). Engineering protein nanocages as carriers for biomedical applications. NPG Asia Mater. *9*, e371.

Bhowmick, N.A., Neilson, E.G., and Moses, H.L. (2004). Stromal fibroblasts in cancer initiation and progression. Nature *432*, 332–337.

Bielenberg, D.R., Pettaway, C.A., Takashima, S., and Klagsbrun, M. (2006). Neuropilins in neoplasms: expression, regulation, and function. Exp. Cell Res. *312*, 584–593.

Bilan, R., Fleury, F., Nabiev, I., and Sukhanova, A. (2015). Quantum dot surface chemistry and functionalization for cell targeting and imaging. Bioconjug. Chem. *26*, 609–624.

Binétruy-Tournaire, R., Demangel, C., Malavaud, B., Vassy, R., Rouyre, S., Kraemer, M., Plouët, J., Derbin, C., Perret, G., and Mazié, J.C. (2000). Identification of a peptide blocking vascular endothelial growth factor (VEGF)-mediated angiogenesis. EMBO J. *19*, 1525–1533.

Bissler, J.J., McCormack, F.X., Young, L.R., Elwing, J.M., Chuck, G., Leonard, J.M., Schmithorst, V.J., Laor, T., Brody, A.S., Bean, J., et al. (2008). Sirolimus for angiomyolipoma in tuberous sclerosis complex or lymphangioleiomyomatosis. N. Engl. J. Med. *358*, 140–151.

Blomberg, O.S., Spagnuolo, L., and de Visser, K.E. (2018). Immune regulation of metastasis: mechanistic insights and therapeutic opportunities. Dis. Model. Mech. *11*.

Bormann, B.J., and Engelman, D.M. (1992). Intramembrane helix-helix association in oligomerization and transmembrane signaling. Annu. Rev. Biophys. Biomol. Struct. *21*, 223–242.

Brose, M.S., Volpe, P., Feldman, M., Kumar, M., Rishi, I., Gerrero, R., Einhorn, E., Herlyn, M., Minna, J., Nicholson, A., et al. (2002). BRAF and RAS mutations in human lung cancer and melanoma. Cancer Res. *62*, 6997–7000.

Brosig, B., and Langosch, D. (1998). The dimerization motif of the glycophorin A transmembrane segment in membranes: importance of glycine residues. Protein Sci. Publ. Protein Soc. *7*, 1052–1056.

Bruckman, M.A., and Steinmetz, N.F. (2014). Chemical modification of the inner and outer surfaces of *Tobacco Mosaic Virus* (TMV). Methods Mol. Biol. Clifton NJ *1108*, 173–185.

Bruckman, M.A., Soto, C.M., McDowell, H., Liu, J.L., Ratna, B.R., Korpany, K.V., Zahr, O.K., and Blum, A.S. (2011). Role of hexahistidine in directed nanoassemblies of *Tobacco mosaic virus* coat protein. ACS Nano *5*, 1606–1616.

Bruckman, M.A., Hern, S., Jiang, K., Flask, C.A., Yu, X., and Steinmetz, N.F. (2013). *Tobacco mosaic* virus rods and spheres as supramolecular high-relaxivity MRI contrast agents. J. Mater. Chem. B *1*, 1482–1490.

Bruckman, M.A., Randolph, L.N., VanMeter, A., Hern, S., Shoffstall, A.J., Taurog, R.E., and Steinmetz, N.F. (2014). Biodistribution, pharmacokinetics, and blood compatibility of native and PEGylated *Tobacco mosaic virus* nano-rods and -spheres in mice. Virology *449*, 163–173.

Bruckman, M.A., Czapar, A.E., VanMeter, A., Randolph, L.N., and Steinmetz, N.F. (2016). *Tobacco mosaic virus*-based protein nanoparticles and nanorods for chemotherapy delivery targeting breast cancer. J. Control. Release Off. J. Control. Release Soc. *231*, 103–113.

Budunova, I.V., and Williams, G.M. (1994). Cell culture assays for chemicals with tumor-promoting or tumor-inhibiting activity based on the modulation of intercellular communication. Cell Biol. Toxicol. *10*, 71–116.

Butler, P.J. (1976). Assembly of *Tobacco mosaic virus*. Philos. Trans. R. Soc. Lond. B. Biol. Sci. *276*, 151–163.

Butler, P.J. (1984). The current picture of the structure and assembly of *Tobacco mosaic virus*. J. Gen. Virol. *65 (Pt 2)*, 253–279.

Butler, P.J., and Klug, A. (1972). Assembly of *Tobacco mosaic virus in vitro*: effect of state of polymerization of the protein component. Proc. Natl. Acad. Sci. U. S. A. *69*, 2950–2953.

Butler, P.J.G., Finch, J.T., and Zimmern, D. (1977). Configuration of *Tobacco mosaic virus* RNA during virus assembly. Nature *265*, 217–219.

Byrski, T., Huzarski, T., Dent, R., Marczyk, E., Jasiowka, M., Gronwald, J., Jakubowicz, J., Cybulski, C., Wisniowski, R., Godlewski, D., et al. (2014). Pathologic complete response to neoadjuvant cisplatin in BRCA1-positive breast cancer patients. Breast Cancer Res. Treat. *147*, 401–405.

Cantley, L.C. (2002). The phosphoinositide 3-kinase pathway. Science *296*, 1655–1657.

Cao, J., Wang, R., Gao, N., Li, M., Tian, X., Yang, W., Ruan, Y., Zhou, C., Wang, G., Liu, X., et al. (2015). A7RC peptide modified paclitaxel liposomes dually target breast cancer. Biomater. Sci. *3*, 1545–1554.

Cao, Y., Chen, Y., Yu, T., Guo, Y., Liu, F., Yao, Y., Li, P., Wang, D., Wang, Z., Chen, Y., et al. (2018). Drug release from phase-changeable nanodroplets triggered by low-intensity focused ultrasound. Theranostics *8*, 1327–1339.

Caponegro, M.D., Moffitt, R.A., and Tsirka, S.E. (2018). Expression of neuropilin-1 is linked to glioma associated microglia and macrophages and correlates with unfavorable prognosis in high grade gliomas. Oncotarget *9*, 35655–35665.

Carretero, R., Sektioglu, I.M., Garbi, N., Salgado, O.C., Beckhove, P., and Hämmerling, G.J. (2015). Eosinophils orchestrate cancer rejection by normalizing tumor vessels and enhancing infiltration of CD8(+) T cells. Nat. Immunol. *16*, 609–617.

Cayuela, A., Soriano, M.L., Carrillo-Carrión, C., and Valcárcel, M. (2016). Semiconductor and carbon-based fluorescent nanodots: the need for consistency. Chem. Commun. Camb. Engl. *52*, 1311–1326.

Chaar, M., Kamta, J., and Ait-Oudhia, S. (2018). Mechanisms, monitoring, and management of tyrosine kinase inhibitors-associated cardiovascular toxicities. OncoTargets Ther. *11*, 6227–6237.

Chan, W.C., and Nie, S. (1998). Quantum dot bioconjugates for ultrasensitive nonisotopic detection. Science *281*, 2016–2018.

Chan, J.A., Krichevsky, A.M., and Kosik, K.S. (2005). MicroRNA-21 is an antiapoptotic factor in human glioblastoma cells. Cancer Res. *65*, 6029–6033.

Chang, Z.L., and Chen, Y.Y. (2017). CARs: synthetic immunoreceptors for cancer therapy and beyond. Trends Mol. Med. *23*, 430–450.

Chang, Y.S., di Tomaso, E., McDonald, D.M., Jones, R., Jain, R.K., and Munn, L.L. (2000). Mosaic blood vessels in tumors: frequency of cancer cells in contact with flowing blood. Proc. Natl. Acad. Sci. U. S. A. *97*, 14608–14613.

Chen, Q., and Lai, H. (2013). Plant-derived virus-like particles as vaccines. Hum. Vaccines Immunother. *9*, 26–49.

Chen, H., Chédotal, A., He, Z., Goodman, C.S., and Tessier-Lavigne, M. (1997). Neuropilin-2, a novel member of the neuropilin family, is a high affinity receptor for the semaphorins Sema E and Sema IV but not Sema III. Neuron *19*, 547–559.

Cherry-Bohannan, J., Baker, K., and Francis, H. (2011). VEGF and cholangiocarcinoma: Feeding the tumor. Transl. Gastrointest. Cancer *1*, 95-102–102.

Chi, C., Du, Y., Ye, J., Kou, D., Qiu, J., Wang, J., Tian, J., and Chen, X. (2014). Intraoperative imaging-guided cancer surgery: from current fluorescence molecular imaging methods to future multi-modality imaging technology. Theranostics *4*, 1072–1084.

Chi, E.Y., Krishnan, S., Randolph, T.W., and Carpenter, J.F. (2003). Physical stability of proteins in aqueous solution: mechanism and driving forces in nonnative protein aggregation. Pharm. Res. *20*, 1325–1336.

Chinnasamy, D., Yu, Z., Theoret, M.R., Zhao, Y., Shrimali, R.K., Morgan, R.A., Feldman, S.A., Restifo, N.P., and Rosenberg, S.A. (2010). Gene therapy using genetically modified lymphocytes targeting VEGFR-2 inhibits the growth of vascularized syngenic tumors in mice. J. Clin. Invest. *120*, 3953–3968.

Chiquet-Ehrismann, R., Orend, G., Chiquet, M., Tucker, R.P., and Midwood, K.S. (2014). Tenascins in stem cell niches. Matrix Biol. J. Int. Soc. Matrix Biol. *37*, 112–123.

Chira, S., Jackson, C.S., Oprea, I., Ozturk, F., Pepper, M.S., Diaconu, I., Braicu, C., Raduly, L.-Z., Calin, G.A., and Berindan-Neagoe, I. (2015). Progresses towards safe and efficient gene therapy vectors. Oncotarget *6*, 30675–30703.

Chu, W., Song, X., Yang, X., Ma, L., Zhu, J., He, M., Wang, Z., and Wu, Y. (2014). Neuropilin-1 promotes epithelial-to-mesenchymal transition by stimulating nuclear factor-kappa B and is associated with poor prognosis in human oral squamous cell carcinoma. PloS One *9*, e101931.

Constantin, C., Neagu, M., Ion, R.-M., Gherghiceanu, M., and Stavaru, C. (2010). Fullerene-porphyrin nanostructures in photodynamic therapy. Nanomed. *5*, 307–317.

Cosset, J.-M. (2016). The dawn of radiotherapy, between strokes of genius, dramas and controversies. Cancer Radiother. J. Soc. Francaise Radiother. Oncol. *20*, 595–600.

Creager, A.N., Scholthof, K.B., Citovsky, V., and Scholthof, H.B. (1999). *Tobacco mosaic virus*. Pioneering research for a century. Plant Cell *11*, 301–308.

Croce, C.M. (2008). Oncogenes and cancer. N. Engl. J. Med. *358*, 502–511.

Cusato, K., Ripps, H., Zakevicius, J., and Spray, D.C. (2006). Gap junctions remain open during cytochrome c-induced cell death: relationship of conductance to “bystander” cell killing. Cell Death Differ. *13*, 1707–1714.

Czapar, A.E., and Steinmetz, N.F. (2017). Plant viruses and bacteriophages for drug delivery in medicine and biotechnology. Curr. Opin. Chem. Biol. *38*, 108–116.

Czapar, A.E., Zheng, Y.-R., Riddell, I.A., Shukla, S., Awuah, S.G., Lippard, S.J., and Steinmetz, N.F. (2016). *Tobacco mosaic virus* delivery of phenanthriplatin for cancer therapy. ACS Nano *10*, 4119–4126.

Czapar, A.E., Tiu, B.D.B., Veliz, F.A., Pokorski, J.K., and Steinmetz, N.F. (2018). Slow-release formulation of *Cowpea mosaic virus* for *in situ* vaccine delivery to treat ovarian cancer. Adv. Sci. Weinh. Baden-Wurtt. Ger. *5*, 1700991.

Danhier, F. (2016). To exploit the tumor microenvironment: since the EPR effect fails in the clinic, what is the future of nanomedicine? J. Control. Release Off. J. Control. Release Soc. *244*, 108–121.

Daniell, M.D., and Hill, J.S. (1991). A history of photodynamic therapy. Aust. N. Z. J. Surg. *61*, 340–348.

Das, P.P., Lin, Q., and Wong, S.-M. (2018). Comparative proteomics of *Tobacco mosaic virus*-infected *Nicotiana tabacum* plants identified major host proteins involved in photosystems and plant defence. J. Proteomics.

Demir, M., and Stowell, M.H.B. (2002). A chemoselective biomolecular template for assembling diverse nanotubular materials. Nanotechnology *13*, 541–544.

Denkert, C., Loibl, S., Noske, A., Roller, M., Müller, B.M., Komor, M., Budczies, J., Darb-Esfahani, S., Kronenwett, R., Hanusch, C., et al. (2010). Tumor-associated lymphocytes as an independent predictor of response to neoadjuvant chemotherapy in breast cancer. J. Clin. Oncol. Off. J. Am. Soc. Clin. Oncol. *28*, 105–113.

Dillon, L.M., and Miller, T.W. (2014). Therapeutic targeting of cancers with loss of PTEN function. Curr. Drug Targets *15*, 65–79.

Dobrovolskaia, M.A., Patri, A.K., Zheng, J., Clogston, J.D., Ayub, N., Aggarwal, P., Neun, B.W., Hall, J.B., and McNeil, S.E. (2009). Interaction of colloidal gold nanoparticles with human blood: effects on particle size and analysis of plasma protein binding profiles. Nanomedicine Nanotechnol. Biol. Med. *5*, 106–117.

Dockery, L., and Daniel, M.-C. (2018). Dendronized systems for the delivery of chemotherapeutics. Adv. Cancer Res. *139*, 85–120.

Dovedi, S.J., Cheadle, E.J., Popple, A.L., Poon, E., Morrow, M., Stewart, R., Yusko, E.C., Sanders, C.M., Vignali, M., Emerson, R.O., et al. (2017). Fractionated radiation therapy stimulates antitumor immunity mediated by both resident and infiltrating polyclonal T-cell populations when combined with PD-1 blockade. Clin. Cancer Res. Off. J. Am. Assoc. Cancer Res. *23*, 5514–5526.

Du, Z.-J., Cui, G.-Q., Zhang, J., Liu, X.-M., Zhang, Z.-H., Jia, Q., Ng, J.C., Peng, C., Bo, C.-X., and Shao, H. (2017). Inhibition of gap junction intercellular communication is involved in silica nanoparticles-induced H9c2 cardiomyocytes apoptosis via the mitochondrial pathway. Int. J. Nanomedicine *12*, 2179–2188.

Dvorak, H.F. (1986). Tumors: wounds that do not heal. Similarities between tumor stroma generation and wound healing. N. Engl. J. Med. *315*, 1650–1659.

Eichmann, A., Makinen, T., and Alitalo, K. (2005). Neural guidance molecules regulate vascular remodeling and vessel navigation. Genes Dev. *19*, 1013–1021.

Elhissi, A.M.A., Ahmed, W., Hassan, I.U., Dhanak, Vinod.R., and D'Emanuele, A. (2012). Carbon nanotubes in cancer therapy and drug delivery. J. Drug Deliv. *2012*.

Ernsting, M.J., Tang, W.-L., MacCallum, N.W., and Li, S.-D. (2012). Preclinical pharmacokinetic, biodistribution, and anti-cancer efficacy studies of a docetaxel-carboxymethylcellulose nanoparticle in mouse models. Biomaterials *33*, 1445–1454.

Escher, C., Cymer, F., and Schneider, D. (2009). Two GxxxG-like motifs facilitate promiscuous interactions of the human ErbB transmembrane domains. J. Mol. Biol. *389*, 10–16.

Fadel, T.R., Sharp, F.A., Vudattu, N., Ragheb, R., Garyu, J., Kim, D., Hong, E., Li, N., Haller, G.L., Pfefferle, L.D., et al. (2014). A carbon nanotube-polymer composite for T-cell therapy. Nat. Nanotechnol. *9*, 639–647.

Fan, C.-H., Cheng, Y.-H., Ting, C.-Y., Ho, Y.-J., Hsu, P.-H., Liu, H.-L., and Yeh, C.-K. (2016). Ultrasound/magnetic targeting with SPIO-DOX-microbubble complex for image-guided drug delivery in brain tumors. Theranostics *6*, 1542–1556.

Filatenkov, A., Baker, J., Mueller, A.M.S., Kenkel, J., Ahn, G.-O., Dutt, S., Zhang, N., Kohrt, H., Jensen, K., Dejbakhsh-Jones, S., et al. (2015). Ablative tumor radiation can change the tumor immune cell microenvironment to induce durable complete remissions. Clin. Cancer Res. Off. J. Am. Assoc. Cancer Res. *21*, 3727–3739.

Finbloom, J.A., Aanei, I.L., Bernard, J.M., Klass, S.H., Elledge, S.K., Han, K., Ozawa, T., Nicolaides, T.P., Berger, M.S., and Francis, M.B. (2018). Evaluation of three morphologically distinct virus-like particles as nanocarriers for convection-enhanced drug delivery to glioblastoma. Nanomater. Basel Switz. *8*.

Finger, L.R., Harvey, R.C., Moore, R.C., Showe, L.C., and Croce, C.M. (1986). A common mechanism of chromosomal translocation in T- and B-cell neoplasia. Science *234*, 982–985.

Foldbjerg, R., Dang, D.A., and Autrup, H. (2011). Cytotoxicity and genotoxicity of silver nanoparticles in the human lung cancer cell line, A549. Arch. Toxicol. *85*, 743–750.

Fraenkel-Conrat, H., and Williams, R.C. (1955). Reconstitution of active *Tobacco mosaic virus* from its inactive protein and nucleic acid components. Proc. Natl. Acad. Sci. U. S. A. *41*, 690–698.

Fraisl, P., Mazzone, M., Schmidt, T., and Carmeliet, P. (2009). Regulation of angiogenesis by oxygen and metabolism. Dev. Cell *16*, 167–179.

Franklin, R.E. (1956). Structure of *Tobacco mosaic virus*: location of the ribonucleic ccid in the *Tobacco mosaic virus* particle. Nature *177*, 928–930.

Frolova, O.Y., Petrunia, I.V., Komarova, T.V., Kosorukov, V.S., Sheval, E.V., Gleba, Y.Y., and Dorokhov, Y.L. (2010). Trastuzumab-binding peptide display by *Tobacco mosaic virus*. Virology *407*, 7–13.

Fuh, G., Garcia, K.C., and de Vos, A.M. (2000). The interaction of neuropilin-1 with vascular endothelial growth factor and its receptor flt-1. J. Biol. Chem. *275*, 26690–26695.

Fujiyama, K., Saejung, W., Yanagihara, I., Nakado, J., Misaki, R., Honda, T., Watanabe, Y., and Seki, T. (2006). *In Planta* production of immunogenic poliovirus peptide using *Tobacco mosaic virus*-based vector system. J. Biosci. Bioeng. *101*, 398–402.

Furthmayr, H., and Marchesi, V.T. (1976). Subunit structure of human erythrocyte glycophorin A. Biochemistry *15*, 1137–1144.

Galon, J., Costes, A., Sanchez-Cabo, F., Kirilovsky, A., Mlecnik, B., Lagorce-Pagès, C., Tosolini, M., Camus, M., Berger, A., Wind, P., et al. (2006). Type, density, and location of immune cells within human colorectal tumors predict clinical outcome. Science *313*, 1960–1964.

Gannon, C.J., Cherukuri, P., Yakobson, B.I., Cognet, L., Kanzius, J.S., Kittrell, C., Weisman, R.B., Pasquali, M., Schmidt, H.K., Smalley, R.E., et al. (2007). Carbon nanotube-enhanced thermal destruction of cancer cells in a noninvasive radiofrequency field. Cancer *110*, 2654–2665.

Gao, P., Mei, C., He, L., Xiao, Z., Chan, L., Zhang, D., Shi, C., Chen, T., and Luo, L. (2018). Designing multifunctional cancer-targeted nanosystem for magnetic resonance molecular imaging-guided theranostics of lung cancer. Drug Deliv. *25*, 1811–1825.

Gao, S., Yang, D., Fang, Y., Lin, X., Jin, X., Wang, Q., Wang, X., Ke, L., and Shi, K. (2019). Engineering nanoparticles for targeted remodeling of the tumor microenvironment to improve cancer immunotherapy. Theranostics *9*, 126–151.

García-Teijido, P., Cabal, M.L., Fernández, I.P., and Pérez, Y.F. (2016). Tumor-infiltrating lymphocytes in triple negative breast Cancer: the future of immune targeting. Clin. Med. Insights Oncol. *10*, 31–39.

Gaudelot, K., Gibier, J.-B., Pottier, N., Hémon, B., Van Seuningen, I., Glowacki, F., Leroy, X., Cauffiez, C., Gnemmi, V., Aubert, S., et al. (2017). Targeting miR-21 decreases expression of multi-drug resistant genes and promotes chemosensitivity of renal carcinoma. Tumour Biol. J. Int. Soc. Oncodevelopmental Biol. Med. *39*, 1010428317707372.

Ge, P., and Zhou, Z.H. (2011). Hydrogen-bonding networks and RNA bases revealed by cryo electron microscopy suggest a triggering mechanism for calcium switches. Proc. Natl. Acad. Sci. U. S. A. *108*, 9637–9642.

Geretti, E., and Klagsbrun, M. (2007). Neuropilins: novel targets for anti-angiogenesis therapies. Cell Adhes. Migr. *1*, 56–61.

Geretto, M., Pulliero, A., Rosano, C., Zhabayeva, D., Bersimbaev, R., and Izzotti, A. (2017). Resistance to cancer chemotherapeutic drugs is determined by pivotal microRNA regulators. Am. J. Cancer Res. *7*, 1350–1371.

Giordano, S.H., Elias, A.D., and Gradishar, W.J. (2018). NCCN Guidelines updates: breast cancer. J. Natl. Compr. Canc. Netw. *16*, 605–610.

Goubran, H.A., Kotb, R.R., Stakiw, J., Emara, M.E., and Burnouf, T. (2014). Regulation of tumor growth and metastasis: the role of tumor microenvironment. Cancer Growth Metastasis *7*, 9–18.

Grant, S., Qiao, L., and Dent, P. (2002). Roles of ERBB family receptor tyrosine kinases, and downstream signaling pathways, in the control of cell growth and survival. Front. Biosci. J. Virtual Libr. *7*, d376-389.

Grenier, P., Viana, I.M. de O., Lima, E.M., and Bertrand, N. (2018). Anti-polyethylene glycol antibodies alter the protein corona deposited on nanoparticles and the physiological pathways regulating their fate *in vivo*. J. Control. Release Off. J. Control. Release Soc. *287*, 121–131.

Grigore, A.D., Jolly, M.K., Jia, D., Farach-Carson, M.C., and Levine, H. (2016). Tumor budding: the name is EMT. Partial EMT. J. Clin. Med. *5*.

Grunewald, M., Avraham, I., Dor, Y., Bachar-Lustig, E., Itin, A., Yung, S., Chimenti, S., Landsman, L., Abramovitch, R., and Keshet, E. (2006). VEGF-induced adult neovascularization: recruitment, retention, and role of accessory cells. Cell *124*, 175–189.

Guo, W., Keckesova, Z., Donaher, J.L., Shibue, T., Tischler, V., Reinhardt, F., Itzkovitz, S., Noske, A., Zürrer-Härdi, U., Bell, G., et al. (2012). Slug and Sox9 cooperatively determine the mammary stem cell state. Cell *148*, 1015–1028.

Gupta, V., Bhavanasi, S., Quadir, M., Singh, K., Ghosh, G., Vasamreddy, K., Ghosh, A., Siahaan, T.J., Banerjee, S., and Banerjee, S.K. (2018). Protein PEGylation for cancer therapy: bench to bedside. J. Cell Commun. Signal.

Hahn, P.F., Stark, D.D., Weissleder, R., Elizondo, G., Saini, S., and Ferrucci, J.T. (1990). Clinical application of superparamagnetic iron oxide to MR imaging of tissue perfusion in vascular liver tumors. Radiology *174*, 361–366.

Hamdy, S., Haddadi, A., Hung, R.W., and Lavasanifar, A. (2011). Targeting dendritic cells with nano-particulate PLGA cancer vaccine formulations. Adv. Drug Deliv. Rev. *63*, 943–955.

Hanahan, D., and Folkman, J. (1996). Patterns and emerging mechanisms of the angiogenic switch during tumorigenesis. Cell *86*, 353–364.

Hanahan, D., and Weinberg, R.A. (2011). Hallmarks of cancer: the next generation. Cell *144*, 646–674.

Hatiboglu, M.A., Akdur, K., and Sawaya, R. (2018). Neurosurgical management of patients with brain metastasis. Neurosurg. Rev.

He, Z., and Tessier-Lavigne, M. (1997). Neuropilin is a receptor for the axonal chemorepellent semaphorin III. Cell *90*, 739–751.

Heister, E., Neves, V., Tîlmaciu, C., Lipert, K., Beltrán, V.S., Coley, H.M., Silva, S.R.P., and McFadden, J. (2009). Triple functionalisation of single-walled carbon nanotubes with doxorubicin, a monoclonal antibody, and a fluorescent marker for targeted cancer therapy. Carbon *47*, 2152–2160.

Her, S., Jaffray, D.A., and Allen, C. (2017). Gold nanoparticles for applications in cancer radiotherapy: mechanisms and recent advancements. Adv. Drug Deliv. Rev. *109*, 84–101.

Hong, R.L., Huang, C.J., Tseng, Y.L., Pang, V.F., Chen, S.T., Liu, J.J., and Chang, F.H. (1999). Direct comparison of liposomal doxorubicin with or without polyethylene glycol coating in C-26 tumor-bearing mice: is surface coating with polyethylene glycol beneficial? Clin. Cancer Res. Off. J. Am. Assoc. Cancer Res. *5*, 3645–3652.

Houdaihed, L., Evans, J.C., and Allen, C. (2018). Codelivery of paclitaxel and everolimus at the optimal synergistic ratio: a promising solution for the treatment of breast cancer. Mol. Pharm. *15*, 3672–3681.

Hsin, Y.-H., Chen, C.-F., Huang, S., Shih, T.-S., Lai, P.-S., and Chueh, P.J. (2008). The apoptotic effect of nanosilver is mediated by a ROS- and JNK-dependent mechanism involving the mitochondrial pathway in NIH3T3 cells. Toxicol. Lett. *179*, 130–139.

Hu, B., Guo, P., Bar-Joseph, I., Imanishi, Y., Jarzynka, M.J., Bogler, O., Mikkelsen, T., Hirose, T., Nishikawa, R., and Cheng, S.Y. (2007). Neuropilin-1 promotes human glioma progression through potentiating the activity of the HGF/SF autocrine pathway. Oncogene *26*, 5577–5586.

Hubert, P., Sawma, P., Duneau, J.-P., Khao, J., Hénin, J., Bagnard, D., and Sturgis, J. (2010). Single-spanning transmembrane domains in cell growth and cell-cell interactions: more than meets the eye? Cell Adhes. Migr. *4*, 313–324.

Hussain, S.M., Hess, K.L., Gearhart, J.M., Geiss, K.T., and Schlager, J.J. (2005). *In vitro* toxicity of nanoparticles in BRL 3A rat liver cells. Toxicol. Vitro Int. J. Publ. Assoc. BIBRA *19*, 975–983.

Hwang, D.J., Roberts, I.M., and Wilson, T.M. (1994). Assembly of *Tobacco mosaic virus* and TMV-like pseudovirus particles in *Escherichia coli*. Arch. Virol. Suppl. *9*, 543–558.

Iijima, S. (1991). Helical microtubules of graphitic carbon. Nature *354*, 56–58.

Insua-Rodríguez, J., Pein, M., Hongu, T., Meier, J., Descot, A., Lowy, C.M., De Braekeleer, E., Sinn, H.-P., Spaich, S., Sütterlin, M., et al. (2018). Stress signaling in breast cancer cells induces matrix components that promote chemoresistant metastasis. EMBO Mol. Med. *10*.

Ittrich, H., Peldschus, K., Raabe, N., Kaul, M., and Adam, G. (2013). Superparamagnetic iron oxide nanoparticles in biomedicine: applications and developments in diagnostics and therapy. ROFO. Fortschr. Geb. Rontgenstr. Nuklearmed. *185*, 1149–1166.

Jacob, L., Sawma, P., Garnier, N., Meyer, L.A.T., Fritz, J., Hussenet, T., Spenlé, C., Goetz, J., Vermot, J., Fernandez, A., et al. (2016). Inhibition of PlexA1-mediated brain tumor growth and tumor-associated angiogenesis using a transmembrane domain targeting peptide. Oncotarget *7*, 57851–57865.

Jia, G., Han, Y., An, Y., Ding, Y., He, C., Wang, X., and Tang, Q. (2018). NRP-1 targeted and cargo-loaded exosomes facilitate simultaneous imaging and therapy of glioma *in vitro* and *in vivo*. Biomaterials *178*, 302–316.

Jin, H.-E., Farr, R., and Lee, S.-W. (2014). Collagen mimetic peptide engineered M13 bacteriophage for collagen targeting and imaging in cancer. Biomaterials *35*, 9236–9245.

Ju, Z., and Sun, W. (2017). Drug delivery vectors based on filamentous bacteriophages and phage-mimetic nanoparticles. Drug Deliv. *24*, 1898–1908.

Jubb, A.M., Strickland, L.A., Liu, S.D., Mak, J., Schmidt, M., and Koeppen, H. (2012). Neuropilin-1 expression in cancer and development. J. Pathol. *226*, 50–60.

Junttila, M.R., and de Sauvage, F.J. (2013). Influence of tumour micro-environment heterogeneity on therapeutic response. Nature *501*, 346–354.

Junttila, T.T., Akita, R.W., Parsons, K., Fields, C., Lewis Phillips, G.D., Friedman, L.S., Sampath, D., and Sliwkowski, M.X. (2009). Ligand-independent HER2/HER3/PI3K complex is disrupted by trastuzumab and is effectively inhibited by the PI3K inhibitor GDC-0941. Cancer Cell *15*, 429–440.

Kalluri, A., Debnath, D., Dharmadhikari, B., and Patra, P. (2018). Graphene quantum dots: synthesis and applications. Methods Enzymol. *609*, 335–354.

Kaminski, J.M., Huber, M.R., Summers, J.B., and Ward, M.B. (2002). Design of a nonviral vector for site-selective, efficient integration into the human genome. FASEB J. Off. Publ. Fed. Am. Soc. Exp. Biol. *16*, 1242–1247.

Kantoff, P.W., Higano, C.S., Shore, N.D., Berger, E.R., Small, E.J., Penson, D.F., Redfern, C.H., Ferrari, A.C., Dreicer, R., Sims, R.B., et al. (2010). Sipuleucel-T immunotherapy for castration-resistant prostate cancer. N. Engl. J. Med. *363*, 411–422.

Karimova, G., Ullmann, A., and Ladant, D. (2001). Protein-protein interaction between *Bacillus stearothermophilus* tyrosyl-tRNA synthetase subdomains revealed by a bacterial two-hybrid system. J. Mol. Microbiol. Biotechnol. *3*, 73–82.

Katano, M., and Torisu, M. (1982). Neutrophil-mediated tumor cell destruction in cancer ascites. Cancer *50*, 62–68.

Kawakami, A., Kitsukawa, T., Takagi, S., and Fujisawa, H. (1996). Developmentally regulated expression of a cell surface protein, neuropilin, in the mouse nervous system. J. Neurobiol. *29*, 1–17.

Kay, M.A. (2011). State-of-the-art gene-based therapies: the road ahead. Nat. Rev. Genet. *12*, 316–328.

Kemnade, J.O., Seethammagari, M., Collinson-Pautz, M., Kaur, H., Spencer, D.M., and McCormick, A.A. (2014). *Tobacco mosaic virus* efficiently targets DC uptake, activation and antigen-specific T cell responses in vivo. Vaccine *32*, 4228–4233.

Kessel, D., Jeffers, R., Fowlkes, J.B., and Cain, C. (1994). Porphyrin-induced enhancement of ultrasound cytotoxicity. Int. J. Radiat. Biol. *66*, 221–228.

Kim, S.T., Chompoosor, A., Yeh, Y.-C., Agasti, S.S., Solfiell, D.J., and Rotello, V.M. (2012). Dendronized gold nanoparticles for siRNA delivery. Small Weinh. Bergstr. Ger. *8*, 3253–3256.

Koch, C., Eber, F.J., Azucena, C., Förste, A., Walheim, S., Schimmel, T., Bittner, A.M., Jeske, H., Gliemann, H., Eiben, S., et al. (2016). Novel roles for well-known players: from *Tobacco mosaic virus* pests to enzymatically active assemblies. Beilstein J. Nanotechnol. *7*, 613–629.

Koch, C., Poghossian, A., Schöning, M.J., and Wege, C. (2018). Penicillin detection by *Tobacco mosaic virus*-assisted colorimetric biosensors. Nanotheranostics *2*, 184–196.

Koo, M., Bendahmane, M., Lettieri, G.A., Paoletti, A.D., Lane, T.E., Fitchen, J.H., Buchmeier, M.J., and Beachy, R.N. (1999). Protective immunity against *Murine hepatitis virus* (MHV) induced by intranasal or subcutaneous administration of hybrids of *Tobacco mosaic virus* that carries an MHV epitope. Proc. Natl. Acad. Sci. U. S. A. *96*, 7774–7779.

Koudelka, K.J., Destito, G., Plummer, E.M., Trauger, S.A., Siuzdak, G., and Manchester, M. (2009). Endothelial targeting of *Cowpea mosaic virus* (CPMV) via surface vimentin. PLoS Pathog. *5*, e1000417.

Kreike, B., van Kouwenhove, M., Horlings, H., Weigelt, B., Peterse, H., Bartelink, H., and van de Vijver, M.J. (2007). Gene expression profiling and histopathological characterization of triple-negative/basal-like breast carcinomas. Breast Cancer Res. BCR *9*, R65.

Kuwahara, Y., Mori, M., Kitahara, S., Fukumoto, M., Ezaki, T., Mori, S., Echigo, S., Ohkubo, Y., and Fukumoto, M. (2014). Targeting of tumor endothelial cells combining 2 Gy/day of X-ray with Everolimus is the effective modality for overcoming clinically relevant radioresistant tumors. Cancer Med. *3*, 310–321.

Laird, D.W., Fistouris, P., Batist, G., Alpert, L., Huynh, H.T., Carystinos, G.D., and Alaoui-Jamali, M.A. (1999). Deficiency of connexin43 gap junctions is an independent marker for breast tumors. Cancer Res. *59*, 4104–4110.

Lam, P., and Steinmetz, N.F. (2018). Plant viral and bacteriophage delivery of nucleic acid therapeutics. Wiley Interdiscip. Rev. Nanomed. Nanobiotechnol. *10*.

Lambert, A.W., Pattabiraman, D.R., and Weinberg, R.A. (2017). Emerging biological principles of metastasis. Cell *168*, 670–691.

Larkins, E., Blumenthal, G.M., Yuan, W., He, K., Sridhara, R., Subramaniam, S., Zhao, H., Liu, C., Yu, J., Goldberg, K.B., et al. (2017). FDA Approval summary: pembrolizumab for the treatment of recurrent or metastatic head and neck squamous cell carcinoma with disease progression on or after platinum-containing chemotherapy. The Oncologist *22*, 873–878.

Laurent, S., Bridot, J.-L., Elst, L.V., and Muller, R.N. (2010). Magnetic iron oxide nanoparticles for biomedical applications. Future Med. Chem. *2*, 427–449.

Lawrie, T.A., Green, J.T., Beresford, M., Wedlake, L., Burden, S., Davidson, S.E., Lal, S., Henson, C.C., and Andreyev, H.J.N. (2018). Interventions to reduce acute and late adverse gastrointestinal effects of pelvic radiotherapy for primary pelvic cancers. Cochrane Database Syst. Rev. *1*, CD012529.

Lebel, M.-È., Chartrand, K., Leclerc, D., and Lamarre, A. (2015). Plant viruses as nanoparticle-based vaccines and adjuvants. Vaccines *3*, 620–637.

Lee, K.L., Carpenter, B.L., Wen, A.M., Ghiladi, R.A., and Steinmetz, N.F. (2016). High aspect ratio nanotubes formed by *Tobacco mosaic virus* for delivery of photodynamic agents targeting melanoma. ACS Biomater. Sci. Eng. *2*, 838–844.

Lee, M.S., Dees, E.C., and Wang, A.Z. (2017). Nanoparticle-delivered chemotherapy: old drugs in new packages. Oncol. Williston Park N *31*, 198–208.

Lemmon, M.A., Flanagan, J.M., Treutlein, H.R., Zhang, J., and Engelman, D.M. (1992a). Sequence specificity in the dimerization of transmembrane alpha-helices. Biochemistry *31*, 12719–12725.

Lemmon, M.A., Flanagan, J.M., Hunt, J.F., Adair, B.D., Bormann, B.J., Dempsey, C.E., and Engelman, D.M. (1992b). Glycophorin A dimerization is driven by specific interactions between transmembrane alpha-helices. J. Biol. Chem. *267*, 7683–7689.

Lemmon, M.A., Treutlein, H.R., Adams, P.D., Brünger, A.T., and Engelman, D.M. (1994). A dimerization motif for transmembrane alpha-helices. Nat. Struct. Biol. *1*, 157–163.

Lepock, J.R. (2005). Measurement of protein stability and protein denaturation in cells using differential scanning calorimetry. Methods San Diego Calif *35*, 117–125.

Li, F., Lv, J.-H., Liang, L., Wang, J.-C., Li, C.-R., Sun, L., and Li, T. (2018a). Downregulation of microRNA-21 inhibited radiation-resistance of esophageal squamous cell carcinoma. Cancer Cell Int. *18*, 39.

Li, J., Kim, S.G., and Blenis, J. (2014). Rapamycin: one drug, many effects. Cell Metab. *19*, 373–379.

Li, K., Giang Nguyen, H., Lu, X., and Wang, Q. (2010). Viruses and their potential in bioimaging and biosensing applications. Analyst *135*, 21–27.

Li, M., Wang, Y., Lin, H., and Qu, F. (2019). Hollow CuS nanocube as nanocarrier for synergetic chemo/photothermal/photodynamic therapy. Mater. Sci. Eng. C Mater. Biol. Appl. *96*, 591–598.

Li, R., Wu, R., Zhao, L., Hu, Z., Guo, S., Pan, X., and Zou, H. (2011). Folate and iron difunctionalized multiwall carbon nanotubes as dual-targeted drug nanocarrier to cancer cells. Carbon *49*, 1797–1805.

Li, W., Li, X., Liu, S., Yang, W., Pan, F., Yang, X.-Y., Du, B., Qin, L., and Pan, Y. (2017). Gold nanoparticles attenuate metastasis by tumor vasculature normalization and epithelial-mesenchymal transition inhibition. Int. J. Nanomedicine *12*, 3509–3520.

Li, Y., Lu, A., Long, M., Cui, L., Chen, Z., and Zhu, L. (2018b). Nitroimidazole derivative incorporated liposomes for hypoxia-triggered drug delivery and enhanced therapeutic efficacy in patient-derived tumor xenografts. Acta Biomater.

Liang, W.-C., Dennis, M.S., Stawicki, S., Chanthery, Y., Pan, Q., Chen, Y., Eigenbrot, C., Yin, J., Koch, A.W., Wu, X., et al. (2007). Function blocking antibodies to neuropilin-1 generated from a designed human synthetic antibody phage library. J. Mol. Biol. *366*, 815–829.

Lim, S., Becker, A., Zimmer, A., Lu, J., Buettner, R., and Kirfel, J. (2013). SNAI1-mediated epithelial-mesenchymal transition confers chemoresistance and cellular plasticity by regulating genes involved in cell death and stem cell maintenance. PLoS One *8*, e66558.

Lin, R.D., and Steinmetz, N.F. (2018). *Tobacco mosaic virus* delivery of mitoxantrone for cancer therapy. Nanoscale.

Liu, C., Wang, Z., Wang, Y., and Gu, W. (2015). MiR-338 suppresses the growth and metastasis of OSCC cells by targeting NRP1. Mol. Cell. Biochem. *398*, 115–122.

Liu, H., Zhang, J., Wang, S., Pang, Z., Wang, Z., Zhou, W., and Wu, M. (2012a). Screening of autoantibodies as potential biomarkers for hepatocellular carcinoma by using T7 phase display system. Cancer Epidemiol. *36*, 82–88.

Liu, L., Ni, F., Zhang, J., Jiang, X., Lu, X., Guo, Z., and Xu, R. (2011). Silver nanocrystals sensitize magnetic-nanoparticle-mediated thermo-induced killing of cancer cells. Acta Biochim. Biophys. Sin. *43*, 316–323.

Liu, R., Vaishnav, R.A., Roberts, A.M., and Friedland, R.P. (2013). Humans have antibodies against a plant virus: evidence from *Tobacco mosaic virus*. PloS One *8*, e60621.

Liu, S., Lachapelle, J., Leung, S., Gao, D., Foulkes, W.D., and Nielsen, T.O. (2012b). CD8+ lymphocyte infiltration is an independent favorable prognostic indicator in basal-like breast cancer. Breast Cancer Res. BCR *14*, R48.

Liu, X., Wu, F., Tian, Y., Wu, M., Zhou, Q., Jiang, S., and Niu, Z. (2016). Size dependent cellular uptake of rod-like bionanoparticles with different aspect ratios. Sci. Rep. *6*, 24567.

Liu, Y., Chen, X., Han, W., and Zhang, Y. (2017). Tisagenlecleucel, an approved anti-CD19 chimeric antigen receptor T-cell therapy for the treatment of leukemia. Drugs Today Barc. Spain 1998 *53*, 597–608.

Liu, Z., Sun, X., Nakayama-Ratchford, N., and Dai, H. (2007). Supramolecular chemistry on water-soluble carbon nanotubes for drug loading and delivery. ACS Nano *1*, 50–56.

Lizotte, P.H., Wen, A.M., Sheen, M.R., Fields, J., Rojanasopondist, P., Steinmetz, N.F., and Fiering, S. (2016). In situ vaccination with *Cowpea mosaic virus* nanoparticles suppresses metastatic cancer. Nat. Nanotechnol. *11*, 295–303.

Loewenstein, W.R. (1979). Junctional intercellular communication and the control of growth. Biochim. Biophys. Acta *560*, 1–65.

Lomonossoff, G.P., and Wege, C. (2018). TMV particles: the journey from fundamental studies to bionanotechnology applications. In Advances in Virus Research, (Elsevier), pp. 149–176.

Long, G.V., Trefzer, U., Davies, M.A., Kefford, R.F., Ascierto, P.A., Chapman, P.B., Puzanov, I., Hauschild, A., Robert, C., Algazi, A., et al. (2012). Dabrafenib in patients with Val600Glu or Val600Lys BRAF-mutant melanoma metastatic to the brain (BREAK-MB): a multicentre, open-label, phase 2 trial. Lancet Oncol. *13*, 1087–1095.

Lucky, S.S., Soo, K.C., and Zhang, Y. (2015). Nanoparticles in photodynamic therapy. Chem. Rev. *115*, 1990–2042.

Ma, Y.-L., Lin, S.-W., Fang, H.-C., Chou, K.-J., Bee, Y.-S., Chu, T.-H., Chang, M.-C., Weng, W.-T., Wu, C.-Y., Cho, C.-L., et al. (2014). A novel poly-naphthol compound ST104P

suppresses angiogenesis by attenuating matrix metalloproteinase-2 expression in endothelial cells. Int. J. Mol. Sci. *15*, 16611–16627.

MacKenzie, K.R., Prestegard, J.H., and Engelman, D.M. (1997). A transmembrane helix dimer: structure and implications. Science *276*, 131–133.

Mahmoud, S., Lee, A., Ellis, I., and Green, A. (2012). CD8(+) T lymphocytes infiltrating breast cancer: A promising new prognostic marker? Oncoimmunology *1*, 364–365.

Mani, S.A., Guo, W., Liao, M.-J., Eaton, E.N., Ayyanan, A., Zhou, A.Y., Brooks, M., Reinhard, F., Zhang, C.C., Shipitsin, M., et al. (2008). The epithelial-mesenchymal transition generates cells with properties of stem cells. Cell *133*, 704–715.

Matsumura, Y., and Maeda, H. (1986). A new concept for macromolecular therapeutics in cancer chemotherapy: mechanism of tumoritropic accumulation of proteins and the antitumor agent smancs. Cancer Res. *46*, 6387–6392.

McCormick, A.A., and Palmer, K.E. (2008). Genetically engineered *Tobacco mosaic virus* as nanoparticle vaccines. Expert Rev. Vaccines *7*, 33–41.

McCormick, A.A., Corbo, T.A., Wykoff-Clary, S., Nguyen, L.V., Smith, M.L., Palmer, K.E., and Pogue, G.P. (2006). TMV-peptide fusion vaccines induce cell-mediated immune responses and tumor protection in two murine models. Vaccine *24*, 6414–6423.

Medina, P.J., and Goodin, S. (2008). Lapatinib: a dual inhibitor of human epidermal growth factor receptor tyrosine kinases. Clin. Ther. *30*, 1426–1447.

Medintz, I.L., Sapsford, K.E., Konnert, J.H., Chatterji, A., Lin, T., Johnson, J.E., and Mattoussi, H. (2005). Decoration of discretely immobilized *Cowpea mosaic virus* with luminescent quantum dots. Langmuir ACS J. Surf. Colloids *21*, 5501–5510.

Mel'nikov, P.A., Baklaushev, V.P., Gabashvili, A.N., Nukolova, N.V., Kuznetsov, I.I., Cherepanov, S.A., Koshkin, F.A., Leopol'd, A.V., and Chekhonin, V.P. (2017). Internalization of vectorized liposomes loaded with plasmid DNA in C6 glioma cells. Bull. Exp. Biol. Med. *163*, 114–122.

Meng, J., Meng, J., Duan, J., Kong, H., Li, L., Wang, C., Xie, S., Chen, S., Gu, N., Xu, H., et al. (2008). Carbon nanotubes conjugated to tumor lysate protein enhance the efficacy of an antitumor immunotherapy. Small Weinh. Bergstr. Ger. *4*, 1364–1370.

Meyer, L.A.T., Fritz, J., Pierdant-Mancera, M., and Bagnard, D. (2016). Current drug design to target the Semaphorin/Neuropilin/Plexin complexes. Cell Adhes. Migr. *10*, 700–708.

Mironov, A.F., Seylanov, A.S., Seylanov, J.A., Pizhik, V.M., Deruzhenko, I.V., and Nockel, A.J. (1992). Haematoporphyrin derivatives: distribution in a living organism. J. Photochem. Photobiol. B *16*, 341–346.

Miyauchi, J.T., Chen, D., Choi, M., Nissen, J.C., Shroyer, K.R., Djordevic, S., Zachary, I.C., Selwood, D., and Tsirka, S.E. (2016). Ablation of neuropilin 1 from glioma-associated microglia and macrophages slows tumor progression. Oncotarget *7*, 9801–9814.

Mocan, T., Matea, C., Tabaran, F., Iancu, C., Orasan, R., and Mocan, L. (2015). *In vitro* administration of gold nanoparticles functionalized with MUC-1 protein fragment generates anticancer aaccine response via macrophage activation and polarization mechanism. J. Cancer *6*, 583–592.

Morin, E., Sjöberg, E., Tjomsland, V., Testini, C., Lindskog, C., Franklin, O., Sund, M., Öhlund, D., Kiflemariam, S., Sjöblom, T., et al. (2018). VEGF receptor-2/neuropilin 1 trans-complex formation between endothelial and tumor cells is an independent predictor of pancreatic cancer survival. J. Pathol. *246*, 311–322.

Mosmann, T. (1983). Rapid colorimetric assay for cellular growth and survival: application to proliferation and cytotoxicity assays. J. Immunol. Methods *65*, 55–63.

Mroz, P., Tegos, G.P., Gali, H., Wharton, T., Sarna, T., and Hamblin, M.R. (2007). Photodynamic therapy with fullerenes. Photochem. Photobiol. Sci. Off. J. Eur. Photochem. Assoc. Eur. Soc. Photobiol. *6*, 1139–1149.

Nakamura, F., Tanaka, M., Takahashi, T., Kalb, R.G., and Strittmatter, S.M. (1998). Neuropilin-1 extracellular domains mediate semaphorin D/III-induced growth cone collapse. Neuron *21*, 1093–1100.

Namba, K., and Stubbs, G. (1986). Structure of *Tobacco mosaic virus* at 3.6 A resolution: implications for assembly. Science *231*, 1401–1406.

Namba, K., Pattanayek, R., and Stubbs, G. (1989). Visualization of protein-nucleic acid interactions in a virus. Refined structure of intact *Tobacco mosaic virus* at 2.9 A resolution by X-ray fiber diffraction. J. Mol. Biol. *208*, 307–325.

Nasarre, C., Roth, M., Jacob, L., Roth, L., Koncina, E., Thien, A., Labourdette, G., Poulet, P., Hubert, P., Crémel, G., et al. (2010). Peptide-based interference of the transmembrane domain of neuropilin-1 inhibits glioma growth *in vivo*. Oncogene *29*, 2381–2392.

Ni, W.-D., Yang, Z.-T., Cui, C.-A., Cui, Y., Fang, L.-Y., and Xuan, Y.-H. (2017). Tenascin-C is a potential cancer-associated fibroblasts marker and predicts poor prognosis in prostate cancer. Biochem. Biophys. Res. Commun. *486*, 607–612.

Nicastro, J., Sheldon, K., and Slavcev, R.A. (2014). Bacteriophage lambda display systems: developments and applications. Appl. Microbiol. Biotechnol. *98*, 2853–2866.

Nichols, J.W., and Bae, Y.H. (2014). EPR: Evidence and fallacy. J. Control. Release Off. J. Control. Release Soc. *190*, 451–464.

Niehl, A., Appaix, F., Boscá, S., van der Sanden, B., Nicoud, J.-F., Bolze, F., and Heinlein, M. (2015). Fluorescent *Tobacco mosaic virus*-derived bio-nanoparticles for intravital two-photon imaging. Front. Plant Sci. *6*, 1244.

Niescioruk, A., Nieciecka, D., Puszko, A.K., Królikowska, A., Kosson, P., Perret, G.Y., Krysinski, P., and Misicka, A. (2017). Physicochemical properties and *in vitro* cytotoxicity of iron oxide-based nanoparticles modified with antiangiogenic and antitumor peptide A7R. J. Nanoparticle Res. Interdiscip. Forum Nanoscale Sci. Technol. *19*, 160.

Nieto, M.A., Sargent, M.G., Wilkinson, D.G., and Cooke, J. (1994). Control of cell behavior during vertebrate development by Slug, a zinc finger gene. Science *264*, 835–839.

Nieto, M.A., Huang, R.Y.-J., Jackson, R.A., and Thiery, J.P. (2016). EMT: 2016. Cell *166*, 21–45.

Ohtani, H. (2007). Focus on TILs: prognostic significance of tumor infiltrating lymphocytes in human colorectal cancer. Cancer Immun. *7*, 4.

Okada, Y. (1975). Mechanism of assembly of *Tobacco mosaic virus in vitro*. Adv. Biophys. *7*, 1–41.

Ormond, A.B., and Freeman, H.S. (2013). Dye sensitizers for photodynamic therapy. Materials *6*, 817–840.

Pai-Scherf, L., Blumenthal, G.M., Li, H., Subramaniam, S., Mishra-Kalyani, P.S., He, K., Zhao, H., Yu, J., Paciga, M., Goldberg, K.B., et al. (2017). FDA Approval summary: pembrolizumab for treatment of metastatic non-small cell lung cancer: first-line therapy and beyond. The Oncologist *22*, 1392–1399.

Palvai, S., Anandi, L., Sarkar, S., Augustus, M., Roy, S., Lahiri, M., and Basu, S. (2017). Drug-triggered self-assembly of linear polymer into nanoparticles for simultaneous delivery of hydrophobic and hydrophilic drugs in breast cancer cells. ACS Omega *2*, 8730–8740.

Park, H.J., Griffin, R.J., Hui, S., Levitt, S.H., and Song, C.W. (2012). Radiation-induced vascular damage in tumors: implications of vascular damage in ablative hypofractionated radiotherapy (SBRT and SRS). Radiat. Res. *177*, 311–327.

Patnaik, A., LoRusso, P.M., Messersmith, W.A., Papadopoulos, K.P., Gore, L., Beeram, M., Ramakrishnan, V., Kim, A.H., Beyer, J.C., Mason Shih, L., et al. (2014). A Phase Ib study evaluating MNRP1685A, a fully human anti-NRP1 monoclonal antibody, in combination with bevacizumab and paclitaxel in patients with advanced solid tumors. Cancer Chemother. Pharmacol. *73*, 951–960.

Pearson, R.M., Sunoqrot, S., Hsu, H.-J., Bae, J.W., and Hong, S. (2012). Dendritic nanoparticles: the next generation of nanocarriers? Ther. Deliv. *3*, 941–959.

Peng, Y., Liu, Y.-M., Li, L.-C., Wang, L.-L., and Wu, X.-L. (2014). MicroRNA-338 inhibits growth, invasion and metastasis of gastric cancer by targeting NRP1 expression. PloS One *9*, e94422.

Pérez Filgueira, D.M., Mozgovoj, M., Wigdorovitz, A., Dus Santos, M.J., Parreño, V., Trono, K., Fernandez, F.M., Carrillo, C., Babiuk, L.A., Morris, T.J., et al. (2004). Passive protection to *Bovine rotavirus* (BRV) infection induced by a BRV VP8* produced in plants using a TMV-based vector. Arch. Virol. *149*, 2337–2348.

Perham, R.N., and Wilson, T.M. (1976). The polarity of stripping of coat protein subunits from the RNA in *Tobacco mosaic virus* under alkaline conditions. FEBS Lett. *62*, 11–15.

Perret, G.Y., Starzec, A., Hauet, N., Vergote, J., Le Pecheur, M., Vassy, R., Léger, G., Verbeke, K.A., Bormans, G., Nicolas, P., et al. (2004). *In vitro* evaluation and biodistribution of a 99mTc-labeled anti-VEGF peptide targeting neuropilin-1. Nucl. Med. Biol. *31*, 575–581.

Pfeffer, S.R., Yang, C.H., and Pfeffer, L.M. (2015). The Role of miR-21 in Cancer. Drug Dev. Res. *76*, 270–277.

Pitzalis, N., and Heinlein, M. (2017). The roles of membranes and associated cytoskeleton in plant virus replication and cell-to-cell movement. J. Exp. Bot. *69*, 117–132.

Pol, J., Kroemer, G., and Galluzzi, L. (2016). First oncolytic virus approved for melanoma immunotherapy. Oncoimmunology *5*, e1115641.

Pramual, S., Lirdprapamongkol, K., Svasti, J., Bergkvist, M., Jouan-Hureaux, V., Arnoux, P., Frochot, C., Barberi-Heyob, M., and Niamsiri, N. (2017). Polymer-lipid-PEG hybrid nanoparticles as photosensitizer carrier for photodynamic therapy. J. Photochem. Photobiol. B *173*, 12–22.

Pranjol, M.Z.I., and Hajitou, A. (2015). Bacteriophage-derived vectors for targeted cancer gene therapy. Viruses *7*, 268–284.

Prasad, S., Cody, V., Saucier-Sawyer, J.K., Saltzman, W.M., Sasaki, C.T., Edelson, R.L., Birchall, M.A., and Hanlon, D.J. (2011). Polymer nanoparticles containing tumor lysates as antigen delivery vehicles for dendritic cell-based antitumor immunotherapy. Nanomedicine Nanotechnol. Biol. Med. *7*, 1–10.

Press, M.F., Bernstein, L., Thomas, P.A., Meisner, L.F., Zhou, J.Y., Ma, Y., Hung, G., Robinson, R.A., Harris, C., El-Naggar, A., et al. (1997). HER-2/neu gene amplification characterized by fluorescence *in situ* hybridization: poor prognosis in node-negative breast carcinomas. J. Clin. Oncol. Off. J. Am. Soc. Clin. Oncol. *15*, 2894–2904.

Prestwich, R.J., Errington, F., Ilett, E.J., Morgan, R.S.M., Scott, K.J., Kottke, T., Thompson, J., Morrison, E.E., Harrington, K.J., Pandha, H.S., et al. (2008). Tumor infection by oncolytic

reovirus primes adaptive antitumor immunity. Clin. Cancer Res. Off. J. Am. Assoc. Cancer Res. *14*, 7358–7366.

Prime, J. (1900). Des accidents toxiques produits par l'éosinate de sodium.

Püschel, A.W. (2002). The function of neuropilin/plexin complexes. Adv. Exp. Med. Biol. *515*, 71–80.

Qin, Y., Han, L., Yang, D., Wei, H., Liu, Y., Xu, J., Autrup, H., Deng, F., and Guo, X. (2018). Silver nanoparticles increase connexin43-mediated gap junctional intercellular communication in HaCaT cells through activation of reactive oxygen species and mitogen-activated protein kinase signal pathway. J. Appl. Toxicol. JAT *38*, 564–574.

Renzi, M.J., Feiner, L., Koppel, A.M., and Raper, J.A. (1999). A dominant negative receptor for specific secreted semaphorins is generated by deleting an extracellular domain from neuropilin-1. J. Neurosci. Off. J. Soc. Neurosci. *19*, 7870–7880.

Riaz, M.K., Riaz, M.A., Zhang, X., Lin, C., Wong, K.H., Chen, X., Zhang, G., Lu, A., and Yang, Z. (2018). Surface functionalization and targeting strategies of liposomes in solid tumor therapy: a review. Int. J. Mol. Sci. *19*.

Ribatti, D., Nico, B., Crivellato, E., and Vacca, A. (2007). The structure of the vascular network of tumors. Cancer Lett. *248*, 18–23.

Ribatti, D., Nico, B., and Crivellato, E. (2011). The role of pericytes in angiogenesis. Int. J. Dev. Biol. *55*, 261–268.

Richter, A.W., and Akerblom, E. (1984). Polyethylene glycol reactive antibodies in man: titer distribution in allergic patients treated with monomethoxy polyethylene glycol modified allergens or placebo, and in healthy blood donors. Int. Arch. Allergy Appl. Immunol. *74*, 36–39.

Ripoll, M., Pierdant, M., Neuberg, P., Bagnard, D., Wagner, A., Kichler, A., and Remy, J.-S. (2018). Co-delivery of anti-PLK-1 siRNA and camptothecin by nanometric polydiacetylenic micelles results in a synergistic cell killing. RSC Adv. *8*, 20758–20763.

Rizzolio, S., Rabinowicz, N., Rainero, E., Lanzetti, L., Serini, G., Norman, J., Neufeld, G., and Tamagnone, L. (2012). Neuropilin-1-dependent regulation of EGF-receptor signaling. Cancer Res. *72*, 5801–5811.

Rizzolio, S., Cagnoni, G., Battistini, C., Bonelli, S., Isella, C., Van Ginderachter, J.A., Bernards, R., Di Nicolantonio, F., Giordano, S., and Tamagnone, L. (2018). Neuropilin-1 upregulation elicits adaptive resistance to oncogene-targeted therapies. J. Clin. Invest. *128*, 3976–3990.

Rochet, N.M., Kottschade, L.A., and Markovic, S.N. (2011). Vemurafenib for melanoma metastases to the brain. N. Engl. J. Med. *365*, 2439–2441.

Röder, J., Fischer, R., and Commandeur, U. (2017). Adoption of the 2A Ribosomal Skip Principle to *Tobacco Mosaic Virus* for Peptide Display. Front. Plant Sci. *8*, 1125.

Roskoski, R. (2018). Small molecule inhibitors targeting the EGFR/ErbB family of protein-tyrosine kinases in human cancers. Pharmacol. Res. *139*, 395–411.

Roth, L., Nasarre, C., Dirrig-Grosch, S., Aunis, D., Crémel, G., Hubert, P., and Bagnard, D. (2008). Transmembrane domain interactions control biological functions of neuropilin-1. Mol. Biol. Cell *19*, 646–654.

Roy, I., Ohulchanskyy, T.Y., Pudavar, H.E., Bergey, E.J., Oseroff, A.R., Morgan, J., Dougherty, T.J., and Prasad, P.N. (2003). Ceramic-based nanoparticles entrapping water-insoluble photosensitizing anticancer drugs: a novel drug-carrier system for photodynamic therapy. J. Am. Chem. Soc. *125*, 7860–7865.

Rudick, J.G., and Percec, V. (2008). Induced helical backbone conformations of self-organizable dendronized polymers. Acc. Chem. Res. *41*, 1641–1652.

Rugo, H.S., Olopade, O.I., DeMichele, A., Yau, C., van 't Veer, L.J., Buxton, M.B., Hogarth, M., Hylton, N.M., Paoloni, M., Perlmutter, J., et al. (2016). Adaptive randomization of veliparib–carboplatin treatment in breast cancer. N. Engl. J. Med. *375*, 23–34.

Rui, M., Qu, Y., Gao, T., Ge, Y., Feng, C., and Xu, X. (2017). Simultaneous delivery of anti-miR21 with doxorubicin prodrug by mimetic lipoprotein nanoparticles for synergistic effect against drug resistance in cancer cells. Int. J. Nanomedicine *12*, 217–237.

Russ, W.P., and Engelman, D.M. (2000). The GxxxG motif: a framework for transmembrane helix-helix association. J. Mol. Biol. *296*, 911–919.

Saejung, W., Fujiyama, K., Takasaki, T., Ito, M., Hori, K., Malasit, P., Watanabe, Y., Kurane, I., and Seki, T. (2007). Production of dengue 2 envelope domain III in plant using TMV-based vector system. Vaccine *25*, 6646–6654.

Saesoo, S., Sathornsumetee, S., Anekwiang, P., Treetidnipa, C., Thuwajit, P., Bunthot, S., Maneeprakorn, W., Maurizi, L., Hofmann, H., Rungsardthong, R.U., et al. (2018). Characterization of liposome-containing SPIONs conjugated with anti-CD20 developed as a novel theranostic agent for central nervous system lymphoma. Colloids Surf. B Biointerfaces *161*, 497–507.

Saunders, K., and Lomonossoff, G.P. (2017). *In planta* synthesis of designer-length *Tobacco mosaic virus*-based nano-rods that can be used to fabricate nano-wires. Front. Plant Sci. *8*, 1335.

Saupe, F., Schwenzer, A., Jia, Y., Gasser, I., Spenlé, C., Langlois, B., Kammerer, M., Lefebvre, O., Hlushchuk, R., Rupp, T., et al. (2013). Tenascin-C downregulates wnt inhibitor dickkopf-1, promoting tumorigenesis in a neuroendocrine tumor model. Cell Rep. *5*, 482–492.

Savagner, P., Kusewitt, D.F., Carver, E.A., Magnino, F., Choi, C., Gridley, T., and Hudson, L.G. (2005). Developmental transcription factor slug is required for effective re-epithelialization by adult keratinocytes. J. Cell. Physiol. *202*, 858–866.

Saw, P.E., Zhang, A., Nie, Y., Zhang, L., Xu, Y., and Xu, X. (2018). Tumor-associated fibronectin targeted liposomal nanoplatform for cyclophilin A siRNA delivery and targeted malignant glioblastoma therapy. Front. Pharmacol. *9*, 1194.

Scholthof, K.-B.G. (2004). *Tobacco mosaic virus*: a model system for plant biology. Annu. Rev. Phytopathol. *42*, 13–34.

Scholthof, K.-B.G., Adkins, S., Czosnek, H., Palukaitis, P., Jacquot, E., Hohn, T., Hohn, B., Saunders, K., Candresse, T., Ahlquist, P., et al. (2011). Top 10 plant viruses in molecular plant pathology. Mol. Plant Pathol. *12*, 938–954.

Schuster, T.M., Scheele, R.B., Adams, M.L., Shire, S.J., Steckert, J.J., and Potschka, M. (1980). Studies on the mechanism of assembly of *Tobacco mosaic virus*. Biophys. J. *32*, 313–329.

Senes, A., Gerstein, M., and Engelman, D.M. (2000). Statistical analysis of amino acid patterns in transmembrane helices: the GxxxG motif occurs frequently and in association with beta-branched residues at neighboring positions. J. Mol. Biol. *296*, 921–936.

Shah, S.P., Roth, A., Goya, R., Oloumi, A., Ha, G., Zhao, Y., Turashvili, G., Ding, J., Tse, K., Haffari, G., et al. (2012). The clonal and mutational evolution spectrum of primary triple-negative breast cancers. Nature *486*, 395–399.

Sharma, V.K., McDonald, T.J., Sohn, M., Anquandah, G.A.K., Pettine, M., and Zboril, R. (2017). Assessment of toxicity of selenium and cadmium selenium quantum dots: A review. Chemosphere *188*, 403–413.

She, W., Li, N., Luo, K., Guo, C., Wang, G., Geng, Y., and Gu, Z. (2013). Dendronized heparin-doxorubicin conjugate based nanoparticle as pH-responsive drug delivery system for cancer therapy. Biomaterials *34*, 2252–2264.

Shi, H., Moriceau, G., Kong, X., Lee, M.-K., Lee, H., Koya, R.C., Ng, C., Chodon, T., Scolyer, R.A., Dahlman, K.B., et al. (2012). Melanoma whole-exome sequencing identifies (V600E)B-RAF amplification-mediated acquired B-RAF inhibitor resistance. Nat. Commun. *3*, 724.

Shukla, S., Eber, F.J., Nagarajan, A.S., DiFranco, N.A., Schmidt, N., Wen, A.M., Eiben, S., Twyman, R.M., Wege, C., and Steinmetz, N.F. (2015). The impact of aspect ratio on the biodistribution and tumor homing of rigid soft-matter nanorods. Adv. Healthc. Mater. *4*, 874–882.

Sim, T., Kim, J.E., Hoang, N.H., Kang, J.K., Lim, C., Kim, D.S., Lee, E.S., Youn, Y.S., Choi, H.-G., Han, H.-K., et al. (2018). Development of a docetaxel micellar formulation using

poly(ethylene glycol)-polylactide-poly(ethylene glycol) (PEG-PLA-PEG) with successful reconstitution for tumor targeted drug delivery. Drug Deliv. *25*, 1362–1371.

Singh, P., Prasuhn, D., Yeh, R.M., Destito, G., Rae, C.S., Osborn, K., Finn, M.G., and Manchester, M. (2007). Bio-distribution, toxicity and pathology of *Cowpea mosaic virus* nanoparticles *in vivo*. J. Control. Release Off. J. Control. Release Soc. *120*, 41–50.

Singh, P., Kim, Y.J., and Yang, D.C. (2016a). A strategic approach for rapid synthesis of gold and silver nanoparticles by *Panax ginseng* leaves. Artif. Cells Nanomedicine Biotechnol. *44*, 1949–1957.

Singh, P., Singh, H., Kim, Y.J., Mathiyalagan, R., Wang, C., and Yang, D.C. (2016b). Extracellular synthesis of silver and gold nanoparticles by *Sporosarcina koreensis* DC4 and their biological applications. Enzyme Microb. Technol. *86*, 75–83.

Siriwon, N., Kim, Y.J., Siegler, E., Chen, X., Rohrs, J.A., Liu, Y., and Wang, P. (2018). CAR-T cells surface-engineered with drug-encapsulated nanoparticles can ameliorate intratumoral T-cell hypofunction. Cancer Immunol. Res. *6*, 812–824.

Sirsi, S., and Borden, M. (2009). Microbubble compositions, properties and biomedical applications. Bubble Sci. Eng. Technol. *1*, 3–17.

Slamon, D.J., Clark, G.M., Wong, S.G., Levin, W.J., Ullrich, A., and McGuire, W.L. (1987). Human breast cancer: correlation of relapse and survival with amplification of the HER-2/neu oncogene. Science *235*, 177–182.

Slebos, R.J., and Rodenhuis, S. (1992). The Ras gene family in human non-small-cell lung cancer. J. Natl. Cancer Inst. Monogr. 23–29.

Smith, M.L., Lindbo, J.A., Dillard-Telm, S., Brosio, P.M., Lasnik, A.B., McCormick, A.A., Nguyen, L.V., and Palmer, K.E. (2006). Modified *Tobacco mosaic virus* particles as scaffolds for display of protein antigens for vaccine applications. Virology *348*, 475–488.

Soda, Y., Marumoto, T., Friedmann-Morvinski, D., Soda, M., Liu, F., Michiue, H., Pastorino, S., Yang, M., Hoffman, R.M., Kesari, S., et al. (2011). Transdifferentiation of glioblastoma cells into vascular endothelial cells. Proc. Natl. Acad. Sci. U. S. A. *108*, 4274–4280.

Soe, Z.C., Thapa, R.K., Ou, W., Gautam, M., Nguyen, H.T., Jin, S.G., Ku, S.K., Oh, K.T., Choi, H.-G., Yong, C.S., et al. (2018). Folate receptor-mediated celastrol and irinotecan combination delivery using liposomes for effective chemotherapy. Colloids Surf. B Biointerfaces *170*, 718–728.

Soker, S., Takashima, S., Miao, H.Q., Neufeld, G., and Klagsbrun, M. (1998). Neuropilin-1 is expressed by endothelial and tumor cells as an isoform-specific receptor for vascular endothelial growth factor. Cell *92*, 735–745.

Soker, S., Miao, H.-Q., Nomi, M., Takashima, S., and Klagsbrun, M. (2002). VEGF165 mediates formation of complexes containing VEGFR-2 and neuropilin-1 that enhance VEGF165-receptor binding. J. Cell. Biochem. *85*, 357–368.

Son, K.H., Hong, J.H., and Lee, J.W. (2016). Carbon nanotubes as cancer therapeutic carriers and mediators. Int. J. Nanomedicine *11*, 5163–5185.

Song, C.W., Sung, J.H., Clement, J.J., and Levitt, S.H. (1974). Vascular changes in neuroblastoma of mice following x-irradiation. Cancer Res. *34*, 2344–2350.

Song, C.W., Park, H.J., Lee, C.K., and Griffin, R. (2005). Implications of increased tumor blood flow and oxygenation caused by mild temperature hyperthermia in tumor treatment. Int. J. Hyperth. Off. J. Eur. Soc. Hyperthermic Oncol. North Am. Hyperth. Group *21*, 761–767.

Song, H.-T., Hoang, N.H., Yun, J.M., Park, Y.J., Song, E.H., Lee, E.S., Youn, Y.S., and Oh, K.T. (2016). Development of a new tri-block copolymer with a functional end and its feasibility for treatment of metastatic breast cancer. Colloids Surf. B Biointerfaces *144*, 73–80.

Soshnikova, V., Kim, Y.J., Singh, P., Huo, Y., Markus, J., Ahn, S., Castro-Aceituno, V., Kang, J., Chokkalingam, M., Mathiyalagan, R., et al. (2018). Cardamom fruits as a green resource for facile synthesis of gold and silver nanoparticles and their biological applications. Artif. Cells Nanomedicine Biotechnol. *46*, 108–117.

Spain, L., Diem, S., and Larkin, J. (2016). Management of toxicities of immune checkpoint inhibitors. Cancer Treat. Rev. *44*, 51–60.

Spikes, J.D. (1990). New trends in photobiology: Chlorins as photosensitizers in biology and medicine. J. Photochem. Photobiol. B *6*, 259–274.

Starzec, A., Vassy, R., Martin, A., Lecouvey, M., Di Benedetto, M., Crépin, M., and Perret, G.Y. (2006). Antiangiogenic and antitumor activities of peptide inhibiting the vascular endothelial growth factor binding to neuropilin-1. Life Sci. *79*, 2370–2381.

Stefan, E., and Bister, K. (2017). MYC and RAF: Key Effectors in cellular signaling and major drivers in human cancer. Curr. Top. Microbiol. Immunol. *407*, 117–151.

Steinmetz, N.F., and Evans, D.J. (2007). Utilisation of plant viruses in bionanotechnology. Org. Biomol. Chem. *5*, 2891–2902.

Steinmetz, N.F., Ablack, A.L., Hickey, J.L., Ablack, J., Manocha, B., Mymryk, J.S., Luyt, L.G., and Lewis, J.D. (2011). Intravital imaging of human prostate cancer using viral nanoparticles targeted to gastrin-releasing peptide receptors. Small Weinh. Bergstr. Ger. *7*, 1664–1672.

Stephan, M.T., Moon, J.J., Um, S.H., Bershteyn, A., and Irvine, D.J. (2010). Therapeutic cell engineering using surface-conjugated synthetic nanoparticles. Nat. Med. *16*, 1035–1041.

Strong, J.E., Coffey, M.C., Tang, D., Sabinin, P., and Lee, P.W. (1998). The molecular basis of viral oncolysis: usurpation of the Ras signaling pathway by reovirus. EMBO J. *17*, 3351–3362.

Suarez, E.R., Chang, D.K., Sun, J., Sui, J., Freeman, G.J., Signoretti, S., Zhu, Q., and Marasco, W.A. (2016). Chimeric antigen receptor T cells secreting anti-PD-L1 antibodies more effectively regress renal cell carcinoma in a humanized mouse model. Oncotarget *7*, 34341–34355.

Sundquist, E., Kauppila, J.H., Veijola, J., Mroueh, R., Lehenkari, P., Laitinen, S., Risteli, J., Soini, Y., Kosma, V.-M., Sawazaki-Calone, I., et al. (2017). Tenascin-C and fibronectin expression divide early stage tongue cancer into low- and high-risk groups. Br. J. Cancer *116*, 640–648.

Takagi, S., Kasuya, Y., Shimizu, M., Matsuura, T., Tsuboi, M., Kawakami, A., and Fujisawa, H. (1995). Expression of a cell adhesion molecule, neuropilin, in the developing chick nervous system. Dev. Biol. *170*, 207–222.

Tamagnone, L., Artigiani, S., Chen, H., He, Z., Ming, G.I., Song, H., Chedotal, A., Winberg, M.L., Goodman, C.S., Poo, M., et al. (1999). Plexins are a large family of receptors for transmembrane, secreted, and GPI-anchored semaphorins in vertebrates. Cell *99*, 71–80.

Taylor, C.W., and Kirby, A.M. (2015). Cardiac side-effects from breast cancer radiotherapy. Clin. Oncol. R. Coll. Radiol. G. B. *27*, 621–629.

Teow, H.M., Zhou, Z., Najlah, M., Yusof, S.R., Abbott, N.J., and D'Emanuele, A. (2013). Delivery of paclitaxel across cellular barriers using a dendrimer-based nanocarrier. Int. J. Pharm. *441*, 701–711.

Thomann, J.-S., Heurtault, B., Weidner, S., Brayé, M., Beyrath, J., Fournel, S., Schuber, F., and Frisch, B. (2011). Antitumor activity of liposomal ErbB2/HER2 epitope peptide-based vaccine constructs incorporating TLR agonists and mannose receptor targeting. Biomaterials *32*, 4574–4583.

Thomas, N., Tirand, L., Chatelut, E., Plénat, F., Frochot, C., Dodeller, M., Guillemin, F., and Barberi-Heyob, M. (2008). Tissue distribution and pharmacokinetics of an ATWLPPR-conjugated chlorin-type photosensitizer targeting neuropilin-1 in glioma-bearing nude mice. Photochem. Photobiol. Sci. Off. J. Eur. Photochem. Assoc. Eur. Soc. Photobiol. *7*, 433–441.

Tirand, L., Frochot, C., Vanderesse, R., Thomas, N., Trinquet, E., Pinel, S., Viriot, M.-L., Guillemin, F., and Barberi-Heyob, M. (2006). A peptide competing with VEGF165

binding on neuropilin-1 mediates targeting of a chlorin-type photosensitizer and potentiates its photodynamic activity in human endothelial cells. J. Control. Release Off. J. Control. Release Soc. *111*, 153–164.

Toda, M., Rabkin, S.D., Kojima, H., and Martuza, R.L. (1999). *Herpes simplex virus* as an *in situ* cancer vaccine for the induction of specific anti-tumor immunity. Hum. Gene Ther. *10*, 385–393.

Truman, J.-P., García-Barros, M., Kaag, M., Hambardzumyan, D., Stancevic, B., Chan, M., Fuks, Z., Kolesnick, R., and Haimovitz-Friedman, A. (2010). Endothelial membrane remodeling is obligate for anti-angiogenic radiosensitization during tumor radiosurgery. PloS One *5*, e12310.

Tsai, H., Werber, J., Davia, M.O., Edelman, M., Tanaka, K.E., Melman, A., Christ, G.J., and Geliebter, J. (1996). Reduced connexin 43 expression in high grade, human prostatic adenocarcinoma cells. Biochem. Biophys. Res. Commun. *227*, 64–69.

Tsimberidou, A.-M. (2015). Targeted therapy in cancer. Cancer Chemother. Pharmacol. *76*, 1113–1132.

Tsubakihara, Y., and Moustakas, A. (2018). Epithelial-mesenchymal transition and metastasis under the control of transforming growth factor β. Int. J. Mol. Sci. *19*, 3672.

Tumeh, P.C., Harview, C.L., Yearley, J.H., Shintaku, I.P., Taylor, E.J.M., Robert, L., Chmielowski, B., Spasic, M., Henry, G., Ciobanu, V., et al. (2014). PD-1 blockade induces responses by inhibiting adaptive immune resistance. Nature *515*, 568–571.

Turpen, T.H., Reinl, S.J., Charoenvit, Y., Hoffman, S.L., Fallarme, V., and Grill, L.K. (1995). Malarial epitopes expressed on the surface of recombinant *Tobacco mosaic virus*. Biotechnol. Nat. Publ. Co. *13*, 53–57.

Vala, I.S., Martins, L.R., Imaizumi, N., Nunes, R.J., Rino, J., Kuonen, F., Carvalho, L.M., Rüegg, C., Grillo, I.M., Barata, J.T., et al. (2010). Low doses of ionizing radiation promote tumor growth and metastasis by enhancing angiogenesis. PLoS One *5*, e11222.

Villa, C.H., Dao, T., Ahearn, I., Fehrenbacher, N., Casey, E., Rey, D.A., Korontsvit, T., Zakhaleva, V., Batt, C.A., Philips, M.R., et al. (2011). Single-walled carbon nanotubes deliver peptide antigen into dendritic cells and enhance IgG responses to tumor-associated antigens. ACS Nano *5*, 5300–5311.

Vinardell, M.P., and Mitjans, M. (2015). Antitumor activities of metal oxide nanoparticles. Nanomater. Basel Switz. *5*, 1004–1021.

Vogelstein, B., Fearon, E.R., Hamilton, S.R., Kern, S.E., Preisinger, A.C., Leppert, M., Nakamura, Y., White, R., Smits, A.M., and Bos, J.L. (1988). Genetic alterations during colorectal-tumor development. N. Engl. J. Med. *319*, 525–532.

Volinia, S., Calin, G.A., Liu, C.-G., Ambs, S., Cimmino, A., Petrocca, F., Visone, R., Iorio, M., Roldo, C., Ferracin, M., et al. (2006). A microRNA expression signature of human solid tumors defines cancer gene targets. Proc. Natl. Acad. Sci. U. S. A. *103*, 2257–2261.

Walling, M.A., Novak, J.A., and Shepard, J.R.E. (2009). Quantum dots for live cell and *in vivo* imaging. Int. J. Mol. Sci. *10*, 441–491.

Wang, L., Zhang, M., Zhang, N., Shi, J., Zhang, H., Li, M., Lu, C., and Zhang, Z. (2011). Synergistic enhancement of cancer therapy using a combination of docetaxel and photothermal ablation induced by single-walled carbon nanotubes. Int. J. Nanomedicine *6*, 2641–2652.

Wang, L., Shi, J., Zhang, H., Li, H., Gao, Y., Wang, Z., Wang, H., Li, L., Zhang, C., Chen, C., et al. (2013). Synergistic anticancer effect of RNAi and photothermal therapy mediated by functionalized single-walled carbon nanotubes. Biomaterials *34*, 262–274.

Wang, T., Srivastava, S., Hartman, M., Buhari, S.A., Chan, C.-W., Iau, P., Khin, L.W., Wong, A., Tan, S.-H., Goh, B.-C., et al. (2016). High expression of intratumoral stromal proteins is associated with chemotherapy resistance in breast cancer. Oncotarget *7*, 55155–55168.

Wang, X., Sun, Q., Cui, C., Li, J., and Wang, Y. (2018). Anti-HER2 functionalized graphene oxide as survivin-siRNA delivery carrier inhibits breast carcinoma growth *in vitro* and *in vivo*. Drug Des. Devel. Ther. *12*, 2841–2855.

Wang, Y., Zhao, Q., Han, N., Bai, L., Li, J., Liu, J., Che, E., Hu, L., Zhang, Q., Jiang, T., et al. (2015). Mesoporous silica nanoparticles in drug delivery and biomedical applications. Nanomedicine Nanotechnol. Biol. Med. *11*, 313–327.

Waugh, D.S. (2016). Crystal structures of MBP fusion proteins. Protein Sci. Publ. Protein Soc. *25*, 559–571.

Weekes, C.D., Beeram, M., Tolcher, A.W., Papadopoulos, K.P., Gore, L., Hegde, P., Xin, Y., Yu, R., Shih, L.M., Xiang, H., et al. (2014). A phase I study of the human monoclonal anti-NRP1 antibody MNRP1685A in patients with advanced solid tumors. Invest. New Drugs *32*, 653–660.

Weiner, D.B., Kokai, Y., Wada, T., Cohen, J.A., Williams, W.V., and Greene, M.I. (1989). Linkage of tyrosine kinase activity with transforming ability of the p185neu oncoprotein. Oncogene *4*, 1175–1183.

Weiss, A., and Schlessinger, J. (1998). Switching signals on or off by receptor dimerization. Cell *94*, 277–280.

Wen, F., and Li, Q. (2016). Treatment dilemmas of cetuximab combined with chemotherapy for metastatic colorectal cancer. World J. Gastroenterol. *22*, 5332–5341.

Wen, A.M., Infusino, M., De Luca, A., Kernan, D.L., Czapar, A.E., Strangi, G., and Steinmetz, N.F. (2015). Interface of physics and biology: engineering virus-based nanoparticles for biophotonics. Bioconjug. Chem. *26*, 51–62.

Wen, A.M., Lee, K.L., Cao, P., Pangilinan, K., Carpenter, B.L., Lam, P., Veliz, F.A., Ghiladi, R.A., Advincula, R.C., and Steinmetz, N.F. (2016). Utilizing viral nanoparticle/dendron hybrid conjugates in photodynamic therapy for dual delivery to macrophages and cancer cells. Bioconjug. Chem. *27*, 1227–1235.

Westra, W.H., Slebos, R.J., Offerhaus, G.J., Goodman, S.N., Evers, S.G., Kensler, T.W., Askin, F.B., Rodenhuis, S., and Hruban, R.H. (1993). K-ras oncogene activation in lung adenocarcinomas from former smokers. Evidence that K-ras mutations are an early and irreversible event in the development of adenocarcinoma of the lung. Cancer *72*, 432–438.

Wilkins, O., Keeler, A.M., and Flotte, T.R. (2017). CAR T-Cell therapy: progress and prospects. Hum. Gene Ther. Methods *28*, 61–66.

Wnęk, M., Górzny, M.L., Ward, M.B., Wälti, C., Davies, A.G., Brydson, R., Evans, S.D., and Stockley, P.G. (2013). Fabrication and characterization of gold nano-wires templated on virus-like arrays of *Tobacco mosaic virus* coat proteins. Nanotechnology *24*, 025605.

Wong, H.H., Song, C.W., and Levitt, S.H. (1973). Early changes in the functional vasculature of Walker carcinoma 256 following irradiation. Radiology *108*, 429–434.

Wucherpfennig, K.W., Gagnon, E., Call, M.J., Huseby, E.S., and Call, M.E. (2010). Structural biology of the T-cell receptor: insights into receptor assembly, ligand recognition, and initiation of signaling. Cold Spring Harb. Perspect. Biol. *2*, a005140.

Xiao, Y., Gao, X., Taratula, O., Treado, S., Urbas, A., Holbrook, R.D., Cavicchi, R.E., Avedisian, C.T., Mitra, S., Savla, R., et al. (2009). Anti-HER2 IgY antibody-functionalized single-walled carbon nanotubes for detection and selective destruction of breast cancer cells. BMC Cancer *9*, 351.

Xiao, Y., Shi, K., Qu, Y., Chu, B., and Qian, Z. (2019). Engineering nanoparticles for targeted delivery of nucleic acid therapeutics in tumor. Mol. Ther. Methods Clin. Dev. *12*, 1–18.

Xu, C., Wang, Y., Guo, Z., Chen, J., Lin, L., Wu, J., Tian, H., and Chen, X. (2018). Pulmonary delivery by exploiting doxorubicin and cisplatin co-loaded nanoparticles for metastatic lung cancer therapy. J. Control. Release Off. J. Control. Release Soc. *295*, 153–163.

Xu, J., Lamouille, S., and Derynck, R. (2009). TGF-beta-induced epithelial to mesenchymal transition. Cell Res. *19*, 156–172.

Yelland, T., and Djordjevic, S. (2016). Crystal structure of the neuropilin-1 MAM domain: completing the neuropilin-1 ectodomain picture. Struct. Lond. Engl. 1993 *24*, 2008–2015.

Yildiz, I., Shukla, S., and Steinmetz, N.F. (2011). Applications of viral nanoparticles in medicine. Curr. Opin. Biotechnol. *22*, 901–908.

Yin, Z., Nguyen, H.G., Chowdhury, S., Bentley, P., Bruckman, M.A., Miermont, A., Gildersleeve, J.C., Wang, Q., and Huang, X. (2012). *Tobacco mosaic virus* as a new carrier for tumor associated carbohydrate antigens. Bioconjug. Chem. *23*, 1694–1703.

Yokoda, R., Nagalo, B.M., Vernon, B., Oklu, R., Albadawi, H., DeLeon, T.T., Zhou, Y., Egan, J.B., Duda, D.G., and Borad, M.J. (2017). Oncolytic virus delivery: from nano-pharmacodynamics to enhanced oncolytic effect. Oncolytic Virotherapy *6*, 39–49.

Yoon, A.-R., Kasala, D., Li, Y., Hong, J., Lee, W., Jung, S.-J., and Yun, C.-O. (2016). Antitumor effect and safety profile of systemically delivered oncolytic adenovirus complexed with EGFR-targeted PAMAM-based dendrimer in orthotopic lung tumor model. J. Control. Release Off. J. Control. Release Soc. *231*, 2–16.

Yoshioka, T., Shien, K., Namba, K., Torigoe, H., Sato, H., Tomida, S., Yamamoto, H., Asano, H., Soh, J., Tsukuda, K., et al. (2018). Antitumor activity of pan-HER inhibitors in HER2-positive gastric cancer. Cancer Sci. *109*, 1166–1176.

Yotti, L.P., Chang, C.C., and Trosko, J.E. (1979). Elimination of metabolic cooperation in Chinese hamster cells by a tumor promoter. Science *206*, 1089–1091.

Zhang, J., Dewilde, A.H., Chinn, P., Foreman, A., Barry, S., Kanne, D., and Braunhut, S.J. (2011a). Herceptin-directed nanoparticles activated by an alternating magnetic field selectively kill HER-2 positive human breast cells *in vitro* via hyperthermia. Int. J. Hyperth. Off. J. Eur. Soc. Hyperthermic Oncol. North Am. Hyperth. Group *27*, 682–697.

Zhang, L., Chan, J.M., Gu, F.X., Rhee, J.-W., Wang, A.Z., Radovic-Moreno, A.F., Alexis, F., Langer, R., and Farokhzad, O.C. (2008). Self-assembled lipid-polymer hybrid nanoparticles: a robust drug delivery platform. ACS Nano *2*, 1696–1702.

Zhang, L., Zhu, S., Qian, L., Pei, Y., Qiu, Y., and Jiang, Y. (2011b). RGD-modified PEG-PAMAM-DOX conjugates: *in vitro* and *in vivo* studies for glioma. Eur. J. Pharm. Biopharm. Off. J. Arbeitsgemeinschaft Pharm. Verfahrenstechnik EV *79*, 232–240.

Zhang, M., Desai, T., and Ferrari, M. (1998). Proteins and cells on PEG immobilized silicon surfaces. Biomaterials *19*, 953–960.

Zhao, M., Liu, Y., Hsieh, R.S., Wang, N., Tai, W., Joo, K.-I., Wang, P., Gu, Z., and Tang, Y. (2014). Clickable protein nanocapsules for targeted delivery of recombinant p53 protein. J. Am. Chem. Soc. *136*, 15319–15325.

Zhao, Y., Tao, L., Yi, J., Song, H., and Chen, L. (2018). The role of canonical Wnt signaling in regulating radioresistance. Cell. Physiol. Biochem. *48*, 419–432.

Zheng, X.-C., Ren, W., Zhang, S., Zhong, T., Duan, X.-C., Yin, Y.-F., Xu, M.-Q., Hao, Y.-L., Li, Z.-T., Li, H., et al. (2018). The theranostic efficiency of tumor-specific, pH-responsive,

peptide-modified, liposome-containing paclitaxel and superparamagnetic iron oxide nanoparticles. Int. J. Nanomedicine *13*, 1495–1504.

Zhou, F., Xing, D., Ou, Z., Wu, B., Resasco, D.E., and Chen, W.R. (2009). Cancer photothermal therapy in the near-infrared region by using single-walled carbon nanotubes. J. Biomed. Opt. *14*, 021009.

Zhou, Y., Wang, S., Ying, X., Wang, Y., Geng, P., Deng, A., and Yu, Z. (2017). Doxorubicin-loaded redox-responsive micelles based on dextran and indomethacin for resistant breast cancer. Int. J. Nanomedicine *12*, 6153–6168.

Zhu, J., Wang, G., Alves, C.S., Tomás, H., Xiong, Z., Shen, M., Rodrigues, J., and Shi, X. (2018). Multifunctional dendrimer-entrapped gold nanoparticles conjugated with doxorubicin for pH-responsive drug delivery and targeted computed tomography imaging. Langmuir *34*, 12428–12435.

Zhu, L., Kate, P., and Torchilin, V.P. (2012). Matrix metalloprotease 2-responsive multifunctional liposomal nanocarrier for enhanced tumor targeting. ACS Nano *6*, 3491–3498.

Zhu, L., Zhou, Z., Mao, H., and Yang, L. (2017). Magnetic nanoparticles for precision oncology: theranostic magnetic iron oxide nanoparticles for image-guided and targeted cancer therapy. Nanomed. *12*, 73–87.

Zielinska, E., Zauszkiewicz-Pawlak, A., Wojcik, M., and Inkielewicz-Stepniak, I. (2018). Silver nanoparticles of different sizes induce a mixed type of programmed cell death in human pancreatic ductal adenocarcinoma. Oncotarget *9*.

IX. Annexes

Research Paper

Inhibition of primary breast tumor growth and metastasis using a neuropilin-1 transmembrane domain interfering peptide

Alexia Arpel[1,2], Coralie Gamper[1], Caroline Spenlé[1], Aurore Fernandez[1], Laurent Jacob[1], Nadège Baumlin[1], Patrice Laquerriere[2], Gertraud Orend[1], Gérard Crémel[1], Dominique Bagnard[1]

[1]INSERM U 1109, MN3T Laboratory, Labex Medalis, Strasbourg University, Strasbourg, France

[2]CNRS UMR 7178, Institut Pluridisciplinaire Hubert Curien, Strasbourg University, Strasbourg, France

Correspondence to: *Dominique Bagnard,* ***email:*** *bagnard@unistra.fr*

Keywords: *neuropilin-1, breast cancer, metastasis, treatment, peptide*

Received: *September 28, 2015* ***Accepted:*** *May 28, 2016* ***Published:*** *June 16, 2016*

ABSTRACT

The transmembrane domains (TMD) in membrane receptors play a key role in cell signaling. As previously shown by us a peptide targeting the TMD of neuropilin-1 (MTP-NRP1), blocks cell proliferation, cell migration and angiogenesis *in vitro*, and decreases glioblastoma growth *in vivo*. We now explored the clinical potential of MTP-NRP1 on breast cancer models and demonstrate that MTP-NRP1 blocks proliferation of several breast cancer lines including the MDA-MB-231, a triple negative human breast cancer cell line. In models with long term *in vivo* administration of the peptide, MTP-NRP1 not only reduced tumor volume but also decreased number and size of breast cancer metastases. Strikingly, treating mice before tumors developed protected from metastasis establishment/formation. Overall, our results report that targeting the TMD of NRP1 in breast cancer is a potent new strategy to fight against breast cancer and related metastasis.

INTRODUCTION

In spite of broad achievements in early breast cancer diagnosis, death due to breast cancer and related metastases remains a sobering fact [1, 2]. This indicates the need to develop new strategies and therapeutic tools with effective anti-metastatic properties. To address this need, we tested a novel strategy inhibiting the recently identified breast cancer target neuropilin-1 (NRP1), a membrane receptor involved in nervous system development and angiogenesis [3]. Mounting evidence now indicates a crucial role in breast cancer tumorigenesis and metastasis. NRP1 promotes breast cancer cell survival [4, 5] and different studies showed a role in cell migration and metastasis [6–8]. Consistently, the expression of NRP1 in human breast cancer tissue [7, 9, 10] negatively correlates with patient survival [7, 9]. Barr and co-workers demonstrated in 2005 [11] that a peptide targeting the VEGF165-binding site of NRP1, antagonises the autocrine anti-apoptotic effects of VEGF in cultured 4T1 and MDA-MB-231 breast carcinoma cells. Moreover, the group of Perret and colleagues described that a heptapeptide also inhibiting VEGF binding to NRP1 reduced tumor volume, blood vessel density in orthotopic mammary MDA-MB-231 tumors [12]. We had previously identified a peptide that antagonizes activities of the transmembrane domain in NRP1 (Membrane Targeting Peptide NRP1, MTP-NRP1). This peptide exhibited *in vitro* and *in vivo* anti-proliferative, anti-migratory and anti-angiogenic properties [13, 14] blocking glioblastoma growth. In the present study, we decided to explore whether targeting NRP1 with our peptide potentially is also suitable for blocking breast cancer growth and metastasis. Because of the lack of targeted therapy for triple negative breast cancer, we focused our study on the aggressive human breast cancer line MDA-MB-231 (Estrogen Receptor ER^-, Progesterone receptor PR^-, $HER2^-$) recapitulating this unfavorable clinical context. We found that long term tri-weekly intraperitoneal administration of MTP-NRP1 significantly improved the overall survival of mice compared to vehicle-treated controls. This benefit could be attributed to reduced primary tumor growth as assessed by bioluminescence *in vivo* imaging and the RECIST criteria [15, 16]. We also report an anti-metastatic effect of MTP-NRP1 preventing establishment and growth of metastases. Hence, we provide data demonstrating the protective effect

of MTP-NRP1 as it reduced metastasis formation and growth when administrated before grafting of tumor cells. Overall, our data not only validate the use of peptides antagonizing NRP1 as very powerful approach to fight triple negative breast cancer growth and metastasis, but also exemplify that drugs targeting the TMD of membrane receptors offer a convincing alternative to conventional drugs targeting extra- or intracellular domains.

RESULTS

MTP-NRP1 inhibits proliferation of 4T1 murine breast cancer cells

The transmembrane domain of NRP1 is 100% conserved across mammalian species thereby simplifying preclinical validation. To address the biological activity of MTP-NRP1 in breast cancer we first focused on a murine setting to evaluate the peptide in an immunocompetent mouse model. To this end, we performed a proliferation MTT assay on murine 4T1 cells expressing NRP1 (Figure 1A). We found a significant dose-dependent reduction of cell proliferation starting at a concentration of the peptide of 10^{-8}M exhibiting a maximal effect at 10^{-6} M. We then produced subcutaneous tumors in Balb/C mice by grafting 4T1 cells. MTP-NRP1 was administrated for a period of three weeks every three days (1 µg/kg) when tumors reached a volume of 200 mm^3. As seen in Figure 1C, the tumor size was 67% reduced in the MTP-NRP1 treated group compared to the vehicle receiving group. This demonstrated the anti-tumor effect of MTP-NRP1 in a syngenic model.

MTP-NRP1 inhibits proliferation of human breast cancer cells

To address the biological activity of MTP-NRP1 on human breast cancer cells we next performed

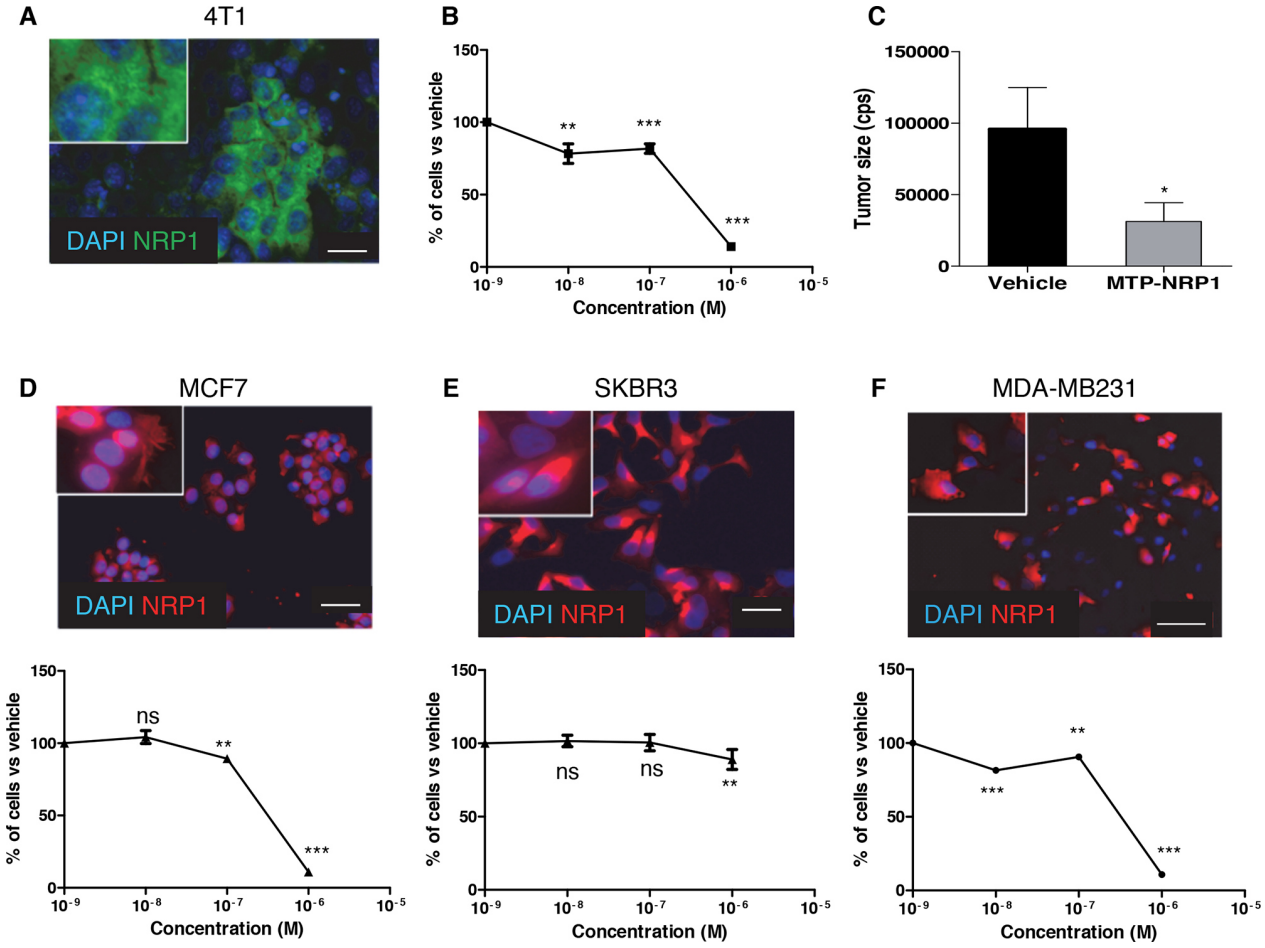

Figure 1: MTP-NRP1 inhibits breast tumor cell proliferation. A. Expression of NRP1 in murine 4T1 cell line. **B.** MTT assay demonstrating the *in vitro* anti-proliferative activity of MTP-NRP1 peptide. **C.** Size of 4T1-derived subcutaneous tumors after 3 weeks every 3 days IP administration of MTP-NRP1 determined with bioluminescence. (* $p < 0.05$, Mann Whitney test). **D.** Expression of NRP1 and anti-proliferative activity of MTP-NRP1 on human MCF7 breast cancer cells. **E.** Expression of NRP1 and anti-proliferative activity of MTP-NRP1 on human SKBR3 breast cancer cells. **F.** Expression of NRP1 and anti-proliferative activity of MTP-NRP1 on human MDA-MB-231 breast cancer cells. (ns: not significant, ** $p < 0.01$ and *** $p < 0.001$, Mann Whitney test).

a proliferation MTT assay on three different NRP1 expressing cell lines, MCF7, SKBR3 and MDA-MB-231 (see Figure 1D-1F showing the expression at protein level). Q-RTPCR analysis confirmed the expression of NRP1 and showed similar amounts of mRNA for all cell lines (see Supplementary Figure S1). Cells were treated with increasing doses of MTP-NRP1 ranging from 10^{-8}M to 10^{-6}M for 24 hours. MTP-NRP1 induced a significant reduction of cell numbers as from 10^{-8}M in MDA-MB-231 (-11% up to -89% at 10^{-6}M), 10^{-7}M in MCF7 cells (-12% up to -90% at 10^{-6}M) and 10^{-6}M in SKBR3 (-12%). Higher concentrations were not possible to test because of a non-specific toxicity of the vehicle. Because the triple negative MDA-MB-231 cells are highly metastatic and represent an important therapeutic challenge we decided to focus on this cell line for in vivo experiments. Strikingly, the addition of MTP-NRP1 (10^{-6}M) fully blocked the Sema3A-induced phosphorylation of AKT (Figure 2). Because of the important role of AKT in the metastatic process this result strengthened the need to investigate the therapeutic potential of MTP-NRP1 in vivo. Considering reported cases of toxicity with anti-NRP1 antibodies we decided to use the 10^{-7} M as a compromise between efficacy and low risk of toxicity. While not producing the maximal anti-proliferative effect in vitro, this concentration was indeed previously proven efficient and safe when treating brain tumors [13]. Hence, we monitored tumor growth by bioluminescence quantification at week 2, 5, 9 and 13 upon injection of luciferase expressing MDA-MB-231 by a life imaging system (NightOwl, Berthold). Initial experimental conditions were standardized by establishing groups of similar cumulated bioluminescence two weeks after grafting of 10^6 cells in the mouse mammary fat pad (average bioluminescence in the vehicle group being 4147 cps and 4189 cps in the MTP-NRP1 group ($p = 0.9$, Mann Whitney). Mice were treated three times a week by intra-peritoneal injection of either the vehicle (LDS, 72 µM) or MTP-NRP1 (10^{-7}M). A total number of 12 animals composed each group. Figure 2A is showing representative examples of the orthotopic tumors detected in the control and the MTP-NRP1 treated groups over time. To analyze extensively the response of each mouse to the treatment a waterfall plot of best response was applied by using the bioluminescence increase between week 9 and 13. This analysis revealed that 100% of the MTP-NRP1 treated animals responded to the treatment with 25% of SD (Stable Disease, < -30% growth decrease compared to averaged growth of control tumors) and 75% responded with PR (Partial Response >-30% growth decrease compared to averaged growth of control tumors) including two individuals above or equal to 90% decrease of tumor volume expansion (Figure 2B). This part of the

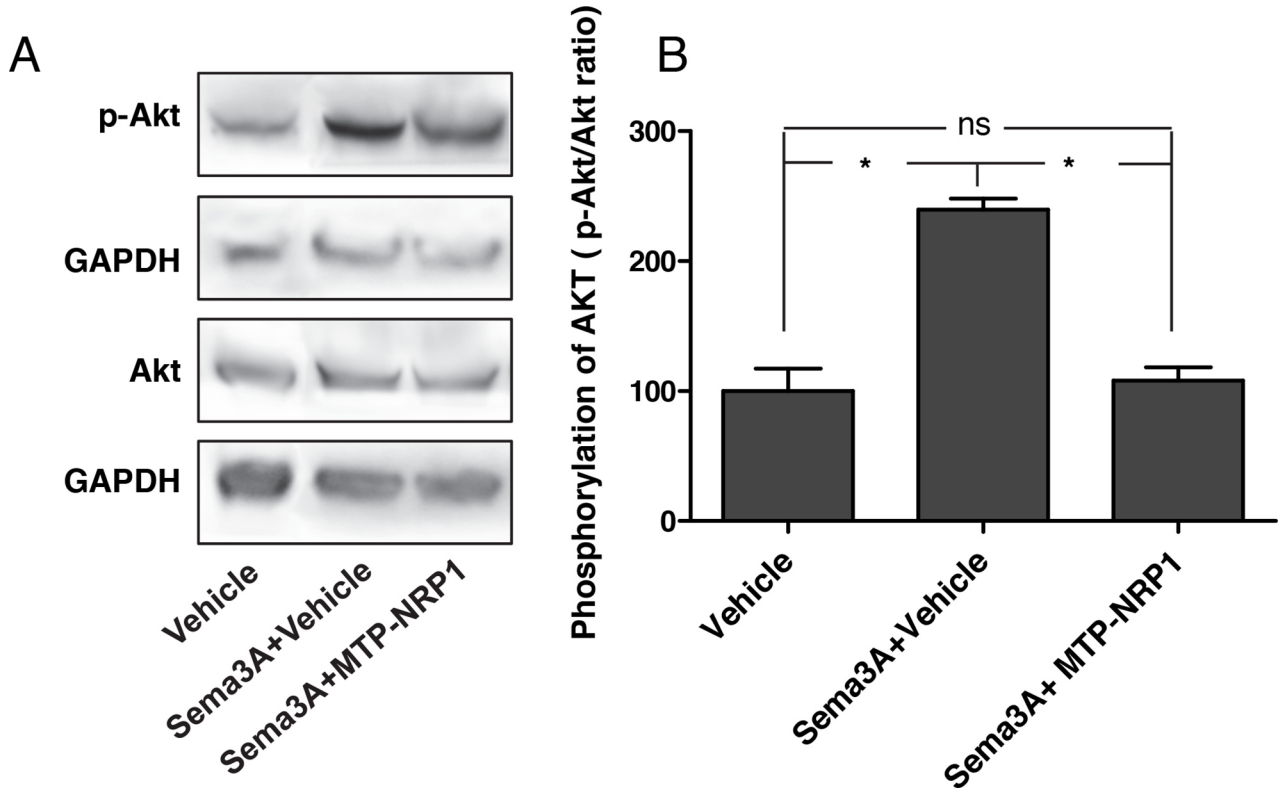

Figure 2: MTP-NRP1 inhibits Sema3A-induced phospho-AKT.A. Representative western blots showing the induction of AKT phosphorylation upon treatments with 200ng/ml Sema3A and with or without MTP-NRP1. Akt and p-AKT expression levels were normalized with GAPDH. **B.** Quantitative analysis of 3 independent experiments showing the relative expression of p-AKT/AKT in the different experimental conditions. (*= $p<0.05$, ns: not significant; Mann Whitney test).

study demonstrated that blocking NRP1 in triple-negative breast tumors significantly blocks tumor growth in all treated mice.

The duration of our protocol was not sufficient to detect metastasis in any organs at bioluminescence or histological level. Therefore, we applied a more sensitive approach by measuring the human specific mRNA coding for the human specific HBMS housekeeping gene and compared expression to the corresponding mouse specific HBMS gene transcript in vehicle or MTP-NRP1 treated mice. This approach allowed us to detect lung metastases in the vehicle group, yet not in other organs such as the brain (Figure 3). Strikingly, we found that MTP-NRP1 significantly reduced lung metastasis issued from the primary tumor almost to background level. Due to insufficient production of metastases we decided to use a different model to evaluate the anti-metastatic effect of MTP-NRP1.

MTP-NRP1 exhibits anti-metastatic properties

The occurrence of lung metastasis is a crucial step in breast cancer progression and is linked to the disease-associated death [17]. Thus, we decided to monitor whether MTP-NRP1 would impede breast cancer metastasis development and progression. Mice were

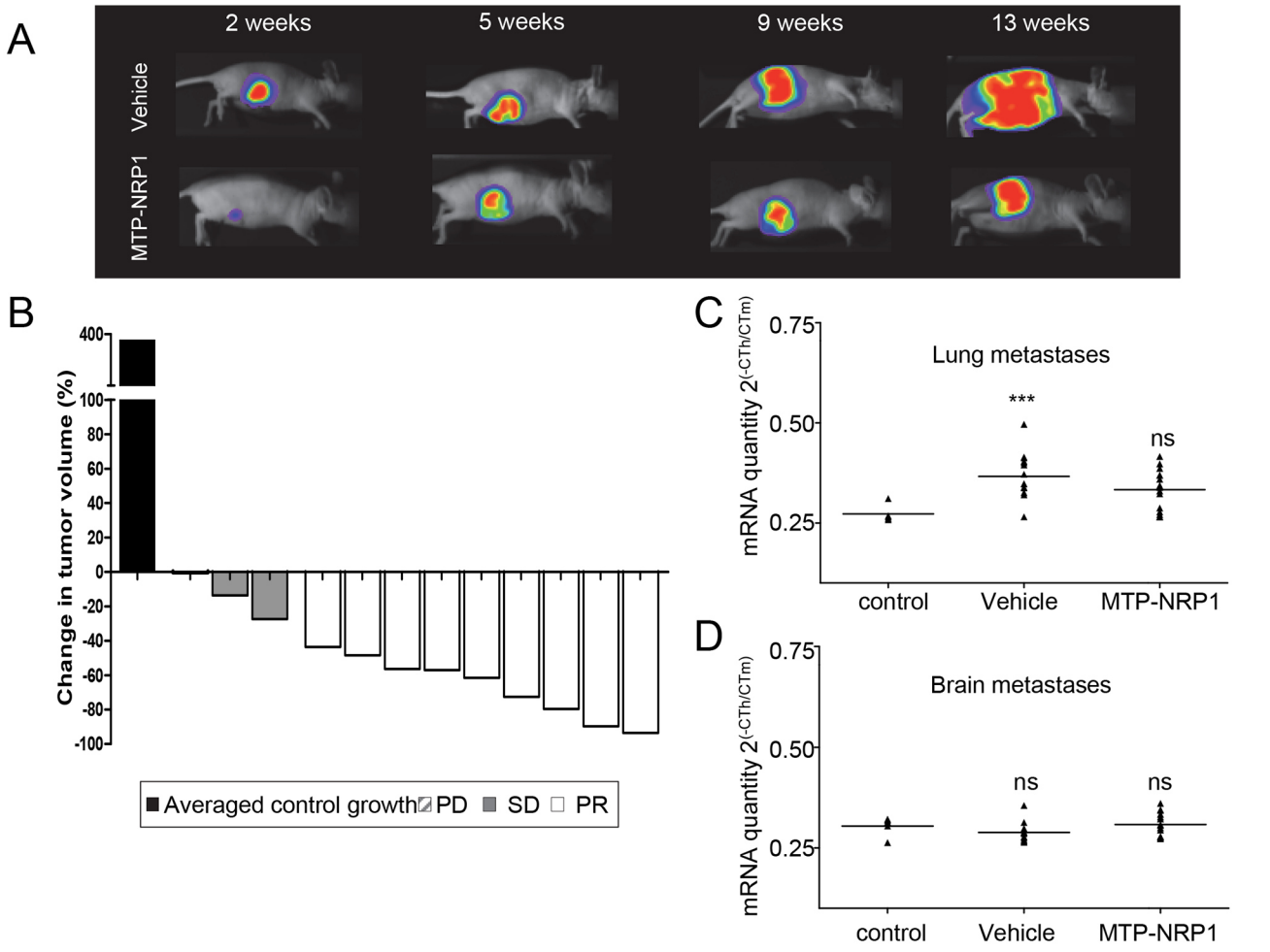

Figure 3: MTP-NRP1 inhibits primary breast tumor growth *in vivo*. A. Representative examples of the orthotopic tumors (MDA-MB-231 cells) detected in the control or the MTP-NRP1 group treated with 1 µg/kg three times a week over time (2, 5, 9 and 13 weeks). **B.** Demonstration of the inhibitory effect of MTP-NRP1 on primary tumor growth between week 9 and 13 of treatment. The Waterfall graph represents the percent change in tumor volume of individual treated animals (grey and white bars, n=12) compared to the averaged tumor volume increased determined in the control group (dark bar, n=12). This demonstrates that 100% of the treated animals responded to MTP-NRP1 treatment including 25% with stable disease (SD grey bars) and 75% with partial response (PR white bars). SD (Stable Disease, < -30% growth decrease compared to averaged growth of control tumors), PR (Partial Response > -30% growth decrease compared to averaged growth of control tumors) (C) RT-QPCR analysis of human specific HMBS mRNA content in the lung to reflect metastasis colonization. Results are mRNA quantity compared to the corresponding mouse specific HMBS housekeeping gene and expressed as $2^{(-CT\_Hs\_HBMS/CT\_Ms\_HBMS)}$. Statistical analysis was done by comparing mRNA content with background signal determined in the lung of control mice without primary tumors (ns= not significant, ** $p < 0.01$, Mann Whitney test). (D) Similar analysis was conducted in the brain. However, no significant human specific HMBS signal was detected in this organ.

here again treated with 1.5 µg/kg of MTP-NRP1 or with the vehicle (LDS, 72µM). Treatment was started 2 days post-intracardiac grafting of 10^5 MDA-MB-231 cells in the left ventricle. Figure 4A is exhibiting representative examples of mice developing metastases over time in the two experimental groups. The location of metastasis was confirmed at histological level in pilot studies to validate accuracy of the method (see Supplementary Figure S2). Strikingly, the quantification of the cumulated bioluminescent signal showed that MTP-NRP1 dramatically reduced the number (-62%, Figure 4C) and size (-83%, Figure 4B) of the arising metastases. Noteworthy, when further addressing the sites of metastasis (in the lung, bone and brain, the major metastatic sites in human breast cancer) we found that the number of metastasis decreased significantly in all analyzed sites upon treatment with MTP-NRP1 (Figure 4D–4G).

MTP-NRP1 improves overall survival

To finally address the therapeutic benefit of MTP-NRP1 we also monitored overall survival (OS) of mice during the whole protocol. Consistently, the high response rate of mice to MTP-NRP1, both in terms of reduced primary tumor volume and number of metastasis, translated into a significant survival benefit (+ 24.7% of the mean survival, p = 0.0109 compared to vehicle, Log-ranked test), a survival benefit also exemplified by a 41.5% increase of the median survival (Figure 5). It is important to note that this protocol lasted for 92 days during which only 16% of the mice died in the MTP-NRP1 group while death reached 58% in the control group. This long term three weekly injection mimicking chronic application provided the possibility to evaluate a potential toxicity of MTP-NRP1 arising after longer term treatment. Blood samples were collected

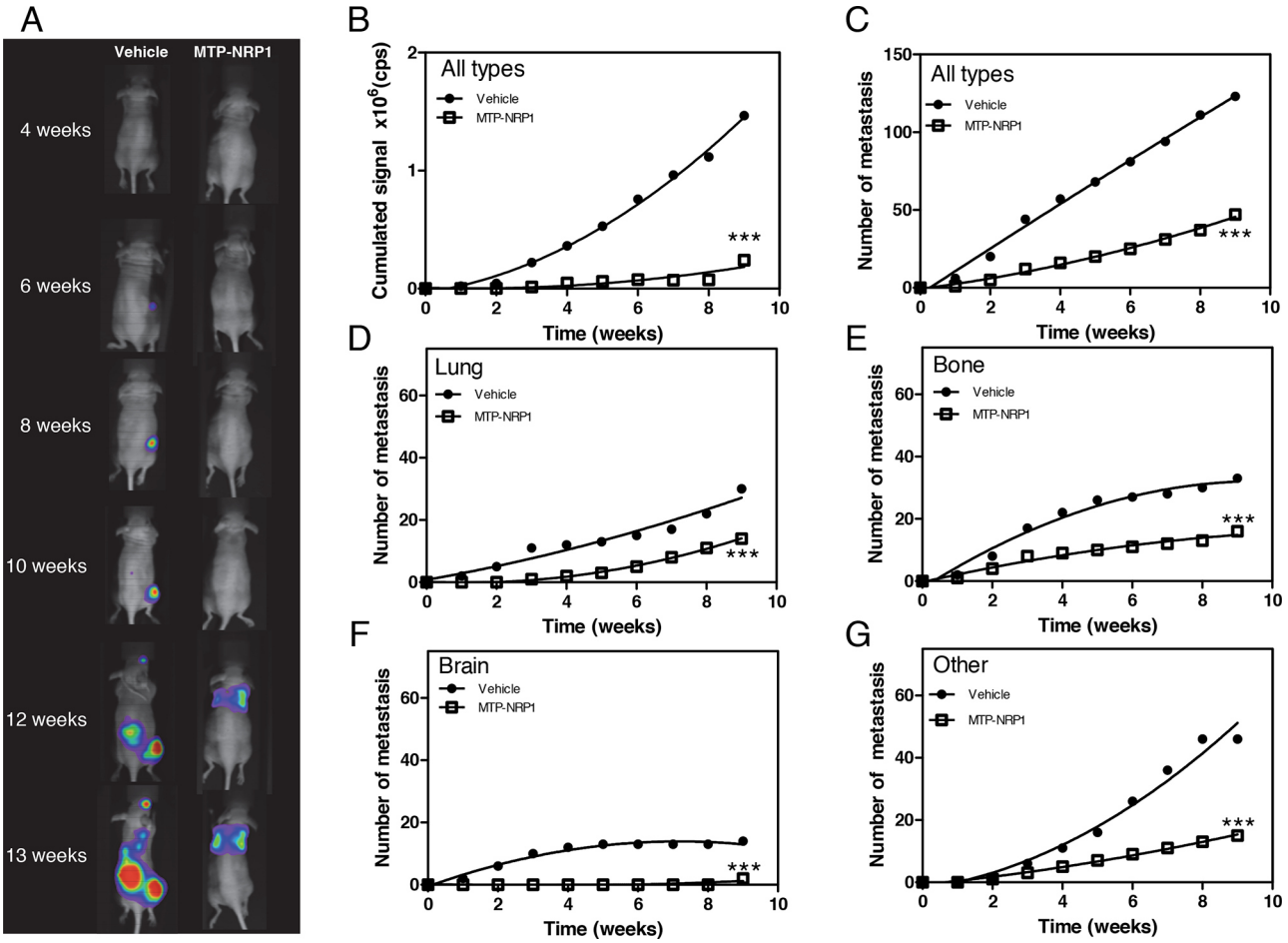

Figure 4: MTP-NRP1 exhibits anti-metastatic properties. A. Representative examples of the metastases (MDA-MB-231 cells) detected in the vehicle and MTP-NRP1 treated groups over time (4, 6, 8, 10, 12 and 13 weeks). **B.** Cumulated bioluminescence signal obtained in vehicle (control) and MTP-NRP1 treated groups over time. **C.** Cumulated number of metastases in entire animals over time. Detailed analysis of cumulated number of metastasis in lung **D.**, bone **E.**, brain **F.** and other sites **G.** in control and MTP-NRP1 treated animals. (*** $p < 0.001$, Extra sum-of-squares F test).

from the cardiac cavity for analysis before sacrifice of animals of both the orthotopic and the systemic metastasis model. In all cases, MTP-NRP1 did not worsen biological parameters of mice including renal, hepatic and cardiac markers. A seen in Supplementary Table S1 and S2, we rather observed a significant lower level of Lactate Dehydrogenase (LDH) reflecting better function of organs in the treated group. Interestingly, the level of platelets was significantly lower in the control group compared to MTP-NRP1 treated mice. Because a transient reduction of platelets in patients treated with an anti-NRP1 antibody was one of the most common (67% of the patients) reported adverse effect in a phase 1 clinical study, this result further demonstrated the good body tolerance for MTP-NRP1.

MTP-NRP1 treatment prevents metastasis formation

The anti-metastatic effect of MTP-NRP1 on primary tumors and induced lung metastases together with the good tolerance of the peptide prompted us to test whether protective treatment of mice by the peptide before grafting the tumor cells potentially was beneficial. We produced metastases by engrafting MDA-MB-231 cells through intra-cardiac injections after 3 days of continuous pre-medication of mice with MTP-NRP1 or by pre-incubating the tumor cells with the peptide 1h before engraftment. We found that both pre-treatments strongly reduced the occurrence of metastases by roughly 60% when determined 3 weeks post grafting (Figure 5B).

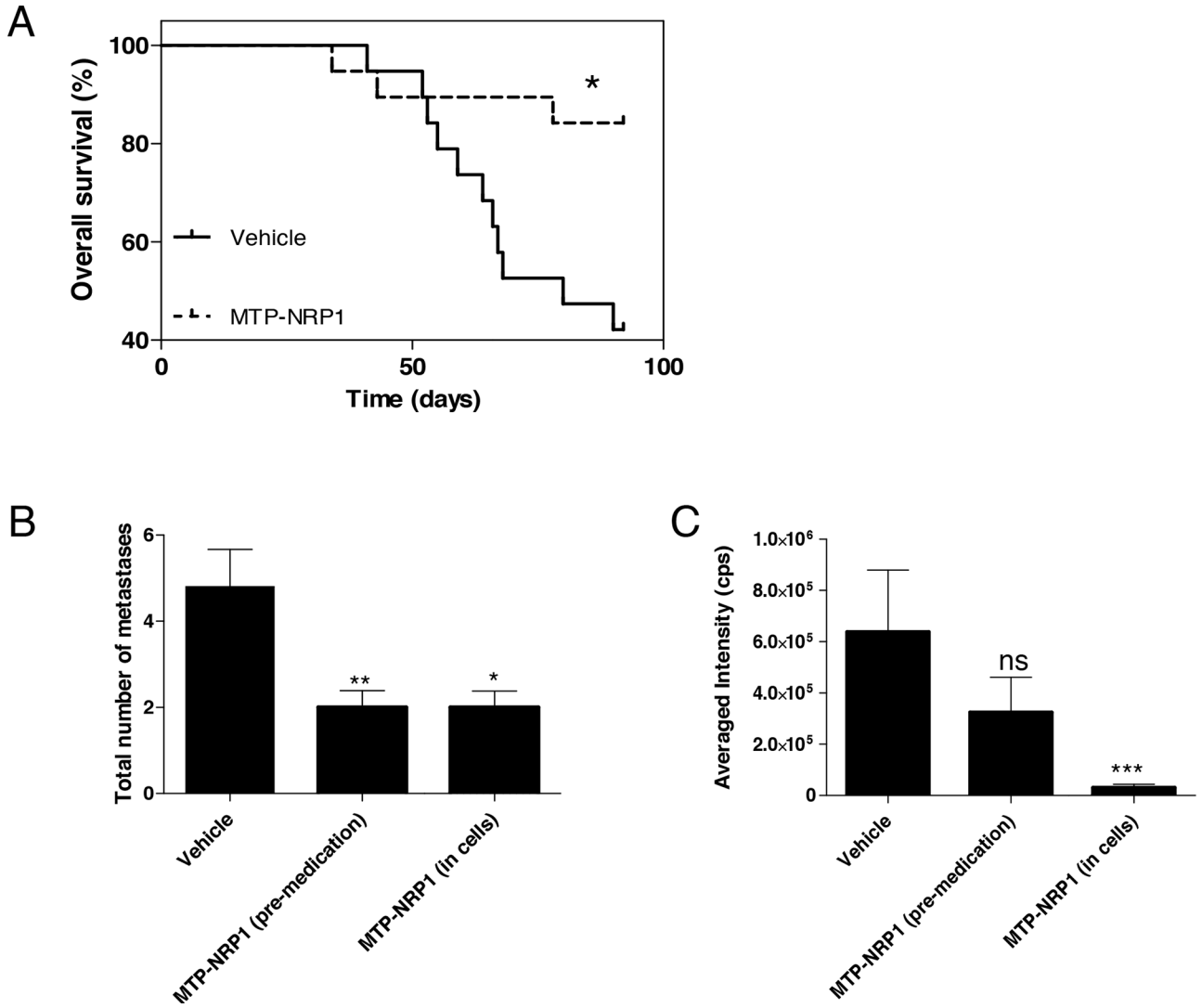

Figure 5: MTP-NRP1 improves overall survival and exhibits protective effect against metastasis. A. Kaplan Meier survival curve demonstrating a significant increased survival of the treated MTP-NRP1 animals compared to the control animals. (* $p < 0.05$, Log Rank test). **B.** Total number of metastases determined in animals that had received IP administration of MTP-NRP1 for 3 days before intracardiac grafting ("pre-medication") or that were grafted with cells (all MDA-MB-231) pre-incubated with the peptide ("in cells"). **C.** Averaged intensity of bioluminescence (cps) emitted by metastases that were able to grow in the different experimental groups. (ns= not significant, * $p < 0.05$, ** $p < 0.01$, *** $p < 0.001$, Mann Whitney test).

This result suggested that blocking NRP1 is able to reduce metastatic colonization. Over the 3 weeks period of survey, the few metastases that had developed in mice receiving premedication were growing similarly well as the control group (Figure 5C). However, those metastases originating from cells that had been pre-incubated with the MTP-NRP1 peptide were 95% smaller (p=0.0006 Mann Whitney test, Figure 5C). These results demonstrated that pre-medication has a beneficial impact on metastasis development and growth. In addition, our results clearly demonstrated a NRP1 cell autonomous metastatic mechanism.

DISCUSSION

The action mechanism of MTP-NRP1 has been well documented and is known to mainly relate to the interference of receptor dimerization [13, 14, 18, 19]. Here, we have shown an anti-proliferative property of MTP-NRP1 in one murine cell line and three different human breast cancer cell lines. The efficacy was stronger in MCF7 and MDA-MB-231 but modest in SKBR3 cells. This milder effect in SKBR3 may be due to the overexpression of HER2 providing a dominant pathway for cell proliferation [20]. Nonetheless, MTP-NRP1 appeared as a very potent inhibitor of primary breast tumor growth generated with 4T1 cells grafted in immunocompetent Balb/C mice. The demonstration of the clinical potential of MTP-NRP1 was confirmed by producing orthotopic breast tumors in nude mice grafted with human MDA-MB-231 cells in the mammary fat pad. When using objective individual tumor growth parameters adapted from the RECIST criteria [15, 16], we found that 100% of mice responded to the treatment. Furthermore, MTP-NRP1 induced a significant decrease of lung metastasis arising from the primary tumors. This anti-metastatic effect was further explored in the intra-cardiac grafting assay that showed both a reduction in the number and in the size of metastasis in all three major sites observed in human, the bone, lung and brain. The anti-tumor effect is obtained with a very low dosage of 1 µg/kg of MTP-NRP1. This is in accordance with our previous work that showed successful inhibition of glioma growth *in vivo* with the same concentration of MTP-NRP1. However, in the case of breast cancer cells, the maximal effect was obtained in vitro with 10^{-6}M, a concentration similar to the one employed for MTP-NeuNT peptide targeting the TMD of the NeuNT receptor [21]. Based on our results future studies can be launched to further explore other parameters such as higher MTP-NRP1 concentrations to reach the maximal anti-tumor effects (optimal dosage, maximum tolerated dose), best therapeutic scheme (duration of treatment, therapeutic window) and potential combinations with other anti-breast cancer drugs. Future PK/PD analyses are necessary that currently are not yet possible due to the lack of tools to detect and measure hydrophobic peptides. Importantly, based on blood analysis after the long period of treatment (13 weeks), the MTP-NRP1 peptide did not show any toxicity. Although we did not reach the maximal tolerated dose here, similar experiments had been done in the glioblastoma model where no toxicity was seen in any tested organ. Noteworthy, no cutaneous lesions were observed on all mice around the intra-peritoneal injection site of the drug. This suggested the lack of peptide accumulation at the injection site avoiding a risk of local toxic side effect. A phase I study of the human monoclonal anti-NRP1 antibody MNRP11685A showed good tolerance when administrated as a single agent. This study only reported cases of transient platelet count reductions without severe impact. We did not observed such a phenomenon in our study thereby suggesting that MTP-NRP1 is extremely well tolerated with the low yet effective dosage we used. It will be interesting to further evaluate the tolerance in future studies dedicated to the identification of the best dosage in stand alone or in combination with other drugs.

Finally, pre-medication using MTP-NRP1 showed a clear reduction of metastasis occurrence/appearance. When administrating the peptide to the mice before grafting tumor cells, the number of metastatic events dropped suggesting that the seeding capacity of the cells is affected when blocking NRP1 in the microenvironment. However, this pretreatment was inefficient on cells that had succeeded extravasation from the blood stream. The cells were able to soil [22] and develop metastases demonstrating that the pre-medication preferentially impacted on tumor cells before breaching blood vessels to enter the lung parenchymal tissue. When the cells were pre-incubated with the peptide, thereby blocking NRP1 cell–autonomous signaling pathways, we found both a reduction of the number and size of metastases. This illustrates that NRP1 is involved in both cell autonomous and non-cell-autonomous mechanisms controlling the metastatic process.

Targeting the TMD of bitopic receptors such as NRP1 provides a new exquisite therapeutic tool. Previous work demonstrated a crucial role of the TMD of NRP1 and suggested that inhibition may present a therapeutic potential in glioma treatment [13, 14]. This strategy has been now validated for another type of cancer, breast cancer and its related metastases. Our results clearly revealed that a peptide mimicking the TMD of NRP1 decreases both the size and the number of breast metastasis translating into a marked improvement of survival. Importantly, this therapeutic benefit was achieved by using the drug in a micromolar dosage with no apparent toxicity. Hence, targeting the TMD of NRP1, with a peptide mimicking its TMD could be a future potent drug in breast cancer therapy particularly to prevent metastasis formation by administrating long term low dose MTP-NRP1 upon reduction or surgical removal of the primary tumor.

MATERIALS AND METHODS

Cell culture

The murine 4T1 cells and human epithelial breast adenocarcinoma derived from pleural effusion MDA-MB-231 (ER-, PR-, HER2-), MCF7 (ER+, PR+, HER2+), SKBR3 (ER-, PR-, HER2+) cells were grown in Dulbecco's modified Eagle medium (DMEM, GIBCO) and HUVEC (Human Umbilical Vein Endothelial Cells, Promo Cell) cells were cultured in Endothelial Cell Growth Medium (Promo Cell). MDA-MB-231 cells were purchased from ECACC (92020424), HUVEC cells were purchased from Promo Cell (C-12200), MCF7 and SKBR3 cells were obtained from our institute collection. All culture media were supplemented with 10% fetal calf serum (FCS) (Gibco), 100 I.U./ml penicillin, 100 µg/ml streptomycin (Sigma), and cultured at 37°C, 5% CO_2. Cells were detached with trypsin-EDTA (0.05 % trypsin, 1X EDTA), spin down and split regularly up to 40 passages before new stocks were thawed.

Peptides

Peptides have been synthesized by Peptide Specialty Laboratories GmbH using automatic peptide synthesis (Fmoc chemistry). The peptide corresponding to the TM sequence of NRP1: ILITIIAMSALGVLLGAVCGVVLYRKR is referred as MTP-NRP1. Peptides purity estimated by RP-HPLC was more than 95% according to manufacturer indication. Peptides were solubilized in LDS (Lithium Dodecyl Sulfate, 72 mM for stock solution) as previously described [13, 14].

RT-QPCR

mRNA was extracted with TriReagent solution according to manufacturer's instruction (Molecular Research Center Inc., Euromedex). mRNA was treated with DNaseI (Invitrogen) and reverse transcribed using the High Capacity cDNA RT Kit (Life Technologies). Quantitative reverse transcriptase polymerase chain reaction (RTQ-PCR) was performed using the Power SYBR Green PCR Master Mix or TaqMan Gene Expression Master Mix (Life Technologies) using the 7500 Real time PCR System (Life Technologies) following the manufacturer's protocol. We used human specific Hs_HMBS (QT 00014462, Quiagen) and mouse specific Ms_HBMS (QT00494130, Quiagen) to quantify lung or brain metastasis contents. Samples were analyzed using 2µl cDNA. Calculation were effectuated as the following: $\Delta ct(\text{MDA-MB-231}^{HBMS}) = ct\ (Hs\_HBMS) - ct\ (Ms\_HBMS)$, mRNA quantity = $2^{(-\Delta ctMDA\text{-}MB\text{-}231HBMS)}$.

Western blot analysis

MDA-MB-231 cells were seeded on 6-well plates overnight, and then treated with 200ng/ml Sema3A (R&D 1250-S3) for 30 minutes prior to addition of 10^{-6}M of MTP-NRP1 for one additional hour. Proteins were extracted in Laemmli buffer complemented with proteinases (Roche, #11836145001) and phosphatases (5mM of Na ortho-vanadate) inhibitors. They were loaded on a 4-15% gradient gel (Biorad). Antibodies for Akt, phospho Akt (Cell Signaling #4060 and #9272 respectively), GAPDH (Santa Cruz #SC-20357) and their respective rabbit and goat–HRP secondary antibodies (GE Healthcare) were used. Revelation was performed using Pierce™ ECL Plus Western Blotting Substrate and the PXi imager apparatus (Syngene Bio Imaging, UK). Quantification was done with Image J software.

Immunocytochemistry

Cells were grown on sterile glass cover slips for one day before immunofluorescence staining. The cells were fixed with freshly made fixative 4% formaldehyde (FA) for 10 minutes. The samples were gently rinsed with PBS (1 wash for 10 minutes) before adding fetal calf serum blocking solution (FCS 5%) for a minimum of 30 minutes. Cells were permeabilized using 1x PBS with 0.1% Tween20 for 5 minutes. Anti-neuropilin-1 (sc-5541; Santa Cruz Biotechnology) diluted in 5% FCS-PBS was added to the cell over night at room temperature. After thorough wash (3 washes of 5 minutes) appropriate secondary antibody (goat anti-rabbit, Nordic Immunology GAM/Fab/TRITC diluted 1/1000 from stock) was added at room temperature for 90 minutes. After washing in PBS, the cell nuclei were stained with DAPI (4',6-diamidino-2-phenylindole, 1/30 000 in water) for 10 minutes. Glass coverslips were finally mounted on microscopy glass slides using a polymerization medium (FluorSave reagent, Calbiochem-Merck, cat#345789).

Cell proliferation

In vitro cell proliferation was monitored using MTT (3-(4,5-Dimethylthiazol-2-yl)-2,5-diphenyl tetrazolium bromide) proliferation assay according to manufacturer's instruction (Sigma, M2128, USA). Cells were seeded at a density of 10 000 cells per well in a 96 well plate before incubation with increasing peptide concentration (ranging from 10^{-9}M to 10^{-6}M) or corresponding vehicle increasing concentration (LDS, ranging from 0.72 µM to 720 µM). After 24h incubation, the culture media were removed from the wells and 100 µl of MTT dye freshly diluted (to 1/50 in GBSS) from stock solution (5 mg/ml) was added to each well for 4h. After this incubation period, isopropanol (100 µl) was added to the MTT solution in each well before reading the optical density at 570 nm using a microplate reader spectrophotometer (EL800, Bio Tek Instruments). For cell fluorescence acquisition, images were acquired with the fluorescence Zeiss Imager Z2 equipped with HXP 120W lamp and structured light ApoTome (Zeiss) system.

Orthotopic grafting of cells in the mouse mammary fat pad

Nude mice (8 weeks of age) were anesthetized (initially 3% isoflurane with air/O_2 mix, then animals were kept under anaesthesia with 1.5% Isoflurane with air/O_2 mix). A cutaneous incision up to the sternum was completed, followed by another angled lateral incision from the initial one towards the posterior leg. The blood vessel emerging between these fat pads was cauterised (Electric cauterizer (FST No 18000-00). Then the needle (BD Microlance; 22G ¼ - Nr 12; 0,7 x 30 mm, REF 300900) of the syringe containing 10^6 cells in 50µl of PBS was inserted in the mammary fat pad from the external side up to the lymph node and the cells were injected behind the lymph node within the mammary fat pad. Skins were then aligned and sutured. The mouse was monitored until it was awakened from the procedure and was moving around the cage normally and then observed on a daily basis until sacrifice. For bioluminescence detection, IP injection of 100µl of a luciferin solution at 30mg/ml was completed on a weekly basis for each mouse. Acquisition was operated for 5min using a live imager (NightOwl, Berthold). All treatments were administrated by IP injection of 100µl solutions containing 72µM LDS (control group) or 1 µg/kg MTP-NRP1. Injections were performed every 3 days once the tumors reached a volume of 200 mm^3. The percent change in bioluminescence intensity at week 9 and 13 was used to quantify response. PD (Progression disease, >20% increase compared to averaged growth of control tumors), SD (Stable Disease, < -30% growth decrease compared to averaged growth of control tumors), PR (Partial Response > -30% growth decrease compared to averaged growth of control tumors), and CR (Complete response, 100% growth decrease compared to averaged growth of control tumors) were defined as per RECIST criteria.

Intra-cardiac grafting model

Cells were detached with Versene (EDTA solution used in order to assess a gentle non-enzymatic cell dissociation), washed and counted for 10^5 in 100µl of PBS before injection into the left ventricle of nude mice (8 weeks old) using a 26G ½ needle with a 1ml syringe. Mice were initially anesthetized with 3% isoflurane with air/O_2 mix and animals were kept under anaesthesia with 1.5% isoflurane with air/O_2 mix during surgery). Monitoring procedure and bioluminescence detection were identical to above described orthotopic injection.

Animal handling and in vivo ethical statement

Experiments were performed according to the Guide for Care and Use of Laboratory Animals (E67-6-482-21) and the European Directive with approval of the regional ethical committee (Reference AL/55/62/02/13). Mice received food and water ad libitum. Animals were sacrificed using CO_2. All necessary precautions were taken to minimize pain or discomfort of the animals. General health status was monitored 3 times a week by independent observers. Mice were sacrificed when reaching ethical endpoints.

Statistics

Statistical analyses were performed using Mann Whitney test (for sample $n < 30$), Log ranked test for survival analysis and sum-of-squares F test using GraphPad software (Prism, USA). P-values are given in the figure legends, and values of $P < 0.05$ were considered to be statistically significant. Normal distribution of the values was checked using GraphPad software (Prism, USA). A minimum of three independent experiments including at least triplicates was performed for *in vitro* proliferation assay. For *in vivo* experiment sample size calculation anticipated a therapeutic effect of 20% for a standard deviation of 14% and confidence interval of confidence 95% (Lamorte's Power calculation, University of Boston). Results from two independent in vivo experiments were pooled only if fully comparable (no statistical differences between control groups).

ACKNOWLEDGMENTS

This work was supported by INCA to GO, ANR "interference TM", ARC and Ligue Régionale contre le Cancer to DB. This work has been published within the LABEX ANR-10-LABX-0034_Medalis and received a financial support from French government managed by "Agence National de la Recherche" under "Programme d'investissement d'avenir". The authors thank Dr Bentires-Alj at the Friedrich Miescher Institute for Biomedical Research (FMI, Basel) for teaching orthotopic breast cancer model. This work is dedicated to our regretted colleague Roseline Lesecq.

CONFLICTS OF INTEREST

The authors declare that they have no conflict of interest.

REFERENCES

1. Lu J, Steeg PS, Price JE, Krishnamurthy S, Mani SA, Reuben J, Cristofanilli M, Dontu G, Bidaut L, Valero V, Hortobagyi GN, Yu D. Breast cancer metastasis: challenges and opportunities. Cancer Res. 2009; 69: 4951–3. doi: 10.1158/0008-5472.CAN-09-0099.
2. Medina D. Mammary developmental fate and breast cancer risk. Endocr Relat Cancer. 2005; 12: 483–95. doi: 10.1677/erc.1.00804.

3. Bagri A, Tessier-Lavigne M. Neuropilins as Semaphorin receptors: in vivo functions in neuronal cell migration and axon guidance. Adv Exp Med Biol. 2002; 515: 13–31.
4. Bachelder RE, Wendt MA, Mercurio AM. Vascular endothelial growth factor promotes breast carcinoma invasion in an autocrine manner by regulating the chemokine receptor CXCR4. Cancer Res. 2002; 62: 7203–6.
5. Pan H, Bachelder RE. Autocrine Semaphorin3A stimulates eukaryotic initiation factor 4E-dependent RhoA translation in breast tumor cells. Exp Cell Res. 2010; 316: 2825–32. doi: 10.1016/j.yexcr.2010.07.012.
6. Fernandis AZ, Prasad A, Band H, Klösel R, Ganju RK. Regulation of CXCR4-mediated chemotaxis and chemoinvasion of breast cancer cells. Oncogene. 2004; 23: 157–67. doi: 10.1038/sj.onc.1206910.
7. Yasuoka H, Kodama R, Tsujimoto M, Yoshidome K, Akamatsu H, Nakahara M, Inagaki M, Sanke T, Nakamura Y. Neuropilin-2 expression in breast cancer: correlation with lymph node metastasis, poor prognosis, and regulation of CXCR4 expression. BMC Cancer. 2009; 9: 220. doi: 10.1186/1471-2407-9-220.
8. Caunt M, Mak J, Liang W-C, Stawicki S, Pan Q, Tong RK, Kowalski J, Ho C, Reslan HB, Ross J, Berry L, Kasman I, Zlot C, et al. Blocking neuropilin-2 function inhibits tumor cell metastasis. Cancer Cell. 2008; 13: 331–42. doi: 10.1016/j.ccr.2008.01.029.
9. Ghosh S, Sullivan CAW, Zerkowski MP, Molinaro AM, Rimm DL, Camp RL, Chung GG. High levels of vascular endothelial growth factor and its receptors (VEGFR-1, VEGFR-2, neuropilin-1) are associated with worse outcome in breast cancer. Hum Pathol. 2008; 39: 1835–43. doi: 10.1016/j.humpath.2008.06.004.
10. Jubb AM, Strickland LA, Liu SD, Mak J, Schmidt M, Koeppen H. Neuropilin-1 expression in cancer and development. J Pathol. 2012; 226: 50–60. doi: 10.1002/path.2989.
11. Barr MP, Byrne AM, Duffy AM, Condron CM, Devocelle M, Harriott P, Bouchier-Hayes DJ, Harmey JH. A peptide corresponding to the neuropilin-1-binding site on VEGF(165) induces apoptosis of neuropilin-1-expressing breast tumour cells. Br J Cancer. 2005; 92: 328–33. doi: 10.1038/sj.bjc.6602308.
12. Starzec A, Vassy R, Martin A, Lecouvey M, Di Benedetto M, Crépin M, Perret GY. Antiangiogenic and antitumor activities of peptide inhibiting the vascular endothelial growth factor binding to neuropilin-1. Life Sci. 2006; 79: 2370–81. doi: 10.1016/j.lfs.2006.08.005.
13. Nasarre C, Roth M, Jacob L, Roth L, Koncina E, Thien A, Labourdette G, Poulet P, Hubert P, Crémel G, Roussel G, Aunis D, Bagnard D. Peptide-based interference of the transmembrane domain of neuropilin-1 inhibits glioma growth in vivo. Oncogene. 2010; 29: 2381–92. doi: 10.1038/onc.2010.9.
14. Roth L, Nasarre C, Dirrig-Grosch S, Aunis D, Crémel G, Hubert P, Bagnard D. Transmembrane domain interactions control biological functions of neuropilin-1. Mol Biol Cell. 2008; 19: 646–54. doi: 10.1091/mbc.E07-06-0625.
15. Eisenhauer EA, Therasse P, Bogaerts J, Schwartz LH, Sargent D, Ford R, Dancey J, Arbuck S, Gwyther S, Mooney M, Rubinstein L, Shankar L, Dodd L, et al. New response evaluation criteria in solid tumours: revised RECIST guideline (version 1.1). Eur J Cancer Oxf Engl 1990. 2009; 45: 228–47. doi: 10.1016/j.ejca.2008.10.026.
16. Roberts PJ, Usary JE, Darr DB, Dillon PM, Pfefferle AD, Whittle MC, Duncan JS, Johnson SM, Combest AJ, Jin J, Zamboni WC, Johnson GL, Perou CM, et al. Combined PI3K/mTOR and MEK inhibition provides broad antitumor activity in faithful murine cancer models. Clin Cancer Res Off J Am Assoc Cancer Res. 2012; 18: 5290–303. doi: 10.1158/1078-0432.CCR-12-0563.
17. Chambers AF, Groom AC, MacDonald IC. Dissemination and growth of cancer cells in metastatic sites. Nat Rev Cancer. 2002; 2: 563–72. doi: 10.1038/nrc865.
18. Aci-Sèche S, Sawma P, Hubert P, Sturgis JN, Bagnard D, Jacob L, Genest M, Garnier N. Transmembrane recognition of the semaphorin co-receptors neuropilin 1 and plexin A1: coarse-grained simulations. PloS One. 2014; 9: e97779. doi: 10.1371/journal.pone.0097779.
19. Sawma P, Roth L, Blanchard C, Bagnard D, Crémel G, Bouveret E, Duneau J-P, Sturgis JN, Hubert P. Evidence for new homotypic and heterotypic interactions between transmembrane helices of proteins involved in receptor tyrosine kinase and neuropilin signaling. J Mol Biol. 2014; 426: 4099–111. doi: 10.1016/j.jmb.2014.10.007.
20. Wu Y, Ginther C, Kim J, Mosher N, Chung S, Slamon D, Vadgama JV. Expression of Wnt3 activates Wnt/β-catenin pathway and promotes EMT-like phenotype in trastuzumab-resistant HER2-overexpressing breast cancer cells. Mol Cancer Res. 2012; 10: 1597–606. doi: 10.1158/1541-7786.MCR-12-0155-T.
21. Arpel A, Sawma P, Spenlé C, Fritz J, Meyer L, Garnier N, Velázquez-Quesada I, Hussenet T, Aci-Sèche S, Baumlin N, Genest M, Brasse D, Hubert P, et al. Transmembrane domain targeting peptide antagonizing ErbB2/Neu inhibits breast tumor growth and metastasis. Cell Rep. 2014; 8: 1714–21. doi: 10.1016/j.celrep.2014.07.044.
22. Ribelles N, Santonja A, Pajares B, Llácer C, Alba E. The seed and soil hypothesis revisited: current state of knowledge of inherited genes on prognosis in breast cancer. Cancer Treat Rev. 2014; 40: 293–9. doi: 10.1016/j.ctrv.2013.09.010.

UNIVERSITE DE STRASBOURG

RESUME DE LA THESE DE DOCTORAT

Discipline : Sciences de la vie

Spécialité (facultative) : Biotechnologie

Présentée par : Gamper Coralie

Titre : Nanoparticules dérivées de virus de plante pour le traitement et l'imagerie du cancer

Unité de Recherche : IBMP-CNRS UPR2357 Institut de Biologie Moléculaire des Plantes

Directeur de Thèse : Heinlein Manfred-Directeur de Recherche

Co-Directeur de Thèse (s'il y a lieu) : Bagnard Dominique-Maître de Conférence Universitaire

Localisation : INSERM U1119-BMNTS

ECOLES DOCTORALES :
(cocher la case)

☐ ED - Sciences de l'Homme et des sociétés ☐ ED 99 – Humanités ☐ ED 101 – Droit, sciences politique et histoire ☐ ED 182 – Physique et chimie physique ☐ ED 221 – Augustin Cournot ☐ ED 222 - Sciences chimiques	☐ ED 269 - Mathématiques, sciences de l'information et de l'ingénieur ☐ ED 270 – Théologie et sciences religieuses ☐ ED 413 – Sciences de la terre, de l'univers et de l'environnement ☒ ED 414 – Sciences de la vie et de la santé

Introduction

Mon projet de thèse porte sur l'élaboration de nanoparticules dérivées du virus de la mosaïque du tabac (TMV) pour l'expression et le transport de molécules d'intérêt (peptides thérapeutiques, peptides de ciblage, fluorochromes, médicaments anti-cancéreux) jusqu'au site tumoral. Il repose sur une collaboration entre l'équipe de M. Heinlein (IBMP-CNRS UPR2357), spécialiste en virologie végétale, et le groupe de D. Bagnard (INSERM U1119, Strasbourg), spécialiste du développement de peptides thérapeutiques.

Le groupe de D. Bagnard a développé un nouveau composé anti-cancéreux, un peptide transmembranaire ciblant le récepteur Neuropiline-1 (MTP-NRP1). Neuropiline-1 est un récepteur membranaire impliqué dans l'angiogenèse et surexprimé dans certains cancers. Sa surexpression est corrélée à un mauvais pronostic pour le patient (Geretti and Klagsburn, 2007). Le peptide MTP-NRP1 empêche la dimérisation du récepteur Nrp-1 nécessaire pour la transduction du signal et bloque ainsi son activité biologique (Nasarre et al., 2010). La difficulté de production et surtout de purification des peptides transmembranaires comme MTP-NRP1 en raison de leur forte hydrophobicité ont poussés le groupe de D. Bagnard à chercher de nouveaux systèmes de production et de vectorisation capables d'améliorer cette stratégie innovante.

Les nanoparticules, qui sont définies comme étant des particules dont la taille est de l'ordre du nanomètre, ont fait l'objet d'un nombre croissant de recherche dans de nombreux domaines d'application et particulièrement dans celui des transporteurs de composés thérapeutiques pour le traitement des maladies, incluant le traitement du cancer du sein (Saadeh et al., 2014) et du glioblastome (Li et al., 2014). L'utilisation de nanoparticules pour l'acheminement de composés thérapeutiques jusqu'au site tumoral présente de nombreux avantages. En effet, les nanoparticules augmentent la demi-vie dans la circulation sanguine des molécules qu'elles transportent, elles réduisent leur adressage non spécifique et elles favorisent l'accumulation des principes actifs au niveau du site tumoral grâce à l'effet d'augmentation de la rétention et de la perméabilité de la tumeur et/ou un ciblage actif par un composé transporté par la particule. Plus particulièrement, les nanoparticules dérivées de virus de plantes ont montré ces dernières années un grand potentiel comme vecteur de molécules thérapeutiques (Lewis et al., 2006; Steinmetz et al., 2006; Steinmetz, 2010; Wen et al., 2012). Ce sont des nanomatériaux biocompatibles et biodégradables. De plus, contrairement aux virus infectant les animaux et l'espèce humaine, les virus de plantes ne sont pas infectieux pour l'Homme (Steinmetz and Evans, 2007). Plus particulièrement, le virus de la mosaïque du tabac (TMV) présente de nombreux avantages. Il est le premier virus à avoir été découvert et son génome est entièrement séquencé (Harrison and Wilson, 1999) rendant ainsi possible la modification par génie génétique de la séquence de la protéine de capside (CP) afin de créer des nanoparticules (ou monomères) portant des peptides d'intérêt. Il possède également une grande stabilité dans des conditions physiologiques (Alonso et al., 2013). La protéine de capside (CP) du TMV est capable de s'auto-assembler *in*

vitro (Fraenkel-Conrat and Williams, 1955) et, sous conditions spécifiques, de former ainsi des structures « 20S » ou « disques », qui consistent en 34 molécules (monomères) de CP. La combinaison (grâce à l'assemblage des CP) de monomères portant un peptide de ciblage et de monomères portant des peptides thérapeutiques permettra de créer des nanoparticules (disques) fonctionnalisées et capables à la fois de cibler et de détruire les cellules tumorales.

L'équipe de M. Heinlein étudie depuis de nombreuses années le TMV et, particulièrement, le mouvement du virus de cellule à cellule dans les plantes infectées. Ainsi, le projet initial reposait sur la production de nanoparticules (disques) dérivées du TMV et présentant des peptides thérapeutiques. Les nanoparticules dérivées de virus de plantes sont aussi développées par d'autres groupes (Steinmetz et al., 2006 ; Steinmetz, 2010) mais pour la première fois, cette stratégie a été appliquée au peptide MTP-NRP1 (appelé par la suite « killing peptide ») en insérant sa séquence peptidique dans une construction His-Maltose Binding Protein-CP. L'expression chez la bactérie de cette construction a permis la production et la purification sur colonne MBP à rendement élevé (plusieurs milligrammes par millilitre) des CP-killing peptides et des CP non couplés au peptide. Des expériences de Western Blot et de DLS (Dynamic Light Scattering) ont montré l'homogénéité des solutions protéiques purifiées et leur solubilité en milieu aqueux. Ces résultats ont montré la validité de la stratégie d'utilisation de la CP afin de produire le peptide MTP-NRP1 à grande échelle et dans une forme hydrophile permettant de s'affranchir de l'utilisation de solvants potentiellement toxiques (Lithium Dodecyl Sulfate ou Diméthylsulfoxyde). Le CP-killing peptide a été testé grâce à la technique de Proximity Ligation Assay (PLA) et a montré des résultats encourageants de liaison au récepteur Nrp-1. Cette avancée majeure a ouvert la possibilité de fabriquer des nanoparticules plus complexes comportant une fonction d'adressage dans les sites tumoraux. Ainsi, nous avons compléter notre arsenal de nanoparticules par des objets comportant cette fois des peptides ciblant la partie extracellulaire du récepteur Nrp-1 ou, via une collaboration avec G. Orend (INSERM U1109) spécialiste de la matrice extracellulaire tumorale), ciblant la ténascine-C (TNC), une protéine de la matrice extracellulaire surexprimée dans le cancer du sein (ces peptides sont appelés « finding peptide »).

Résultats

1) Evaluation des CP monomères

1.1 Evaluation in vitro

Durant ma première année de thèse j'ai évalué l'activité biologique des CP-killing peptides ciblant le domaine transmembranaire du récepteur Nrp1 produit précédemment en utilisant un test d'angiogenèse sur cellules HUVEC (Human Umbilical Vein Endothelial Cells). Ces expériences ont démontré que les CP-killing peptides sont capables d'inhiber la formation de tubes par les cellules HUVEC d'environ 30% et, de plus, que les monomères de

CP sans peptide n'ont pas d'effet anti-angiogénique. J'ai ensuite testé l'effet anti-migratoire du CP-killing peptide dans un test de migration en matrice tridimensionnelle sur cellules U118, une lignée humaine de glioblastome. Les résultats obtenus ont montré une inhibition de la migration cellulaire de 40% pour le CP-killing peptide et une absence d'effet du CP non couplé au peptide. J'ai également testé la toxicité aigüe du CP-killing Nrp-1 sur cellules MDA-MB-231 grâce au test MTT et les résultats ont montré que ni le CP-killing ni le CP non couplé ne présentent une toxicité non spécifique.

Afin de développer la stratégie de ciblage des cellules tumorales, j'ai cloné et produit le monomère de CP couplé au « finding Nrp-1 peptide » (appelés CP-finding Nrp1) et produit le monomère de CP couplé au « finding TNC peptide (appelés CP-finding TNC). J'ai utilisé la technique de Proximity Ligation Assay (PLA) afin de valider la capacité du CP-finding Nrp-1 à se lier au récepteur Nrp-1 sur les cellules MDA-MB-231, une lignée de cancer du sein. Le CP-finding TNC a été testé sur lames recouvertes de TNC ainsi que sur coupe histologique de tumeur exprimant la TNC et a montré des résultats encourageant de liaison spécifique à la TNC.

1.2 Evaluation *in vivo*

Après avoir vérifié la capacité de liaison du CP-finding Nrp-1 à son récepteur *in vitro*, je l'ai marqué avec un fluorochrome afin d'évaluer sa biodistribution. Le CP-finding Nrp-1 marqué a été injecté en intrapéritonéal chez des souris immunodéficientes. Le suivi du signal a été effectué grâce au système d'imagerie NightOwl et a montré une élimination hépatique et rénale du composé. La même expérience a été menée avec le CP-killing Nrp-1 et a amené à des résultats similaires.

Après avoir validé l'absence de rétention dans des organes non pathologiques du CP-finding Nrp-1, j'ai mené une expérience afin de valider la capacité de ciblage des tumeurs de ces monomères. Pour cela j'ai utilisé un modèle de souris immunodéficientes greffées en sous-cutané avec deux types de cellules tumorales, des cellules MDA-MB-231 wild-type (exprimant Nrp-1) dans le flanc gauche et des cellules MDA-MB-231 knock-down pour Nrp-1 (99% d'extinction, validation en western blot) dans le flanc droit. Lorsque les tumeurs ont atteint un volume de 100 mm^3 le « finding peptide » couplé à un fluorochrome a été injecté en intrapéritonéal et le signal a été suivi dans l'animal vivant. Le signal a été acquis à trois temps différents : cinq minutes, une heure et vingt-quatre heures après l'injection. Les animaux ont été sacrifiés après l'acquisition à vingt-quatre heures et les organes ainsi que les tumeurs ont été disséqués et analysés (mesure de la fluorescence) dans le système d'imagerie. Les données ainsi recueillies ont montré un signal plus faible dans les tumeurs knock-down pour Nrp-1 comparé au signal obtenu dans les tumeurs wild-type chez les souris injectées avec le finding peptide et aucune différence de signal significative entre les tumeurs exprimant ou non Nrp-1 chez les souris injectées avec les monomères de CP non couplés au finding peptide.

2) Evaluation des disques formés par les CP monomères

Après avoir confirmé la conservation de l'activité biologique des CP-killing peptide et CP-finding Nrp-1 peptide, j'ai procédé à l'assemblage de ces deux monomères afin de créer des disques réunissant la stratégie de destruction des cellules tumorales et la stratégie de ciblage des cellules tumorales. Pour cela j'ai effectué par dialyse une diminution du pH pour atteindre une valeur de 6 favorisant l'auto-assemblage de la CP. La formation de disques a été vérifiée par microscopie électronique à transmission et j'ai commencé leur caractérisation *in vitro* (capacité de liaison au récepteur Nrp-1) grâce à la technique PLA sur cellules MDA-MB-231.

La poursuite de l'évaluation *in vitro* des disques a montré leur capacité d'inhibition de l'angiogenèse sur cellules HUVEC et leur absence de toxicité non spécifique.

Conclusion

Les résultats obtenus durant ma thèse ont permis de démontrer que la fusion de peptides à la CP du TMV permet de produire facilement et grande quantité des peptides TM qui conservent leur activité biologique *in vitro* (liaison au récepteur, inhibition de l'angiogenèse et de la migration cellulaire). Les résultats obtenus *in vivo* ont montré que le CP-killing peptide et le CP-finding Nrp-1 peptide subissent une élimination hépatique et rénale classique en l'absence de tumeur. De plus, le « finding peptide » a montré une capacité de ciblage des tumeurs exprimant Nrp-1. Les résultats obtenus en microscopie électronique ont également permis de confirmer la capacité des monomères de CP fusionnés aux peptides à s'auto-assembler *in vitro*. Les disques ainsi formés présentent également une capacité de liaison au récepteur Nrp-1 et une activité anti-angiogénique.

Publication

Inhibition of primary breast tumor growth and metastasis using a neuropilin-1 transmembrane domain interfering peptide. Arpel A, Gamper C, Spenlé C, Fernandez A, Jacob L, Baumlin N, Laquerriere P, Orend G, Crémel G, Bagnard D. Oncotarget, 2016.

Communications

TMV-derived nanoparticles for the targeting and treatment of cancer. Gamper C, Spenlé C, Bosca-San José S, Orend G, Bagnard D and Heinlein M.
18e Journée scientifique régionale de la Ligue contre le Cancer, 30 Novembre 2017, Ecole Supérieure de Biotechnologie de Strasbourg, Illkirch.

Références

Alonso JM, Gorzny M, Bittner AM (2013) The physics of Tobacco mosaic virus and virus-based devices in biotechnology. Trends Biotechnol 31, 530-538

Fraenkel-Conrat H, Williams RC (1955) Reconstitution of active Tobacco mosaic virus froms its inactive protein and nucleic acid components. Proc Natl Acad Sci USA 41, 690-698

Geretti E, Klagsburn M (2007) Neuropilins : novel targets for anti-angiogenesis therapies. Cell Adh Migr. Apr- Jun;1(2):56-61

Harrison BD, Wilson TMA (1999) Tobacco mosaic virus: pioneering research for a century. Phil. Trans. R. Soc. Lond.B

Lewis JD, Destito G, Zijlstra A, Gonzalez MJ, Quigley JP, Manchester M, Stuhlmann H (2006) Viral nanoparticles as tools for intravital vascular imaging. Nat Med 12, 354-360

Li M, Deng H, Peng H, Wang Q (2014) Functional nanoparticles in targeting glioma diagnosis and therapies. J Nanosci Nanotechnol 14, 415-432

Nasarre C, Roth M, Jacob L, Roth L, Koncina E, Thien A, Labourdette G, Poulet P, Hubert P, Cremel G, Roussel G,Aunis D, Bagnard D (2010) Peptide-based interference of the transmembrane domain of neuropilin-1 Inhibits glioma growth in vivo. Oncogene 29, 2381-2392

Orend G (2005) Potential oncogenic action of tenascin-C in tumorigenesis. Int J Biochem Cell Biol 37: 1066

Saadeh Y, Leung T, Vyas A, Chaturvedi LS, Perumal O, Vyas D (2014) Applications of nanomedicine in breast cancer detection, imaging, and therapy. J Nanosci Nanotechnol 14, 913-923.

Steinmetz NF, Calder G, Lomonossoff GP, Evans DJ (2006) Plant viral capsids as nanobuilding blocks: construction of arrays on solid supports. Langmuir 22, 10032-10037

Steinmetz NF (2010) Viral nanoparticles as platforms for next-generation therapeutics and imaging devices. Nanomedicine 6, 634-641

Wen AM, Lee KL, Yildiz I, Bruckman MA, Shukla S, Steinmetz NF (2012) Viral nanoparticles for in vivo tumor imaging. J Vis Exp 16, e4352

Coralie GAMPER

Nanoparticules dérivées de virus de plante pour le traitement et l'imagerie du cancer

Résumé

Les possibilités de combinaison thérapeutiques offertes par les nanoparticules ont ouvert un nouveau champ d'investigation pour la recherche sur le cancer. Dans ce projet de recherche, des nanoparticules dérivées de la protéine de capside du virus de la mosaïque du tabac (TMV) ont été utilisées afin de transporter différents peptides thérapeutiques ciblant le récepteur neuropiline-1. Cette stratégie a permis de solubiliser un peptide fortement hydrophobe ayant préalablement démontré son efficacité anticancéreuse sur des lignées de cancer du sein humain et de glioblastome. Les résultats obtenus ont également permis de démontrer la possibilité de combiner différents peptides thérapeutiques via l'auto-assemblage de la protéine de capside du TMV.

Mots-clés : Nanoparticule, neuropiline-1, cancer du sein, peptide, TMV.

Résumé en anglais

Nanoparticles play an ever increase role in carrying therapeutic compounds in the cancer field. In this research project, the coat protein of Tobacco mosaic virus (TMV) was used as nanocarrier to solubilize an hydrophobic peptide interfering with the transmembrane domain of neuropilin-1. The nanoparticles created have conserved the antiangiogenic and antimigratory effect of the therapeutic peptide. This strategy was also used to create nanoparticles carrying a peptide targeting the ectodomain of neuropilin-1. The two types of nanoparticles were then assemble through auto-assembling ability of the coat protein. These nanoparticles also exhibit antiangiogenic ability thus, confirming the validity of this approach to combine therapeutic peptides.

Key-words: Nanoparticle, neuropilin-1, breast cancer, theranostic, therapeutic peptide, TMV.